UNIVERSITÉ DE GENÈVE
Département de physique théorique

FACULTÉ DES SCIENCES
Professeur Michel Droz

# On a Class of Nonequilibrium Dissipative Systems

THÈSE

présentée à la Faculté des sciences de l'Université de Genève
pour obtenir le grade de Docteur ès Sciences, mention physique

par

**François COPPEX**
de
Vouvry (VS)

Thèse N° 3610

GENÈVE
Atelier de reproduction de la Section de physique
2005

La Faculté des sciences, sur le préavis de Messieurs M. DROZ, professeur titulaire et directeur de thèse (Département de physique théorique), P.-A. MARTIN, professeur titulaire (Ecole Polytechnique Fédérale de Lausanne – Faculté des sciences de base – institut de théorie des phénomènes physiques – groupe de mécanique quantique – Lausanne, Suisse) et E. TRIZAC, professeur (Université de Paris-Sud XI – Faculté des sciences d'Orsay – UMR 8626 – laboratoire de physique théorique et modèles statistiques – Orsay, France), autorise l'impression de la présente thèse, sans exprimer d'opinion sur les propositions qui y sont énoncées.

Genève, le 18 mars 2005

P. Spierer

**Thèse - 3610 -**

**Le Doyen, Pierre SPIERER**

# Remerciements

Je tiens à remercier tout particulièrement mon directeur de thèse, le Professeur Michel Droz, de m'avoir accepté comme étudiant et m'avoir encadré avec compétence tout au long de ma thèse. Malgré ses très nombreuses tâches académiques, il a toujours su trouver le temps de se rendre disponible lorsque cela m'était nécessaire. J'ai aussi grandement bénéficié de sa connaissance encyclopédique du monde scientifique. Outre les compétences professionnelles, ses qualités humaines et sa sagesse m'ont apporté un enseignement complémentaire tout aussi précieux que la recherce scientifique elle-même.

Je remercie les Professeurs Emmanuel Trizac et Philippe-André Martin d'avoir accepté d'être rapporteurs de ma thèse. En particulier, mes remerciements vont au Prof. Emmanuel Trizac avec qui j'ai eu la chance de collaborer dès le début de ma thèse. J'ai pu bénéficier de sa grande compétence et de ses conseils avisés qui m'ont efficacement guidés durant ma recherche. Je remercie le Prof. Philippe-André Martin de m'avoir initié à la recherche, avec son enthousiasme caractéristique, alors que je réalisais mon diplôme sous sa direction.

Que soient remerciées toutes les autres personnes avec qui j'ai collaboré durant cette période. En particulier, je remercie le Professeur Adam Lipowski avec qui j'ai partagé le même bureau depuis le début de ma thèse et durant deux années; j'ai grandement bénéficié au quotidien de ses fortes aptitudes pédagogiques. La Dr. Ioana Bena qui a fait une lecture très attentive de ce mémoire en suggérant un grand nombre d'améliorations; les Professeurs Jarosław Piasecki, Zoltán Rácz, et Peter Wittwer avec qui j'ai eu la chance de pouvoir collaborer; le Dr. Andreas Malaspinas qui a toujours résolu mes problèmes informatiques avec beaucoup de gentillesse et d'amabilité, les Drs. Tibor Antal et Eric Bertin avec qui j'ai partagé de si nombreuses heures de lunch; enfin, les secrétaires du Département de Physique Théorique, Danièle Chevalier, Francine Gennai-Nicole, et Cécile Jaggi, qui m'ont guidé avec compétence et bonne humeur à travers les méandres administratifs.

Enfin, je remercie le Fonds National Suisse de la Recherche Scientifique ainsi que l'Etat de Genève pour le support financier.

François Coppex

# Contents

# Résumé en français

## 0.1 Introduction

Dans cette thèse nous considérons une classe de systèmes dissipatifs hors d'équilibre. Avant de définir plus précisément quelle est cette classe, il est utile d'aborder les notions de dissipation et de non-équilibre.

Soit un système macroscopique constitué de $N$ particules classiques en interaction dans un volume donné. Comme un tel système est formé de beaucoup de particules (typiquement $N$ est de l'ordre du nombre d'Avogadro, $N \sim 10^{23}$), la description des trajectoires individuelles est en général un objectif non réalisable. On est donc amené à adopter une description probabiliste. Une configuration du système (correspondant à une certaine échelle spatio-temporelle, ou degré de "coarse-graining") sera notée $\omega$. Alors l'état du système à un moment $t$ sera décrit par la distribution de probabilité $P(\omega, t)$ associée aux configurations possibles $\{\omega\}$ du système. Supposons que le niveau de "coarse-graining" soit tel que l'évolution du système soit markovienne et donc descriptible par une équation maîtresse. La dynamique du système peut être telle qu'aucun état stationnaire n'est atteint durant la période d'observation (e.g., le système peut présenter un cycle limite ou un comportement chaotique). Il est évident qu'un tel système est hors d'équilibre. Au contraire, supposons qu'un état stationnaire soit atteint ; l'ensemble des taux de transition $\mathcal{W}_s(\omega|\omega')$ devient stationnaire, ainsi que la distribution des configurations possibles $P_s(\omega)$. Un état d'équilibre est un cas bien particulier d'état stationnaire. Outre l'indépendance temporelle des grandeurs caractéristiques du système, il n'y a pas d'échange macroscopique entre le système et l'extérieur (i.e., aucun flux ne parcourt le système et ses frontières). Du point de vue stochastique, ceci se traduit par la condition de bilan détaillé dans l'espace des configurations, i.e., à l'équilibre $P_s(\omega)\mathcal{W}_s(\omega|\omega') = P_s(\omega')\mathcal{W}_s(\omega'|\omega)$, $\forall \omega, \omega'$. Au contraire, un état stationnaire de non-équilibre correspond à un système parcouru par au moins un flux macroscopique à l'intérieur ainsi qu'à travers ses frontières (le système est nécessairement ouvert). Ce flux macroscopique correspond à des "boucles de courant" dans l'espace des configurations, plus précisément, à une violation du bilan détaillé pour certaines configurations : il existe $\omega$ et $\omega'$ tels que $P_s(\omega)\mathcal{W}_s(\omega|\omega') \neq P_s(\omega')\mathcal{W}_s(\omega'|\omega)$. Ceci est la caractéristique générale des systèmes stochastiques dans un état stationnaire de non-équilibre.

Qu'entend-on par système dissipatif ? Une définition courante est de dire que l'évolution d'un tel système ne conserve pas l'énergie. Nous adoptons ici une définition plus générale. Considérons les grandeurs nécessaires (nombre de particules, énergie, etc.) pour décrire l'état d'un système. Il y a alors deux scénarios possibles permettant de définir un système dissipatif. Le premier est le cas d'un système pour lequel au moins une des grandeurs caractéristiques n'est pas conservée au cours de l'évolution. Par exemple l'énergie totale diminue (collisions inélastiques), ou le nombre total de particules diminue (réactions d'annihilation). Le second scénario est tel que le système atteint un état stationnaire dans lequel il existe un flux –imposé par l'environnement– d'au moins une de ces grandeurs caractéristiques. Il s'agit par exemple de matière granulaire soumise à une excitation externe : malgré les collisions inélastiques dissipant de l'énergie, cette excitation représente une injection d'énergie compensant exactement la perte due aux collisions.

Nous étudions dans un premier temps un gaz dilué en dimension $d \geqslant 2$ formé de particules ayant des trajectoires balistiques entre collisions. Lorsque deux particules entrent en collision, elles disparaissent avec probabilité $p$ et subissent une collision élastique avec probabilité $(1-p)$. Il est alors possible d'établir une description hydrodynamique d'un tel système en se basant sur la théorie cinétique. L'étude d'une telle description peut révéler d'importantes conséquences sur la question de la validité de l'hydrodynamique des systèmes dissipatifs. Les réalisations expérimentales d'une telle dynamique sont néanmoins difficiles à trouver, même si la dynamique des défauts ponctuels dans des cristaux liquides nématiques de géométrie particulière peut révéler des similitudes. Dans un second temps, nous étudions un modèle pour la séparation de la matière granulaire. Des particules granulaires (qui subissent des collisions inélastiques) sont réparties dans des urnes communiquantes secouées verticalement (ce qui correspond à une injection d'énergie). Ce modèle simple reproduit certains résultats expérimentaux, comme par exemple la brisure spontanée de symétrie de la répartition des particules entre les urnes ainsi que la formation spontanée d'inhomogénéités spatiales. L'approche théorique est cette fois basée sur une description en terme d'équations maîtresses.

La classe considérée est donc formée de systèmes dissipatifs dilués hors d'équilibre. Le formalisme hydrodynamique développé s'applique à plusieurs types de tels systèmes (mélanges granulaires, annihilation pure, annihilation probabiliste). Un pendant de ces systèmes est le modèle pour la matière granulaire.

Nous commençons par décrire le contexte et les outils théoriques principaux pour l'étude de la description hydrodynamique d'un système dissipatif.

### 0.1.1 Contexte général

Soit un gaz dilué de particules dont les trajectoires sont balistiques entre collisions. Les particules subissent des collisions binaires élastiques. La théorie cinétique d'un tel système est un sujet bien établi dont l'étude remonte à plus de 40 ans. L'existence d'invariants collisionnels permet d'établir de façon naturelle une description hydrodynamique basée sur la théorie cinétique. Au contraire, on peut considérer une dynamique telle que lors des collisions soit le nombre de particules, leur impulsion, ou leur énergie cinétique n'est plus conservée. La théorie cinétique ainsi que la description hydrodynamique d'un tel système sont bien plus délicates et de nombreuses questions restent sans réponse. Plusieurs travaux visant à établir une description hydrodynamique ont été réalisés pour le gaz granulaire. Un tel système se caractérise par des collisions inélastiques entre particules, où l'inélasticité est caractérisée par un coefficient de restitution $\alpha \in [0,1]$ (la limite élastique correspond à $\alpha = 1$). Néanmoins, la dynamique d'un tel système fait apparaître un inconvénient majeur. En effet, l'évolution est telle que des régions de plus en plus denses se forment. Dans de telles régions, le gaz devient si dense que les corrélations prennent une importance majeure. Or la description cinétique d'un tel système se base sur l'équation de Boltzmann, qui fait intervenir l'hypothèse du chaos moléculaire (factorisation des fonctions de distribution à deux points des vitesses, ce qui revient à négliger les corrélations des vitesses des particules sur le point d'entrer en collision). Dans ces régions de haute densité de particules, qui apparaissent dans la limite des temps longs, l'équation de Boltzmann n'est plus en mesure de fournir une description adéquate.

Considérons à présent un système tel que lorsque deux particules entrent en collision elles disparaissent (annihilation). Il a été montré que l'équation de Boltzmann devient alors asymptotiquement exacte (dans la limite des temps longs). Par contre, un tel système est hautement dissipatif (dans le sens où aucun des champs hydrodynamiques densité $n$, vitesse $\mathbf{u}$, et température $T$ n'est conservé). Une description hydrodynamique soulève donc des problèmes fondamentaux dont la solution n'est actuellement pas connue. Pour contourner ces difficultés, une idée est de concevoir un modèle tel qu'il soit possible de contrôler l'amplitude de la dissipation tout en gardant une dynamique adéquatement décrite par l'équation de Boltzmann. Un tel modèle est fourni par l'annihilation balistique probabiliste.

Considérons un système tel que lorsque deux particules entrent en collision, elles disparaissent avec probabilité $p$ (annihilation) ou subissent une collision élastique avec probabilité $(1-p)$. On parle alors d'annihilation balistique probabiliste. La dissipation peut être choisie aussi faible que désiré ($p \simeq 0$). Ceci permet de diminuer arbitrairement l'ampleur des effets remettant en cause une théorie cinétique de l'hydrodynamique des systèmes dissipatifs. De plus, le problème des corrélations des vitesses dans la limite des temps longs ne se pose pas. En effet, l'équation de Boltzmann de l'annihilation balistique probabiliste fournit une description adéquate de l'évolution pour temps longs si $p \neq 0$.

Notre objectif majeur est donc de fournir une description cinétique bien établie de l'hydrodynamique de l'annihilation balistique probabiliste. Une telle description est particulièrement bien adaptée pour permettre, dans un second temps, une vérification quantitative de la validité de l'hydrodynamique d'un tel système. Nous rappelons brièvement les outils principaux permettant d'établir cette description, plus précisément l'équation de Boltzmann et le développement de Chapman-Enskog.

### 0.1.2 L'équation de Boltzmann

L'équation de Boltzmann s'obtient sur la base de l'hypothèse du *chaos moléculaire*. Plus précisément, il s'agit de la factorisation de la fonction de distribution des vitesses à deux points des particules sur le point d'entrer en collision. Cela revient à dire que les corrélations des vitesses avant collision sont négligées. Une telle approximation est justifiée dans le cas d'un gaz suffisamment dilué. On fait l'hypothèse supplémentaire (d'autant mieux justifiée que la densité est faible) selon laquelle toutes les corrélations d'ordre supérieur sont négligées. Seules les collisions binaires sont prises en considération.

Soit un gaz dilué dans un espace $d$-dimensionnel constitué $N \gg 1$ particules sphériques de masse $m$ et diamètre $\sigma$, sous l'influence d'une force externe $\mathbf{F}$. Nous supposerons que ces particules iteragissent par un potentiel binaire de contact, i.e., que les particules subissent des collisions à deux corps instantanées. Entre ces collisions elles ont une trajectoire balistique. Soit $f(\mathbf{r},\mathbf{v};t)$ la fonction de distribution du gaz donnant la probabilité de trouver une particule de vitesse $\mathbf{v}$ à la position $\mathbf{r}$ au temps $t$. L'équation de Boltzmann décrit alors l'évolution de $f$ :

$$\frac{\partial}{\partial t}f(\mathbf{r},\mathbf{v}_1;t)+\mathbf{v}\cdot\boldsymbol{\nabla}_{\mathbf{r}}f(\mathbf{r},\mathbf{v}_1;t)+\boldsymbol{\nabla}_{\mathbf{v}}\cdot\frac{\mathbf{F}(\mathbf{r},\mathbf{v}_1)f(\mathbf{r},\mathbf{v}_1;t)}{m}=J[f,f], \tag{1}$$

où l'opérateur de collision $J$ est défini par

$$J[f,f]=\sigma^{d-1}\int_{\mathbb{R}^d}\mathrm{d}\mathbf{v}_2\int \mathrm{d}\widehat{\boldsymbol{\sigma}}\,\theta(\mathbf{g}\cdot\widehat{\boldsymbol{\sigma}})(\mathbf{g}\cdot\widehat{\boldsymbol{\sigma}})(b^{-1}-1)f(\mathbf{r},\mathbf{v}_1;t)f(\mathbf{r},\mathbf{v}_2;t), \tag{2}$$

et $\widehat{\boldsymbol{\sigma}}$ est un vecteur unitaire rejoignant le centre des particules au contact. Nous avons noté $\mathbf{g}=\mathbf{v}_1-\mathbf{v}_2$ la vitesse relative, $\theta$ la fonction de Heaviside, et $b^{-1}$ l'opérateur restituant les vitesses de collision dont l'action est définie par

$$b^{-1}\mathbf{v}_1=\mathbf{v}_1'=\mathbf{v}_1-(\mathbf{g}\cdot\widehat{\boldsymbol{\sigma}})\widehat{\boldsymbol{\sigma}}, \tag{3a}$$
$$b^{-1}\mathbf{v}_2=\mathbf{v}_2'=\mathbf{v}_2+(\mathbf{g}\cdot\widehat{\boldsymbol{\sigma}})\widehat{\boldsymbol{\sigma}}. \tag{3b}$$

Dans l'opérateur de collision (2), le terme multiplié par $b^{-1}$ est un terme de gain, tandis que le second représente une perte.

L'opérateur de collision de l'annihilation s'obtient de l'Eq. (2) en gardant uniquement le terme de perte.

Les calculs analytiques basés sur le modèle des sphères dures sont néanmoins très conséquents. Cette difficulté calculatoire découle de la présence du module d'une vitesse relative $g=|\mathbf{v}_1-\mathbf{v}_2|$ dans l'opérateur de collision. Il est alors instructif d'étudier d'autres modèles plus simples dans l'espoir qu'ils capturent la même physique que celle de l'annihilation balistique probabiliste des sphères dures. Considérons donc deux autres modèles d'interaction entre particules. Les modèles de Maxwell et des sphères très dures (VHP) peuvent être caractérisés par leur section efficace. La section efficace est proportionnelle à la vitesse relative pour le premier modèle, et à son inverse pour le second. L'opérateur de collision de ces modèles s'obtient de l'Eq. (2) par une moyenne de la fréquence de collision $(\mathbf{g}\cdot\widehat{\boldsymbol{\sigma}})$ sur l'angle solide. Les effets de la section efficace sont alors inclus dans une fréquence de collision effective $n\sigma^{d-1}\phi v_T^{1-x}$. Le paramètre libre $\phi(x)$ définit l'échelle de temps du système, où $x$ permet de sélectionner un modèle, i.e., $x=0$ pour le modèle de Maxwell, $x=2$ pour le modèle VHP, tandis que la dynamique des sphères dures correspond au cas $x=1$. $v_T$ est la vitesse thermique définie par $v_T=\sqrt{2k_BT/m}$ où $k_B$ est la constante de Boltzmann, $T(t)$ la température cinétique dépendante du temps, et $\sigma$ la portée du potentiel d'interaction. L'opérateur de collision prend la forme

$$J[f,f] = \sigma^{d-1}\frac{\phi(x)v_T^{1-x}}{S_d}\int_{\mathbb{R}^d}\mathrm{d}\mathbf{v}_2\, v_{12}^x \int \mathrm{d}\widehat{\boldsymbol{\sigma}}\,(b^{-1}-1)f(\mathbf{r},\mathbf{v}_1;t)f(\mathbf{r},\mathbf{v}_2;t), \tag{4}$$

où $S_d = 2\pi^{d/2}/\Gamma(d/2)$ est la surface de l'angle solide, et $\Gamma$ la fonction gamma d'Euler.

Enfin, il est utile de considérer un autre système souvent étudié dans la littérature : le gaz granulaire. Dans ce cas, les collisions sont inélastiques. On a alors

$$b^{-1}\mathbf{v}_1 = \mathbf{v}_1' = \mathbf{v}_1 - \frac{1+\alpha}{2\alpha}(\mathbf{g}\cdot\widehat{\boldsymbol{\sigma}})\widehat{\boldsymbol{\sigma}}, \tag{5a}$$

$$b^{-1}\mathbf{v}_2 = \mathbf{v}_2' = \mathbf{v}_2 + \frac{1+\alpha}{2\alpha}(\mathbf{g}\cdot\widehat{\boldsymbol{\sigma}})\widehat{\boldsymbol{\sigma}}, \tag{5b}$$

où $\alpha \in [0,1]$ est le coefficient de restitution de la composante normale des vitesses. L'opérateur de collision s'obtient par un simple changement de variables :

$$J[f,f] = \sigma^{d-1}\int_{\mathbb{R}^d}\mathrm{d}\mathbf{v}_2\int \mathrm{d}\widehat{\boldsymbol{\sigma}}\,\theta(\mathbf{g}\cdot\widehat{\boldsymbol{\sigma}})(\mathbf{g}\cdot\widehat{\boldsymbol{\sigma}})(\alpha^{-2}b^{-1}-1)f(\mathbf{r},\mathbf{v}_1;t)f(\mathbf{r},\mathbf{v}_2;t). \tag{6}$$

Le gaz granulaire va nous permettre de réaliser une comparaison de résultats connus avec ceux issus d'une nouvelle méthode générale (qui s'applique à une classe de systèmes bien plus large que le gaz granulaire) que nous avons développée.

Nous abordons à présent un autre développement théorique majeur utilisé dans ce mémoire.

### 0.1.3 Le développement de Chapman-Enskog

Le développement de Chapman-Enskog se base sur le concept général de séparation des échelles de temps. La dynamique d'un système peut être telle que différents phénomènes physiques se déroulent sur différentes échelles de temps. L'hypothèse de séparation des échelles de temps sous-tendant le développement de Chapman-Enskog mène à deux conséquences fortement reliées.

La première est l'existence d'une solution normale, i.e., toute dépendance spatiale et temporelle de la fonction de distribution $f(\mathbf{r},\mathbf{v};t)$ s'exprime par dépendance fonctionnelle dans les champs hydrodynamiques. La fonction de distribution $f$ prend alors la forme

$$f(\mathbf{r},\mathbf{v};t) = f[\mathbf{v}, n(\mathbf{r},t), \mathbf{u}(\mathbf{r},t), T(\mathbf{r},t)]. \tag{7}$$

Quelle est la justification d'une telle solution ? Soit $\ell$ le libre parcours moyen. Supposons que la variation des champs hydrodynamiques sur une échelle de longueur $\ell$ soit faible, e.g., $\ell|\boldsymbol{\nabla}\ln n| \ll 1$. On associe les échelles de temps correspondantes $\tau$ (pour $\ell$) et $\tau_h$ (pour $|\boldsymbol{\nabla}\ln n| \doteqdot \ell_h^{-1}$). $\tau$ est bien entendu le temps moyen de collision. Sur des échelles $t$ telles que $t \gg \tau_h \gg \tau$, les particules se sont déplacées de plusieurs fois la distance $\ell_h$. Ce *régime hydrodynamique* est alors indépendant des conditions initiales (à distinguer du *régime cinétique* pour des temps de l'ordre de $\tau$). Par conséquent, pour $t \gg \tau_h$ l'état est entièrement caractérisé par les champs $n$, $\mathbf{u}$, et $T$. Toute dépendance spatiale et temporelle de la fonction de distribution peut donc être exprimée par une dépendance fonctionnelle dans les champs hydrodynamiques, menant à l'Eq. (7). L'existence d'une solution normale repose donc sur la séparation d'échelles de temps $\tau_h \gg \tau$, ce qui mène aussi à la seconde conséquence.

La seconde conséquence se base aussi sur l'existence de ces deux échelles de temps distinctes : l'échelle microscopique définie par le temps moyen de collision $\tau$ et l'échelle macroscopique définie par le temps $\tau_h$ associé aux variations des champs hydrodynamiques et de leur inhomogénéités. Par définition $\tau_h \gg \tau$, ce qui revient à dire que sur des échelles de temps microscopiques $\tau$ les champs hydrodynamiques ne varient que faiblement, i.e., ces champs ne sont donc que faiblement inhomogènes. Ceci permet de réaliser un développement de la fonction de distribution dans les gradients :

$$f = f^{(0)} + \lambda f^{(1)} + \lambda^2 f^{(2)} + \ldots . \tag{8}$$

L'ordre $f^{(0)}$ représente donc la fonction de distribution homogène qui apparaît après de courts temps $t$ tels que $\tau \ll t \ll \tau_h$. On doit avoir $\tau \ll t$ pour satisfaire l'équilibre local. Chaque puissance dans le paramètre formel $\lambda$ signifie un ordre donné dans les gradients. Le paramètre $\lambda \ll 1$ s'interprète comme le rapport $\tau/\tau_h \sim \ell/\ell_h$. On suppose de même l'existence d'une hiérarchie d'échelle de temps donc

$$\frac{\partial}{\partial t} = \frac{\partial^{(0)}}{\partial t} + \lambda \frac{\partial^{(1)}}{\partial t} + \lambda^2 \frac{\partial^{(2)}}{\partial t} + \ldots , \tag{9}$$

où $\partial^{(k)}/\partial t$ décrit l'évolution sur l'échelle de temps $k$. Le développement de Chapman-Enskog s'obtient en insérant les séries (8) et (9) dans l'équation de Boltzmann. Récoltant les termes de même ordre en $\lambda$ puis résolvant ces équations ordre par ordre il est possible de construire explicitement la solution.

Supposons à présent que certains champs hydrodynamiques ne soient plus conservés par la dynamique. L'intégration de l'équation de Boltzmann sur les vitesses $\mathbf{v}$ avec poids 1, $m\mathbf{v}$, $mv^2/2$ fournit les équations de bilan des champs $n$, $\mathbf{u}$, et $T$, respectivement. Il s'agit des *équations hydrodynamiques* décrivant l'évolution de ces champs. A chaque champ non conservé est alors associé un taux de déclin apparaissant dans ces équations. Chaque taux définit une échelle de temps qui lui est inversement proportionnelle. Le problème est alors de déterminer si ces nouvelles échelles de temps peuvent être si petites (forte dissipation) qu'elles deviennent de l'ordre du temps caractéristique microscopique $\tau$. L'existence d'une solution normale serait alors invalidée, et la validité d'une description hydrodynamique remise en question.

L'annihilation balistique probabiliste permet d'avoir une dissipation aussi faible que désirée. En effet, pour de petites probabilités d'annihilation $p \simeq 0$ la dynamique est essentiellement donnée par celle des sphères dures. Ce paramètre continu $p$ permet donc de placer la dynamique aussi proche de la limite de validité de la description hydrodynamique d'un système dissipatif que voulu. De plus, la dynamique à long temps de l'annihilation balistique probabiliste est adéquatement décrite par l'équation de Boltzmann. Nous commençons donc par l'étude de l'annihilation pure, i.e., $p = 1$, confrontant une solution exacte de l'équation de Boltzmann avec des simulations de dynamique moléculaire pour vérifier l'hypothèse sous-jacente du chaos moléculaire.

## 0.2 Résultats exacts sur la dynamique d'annihilation de Boltzmann

Soit un système de sphères de diamètre $\sigma$ se mouvant balistiquement dans $\mathbb{R}^d$. Lorsque deux particules entrent en contact, elles disparaissent. Nous supposons la distribution de particules initialement spatialement homogène, et que cette propriété est conservée par l'évolution. La fonction de distribution prend alors la forme $f(\mathbf{v};t) = n(t)\varphi(\mathbf{v};t)$, où $n(t)$ est la densité de particules et $\varphi(\mathbf{v};t)$ est la distribution de probabilité des vitesses. Le problème se simplifie considérant une distribution initiale des vitesses de spectre discret. Un tel spectre est alors conservé par la dynamique. Un cas simple en dimension $d = 2$ est

$$f(v;t) = X(t)\frac{1}{2\pi c_1}\delta(v - c_1) + Y(t)\frac{1}{2\pi c_2}\delta(v - c_2), \tag{10}$$

où $c_2 > c_1 \geqslant 0$. $X(t)$ et $Y(t)$ sont les densités de particules de module de vitesse $c_1$ et $c_2$, respectivement. Ces densités vérifient $X(t) + Y(t) = n(t)$. Nous établissons alors analytiquement une équation implicite donnant la solution de l'équation de Boltzmann. Dans la limite des temps longs, nous trouvons les relations explicites

$$X(\tau) \overset{\tau\to\infty}{\simeq} \frac{1}{4\gamma}\tau^{-1}, \tag{11a}$$

$$Y(\tau) \overset{\tau\to\infty}{\simeq} \frac{V_0}{4\gamma}(4\gamma X_0)^{-1/\alpha}\left(\frac{4-\kappa}{\kappa-4\gamma}V_0+1\right)^{\beta/\alpha}\tau^{-\kappa/4\gamma}, \tag{11b}$$

avec $\tau = 2\pi\sigma c_2 t$, $\gamma = c_1/c_2$, $\alpha = 4\gamma/(\kappa - 4\gamma)$, $\beta = \kappa/(4-\kappa)$, $V_0 = Y_0/X_0$, $X_0 = X(0)$, $Y_0 = Y(0)$, et $\kappa = \int_0^\pi \mathrm{d}\varphi\sqrt{1+\gamma^2-2\gamma\cos\varphi}$.

Considérons à présent le problème de l'annihilation balistique où une partie $X(t)$ des particules est immobile, $c_1 = 0$. Ce système décrit le problème de l'annihilation balistique en présence de pièges statiques. A nouveau, nous obtenons une solution analytique, dont la limite des temps longs donne les relations explicites

$$X(\tau) \overset{\tau\to\infty}{\simeq} X_\infty[1+\varepsilon_2(X_0,Y_0;\tau)], \tag{12a}$$

$$Y(\tau) \overset{\tau\to\infty}{\simeq} X_\infty\varepsilon_2(X_0,Y_0;\tau), \tag{12b}$$

où $\beta = \pi/(4-\pi)$ et

$$\varepsilon_2(X_0,Y_0;\tau) = V_0^{1/(1+V_0/\beta)^{\beta+1}}\exp\left(-JX_\infty/X_0\right)\exp\left(-X_\infty\tau\right), \tag{13}$$

avec

$$J = \int_0^{V_0}\mathrm{d}u\,\ln(u)\frac{\mathrm{d}^2}{\mathrm{d}u^2}\left[-\left(\frac{\beta+V_0}{\beta+u}\right)^\beta\right]. \tag{14}$$

$X_\infty = X(t\to\infty) = X_0/(1+V_0/\beta)^\beta \neq 0$ est la concentration asymptotique de pièges.

Des simulations de dynamique moléculaire permettent de tester la validité de l'hypothèse du chaos moléculaire sous-jacente à l'équation de Boltzmann. Pour un système de l'ordre de $10^5$ sphères, nous avons pu vérifier aussi bien l'établissement du régime asymptotique que les prédictions des Eqs. (11) et (12). En conclusion, nous avons montré que la théorie cinétique de Boltzmann fournit une description adéquate de la dynamique de l'annihilation pour une classe particulière de conditions initiales.

L'hydrodynamique d'un gaz de sphères dures est connue depuis longtemps. Pour un gaz suffisamment dilué cette dynamique ne génère pas de fortes corrélations des vitesses. D'autre part, nous avons montré que l'équation de Boltzmann fournit une description adéquate de l'annihilation pure. Ainsi, l'équation de Boltzmann reste pour des temps longs une description adéquate si les particules subissent une collision élastique avec probabilité $(1-p)$, $p \neq 0$.

Notre but est d'étudier l'annihilation balistique probabiliste. Pour cela, dans un premier temps, nous établissons et testons une nouvelle méthode permettant de calculer de manière approximative la fonction de distribution des vitesses décrivant l'état homogène pour une large classe de systèmes. Pour estimer les avantages de cette nouvelle méthode il est utile de considérer d'abord le gaz granulaire pour lequel des résultats basés sur la "méthode traditionnelle" sont disponibles dans la littérature.

## 0.3 La première correction de Sonine

Soit un système homogène sans forces externes et admettant $(d+2)$ invariants de collision (la densité, chaque composante de l'impulsion, et l'énergie cinétique). La fonction de distribution peut alors être obtenue exactement et est une Maxwellienne. Par contre, si un des champs hydrodynamiques n'est pas conservé [i.e., il existe moins de $(d+2)$ invariants de collision], il n'est pas possible en général de trouver exactement la fonction de distribution décrivant l'état homogène. Une méthode approximative pour la trouver est la suivante.

De nombreux travaux montrent que la fonction de distribution isotrope pour différents systèmes [annihilation balistique (probabiliste), gaz granulaires, ou encore agrégation balistique] prend la forme d'une solution d'échelle (ou de "scaling")

$$f(\mathbf{v};t) = \frac{n}{\overline{v}^d(t)}\widetilde{f}(c), \tag{15}$$

où $\overline{v}(t) = \sqrt{2\langle v^2\rangle/d}$ et $c = v/\overline{v}$. La méthode de calcul de $\widetilde{f}(c)$ consiste à développer cette distribution dans la base des polynômes $S_i(c^2)$ orthogonaux par rapport à la mesure Maxwellienne $\widetilde{\mathcal{M}}(c) = \pi^{-d/2}\exp(-c^2)$ :

$$\widetilde{f}(c) = \widetilde{\mathcal{M}}(c)\left[1 + \sum_{i\geqslant 1} a_i S_i(c^2)\right]. \tag{16}$$

Les $S_i$ sont appelés *polynômes de Sonine*, et $a_2$ fournit la *première correction de Sonine* (la contrainte $\langle c^2\rangle = d/2$ impose la nullité du coefficient $a_1$).

Nous savons que pour une large classe de systèmes dissipatifs, la "queue" de la distribution des vitesses est surpeuplée (décroissance moins rapide que gaussienne). Par conséquent, une distribution de la forme $\widetilde{\mathcal{M}}(1 + a_2 S_2)$ ne fournit pas une bonne description pour de grandes vitesses et cela quelle que soit la valeur de $a_2$. Par contre, nous sommes en général amenés à calculer des moments de petit ordre, ce qui requiert une meilleure précision de la fonction de distribution près de l'origine. La méthode traditionnelle permettant le calcul de $a_2$ fait intervenir des moments d'ordre 4 dans les vitesses. Donc, s'il est possible de développer une méthode impliquant des moments d'ordre inférieur, les erreurs issues des grandes vitesses seront minimisées. Ceci mène à conclure que la limite des faibles vitesses de l'équation de Boltzmann "rescalée"

$$\frac{\mu_2}{d}\left(d + c_1\frac{\mathrm{d}}{\mathrm{d}c_1}\right)\widetilde{f}(c_1) = \widetilde{I}(\widetilde{f},\widetilde{f}) \tag{17}$$

contient une information utile. Une telle limite revient en effet à attribuer plus de poids près de l'origine. Dans l'Eq. (17) on a

$$\widetilde{I}(\widetilde{f},\widetilde{f}) = \int_{\mathbb{R}^d}\mathrm{d}\mathbf{c}_2\int \mathrm{d}\widehat{\boldsymbol{\sigma}}\,\theta(\widehat{\boldsymbol{\sigma}}\cdot\widehat{\mathbf{c}}_{12})(\widehat{\boldsymbol{\sigma}}\cdot\mathbf{c}_{12})\left[\alpha^{-2}\widetilde{f}(c_1')\widetilde{f}(c_2') - \widetilde{f}(c_1)\widetilde{f}(c_2)\right], \tag{18}$$

et $\mu_p = \mu_2 p\langle c^p\rangle/d$. Cette limite fournit l'équation $\mu_2\widetilde{f}(0) = \lim_{c_1\to 0}\widetilde{I}(\widetilde{f},\widetilde{f})$. Le calcul à l'ordre linéaire en $a_2$ fournit

$$a_2 = \frac{4(\alpha^2+1)^2(\alpha^2-1)\left[\sqrt{2}(\alpha^2+1)-2\right]}{A(\alpha,d)}, \tag{19}$$

où

$$\begin{aligned}A(\alpha,d) = 5 + d(2-d) + 8\alpha(\alpha^2+1)(d-1) - \alpha^2(23-6d+d^2) + \alpha^4(3+6d+d^2)\\ + \alpha^6(-1+2d+d^2) - \sqrt{2}(\alpha^2+1)^3(\alpha^2-1)(3+4d+2d^2)/4.\end{aligned} \tag{20}$$

Nous avons réalisé des simulations Monte Carlo aussi bien pour le gaz libre que pour un gaz chauffé à l'aide d'un thermostat stochastique. Ces simulations permettent de conclure que la méthode de la limite fournit de très précises prédictions dans le domaine d'intérêt des petites vitesses. Par contre, dans le régime de moindre intérêt des grandes vitesses les résultats obtenus sont moins précis que ceux issus de la méthode "traditionnelle". En effet, cette méthode consiste en une interpolation globale de la fonction de distribution des vitesses.

Comme discuté auparavant, notre but est de fournir une description de l'annihilation balistique probabiliste. Ayant donc vérifié la précision de la méthode de la limite pour la première correction de Sonine, nous pouvons à présent l'appliquer à ce système.

## 0.4 Annihilation balistique probabiliste

Soit à présent un système tel que lorsque deux particules entrent en contact elles disparaissent avec probabilité $p$ et subissent une collision élastique avec probabilité $(1-p)$. L'opérateur de collision est donc composé de la somme des opérateurs de collision de l'annihilation avec poids $p$ et de collision élastique avec poids $(1-p)$. Nous considérons d'abord un système homogène et appliquons la méthode de la limite pour établir la première correction de Sonine. La connaissance de cette solution homogène permettra ensuite d'appliquer le développement de Chapman-Enskog pour étudier les inhomogénéités ainsi que l'hydrodynamique de l'annihilation balistique probabiliste.

## 0.4.1 La solution homogène

### 0.4.1.1 Les exposants de déclin

La dynamique est telle que ni le nombre de particules ni l'énergie ne sont conservés. Dans le régime de l'Eq. (15) nous avons établi exactement les exposants de déclin de la densité $\xi$ et de l'énergie $\gamma$ :

$$\frac{n}{n_0} = \left(1 + p\frac{1+\alpha_e}{2}\omega_0 t\right)^{-\xi}, \tag{21a}$$

$$\frac{\overline{v}}{\overline{v}_0} = \left(1 + p\frac{1+\alpha_e}{2}\omega_0 t\right)^{-\gamma}, \tag{21b}$$

où la fréquence de collision $\omega$ est donnée par

$$\omega(t) = n(t)\overline{v}(t)\sigma^{d-1}\int \mathrm{d}\mathbf{c}_1\mathrm{d}\mathbf{c}_2\mathrm{d}\widehat{\boldsymbol{\sigma}}\ (\widehat{\boldsymbol{\sigma}}\cdot\mathbf{c}_{12})\,\theta\,(\widehat{\boldsymbol{\sigma}}\cdot\mathbf{c}_{12})\,\widetilde{f}(c_1)\widetilde{f}(c_2), \tag{22}$$

et le paramètre de dissipation d'énergie $\alpha_e$ par

$$\alpha_e = \frac{\int \mathrm{d}\mathbf{c}_1\mathrm{d}\mathbf{c}_2\mathrm{d}\widehat{\boldsymbol{\sigma}}\ (\widehat{\boldsymbol{\sigma}}\cdot\mathbf{c}_{12})\,\theta\,(\widehat{\boldsymbol{\sigma}}\cdot\mathbf{c}_{12})\,c_1^2\widetilde{f}(c_1)\widetilde{f}(c_2)}{\left[\int \mathrm{d}\mathbf{c}c^2\widetilde{f}(c)\right]\left[\int \mathrm{d}\mathbf{c}_1\mathrm{d}\mathbf{c}_2\mathrm{d}\widehat{\boldsymbol{\sigma}}\ (\widehat{\boldsymbol{\sigma}}\cdot\mathbf{c}_{12})\,\theta\,(\widehat{\boldsymbol{\sigma}}\cdot\mathbf{c}_{12})\,\widetilde{f}(c_1)\widetilde{f}(c_2)\right]}. \tag{23}$$

Dans l'Eq. (21) on a $\omega_0 = \omega(t=0)$, $\overline{v}_0 = \overline{v}(t=0)$, et les exposants de déclin

$$\xi = \frac{2}{1+\alpha_e}, \tag{24a}$$

$$\gamma = \frac{\alpha_e - 1}{\alpha_e + 1}. \tag{24b}$$

Ce résultat est exact (dans le contexte du chaos moléculaire) car aucune approximation n'est faite sur $\widetilde{f}$ dans les Eqs. (22) et (23). Supposant à présent un développement de la forme (16) tronqué au premier coefficient non nul $a_2$, il résulte

$$\alpha_e = 1 + \frac{1}{2d} + a_2\frac{1}{8}\left(1+\frac{3}{d}\right) + \mathcal{O}(a_2^2). \tag{25}$$

L'évaluation explicite des exposants $\xi$ et $\gamma$ nécessite donc la connaissance de la première correction de Sonine $a_2$.

#### 0.4.1.2 La première correction de Sonine

L'application de la méthode de la limite présentée dans la Sec. 0.3 fournit

$$a_2(p) = 8\frac{3-2\sqrt{2}}{4d+6-\sqrt{2}+\frac{1-p}{p}8\sqrt{2}(d-1)}. \tag{26}$$

Les exposants de déclin sont donc donnés par l'insertion des Eqs. (26) et (25) dans (24).

Nous avons implémenté un schéma numérique Monte Carlo simulant la dynamique de l'annihilation balistique probabiliste. Ces simulations sont en très bon accord avec les exposants de déclin prédits, ainsi qu'avec la distribution des vitesses issue du $a_2$ donné par l'Eq. (26).

Soit $\mu$ tel que $\widetilde{f}(c) \propto c^{\mu}$ pour $c \to 0$. Dans le cas de l'annihilation pure, il est connu que l'évolution préserve $\mu$. Plus précisément, pour une distribution initiale continue caractérisée par un $\mu$ donné, l'évolution sera telle que pour tout temps la fonction de distribution des vitesses sera caractérisée par le même $\mu$. Une classe d'universalité correspond donc à un $\mu$ donné. Ceci n'est plus vrai pour l'annihilation balistique probabiliste. En effet, les simulations numériques mènent à conjecturer l'universalité des distributions des vitesses. Pour toute distribution initiale de $\mu$ quelconque, l'évolution est telle que la distribution est attirée asymptotiquement vers celle caractérisée par $\mu = 0$.

### 0.4.2 La description hydrodynamique des sphères dures pour l'annihilation balistique probabiliste

Soit un système qui à présent est inhomogène. Définissons les champs hydrodynamiques locaux de densité $n$, vitesse $\mathbf{u}$, et de température $T$ par

$$n(\mathbf{r},t) = \int_{\mathbb{R}^d} \mathrm{d}\mathbf{v}\, f(\mathbf{r},\mathbf{v};t), \tag{27a}$$

$$\mathbf{u}(\mathbf{r},t) = \frac{1}{n(\mathbf{r},t)} \int_{\mathbb{R}^d} \mathrm{d}\mathbf{v}\, \mathbf{v} f(\mathbf{r},\mathbf{v};t), \tag{27b}$$

$$T(\mathbf{r},t) = \frac{m}{n(\mathbf{r},t)k_B d} \int_{\mathbb{R}^d} \mathrm{d}\mathbf{v}\, \mathbf{V}^2 f(\mathbf{r},\mathbf{v};t), \tag{27c}$$

où $\mathbf{V} = \mathbf{v} - \mathbf{u}(\mathbf{r},t)$ est la déviation à la vitesse moyenne. L'intégration de l'équation de Boltzmann avec moments 1, $m\mathbf{v}$, et $mv^2/2$ fournit les équations de bilan des champs hydrodynamiques. Ces équations font apparaître des taux de déclin qui dépendent de la fonction de distribution $f$. Il est donc nécessaire d'appliquer le développement de Chapman-Enskog pour déterminer $f$. Le premier terme $f^{(0)}$ du développement de $f$ étant déjà connu, nous calculons approximativement (par un développement de Sonine au premier ordre) la première correction $f^{(1)}$ à la distribution $f^{(0)}$ caractérisant le système homogène.

Les équations de bilan au premier ordre sont ainsi

$$\partial_t n + \nabla_i(nu_i) = -pn[\xi_n^{(0)} + \xi_n^{(1)}], \tag{28a}$$
$$\partial_t u_i + \frac{1}{mn}\nabla_j P_{ij} + u_j\nabla_j u_i = -pv_T[\xi_{u_i}^{(0)} + \xi_{u_i}^{(1)}], \qquad i = 1,\ldots,d, \tag{28b}$$
$$\partial_t T + u_i\nabla_i T + \frac{2}{nk_Bd}(P_{ij}\nabla_i u_j + \nabla_i q_i) = -pT[\xi_T^{(0)} + \xi_T^{(1)}]. \tag{28c}$$

Les $\xi_A^{(n)}$ sont les taux de déclin de la grandeur $A$ obtenus à l'ordre $n$. Ainsi

$$\xi_n^{(0)} = \frac{d+2}{4}\left(1 - a_2\frac{1}{16}\right)\nu_0, \tag{29a}$$
$$\xi_{u_i}^{(0)} = 0, \qquad i = 1,\ldots,d, \tag{29b}$$
$$\xi_T^{(0)} = \frac{d+2}{8d}\left(1 + a_2\frac{8d+11}{16}\right)\nu_0, \tag{29c}$$

et

$$\xi_n^{(1)} = 0, \tag{30a}$$
$$\xi_{u_i}^{(1)} = -v_T\left(\kappa^*\frac{1}{T}\nabla_i T + \mu^*\frac{1}{n}\nabla_i n\right)\xi_u^*, \tag{30b}$$
$$\xi_T^{(1)} = 0, \tag{30c}$$

où

$$\xi_u^* = \frac{(d+2)^2}{32(d-1)}\left[1 + a_2\frac{-86 - 101d + 32d^2 + 88d^3 + 28d^4}{32(d+2)}\right]. \tag{31}$$

Le coefficient $\nu_0$ est défini par le rapport $\nu_0 = p^{(0)}/\eta_0$, où $p^{(0)} = nk_BT$ est la pression à l'ordre zéro et

$$\eta_0 = \frac{d+2}{8}\frac{\Gamma(d/2)}{\pi^{(d-1)/2}}\frac{\sqrt{mk_BT}}{\sigma^{d-1}} \tag{32}$$

est la viscosité du gaz homogène de sphères dures. Le tenseur de pression $P_{ij}$ est donné par

$$P_{ij}(\mathbf{r},t) = p^{(0)}\delta_{ij} - \eta\left(\nabla_i u_j + \nabla_j u_i - \frac{2}{d}\delta_{ij}\nabla_k u_k\right), \tag{33}$$

où $\eta$ est le coefficient de viscosité de cisaillement. Le courant de chaleur $q_i$ est donné par la loi linéaire de Fourier :

$$q_i = -\kappa\nabla_i T - \mu\nabla_i n, \tag{34}$$

où $\kappa$ est le coefficient de conductivité thermique et $\mu$ un coefficient de transport qui n'a pas d'analogue dans le cas sans dissipation (ce coefficient est responsable du phénomène d'inversion de température qui sera présenté plus loin). Ces relations ainsi que les coefficients de transport sont, bien entendu, issus de la théorie cinétique. Les coefficients de transport sont solutions du système linéaire

$$\eta^* = \frac{\eta}{\eta_0} = \frac{1}{\nu_\eta^* - \frac{1}{2}p\xi_T^{(0)*}}, \tag{35a}$$

$$\kappa^* = \frac{\kappa}{\kappa_0} = \frac{1}{\nu_\kappa^* - 2p\xi_T^{(0)*}}\left[\frac{1}{2}p\xi_n^{(0)*}\mu^* + \frac{d-1}{d}(2a_2+1)\right], \tag{35b}$$

$$\mu^* = \frac{n\mu}{T\kappa_0} = \frac{2}{2\nu_\mu^* - 3p\xi_T^{(0)*} - 2p\xi_n^{(0)*}}\left[p\xi_T^{(0)*}\kappa^* + \frac{d-1}{d}a_2\right]. \tag{35c}$$

Dans les Eqs. (35), les taux de déclin sans dimensions sont $\xi_A^{(n)*} = \xi_A^{(n)}/\nu_0$. Les coefficients $\nu_\kappa^*$, $\nu_\mu^*$, et $\nu_\eta^*$ sont donnés par

$$\begin{aligned}\nu_\kappa^* = \nu_\mu^* = {} & p\frac{1}{32d}\left[16+27d+8d^2+a_2\frac{2880+1544d-2658d^2-1539d^3-200d^4}{32d(d+2)}\right]\\ & +(1-p)\frac{d-1}{d}\left(1+a_2\frac{1}{32}\right),\end{aligned} \tag{36a}$$

$$\begin{aligned}\nu_\eta^* = {} & p\frac{1}{8d}\left[3+6d+2d^2-a_2\frac{278+375d+96d^2+2d^3}{32(d+2)}\right]\\ & +(1-p)\left(1-a_2\frac{1}{32}\right).\end{aligned} \tag{36b}$$

Les Eqs. (28) forment ainsi un ensemble de $(d+2)$ équations pour les $(d+2)$ champs hydrodynamiques au premier ordre (i.e., l'ordre *Navier-Stokes*). Ces équations ne sont en général pas solubles analytiquement. Afin de faire une analyse de stabilité nous les linéarisons en considérant une légère déviation $\delta y(\mathbf{r},t)$ de l'état homogène $y_H(t)$ : $\delta y(\mathbf{r},t) = y(\mathbf{r},t) - y_H(t)$, où $y = \{n, \mathbf{u}, T\}$. Insérant cette forme dans l'équation de Navier-Stokes, on obtient des équations aux dérivées partielles dont les coefficients dépendent du temps. Cette dépendance peut être éliminée par un changement de variables spatiale $\mathbf{l} = \nu_{0H}(t)\sqrt{m/[k_BT_H(t)]}\mathbf{r}/2$ et temporelle $\tau = \int_0^t \mathrm{d}s\,\nu_{0H}(s)/2$, ainsi qu'en définissant les champs de Fourier adimensionnels $\rho_{\mathbf{k}}(\tau) = \delta n_{\mathbf{k}}(\tau)/n_H(\tau)$, $\mathbf{w}_{\mathbf{k}}(\tau) = \sqrt{m/[k_BT_H(\tau)]}\delta\mathbf{u}_{\mathbf{k}}(\tau)$, et $\theta_{\mathbf{k}}(\tau) = \delta T_{\mathbf{k}}(\tau)/T_H(\tau)$, où la transformée de Fourier est $\delta y_{\mathbf{k}}(\tau) = \int_{\mathbb{R}^d}\mathrm{d}\mathbf{l}\,\mathrm{e}^{-i\mathbf{k}\cdot\mathbf{l}}\delta y(\mathbf{l},\tau)$. L'indice $H$ indique une grandeur évaluée dans l'état homogène. Notons que $\mathbf{l}$ est défini (à une constate près) en unités de libre parcours moyen d'un gaz homogène de densité $n_H(t)$.

Les équations hydrodynamiques ainsi linéarisées montrent l'existence d'un mode de vitesse $\mathbf{w}_{\mathbf{k}_\perp}$ découplé des autres modes. Ce mode $\mathbf{w}_{\mathbf{k}_\perp} = \mathbf{w}_{\mathbf{k}} - \mathbf{w}_{\mathbf{k}_\parallel}$ est par définition transverse à la perturbation de nombre d'onde $\mathbf{k}$. Le mode de vitesse longitudinal est défini par $\mathbf{w}_{\mathbf{k}_\parallel} = (\mathbf{w}_{\mathbf{k}}\cdot\widehat{\mathbf{e}}_{\mathbf{k}})\widehat{\mathbf{e}}_{\mathbf{k}}$ où $\widehat{\mathbf{e}}_{\mathbf{k}}$ est le vecteur unitaire dans la direction $\mathbf{k}$. Nous trouvons que pour toute perturbation de nombre d'onde $k$ telle que $k > k_\perp = [2p\xi_T^{(0)*}/\eta^*]^{1/2}$, $\mathbf{w}_{\mathbf{k}_\perp}$ est linéairement stable. De façon similaire, les $(d+1)$ autres modes étant couplés, on définit $k_\parallel$ tel que pour tout $k > k_\parallel$ ces modes sont linéairement stables. Nous trouvons néanmoins $k_\parallel < k_\perp$. Bien que $\mathbf{w}_{\mathbf{k}_\perp}$ soit linéairement découplé des autres modes, il peut leur être couplé non linéairement (par exemple pour le gaz granulaire, ce couplage non linéaire est responsable de la perte de stabilité de l'état homogène). Par conséquent, comme $k_\parallel < k_\perp$ et grâce à ce couplage, la limite de stabilité est issue des conditions sur $k_\perp$ uniquement. Soit par exemple une boîte cubique de volume $L^d$, alors dans l'espace adimensionnel le plus petit nombre d'onde d'une perturbation est $k_{\min} = 2\pi/(Ln\sigma^{d-1}\mathcal{C})$, où $\mathcal{C}$ est une constante. Etant donné que la densité $n(t)$ décroît en fonction du temps, $k_{\min}(t)$ croît de façon monotone. Il existe donc un temps tel que $k_{\min}(t) = k_\perp$. Ainsi la borne inférieure $k_{\min}(t)$ entre inévitablement dans la région où la solution homogène est stable. Même si cette affirmation n'est pas rigoureusement dérivée, on en conclut que toute instabilité ne peut être qu'un phénomène transitoire. Par un argument approximatif, nous avons estimé pour $p = 0.1$ (et pour des conditions typiques correspondant à celles requises pour une implémentation de dynamique moléculaire) que l'état homogène redevient stable après que la densité ne soit plus que d'environ la moitié de la densité initiale. Ceci correspond à moins de 10 collisions par particule. Par analogie, les inhomogénéités dans un gaz granulaire ne sont observées qu'après quelques centaines de collisions par particule. Il est ainsi improbable que des simulations de dynamique moléculaire puissent révéler des inhomogénéités pour l'annihilation balistique probabiliste. Nous n'avons en effet pas observé d'inhomogénéités à l'aide de nos simulations.

Les nombres d'ondes $k_\perp$ et $k_\parallel$ sont des fonctions croissantes de la probabilité d'annihilation $p$. Ainsi, plus la dissipation augmente plus la plage de modes stables se réduit. Néanmoins, comme $k_\perp$ augmente rapidement en fonction de $p$, la région stable $k > k_\perp$ peut correspondre à un régime “non hydrodynamique” lorsque $p$ est supérieur à une valeur critique (difficile à quantifier). En effet, notre description est restreinte à des valeurs $k \ll 1$. Dans l'espace réel, $k$ est proportionnel au libre parcours moyen. Ce dernier est inversément proportionnel à la densité $n$ qui décroît en fonction du temps. Ainsi les grandes valeurs de $k$ correspondent à de très faibles densités. Or lorsque la densité est faible le temps de libre parcours moyen devient grand, éventuellement de l'ordre de gandeur de la variation des champs hydrodynamiques. Il n'y a alors plus séparation des échelles de temps, ce qui invalide la méthode de dérivation des équations de Navier-Stokes. $k \ll 1$ assure donc que le temps de variation des champs hydrodynamiques soit sensiblement supérieur au temps de libre parcours moyen.

Comme déjà mentionné dans la Sec. 0.1.2, les calculs analytiques basés sur le modèle des sphères dures sont lourds. Il est alors instructif d'étudier d'autres modèles plus simples, dans l'espoir qu'ils capturent la même physique que celle de l'annihilation balistique probabiliste des sphères dures. Nous étudions donc les modèles de Maxwell et VHP.

### 0.4.3 La description hydrodynamique des modèles de Maxwell et VHP

L'analyse est similaire à celle basée sur l'annihilation balistique probabiliste des sphères dures, mais fait à présent usage de l'équation de Boltzmann sous la forme (4).

#### 0.4.3.1 Le modèle de Maxwell

Nous établissons le résultat exact $a_2 = 0$ et choisissons l'échelle de temps $\phi$ de sorte à ce que les coefficients de transports soient normalisés pour $p = 0$. Un calcul exact [i.e., sans hypothèse sur la forme de la fonction de distribution $f^{(1)}$] fournit

$$\eta^* = \frac{1}{p\frac{d+2}{2} + (1-p)}, \tag{37a}$$

$$\kappa^* = \frac{1}{p\frac{d(d+2)}{2(d-1)} + (1-p)}, \tag{37b}$$

$$\mu^* = 0. \tag{37c}$$

Les équations hydrodynamiques ont la forme (28), avec comme seul taux de déclin non nul

$$\xi_n^{(0)} = \frac{d+2}{2}\nu_0. \tag{38}$$

#### 0.4.3.2 Le modèle VHP

Un calcul exact de la première correction de Sonine (i.e., en tenant compte des termes non linéaires en $a_2$) fournit à nouveau $a_2 = 0$. En choisissant l'échelle de temps $\phi$ de sorte à ce que $\eta^*(p=0) = 1$, un calcul contenant des approximations similaires à celles pour les sphères dures donne

$$\eta^* = \frac{1}{\nu_\eta^* - \frac{1}{2}p\xi_T^{(0)*}}, \tag{39a}$$

$$\kappa^* = \frac{d-1}{d}\frac{2\nu_\mu^* - 2p\xi_n^{(0)*} - 3p\xi_T^{(0)*}}{X}, \tag{39b}$$

$$\mu^* = 2p\frac{d-1}{d}\frac{\xi_T^{(0)*}}{X}, \tag{39c}$$

où $X = \nu_\kappa^*[2\nu_\mu^* - 2p\xi_n^{(0)*} - 3p\xi_T^{(0)*}] + p\xi_T^{(0)*}\{-4\nu_\mu^* + 3p[\xi_n^{(0)*} + 2\xi_T^{(0)*}]\}$ et

$$\nu_\eta^* = p\frac{2(d+2)}{d+4} + (1-p), \tag{40a}$$

$$\nu_\kappa^* = \nu_\mu^* = p\frac{2(d+3)}{d+4} + (1-p)\frac{4(d-1)}{d(d+2)}. \tag{40b}$$

Les équations hydrodynamiques ont la forme (28), avec comme seuls taux de déclin non nuls

$$\xi_n^{(0)} = \frac{2d}{d+4}\,\nu_0, \tag{41a}$$

$$\xi_{u_i}^{(1)} = -v_T\left(\kappa^*\frac{1}{T}\nabla_i T + \mu^*\frac{1}{n}\nabla_i n\right)\frac{d^2(d+2)}{2(d-1)(d+4)}, \tag{41b}$$

$$\xi_T^{(0)} = \frac{2}{d+4}\,\nu_0. \tag{41c}$$

#### 0.4.3.3 Comparaisons avec les sphères dures

Nous avons calculé les taux de déclin de densité $n$ et de la vitesse thermique $\overline{v} = \sqrt{2\langle v^2\rangle/d}$. Les modèles de Maxwell et VHP fournissent des bornes inférieures et supérieures aux taux de déclin des sphères dures $\xi$ et $\gamma$ :

$$\frac{2d}{2d+1} < \xi < 1, \qquad 0 < \gamma < \frac{1}{2d+1}, \tag{42}$$

où $\xi$ est le taux de déclin de la densité donné par l'Eq. (24a) et $\gamma$ celui de $\overline{v}$ donné par l'Eq. (24b) [en faisant encore usage des Eqs. (25) et (26)]. Notons qu'aucun des taux de déclin des modèles de Maxwell ou VHP ne dépend de $p$. Nous implémentons des simulations Monte Carlo et montrons l'excellent accord avec les taux de déclin du modèle VHP.

La comparaison des coefficients de transport (35), (37), et (39) montre que les modèles de Maxwell et VHP génèrent une dépendance en $p$ similaire à celle des sphères dures. De plus, le modèle de Maxwell (VHP) fournit, respectivement, une borne inférieure (supérieure) à chacun des coefficients de transport des sphères dures.

Nous réalisons à nouveau une analyse de stabilité linéaire des équations hydrodynamiques pour de faibles perturbations autour de la solution homogène. Le modèle de Maxwell est tel que tous les modes sont stables. Par contre, le modèle VHP montre un comportement qualitativement similaire à celui des sphères dures. Comparant les limites de stabilité linéaires, on conclut à nouveau que les modèles de Maxwell et VHP fournissent respectivement une borne inférieure et supérieure aux sphères dures.

En conclusion, les modèles de Maxwell et VHP capturent les mêmes phénomènes physiques que l'annihilation balistique probabiliste de sphères dures. Ces derniers modèles fournissent des bornes inférieures et supérieures à toutes les grandeurs physiques pertinentes et comparables. De plus, la simplicité technique liée à ces modèles ouvre des perspectives pour l'étude de l'influence des termes d'ordre supérieur entrant dans les équations de Navier-Stokes.

Même si ce résultat n'est pas rigoureusement dérivé, l'analyse des équations de Navier-Stokes a permis de conclure que les inhomogénéités de l'annihilation balistique probabiliste sont un phénomène transitoire. Au contraire, il est connu que pour le gaz granulaire la dynamique génère des zones de plus en plus denses, menant éventuellement à une singularité de la fréquence de collision dans ces régions. Exploitant cette idée, nous formulons un modèle reproduisant ces inhomogénéités pour étudier la séparation de matière granulaire.

## 0.5 Le modèle d'urnes

### 0.5.1 Définition générale du modèle

Nous étudions un modèle d'urnes pour la séparation de matière granulaire. Soient $L \geqslant 2$ urnes connectées séquentiellement par une fente à hauteur $h$. L'urne numéro $i$ est donc directement reliée aux urnes $(i-1)$ et $(i+1)$. Les conditions aux bords sont périodiques. $N$ particules granulaires sont distribuées dans les $L$ urnes. Le nombre de particules dans l'urne $i$ est noté $N_i$, et $n_i = N_i/N$. Les particules peuvent changer d'urne si elles ont une énergie cinétique suffisante leur permettant d'atteindre la hauteur $h$. Ces urnes sont soumises à une oscillation verticale, et les particules subissent des collisions inélastiques. Il s'agit donc à nouveau d'un système hors d'équilibre dans le sens où il y a dissipation d'énergie par les collisions inélastiques, dissipation compensée par un mécanisme d'injection lié au mouvement vertical périodique du système d'urnes. Plutôt que de recourir à la théorie cinétique, nous énonçons un modèle phénoménologique capturant l'essentiel des propriétés physiques d'intérêt.

Nous savons que pour un système granulaire la température cinétique est une fonction décroissante de la densité. Le modèle le plus simple qui reproduise la décroissance de la température $T$ dans l'urne $i$ en fonction de sa densité $n_i$ est $T(n_i) = T_0 + \Delta(1 - n_i)$, où $T_0$ et $\Delta$ sont des constantes positives. On suppose de plus que la distribution de particules en fonction de la hauteur depuis le fond d'une urne satisfait la distribution de Boltzmann. On mesure la température en unités $mgh/k_B$, où $m$ est la masse des particules, $g$ la constante de gravitation, et $k_B$ la constante de Boltzmann. La dynamique du modèle est définie par :

(i) une des $N$ particules est sélectionnée au hasard,

(ii) avec probabilité $\exp[-1/T(n_i)]$ la particule sélectionnée est placée aléatoirement dans une des deux urnes voisines, où $i$ est l'urne à laquelle appartient initialement la particule.

Le flux de particules quittant l'urne $i$ est alors donné par

$$F(n_i) = n_i \exp\left[-1/T(n_i)\right]. \tag{43}$$

En fonction des paramètres $T_0$ et $\Delta$, ce modèle permet de décrire la transition de phase entre une distribution symétrique et asymétrique des particules dans les urnes. Pour reproduire une telle brisure de symétrie, il suffit que le flux $F(n)$ possède un seul maximum.

### 0.5.2 Le diagramme de phase et les propriétés dynamiques

Nous étudions dans un premier temps le modèle à $L = 3$ urnes sur la base des équations maîtresses. Nous établissons le diagramme de phase en fonction des deux paramètres $T_0$ et $\Delta$ (partiellement analytiquement). Il existe ainsi deux phases : la phase symétrique (chaque urne contient le même nombre de particules) et la phase asymétrique. Pour de faibles valeurs de $T_0$ et $\Delta$, l'état asymétrique ($n_1 > n_2 = n_3$) est stable (région II). Augmentant $T_0$ (pour $\Delta$ fixé), l'état symétrique ($n_1 = n_2 = n_3$) devient métastable (région III) jusqu'à une ligne spinodale où l'état symétrique devient stable et l'état asymétrique métastable (région IV). Enfin, augmentant encore $T_0$ l'état asymétrique perd sa métastabilité et seul l'état symétrique est stable (région I). Les valeurs de $T_0$ définissant ces régions dépendent évidemment de la valeur de $\Delta$. Contrairement au cas à $L = 2$ urnes, le point tricritique est ici localisé à l'origine $T_0 = \Delta = 0$. Ainsi une transition de phase sera toujours de premier ordre et accompagnée d'hystérèse.

Le recours à des simulations Monte Carlo permet d'avoir accès pas seulement aux valeurs moyennes, mais à toute la dynamique incluant les fluctuations.

Définissons le temps de vie $\tau$ d'un cluster. Soit un état initial asymétrique métastable donné par la solution des équations maîtresses (pour des paramètres $T_0$ et $\Delta$ situés dans la région IV où l'état asymétrique est métastable). Une des urnes contient donc une majorité de particules, notée $N_0$. On convient que cet état asymétrique est détruit si le nombre de particules dans cette urne devient inférieur ou égal à, par exemple, $0.99N_0$. $\tau$ est alors défini par le temps nécessaire pour que cet état asymétrique soit détruit.

En approchant la ligne séparant les régions IV et III (i.e., partant d'un état asymétrique métastable et en se rapprochant de la limite de stabilité de cet état), selon la théorie des phénomènes critiques, $\tau$ diverge comme $\tau \propto N^z$, $z > 0$. Nous avons réalisé des simulations pour différentes valeurs de $L \geqslant 2$ qui indiquent bien un tel comportement, avec de plus $z = 1/3$.

Enfin, pour $L \gg 1$ nous avons étudié numériquement la diffusion d'un cluster dans les urnes après perte de stabilité. Plus précisément, nous considérons un état asymétrique qui perd sa stabilité à cause des fluctuations. Le cluster de particules est donc détruit, et les particules diffusent dans les urnes adjacentes. Cette diffusion est normale avec exposant 1/2 (i.e., décrite par l'équation de diffusion usuelle). La taille $y$ du cluster ayant perdu sa stabilité décroît en fonction du temps $t$ selon $y \propto t^{-1/2}$.

On peut reproduire une diffusion anomale en considérant les collisions à deux particules, comme nous l'expliquons dans le paragraphe suivant.

### 0.5.3 Le modèle de paires

Il est possible de définir plusieurs modèles décrivant la brisure de symétrie des particules dans les urnes. Pour cela, il suffit que la fonction flux $F(n)$ n'ait qu'un seul maximum. Considérons donc un modèle tenant compte de certaines des corrélations à deux points et dont la dynamique est définie par :

(i) deux des $N$ particules sont sélectionnées au hasard,

(ii) si et seulement si les particules sont dans la même urne, avec probabilité $\exp[-Bn_i^2]$ les deux particules sont placées aléatoirement dans une des deux urnes voisines, où $i$ est l'urne à laquelle appartiennent initialement les deux particules et $B > 0$ est une constante positive.

La probabilité que deux particules sélectionnées au hasard appartiennent à la même urne est $N_i(N_i - 1)/[N(N-1)]$, qui dans la limite $N \to \infty$ devient $n_i^2$. La fonction flux est alors celle du modèle de Eggers : $F(n_i) = n_i^2 \exp(-Bn_i^2)$. Pour $L = 2$ la valeur critique $B_c = 4$ donne la transition entre les phases symétrique ($B < 4$) et asymétrique ($B > 4$). Pour $L = 3$, il existe deux points critiques $B_1 = 6.552703411\ldots$ et $B_2 = 9$. Pour $B < B_1$ la solution symétrique est stable alors que la solution asymétrique est stable pour $B > B_2$. Dans l'intervalle $B \in [B_1, B_2]$ les deux solutions sont stables, et il y a hystérèse. A nouveau, des simulations numériques indiquent que $\tau \propto N^z$, $z = 1/3$. La diffusion d'un cluster devient anomale d'exposant 1/3.

### 0.5.4 Les zéros de Yang-Lee

Il est possible d'établir de façon analytique la distribution de probabilité dans l'état stationnaire en terme de la fonction de flux $F(n)$. Ceci peut être aisément réalisé dans le cas général $L \geqslant 2$ à l'aide du formalisme des “zero-range processes”. Dans le cas $L = 2$, on trouve

$$p_s(M) = \frac{1}{Z_N} \prod_{i=1}^{N} \frac{F\left(\frac{N-i+1}{N}\right)}{F\left(\frac{i}{N}\right)}, \tag{44}$$

où le facteur de normalisation (fonction de partition) $Z_N$ est

$$Z_N = 1 + \sum_{M=1}^{N} \prod_{i=1}^{N} \frac{F\left(\frac{N-i+1}{N}\right)}{F\left(\frac{i}{N}\right)}. \tag{45}$$

Le choix le plus simple pour un flux $F(n)$ reproduisant la brisure de symétrie est $F(n) = n\exp(-An)$, $A > 0$. Dans la limite thermodynamique $N \to \infty$ la brisure de symétrie pour $A = 2$ est une transition de phase de second ordre (pour $A < 2$ l'état symétrique est stable). Avec ce choix pour $F(n)$ la fonction de partition (45) prend la forme

$$Z_N = \sum_{M=0}^{N} \binom{N}{M} z^{M(N-M)}, \tag{46}$$

où $\binom{N}{M} = N!/[M!(N-M)!]$ est le coefficient binômial et $z = \exp(-A/N)$ est la fugacité effective.

Il est important de constater que $z$ est une fugacité qui *dépend de la taille du système* $N$. Notons aussi que la fonction de partition (46) est mathématiquement équivalente (avec un changement de variables approprié) à la fonction de partition du modèle de Weiss-Ising en champ moyen. Néanmoins et malgré l'équilibre détaillé, notre système est *physiquement hors d'équilibre*. En effet, il y a balance entre l'injection d'énergie (oscillations verticales des urnes) et dissipation (par les collisions inélastiques).

Nous étudions la théorie de Yang-Lee des transitions de phases sur la base de la fonction de partition (46), avec une fugacité dépendant de la taille du système. Les zéros de (46) sont obtenus numériquement pour différentes valeurs de $N$. Dans la limite thermodynamique ces derniers s'approchent du cercle unité dans le plan des fugacités $z$ complexes. Dans le plan complexe du paramètre de contrôle $A$, les zéros approchent le point critique $A = 2$ avec une pente de $\pi/4$. Ceci confirme l'existence d'une transition de second ordre. Enfin, nous montrons analytiquement que la densité de zéros sur la ligne de zéros dans le plan complexe de $A$ s'annule en loi de puissance à l'approche du point critique. Il s'agit à nouveau d'une caractéristique de la théorie d'équilibre des transitions de phase du second ordre.

## 0.6 Conclusions, extensions et problèmes ouverts

Nous avons étudié une classe de systèmes hors équilibre dissipatifs dilués. Un objectif majeur du travail reporté dans ce mémoire était de fournir une description hydrodynamique basée sur la théorie cinétique. Nous avons donc étudié plusieurs propriétés de l'hydrodynamique de l'annihilation balistique probabiliste. L'analyse de stabilité des équations hydrodynamiques a montré entre autres que les inhomogénéités étaient transitoires, contrairement à ce qui est connu des gaz granulaires où la dynamique génère des zones de plus en plus denses. Nous avons ensuite formulé un modèle pour étudier la séparation de matière granulaire dans des urnes, permettant ainsi de reproduire certaines observations expérimentales.

### 0.6.1 Résumé des résultats obtenus

Nous avons trouvé la solution analytique de l'équation de Boltzmann pour un modèle d'annihilation pure en dimension $d \geqslant 2$. Ce modèle est formé de sphères dures avec distribution initiale isotrope bimodale des vitesses. Des simulations de dynamique moléculaire ont été confrontées avec la solution analytique. Ceci a permis de conclure que l'équation de Boltzmann fournit une bonne description de la dynamique déjà en dimension $d = 2$ (en dimension supérieure $d > 2$ on s'attend à ce que le rôle des corrélations diminue encore, alors qu'en dimension $d = 1$ l'équation de Boltzmann n'est pas adéquate).

Considérant ensuite des distributions initiales continues, nous avons développé une nouvelle méthode pour calculer la première correction à la maxwellienne pour un gaz balistique homogène. Des simulations Monte Carlo ont permis de tester la précision de la méthode. Non seulement notre méthode est techniquement plus simple à implémenter, mais en plus elle fournit des résultats bien plus précis que la méthode “traditionnelle” dans le régime d'intérêt des faibles vitesses pour les grandeurs physiques pertinentes.

Ayant développé cette nouvelle méthode générale et testé la précision de l'équation de Boltzmann pour décrire l'annihilation pure, nous avons tourné notre attention vers l'annihilation balistique probabiliste. Ainsi, les particules qui entrent en collision disparaissent avec probabilité $p$ ou subissent une collision élastique avec probabilité $(1-p)$. Nous avons établi la première correction à la distribution des vitesses maxwellienne pour le système homogène. Des simulations Monte Carlo ont montré la grande précision de nos résultats analytiques. De plus, ces simulations mènent à postuler l'universalité des distributions des vitesses $\widetilde{f}(c)$. En effet, soit $\mu$ tel que $\widetilde{f}(c) \propto c^\mu$ pour $c \to 0$, alors pour toute distribution initiale de $\mu$ quelconque cette distribution est asymptotiquement menée par la dynamique vers la distribution caractérisée par $\mu = 0$.

Nous avons ensuite étudié les inhomogénéités du gaz grâce à un développement de Chapman-Enskog. Nous avons ainsi établi une description hydrodynamique d'un système pour lequel aucun des champs hydrodynamiques n'est associé à une grandeur conservée. L'analyse de stabilité linéaire des équations hydrodynamiques indique que toute inhomogénéité ne peut être qu'un phénomène transitoire. Nous avons aussi montré que les modèles simplifiés de Maxwell et des particules très dures (VHP) capturent l'essentiel de la physique de l'annihilation balistique probabiliste du gaz de sphères dures. De plus, ces modèles fournissent respectivement des bornes inférieures et supérieures à toutes les grandeurs physiques pertinentes comparables.

Enfin, se basant sur une description en terme d'équations maîtresses (et recourant à des simulations Monte Carlo) nous avons étudié un modèle reproduisant la séparation de matière granulaire répartie dans des urnes communiquantes. Cela nous a permis d'illustrer des aspects contre-intuitifs comme par exemple la brisure spontanée de symétrie, ainsi que de reproduire certaines observations expérimentales. La dynamique de ce modèle est telle que le système est hors d'équilibre. Néanmoins, au niveau de "coarse-graining" de la modélisation considérée, le bilan détaillé est vérifié ce qui en fait un système d'équilibre. Nous avons montré que la théorie de l'équilibre de Yang-Lee des transitions de phase fournit une description adéquate de la transition de second ordre dans un cas où la fonction de partition est exprimée en terme d'une fugacité dépendant de la taille du système.

### 0.6.2 Extensions et problèmes ouverts

Mentionnons certains problèmes ouverts vers lesquels pointe ce mémoire.

Une caractéristique de l'annihilation balistique probabiliste est que pour les temps longs l'équation de Boltzmann fournit une description adéquate de la dynamique. D'un autre côté, la dynamique moléculaire permet de simuler la dynamique sans aucune approximation. Par conséquent, l'implémentation de simulations de dynamique moléculaire de l'annihilation balistique probabiliste permettrait un test direct de la validité de la description hydrodynamique. Cette comparaison serait donc indépendante de l'hypothèse du chaos moléculaire. L'implémentation de telles simulations représente cependant un travail considérable qui va au-delà du cadre de cette thèse.

Nous avons vu que les inhomogénéités pour l'hydrodynamique de l'annihilation balistique probabiliste sont transitoires, contrairement au cas du gaz granulaire. La physique de l'annihilation balistique probabiliste révèle donc des différences importantes avec la physique du gaz granulaire. On peut donc s'attendre à découvrir d'autres comportements a priori inattendus en considérant d'autres variantes de la dynamique de l'annihilation balistique probabiliste, comme discuté ci-dessous.

La dynamique de l'annihilation balistique probabiliste est telle qu'aucun des champs hydrodynamiques ne peut être associé à une grandeur conservée. Cependant, par l'action d'un thermostat et d'un réservoir de particules il serait possible de compenser exactement la perte de particules, d'impulsion, et d'énergie cinétique. La densité étant alors conservée, il est possible que les inhomogénéités ne soient plus transitoires. Il serait alors envisageable de les étudier à l'aide de la dynamique moléculaire.

A part le test numérique de la validité de l'hydrodynamique, il existe un grand nombre d'études pouvant être réalisées sur la base du formalisme présenté dans ce mémoire et apportant donc des résultats concernant l'annihilation balistique probabiliste. Plusieurs modèles –initialement utilisés pour les gaz granulaires– peuvent être traduits dans le langage de l'annihilation balistique probabiliste (thermostats, mélanges de particules, particules avec degrés de liberté interne, ou avec des règles de collision plus complexes, ...), pour différentes interactions (modèles de Maxwell, des sphères dures, ou VHP) ou approches numériques (gaz sur réseau, dynamique moléculaire, ou méthodes Monte Carlo).

Finalement, il est possible de généraliser les résultats de ce mémoire aux collisions inélastiques. Ceci mènerait à une théorie unifiée de l'annihilation balistique probabiliste granulaire. A nouveau, des extensions possibles du modèle seraient de considérer la dépendance du coefficient de restitution dans la vitesse (annihilation balistique probabiliste viscoélastique), un coefficient de restitution aléatoire, ou encore un coefficient de restitution tangentiel différent de l'unité. Il est bien connu que les inhomogénéités du gaz viscoélastique sont transitoires. Par conséquent, il serait instructif d'étudier les conséquences de la dépendance du coefficient de restitution dans la vitesse sur la stabilité linéaire de l'annihilation balistique probabiliste viscoélastique.

# Chapter 1

# Introduction

## 1.1 General introduction

In this thesis we shall focus on a class of out-of-equilibrium dissipative systems. Let us define first the general frame defining these systems.

### 1.1.1 General context

Let us consider a low density gas of hard spheres that move ballistically in the interval between binary elastic collisions. The kinetic description of this problem was initiated more than 40 years ago, and is now well established. For this model the number of particles, the momentum, and the kinetic energy are all conserved. More generally, one may consider a system for which the dynamics does not conserve one of the above quantities. The fundamental theoretical background for the hydrodynamic description of such a system remains a controversial issue. The difficulty to establish the validity of such a description is due to the following point.

A hydrodynamic description rooted in the kinetic theory is based on the general concept of separation of time scales. A first time scale is the microscopic time scale defined by the average mean free collision time between particles. The second one characterizes the variations of the coarse-grained hydrodynamic fields. The hydrodynamic description of a ballistic gas based on the kinetic theory exploits explicitly the separation between these time scales, through a Chapman-Enskog perturbation expansion. However, the picture of well-separated time scales changes if any of the coarse-grained hydrodynamic fields is not conserved by the dynamics. Indeed, to each non conserved field there is an associated decay rate due to the loss term in the hydrodynamic equations. The inverse of each decay rate defines a new time scale. Hence, if the decay rate increases, the associated time scale decreases. For strong dissipation (large decay rates), one of the decay rates may become of the order of the mean collision time. Consequently, this would invalidate the derivation of the hydrodynamic description of the system.

This problem has been much investigated in the case of granular gases where particles collide inelastically. However, no clear conclusion has been drawn yet concerning the domain of validity of the corresponding hydrodynamic description. The only common-sense conclusion was that the description should be valid "significantly" close to the elastic limit. The granular gases show some intrinsic "drawbacks" that complicate the answer to the question of validity of a hydrodynamic description. Indeed, it is known that the dynamics is such that density inhomogeneities and clusters of particles form. Some clusters may become so dense that the velocity correlations of the particles become essential in describing the dynamics. Eventually, the granular gas may collapse. In such conditions, the Boltzmann description underlying the hydrodynamics would be invalidated. On the other hand, one may consider a different system which does not show the emergence of such strong correlations generated by the dynamics: annihilation dynamics. In such a system, when two particles collide they instantaneously disappear from the system. A great advantage of ballistic annihilation is that in the long time limit the Boltzmann equation becomes an exact description of the dynamics. On the other hand, such a system is highly dissipative in the sense that neither the density, nor the momentum, or the kinetic energy are conserved. In view of the discussion above, it would be desirable to control the amplitude of the dissipation with an additional parameter. To this purpose we introduce the annihilation probability $p \in [0, 1]$. When two particles meet, they either disappear from the system with probability $p$ or scatter *elastically* with probability $(1-p)$. This mechanism is referred to as *probabilistic ballistic annihilation* (PBA).

To sum up, we have at our disposal a system such that for $p \neq 0$ the Boltzmann equation is likely to describe exactly the dynamics. Moreover, the continuous control parameter $p$ allows the system to be in a regime that is as close as desired to the elastic limit ($p \simeq 0$) in order to avoid the problem of non-separation of time scales.

### 1.1.2 Objectives

The major objective of this work is to provide a well-established kinetic description of probabilistic ballistic annihilation. Such a description then provides an adequate framework for probing the validity of hydrodynamics of dissipative systems.

In order to achieve this goal, many properties of PBA (or kinetic theory of dilute gases in general) have to be studied. We shall first focus on an exactly solvable model for pure annihilation. For this system, we confront the exact asymptotic Boltztmann solution to molecular dynamics in order to probe the hypothesis of molecular chaos. It is known that the velocity function distribution describing the homogeneous state of the granular gas is non Gaussian in several aspects. We develop a new method to compute the first nonzero correction to the Maxwellian distribution in the small velocity domain (the so-called first Sonine correction). Monte Carlo simulations show that this method turns out to be much more accurate than the "traditional" method. This new method is used next to establish analytically the velocity distribution function in a homogeneous gas for PBA and for different continuous initial conditions. These results are confronted to Monte Carlo simulations. Starting from different *continuous* initial conditions, the simulations lead to conjecture that for long times the velocity distribution becomes universal: it does not depend on its initial form. The next step is to study inhomogeneities. This is achieved with a first order Chapman-Enskog expansion in the gradients of the spatial inhomogeneities, leading to the Navier-Stokes hydrodynamic description of PBA. A linear stability analysis is performed. It shows that inhomogeneities in PBA are only a transient effect, which is unlikely to be observable by molecular dynamics simulations. It means that if for short times some dense clusters form, they will inevitably be destroyed by the dynamics for longer times. Therefore, and contrarily to granular gases with constant restitution coefficient, the molecular chaos assumption is likely to be well-justified for all times beyond this short transient regime. The analytical treatment of PBA of the hard sphere gas is however quite involved. We therefore study two other models associated with two different forms of the interaction between particles. Those models not only capture the essential features of the hard sphere gas, but provide as well analytical upper and lower bounds for all comparable quantities. The whole study therefore provides a well established framework that may be further used in order to probe the validity of hydrodynamics of dissipative systems. The above-mentioned systems are nonequilibrium dissipative ones, in the sense that is stated below.

## 1.2 Nonequilibrium systems

The macroscopic system $\Lambda$ we are considering is made of $N \gg 1$ interacting classical particles in a given volume. Since the typical system of interest is made of many particles (of the order of the Avogadro number, $N \sim 10^{23}$), the knowledge of all individual trajectories in the phase space is in general an unrealistic goal. A more tractable description can thus be obtained from a statistical approach. A microscopic configuration of the system (corresponding to a given level of coarse-graining) is denoted $\omega$. The definition of a nonequilibrium system may be understood best if we start from the definition of a system at *equilibrium*.

Depending on the constraints imposed on the system, several descriptions are possible. Imposing constant energy $E$, number of particles $N$, and volume $V$ yields (assuming ergodicity) the micro-canonical statistical ensemble for the distribution of configurations $\{\omega\}$. If the constraint of constant energy is relaxed and the system $\Lambda$ is put in contact with a thermal bath at temperature $T$, then it is described by the canonical ensemble. The distribution function of the configurations $\{\omega\}$ is given by the canonical distribution $P_e(\omega) = \exp[-\beta E(\omega)]/Z$, where $\beta = 1/(k_B T)$ (with $k_B$ the Boltzmann constant and $Z$ the partition function). If moreover the constraint of constant number of particles $N$ is relaxed and that the system is put in contact with a reservoir of particles, then it is described by the grand canonical ensemble. Depending on the constraints, other statistical ensembles can be obtained.

We now turn to the *dynamics*. The description is then obtained from the theory of stochastic processes. We suppose that the evolution of the system is Markovian. Let $\omega$ and $\omega'$ be two different configurations of the system, and the transition rate from $\omega$ to $\omega'$ denoted by $\mathcal{W}(\omega|\omega')$. The time-dependent probability distribution is $P(\omega; t)$. It is therefore possible to describe the dynamics of $\Lambda$ through a master equation. A system at equilibrium is such that there are in average no fluxes inside

$\Lambda$ and through its boundaries. In the canonical ensemble this property translates into the *detailed balance* condition $P_e(\omega)\mathcal{W}_e(\omega|\omega') = P_e(\omega')\mathcal{W}_e(\omega'|\omega)$, $\forall\omega,\omega'$ for the stationary equilibrium distribution $P_e$ and the equilibrium transition rates $\mathcal{W}_e$. In the microcanonical ensemble the probability distribution $P_e(\omega)$ is uniform on a surface of constant energy and the detailed balance condition therefore becomes $\mathcal{W}_e(\omega|\omega') = \mathcal{W}_e(\omega'|\omega)$, $\forall\omega,\omega'$, which expresses the microreversibility. For example, a Hamiltonian description (with the underlying time reversal symmetry) obeys the microreversibility condition [1].

We now consider a *nonequilibrium* system. The dynamics of a nonequilibrium system $\Lambda$ is driven by open boundaries. There is a nonzero (average) flux between $\Lambda$ and its environment. As a consequence, there is a nonzero (average) flux *inside* the system.

The asymptotic *dynamics* of $\Lambda$ may not reach a steady state, but instead show a limit cycle or a chaotic behavior. It is clear that such a system is out of equilibrium. Suppose on the other hand that the system reaches asymptotically a steady state $P_s(\omega)$ (the corresponding transition rates are denoted $\mathcal{W}_s$). Of course, the equilibrium state (defined by the constraints discussed above) is a very particular case of stationary state.[1] But in a nonequilibrium steady state there exist fluxes inside the system and through its boundaries. These macroscopic fluxes correspond to "loops" of current in the configuration space. From a stochastic point of view, a nonequilibrium steady-state is such that the micro-dynamics *does not obey detailed balance*: there exist $\omega$ and $\omega'$ such that $P_s(\omega)\mathcal{W}_s(\omega|\omega') \neq P_s(\omega')\mathcal{W}_s(\omega'|\omega)$ [3, 4].

Note that the definition given here may not be appropriated in some cases where a given coarse-grained description of a system is taken into account. As a matter of illustration, we shall consider the urn model defined in Chap. 6. Although detailed balance is verified at a certain coarse-grained level, the urn model describes a nonequilibrium system. The dynamics is generated by an energy injection mechanism (through the vertical shaking of the sand beads) which compensates exactly the loss of energy due to inelastic collisions between the particles. In the thermodynamic limit the coarse-grained steady state is such that the number of particles in each of the urns remains constant. Therefore this system is at equilibrium at the coarse-grained macroscopic scale, but out-of-equilibrium at a microscopic scale.

## 1.3 Dissipative systems

What are dissipative systems? An common definition is that the evolution of the system does not conserve the energy. We shall here consider a broader definition. Let $\Lambda$ be the dynamical system of $N$ interacting particles, and $\Omega$ the environment. We consider the total number of particles, the total momentum, the total energy of the system, or any other pertinent quantity that is needed to formulate a coarse-grained description of $\Lambda$. Alternatively, one may consider the microscopic rules defin-

[1] Note that the time scale of the dynamical relaxation process in glassy systems may be so large compared to experimental scales that the system may merely be considered as relaxing to equilibrium [2].

ing the dynamics of the particles (two or many body collisions of non spherical objects, charged particles interacting through the Coulomb potential, ...) and the corresponding local quantities (number of particles, impulsion, kinetic energy, electric charge, etc.). The global counterpart of those quantities (i.e., their average in $\Lambda$) are denoted by $X$. We shall distinguish two different class of dissipative systems.

The first one corresponds to the case of a non stationary state where one or more of the quantities $X$ is not conserved by the dynamics of $\Lambda$. For example, the total number of particles diminishes (annihilation reactions), or the total energy decreases (inelastic collisions).

The second one is such that the stationary state of $\Lambda$ requires a flow of any such a quantity $X$ between $\Lambda$ and $\Omega$. This is for example the case of a granular material which is shaken: although the inelastic collisions dissipate energy, there is a constant energy injection mechanism through the shaking which exactly compensates the energy loss due to the collisions.

## 1.4 The Boltzmann equation

### 1.4.1 Introduction and hypothesis

We consider a dilute gaz of $N \gg 1$ identical particles of mass $m$ in a $d$-dimensional volume which may be under the influence of an *external* force $\mathbf{F}$. The particles interact through a two-body potential. Let $f(\mathbf{r}, \mathbf{v}; t)$ be the one-particle distribution function of the system. $f(\mathbf{r}, \mathbf{v}; t)\mathrm{d}\mathbf{r}\mathrm{d}\mathbf{v}$ gives the average number of particles at time $t$ in the volume $\mathrm{d}\mathbf{r}$ centered at position $\mathbf{r}$, with speed $\mathrm{d}\mathbf{v}$ around $\mathbf{v}$. We define the average number of particles at position $r$ at time $t$ by

$$n(\mathbf{r}, t) = \int_{\mathbb{R}^d} \mathrm{d}\mathbf{v}\, f(\mathbf{r}, \mathbf{v}; t), \tag{1.1}$$

and the local flow velocity density $\mathbf{u}(\mathbf{r}, t)$ by

$$\mathbf{u}(\mathbf{r}, t) = \frac{1}{n(\mathbf{r}; t)} \int_{\mathbb{R}^d} \mathrm{d}\mathbf{v}\, \mathbf{v}\, f(\mathbf{r}, \mathbf{v}; t), \tag{1.2}$$

such that the local flow velocity field is given by $n(\mathbf{r}, t)\mathbf{u}(\mathbf{r}, t)$. The average kinetic energy $T(\mathbf{r}, t)$ is defined from the principle of energy equipartition

$$\frac{d}{2} n(\mathbf{r}, t) k_B T(\mathbf{r}, t) = \int_{\mathbb{R}^d} \mathrm{d}\mathbf{v}\, \frac{1}{2} m \mathbf{V}^2 f(\mathbf{r}, \mathbf{v}; t), \tag{1.3}$$

where $\mathbf{V} = \mathbf{v} - \mathbf{u}(\mathbf{r}, t)$ describes the deviation around the mean local flow, and $k_B$ is the Boltzmann constant. It follows that

$$T(\mathbf{r}, t) = \frac{m}{n(\mathbf{r}, t) k_B d} \int_{\mathbb{R}^d} \mathrm{d}\mathbf{v}\, \mathbf{V}^2 f(\mathbf{r}, \mathbf{v}; t). \tag{1.4}$$

We shall establish an evolution equation, a *kinetic equation*, for the distribution function $f(\mathbf{r}, \mathbf{v}; t)$. An evolution equation involves an expression for $\partial f / \partial t$, and thus introduces a time scale $\tau$ (roughly, the mean time between two successive collisions of the particles) on which there is a "significant" change of the velocity distribution function. Let $\tau_c$ be the duration of such a collision event.

A first approximation of Boltzmann's description is to assume $\tau_c \ll \tau$, which means that the collisions are *instantaneous* on a scale $\tau$. As shown below, this condition is intimately related with the condition of having a dilute gas.

Let $\sigma$ be the diameter of the particles (the domain-size of the interaction potential). For a low density gas, $n^{-1/d} \gg \sigma$, which means that the average distance between two particles is much larger that the range of the interaction. This may be rewritten in the form $n\sigma^d \ll 1$. The mean free path is $\ell \approx 1/(n\sigma^{d-1})$, and the condition $n\sigma^d \ll 1$ translates into $\sigma \ll \ell$. Let $v_T = \sqrt{2k_BT/m}$ be the thermal velocity, then $\tau_c \approx \sigma/v_T$ is the collision time and $\tau \approx \ell/v_T$ is the mean free time. The condition $n\sigma^d \ll 1$ then translates into $\tau_c \ll \tau$, and we recover the assumption of instantaneous (and spatially localized) collisions.

This will also allow to take into account only *binary* collisions. Since $\sigma \ll \ell$ one may neglect the diameter of the particles at contact and state that they collide only if they are at the same position $\mathbf{r}$ at time $t$. For instance, a Helium gas under normal conditions is characterized by $\sigma \approx 3$ Å, $n^{-1/3} \approx 30$ Å, $v_T \approx 1'000$ m/s, and $\lambda \approx 1'500$ Å, which gives $\tau_c/\tau \approx 2 \times 10^{-3} \ll 1$. Finally, the last hypothesis is to neglect the correlations of the *pre-collisional* velocities of the particles that are about to scatter. This hypothesis is known under the name of *molecular chaos* assumption. Molecular chaos is expected to fail for dense gases. It is also an inappropriate approximation in $d = 1$, but it holds with a good accuracy for $d \geqslant 2$. Note that the post-collisional velocities (i.e., the velocities after the collision event) are strongly correlated.

### 1.4.2 The Knudsen gas

One may write the Boltzmann equation under the form

$$\frac{\partial f}{\partial t} = \left.\frac{\partial f}{\partial t}\right|_{\text{free}} + \left.\frac{\partial f}{\partial t}\right|_{\text{coll}}, \tag{1.5}$$

where $\partial f/\partial t|_{\text{free}}$ describes the change of $f$ due to the motion of the particles between collisions. $\partial f/\partial t|_{\text{coll}}$ describes the change of $f$ due to the mutual interactions between the particles. We first turn to the evaluation of $\partial f/\partial t|_{\text{free}}$. For this purpose, we consider the Knudsen gas where collisions between particles are neglected. The evolution of each particle is then governed by Newton's equation $\mathrm{d}\mathbf{v}_i(t)/\mathrm{d}t = m^{-1}\mathbf{F}[\mathbf{r}_i(t), \mathbf{v}_i(t)]$, $i = 1, \ldots, N$. A particle at position $\mathbf{r}$ and with velocity $\mathbf{v}$ at time $t$ is at position $\mathbf{r}' = \mathbf{r} + \mathbf{v}\delta t$ with velocity $\mathbf{v}' = \mathbf{v} + m^{-1}\mathbf{F}\delta t$ at time $t + \delta t$. Therefore

$$f(\mathbf{r}, \mathbf{v}; t)\mathrm{d}\mathbf{r}\mathrm{d}\mathbf{v} = f(\mathbf{r}', \mathbf{v}'; t)\mathrm{d}\mathbf{r}'\mathrm{d}\mathbf{v}', \tag{1.6}$$

where

$$\mathrm{d}\mathbf{r}'\mathrm{d}\mathbf{v}' = \left(1 + \frac{1}{m}\boldsymbol{\nabla}_{\mathbf{v}} \cdot \mathbf{F}\delta t + \frac{1}{m}\boldsymbol{\nabla}_{\mathbf{r}} \cdot \mathbf{F}\delta t^2\right)\mathrm{d}\mathbf{r}\mathrm{d}\mathbf{v}. \tag{1.7}$$

A first-order expansion for small $\delta t$ yields

$$f(\mathbf{r}', \mathbf{v}'; t') = f(\mathbf{r}, \mathbf{v}; t) + \mathbf{v} \cdot \boldsymbol{\nabla}_{\mathbf{r}} f \delta t + \frac{\mathbf{F}}{m} \cdot \boldsymbol{\nabla}_{\mathbf{v}} f \delta t + \frac{\partial f}{\partial t} \delta t + \mathcal{O}(\delta t^2). \tag{1.8}$$

Inserting Eqs. (1.8) and (1.7) in (1.6) one obtains

$$\left.\frac{\partial f}{\partial t}\right|_{\text{free}} = -\mathbf{v} \cdot \boldsymbol{\nabla}_{\mathbf{r}} f - \boldsymbol{\nabla}_{\mathbf{v}} \cdot \frac{\mathbf{F}}{m} f. \tag{1.9}$$

This result is not restricted to conservative forces since the field $\mathbf{F}$ may depend on the velocity $\mathbf{v}$.

### 1.4.3 The binary encounter

The collision term $\partial f / \partial t|_{\text{coll}}$ may be obtained from the truncation to first order of a hierarchy of equations for the many body distribution functions (BBGKY hierarchy [5]). We decide however to present another route in order to derive the equation, that is closer to the original derivation by Ludwig Boltzmann and maybe contains more physical insight into the mechanisms of the collisions.

We consider two particles with velocities $\mathbf{v}_1$ and $\mathbf{v}_2$ The interaction is described by an isotropic binary potential $V(|\mathbf{r}_1 - \mathbf{r}_2|)$. The post-collisional velocities are given by $\mathbf{v}_1'$ and $\mathbf{v}_2'$, respectively (c.f. Fig. 1.1).

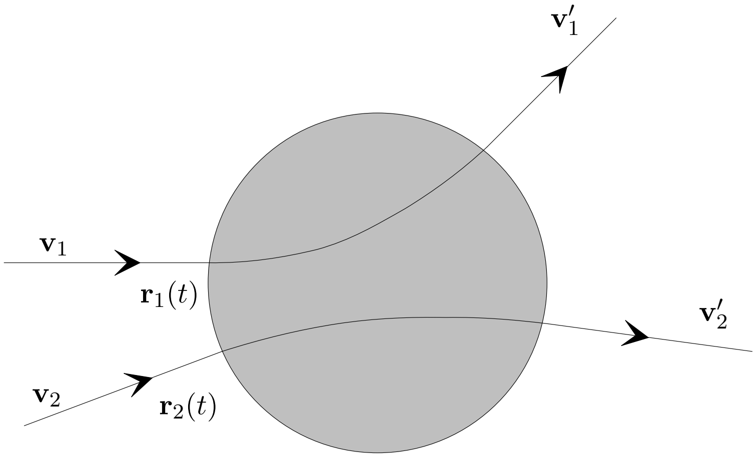


Figure 1.1: Sketch of a binary collision, where the domain of interaction of the two particles is given by the dark-gray region.

The impulsion and energy are conserved in an elastic binary encounter, i.e., $\mathbf{v}_1 + \mathbf{v}_2 = \mathbf{v}_1' + \mathbf{v}_2'$ and $v_1^2 + v_2^2 = v_1'^2 + v_2'^2$, respectively, where we have written $v = |\mathbf{v}|$. Making use of the last two conservation laws one obtains $|\mathbf{v}_1 - \mathbf{v}_2|^2 = |\mathbf{v}_1' - \mathbf{v}_2'|^2$. It is instructive to consider the binary encounter in the frame of the center of mass. The velocity of the center of mass is $\mathbf{u} = (\mathbf{v}_1 + \mathbf{v}_2)/2$, the relative velocity $\mathbf{g} = \mathbf{v}_1 - \mathbf{v}_2$, and the relative position $\boldsymbol{\rho} = \mathbf{r}_1 - \mathbf{r}_2$. The conservation laws thus give

$$\mathbf{u} = \mathbf{u}', \tag{1.10a}$$
$$g = g', \tag{1.10b}$$

which simply mean that the center of mass undergoes an uniform translation and that the relative energy is conserved. Consequently, the problem in the center of mass frame is equivalent to the diffusion of one particle of velocity $\mathbf{u}$ by the central potential $V(|\boldsymbol{\rho}|)$, for which only the direction of the relative velocity changes at collision (see Fig. 1.2).

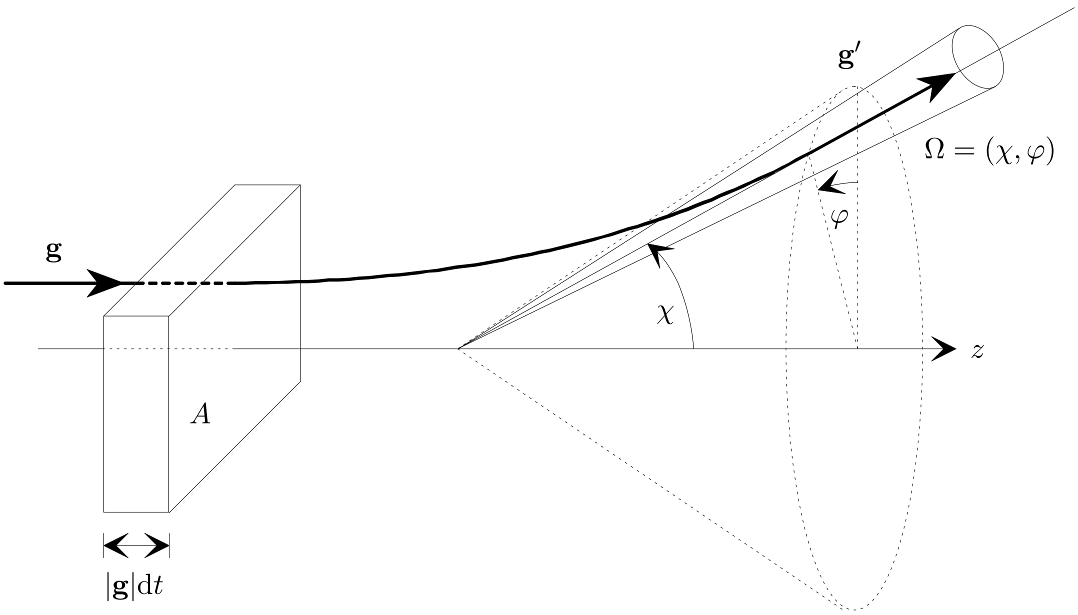


Figure 1.2: Sketch of the geometry of a binary encounter in the center of mass frame for a repulsive potential. The surface $A$ is defined as being orthogonal to $\mathbf{g}$. The incident particle approaches the target with initial velocity $\mathbf{g}$ along the $z$ axis, and after the interaction leaves with a relative velocity $\mathbf{g}'$. The scattering angle is given by $\chi$.

Since $g = g'$, the final velocity depends only on $g$ and on the solid angle $\Omega = (\chi, \varphi)$. The collision process is therefore governed by the interaction potential through the differential cross section $B(g, \Omega)$. Let $I$ be the flux of incoming particles with speed $\mathbf{g}$, i.e., $I$ is the number of particles passing per unit time through a unit surface orthogonal to $\mathbf{g}$. That is, $I = n(\mathbf{g})Ag\mathrm{d}t/(A\mathrm{d}t) = n(\mathbf{g})g$, where $n(\mathbf{g})$ is the number of particles with velocity $\mathbf{g}$ per unit volume. $B(g, \Omega)$ is defined through the relation $I = B(g, \Omega)\mathrm{d}\Omega$. $B$ therefore represents the number of particles scattered in the solid angle $\mathrm{d}\Omega$ around $\Omega$ per unit time with incoming flux $I$. Since we consider a symmetrically spherical potential, the cross section depends only on $g$ and the scattering angle $\chi$.

### 1.4.4 The collision term

The collision term is obtained from the difference of a *gain* term $C_g$ and of a loss term $C_l$, i.e.,

$$\partial f/\partial t|_{\text{coll}} = C_g - C_l. \tag{1.11}$$

Let $\mathrm{d}\mathbf{r}$ be an infinitesimal volume centered around $\mathbf{r}$, and $\mathrm{d}\mathbf{v}$ an infinitesimal volume centered around $\mathbf{v}$ in the velocity space. $C_l\mathrm{d}\mathbf{r}\mathrm{d}\mathbf{v}\mathrm{d}t$ gives the number of collisions during $t$ and $t+\mathrm{d}t$ such that a particle of velocity $\mathbf{v}$ in $\mathrm{d}\mathbf{r}$ acquires a post-collisional velocity $\mathbf{v}' \notin \mathrm{d}\mathbf{v}$. $C_g\mathrm{d}\mathbf{r}\mathrm{d}\mathbf{v}\mathrm{d}t$ gives the number of collisions during $t$ and $t+\mathrm{d}t$ such that a particle with initial arbitrary velocity $\mathbf{v}'$ in $\mathrm{d}\mathbf{r}$ acquires a post-collisional velocity $\mathbf{v} \in \mathrm{d}\mathbf{v}$ (those are the inverse collisions of the kind $\{\mathbf{v}_1', \mathbf{v}_2'\} \to \{\mathbf{v}_1, \mathbf{v}_2\}$).

We first turn our attention to the loss term $C_l$. In the center of mass we consider the target and incident particles of velocity $\mathbf{v}_1$ and $\mathbf{v}_2$, respectively. Since $f(\mathbf{r}, \mathbf{v}_2; t)\mathrm{d}\mathbf{v}_2$ is the number of particles per unit volume with velocity in $\mathrm{d}\mathbf{v}_2$, a similar argument to that of the previous paragraph gives the corresponding flux of particles $f(\mathbf{r}, \mathbf{v}_2; t)\mathrm{d}\mathbf{v}_2 g$. The number of particles scattered per unit time into the element $\mathrm{d}\Omega$ is therefore $f(\mathbf{r}, \mathbf{v}_2; t)\mathrm{d}\mathbf{v}_2 gB(g, \Omega)$. Since in $\mathrm{d}\mathbf{r}$ there are $f(\mathbf{r}, \mathbf{v}_1; t)\mathrm{d}\mathbf{r}\mathrm{d}\mathbf{v}_1$ target particles with velocity between $\mathbf{v}_1$ and $\mathbf{v}_1 + \mathrm{d}\mathbf{v}_1$, the number of particles scattered into the element $\mathrm{d}\Omega$ reads

$$f(\mathbf{r}, \mathbf{v}_1; t)f(\mathbf{r}, \mathbf{v}_2; t)\mathrm{d}\mathbf{v}_1\mathrm{d}\mathbf{v}_2\mathrm{d}\mathbf{r}gB(g, \Omega). \tag{1.12}$$

Note that in the latter expression we have made use explicitly of the molecular chaos assumption. The total number of scattered particles is obtained upon integrating over all scattering directions and all velocities $\mathbf{v}_2$ of incoming particles. It follows

$$C_l\mathrm{d}\mathbf{r}\mathrm{d}\mathbf{v}_1 = \int_{\mathbb{R}^d} \mathrm{d}\mathbf{v}_2 \int \mathrm{d}\Omega\, f(\mathbf{r}, \mathbf{v}_1; t)f(\mathbf{r}, \mathbf{v}_2; t)\mathrm{d}\mathbf{v}_1\mathrm{d}\mathbf{r}gB(g, \Omega), \tag{1.13}$$

so that

$$C_l = \int_{\mathbb{R}^d} \mathrm{d}\mathbf{v}_2 \int \mathrm{d}\Omega\, gB(g, \Omega)f(\mathbf{r}, \mathbf{v}_1; t)f(\mathbf{r}, \mathbf{v}_2; t). \tag{1.14}$$

In order to find the gain term $C_g$, we consider the *inverse* collisions $\{\mathbf{v}_1', \mathbf{v}_2'\} \to \{\mathbf{v}_1, \mathbf{v}_2\}$ such that the final velocity $\mathbf{v}_1 \in \mathrm{d}\mathbf{v}_1$. Following the same route as for the loss term, the number of such collisions per unit time in $\mathrm{d}\mathbf{r}$ is given by

$$C_g\mathrm{d}\mathbf{v}_1 = \int_{\mathbf{v}_1(\mathbf{v}_1', \mathbf{v}_2') \in \mathrm{d}\mathbf{v}_1} \mathrm{d}\mathbf{v}_1'\mathrm{d}\mathbf{v}_2' \int \mathrm{d}\Omega\, g'B(g', \Omega)f(\mathbf{r}, \mathbf{v}_1'; t)f(\mathbf{r}, \mathbf{v}_2'; t), \tag{1.15}$$

where the final velocity $\mathbf{v}_1(\mathbf{v}_1', \mathbf{v}_2')$ of target particles depends on the initial velocities $\mathbf{v}_1'$ and $\mathbf{v}_2'$. Let $\widehat{\boldsymbol{\sigma}}$ be the unit vector joining the center of the particles at their closest approach (chosen such that $\widehat{\boldsymbol{\sigma}}$ points from the incident particle to the target particle). The conservation laws (1.10) then give the relation between the pre-collisional $\{\mathbf{v}_1', \mathbf{v}_2'\}$ and post-collisional velocities $\{\mathbf{v}_1, \mathbf{v}_2\}$:

$$\mathbf{v}_1' = \mathbf{v}_1 - (\mathbf{g} \cdot \widehat{\boldsymbol{\sigma}})\widehat{\boldsymbol{\sigma}}, \tag{1.16a}$$

$$\mathbf{v}_2' = \mathbf{v}_2 + (\mathbf{g} \cdot \widehat{\boldsymbol{\sigma}})\widehat{\boldsymbol{\sigma}}. \tag{1.16b}$$

The Jacobian of the transformation $(\mathbf{v}_1', \mathbf{v}_2') \to (\mathbf{v}_1, \mathbf{v}_2)$ is equal to 1 (for an inverse collision, the unit vector joining the centers of the particles at collision is $-\widehat{\boldsymbol{\sigma}}$). Since from Eq. (1.10b) we have $g = g'$, upon simplifying both sides of Eq. (1.15) by $\mathrm{d}\mathbf{v}_1$ one obtains

$$C_g = \int_{\mathbb{R}^d} \mathrm{d}\mathbf{v}_2 \int \mathrm{d}\Omega\, gB(g,\Omega) f(\mathbf{r},\mathbf{v}_1';t) f(\mathbf{r},\mathbf{v}_2';t). \tag{1.17}$$

Inserting Eqs. (1.14) and (1.17) in (1.11), from Eqs (1.5) and (1.9) the *Boltzmann equation* reads

$$\boxed{\frac{\partial}{\partial t} f(\mathbf{r},\mathbf{v}_1;t) + \mathbf{v}\cdot\boldsymbol{\nabla}_{\mathbf{r}} f(\mathbf{r},\mathbf{v}_1;t) + \boldsymbol{\nabla}_{\mathbf{v}} \cdot \frac{\mathbf{F}(\mathbf{r},\mathbf{v}_1) f(\mathbf{r},\mathbf{v}_1;t)}{m} = J[f,f],} \tag{1.18}$$

where the collision operator $J$ is defined by

$$J[f,f] = \int_{\mathbb{R}^d} \mathrm{d}\mathbf{v}_2 \int \mathrm{d}\Omega\, gB(g,\Omega) \left[ f(\mathbf{r},\mathbf{v}_1';t) f(\mathbf{r},\mathbf{v}_2';t) - f(\mathbf{r},\mathbf{v}_1;t) f(\mathbf{r},\mathbf{v}_2;t) \right]. \tag{1.19}$$

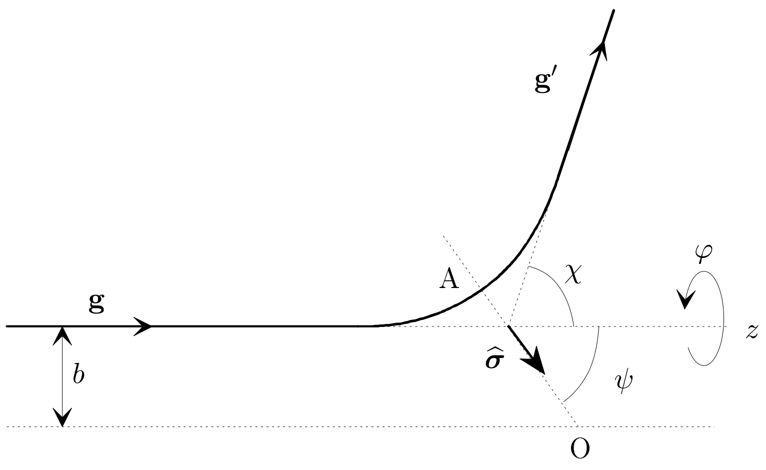


Figure 1.3: Sketch of the geometry of a binary encounter in the center of mass frame for a repulsive potential. The line joining the point $A$ of maximum approach and the target particle $O$ defines the vector $\widehat{\boldsymbol{\sigma}}$.

In the following, for the sake of simplicity we consider the particular case of $d = 3$ dimensions. The results may however be generalized to arbitrary dimensions. We would like to change variables from an integration over the solid angle $\mathrm{d}\Omega = \sin\chi \mathrm{d}\chi \mathrm{d}\varphi$ about $\mathbf{g}'$ to the solid angle $\mathrm{d}\widehat{\boldsymbol{\sigma}} = \sin\psi \mathrm{d}\psi \mathrm{d}\varphi$ about $\widehat{\boldsymbol{\sigma}}$. The scattering angle $\chi$ satisfies $\pi - \chi = 2\psi$, where $\psi$ is the angle between $\mathbf{g}$ and $\widehat{\boldsymbol{\sigma}}$ (see Fig. 1.3). Therefore $2\sin\psi\cos\psi = \sin\chi$ and one obtains

$$g\mathrm{d}\Omega = 4\theta(\mathbf{g}\cdot\widehat{\boldsymbol{\sigma}})(\mathbf{g}\cdot\widehat{\boldsymbol{\sigma}})\mathrm{d}\widehat{\boldsymbol{\sigma}}, \tag{1.20}$$

where the integration is restricted to a hemisphere with the help of the Heaviside function $\theta$ (for example the one defined by $\mathbf{g}\cdot\widehat{\boldsymbol{\sigma}} > 0$). In Eq. (1.19) the gain term is such that $\{\mathbf{v}_1', \mathbf{v}_2'\}$ are the pre-collisional velocities of the collision $\{\mathbf{v}_1', \mathbf{v}_2'\} \to \{\mathbf{v}_1, \mathbf{v}_2\}$, and thus we need to express the pre-collisional velocities as a function of the post-collisional ones. We therefore introduce the operator for restituting collisions $b^{-1}$ such that

$$b^{-1}\mathbf{v}_1 = \mathbf{v}_1' = \mathbf{v}_1 - (\mathbf{g} \cdot \widehat{\boldsymbol{\sigma}})\widehat{\boldsymbol{\sigma}}, \tag{1.21a}$$

$$b^{-1}\mathbf{v}_2 = \mathbf{v}_2' = \mathbf{v}_2 + (\mathbf{g} \cdot \widehat{\boldsymbol{\sigma}})\widehat{\boldsymbol{\sigma}}, \tag{1.21b}$$

and $b^{-1}h(\{\mathbf{v}_i\}) = h(b^{-1}\{\mathbf{v}_i\})$ for any function $h$ of the velocities. The operator $b$ gives the post-collisionnal velocities as a function of the pre-collisional ones. Note that the velocity of the center of mass $(\mathbf{v}_1 + \mathbf{v}_2)/2$ is invariant under the action of $b$. For hard spheres of diameter $\sigma$, the differential cross section is simply the geometrical radius $B(g, \chi) = (\sigma/2)^d$ which is independent of both relative velocity $g$ and scattering angle $\chi$ [6, 7]. The latter expression combined with Eqs. (1.20) and (1.19) gives in arbitrary dimension $d$:

$$\boxed{J[f,f] = \sigma^{d-1}\int_{\mathbb{R}^d} \mathrm{d}\mathbf{v}_2 \int \mathrm{d}\widehat{\boldsymbol{\sigma}}\, \theta(\mathbf{g} \cdot \widehat{\boldsymbol{\sigma}})(\mathbf{g} \cdot \widehat{\boldsymbol{\sigma}})(b^{-1} - 1) f(\mathbf{r}, \mathbf{v}_1; t) f(\mathbf{r}, \mathbf{v}_2; t).} \tag{1.22}$$

The Boltzmann equation

$$\begin{aligned} \frac{\partial}{\partial t} f(\mathbf{r}, \mathbf{v}_1; t) + \mathbf{v} \cdot \boldsymbol{\nabla}_{\mathbf{r}} f(\mathbf{r}, \mathbf{v}_1; t) + \boldsymbol{\nabla}_{\mathbf{v}} \cdot \frac{\mathbf{F}(\mathbf{r}, \mathbf{v}_1) f(\mathbf{r}, \mathbf{v}_1; t)}{m} \\ = \sigma^{d-1}\int_{\mathbb{R}^d} \mathrm{d}\mathbf{v}_2 \int \mathrm{d}\widehat{\boldsymbol{\sigma}}\, \theta(\mathbf{g} \cdot \widehat{\boldsymbol{\sigma}})(\mathbf{g} \cdot \widehat{\boldsymbol{\sigma}})(b^{-1} - 1) f(\mathbf{r}, \mathbf{v}_1; t) f(\mathbf{r}, \mathbf{v}_2; t) \end{aligned} \tag{1.23}$$

is a nonlinear integro-differential equation for the one particle distribution function $f(\mathbf{r}, \mathbf{v}; t)$. For a homogeneous system, the stationary velocity distribution is given by the Maxwellian $f(\mathbf{v}) = A \exp(-Bv^2)$, where the constants $A$ and $B$ are found from the definitions (1.1) and (1.3).

## 1.5 The collision operator for several systems

### 1.5.1 The Enskog equation

For dense gases, the Boltzman equation (1.18) is not expected to provide an accurate description due to a violation of the basic hypothesis that led to it (finite density effects). A heuristic modification of the Boltzmann equation was proposed by Enskog in 1922, known under the name of *Enskog equation*. This equation is based on the two following ideas. First, the particles (which have a spherical shape) are separated by the distance $\sigma$ (their diameter) at contact. Second, the collision frequency must be modified by a factor $C$ corresponding to excluded volume effects. The Enskog collision operator is thus given by [5, 7]

$$\begin{aligned} J_E[f,f] = \sigma^{d-1}\int_{\mathbb{R}^d} \mathrm{d}\mathbf{v}_2 \int \mathrm{d}\widehat{\boldsymbol{\sigma}}\, \theta(\mathbf{g} \cdot \widehat{\boldsymbol{\sigma}})(\mathbf{g} \cdot \widehat{\boldsymbol{\sigma}}) \\ \times \left[C(\mathbf{r}, \mathbf{r} - \widehat{\boldsymbol{\sigma}}) f(\mathbf{r}, \mathbf{v}_1'; t) f(\mathbf{r} - \widehat{\boldsymbol{\sigma}}, \mathbf{v}_2'; t) - C(\mathbf{r}, \mathbf{r} + \widehat{\boldsymbol{\sigma}}) f(\mathbf{r}, \mathbf{v}_1; t) f(\mathbf{r} + \widehat{\boldsymbol{\sigma}}, \mathbf{v}_2; t)\right], \end{aligned} \tag{1.24}$$

where $C(\mathbf{r}, \mathbf{r} \pm \widehat{\boldsymbol{\sigma}})$ is the equilibrium pair correlation function at contact as a functional of the nonequilibrium density $n(\mathbf{r}, t)$ defined by Eq. (1.1). Further investigations have shown that the Enskog equation needs a slight modification in order to be compatible with the Onsager reciprocity relations in nonequilibrium thermodynamics (leading to the *modified Enskog equation*) [8, 9, 10]. Moreover, it was recently shown that for granular mixtures the range of densities for which the Enskog equation applies decreases with increasing dissipation [11].

### 1.5.2 The granular gas

The granular gas is a system of hard spheres that upon contact scatter inelastically with constant normal restitution coefficient $\alpha \in [0, 1]$ (i.e., $\alpha$ does not depend on time or on the velocities). This is a minimal model for the collisions, which still captures many interesting features reproduced by experiments, see below. Some refinements have also been considered. For instance, the gas of viscoelastic particles where the restitution coefficient depends on the relative velocity modulus $g$ [12, 13], the case where particles have rotational degrees of freedom [14, 15], or collision rules involving a non-unity tangential restitution coefficient [16]. The elastic case described in Sec. 1.4 corresponds to the limit $\alpha = 1$. If $\{\mathbf{v}_1', \mathbf{v}_2'\}$ are the pre-collisional velocities, $\{\mathbf{v}_1^*, \mathbf{v}_2^*\}$ the post-collisionnal ones, then the operator $b$ [first introduced in Eq. (1.21)] acts as

$$b^{-1}\mathbf{v}_1 = \mathbf{v}_1' = \mathbf{v}_1 - \frac{1+\alpha}{2\alpha}(\mathbf{g} \cdot \widehat{\boldsymbol{\sigma}})\widehat{\boldsymbol{\sigma}}, \tag{1.25a}$$

$$b^{-1}\mathbf{v}_2 = \mathbf{v}_2' = \mathbf{v}_2 + \frac{1+\alpha}{2\alpha}(\mathbf{g} \cdot \widehat{\boldsymbol{\sigma}})\widehat{\boldsymbol{\sigma}}, \tag{1.25b}$$

and

$$b\mathbf{v}_1 = \mathbf{v}_1^* = \mathbf{v}_1 - \frac{1+\alpha}{2}(\mathbf{g} \cdot \widehat{\boldsymbol{\sigma}})\widehat{\boldsymbol{\sigma}}, \tag{1.26a}$$

$$b\mathbf{v}_2 = \mathbf{v}_2^* = \mathbf{v}_2 + \frac{1+\alpha}{2}(\mathbf{g} \cdot \widehat{\boldsymbol{\sigma}})\widehat{\boldsymbol{\sigma}}. \tag{1.26b}$$

From the rule (1.26), the tangential component of the velocity $\mathbf{v}_\parallel = \mathbf{v} - (\mathbf{g} \cdot \widehat{\boldsymbol{\sigma}})\widehat{\boldsymbol{\sigma}}$ is not modified by the collisions. In the inelastic limit $\alpha = 0$, the post-collisional velocity reduces to its tangential component.

From Eq. (1.25), the Jacobian of the transformation $(\mathbf{v}_1', \mathbf{v}_2') \to (\mathbf{v}_1, \mathbf{v}_2)$ is equal to $\alpha^{-2}$ and Eq. (1.17) must therefore be multiplied by $\alpha^{-2}$. The equivalent of the collision term (1.22) for inelastic hard spheres thus reads

$$J[f,f] = \sigma^{d-1} \int_{\mathbb{R}^d} \mathrm{d}\mathbf{v}_2 \int \mathrm{d}\widehat{\boldsymbol{\sigma}}\, \theta(\mathbf{g} \cdot \widehat{\boldsymbol{\sigma}})(\mathbf{g} \cdot \widehat{\boldsymbol{\sigma}})(\alpha^{-2}b^{-1} - 1) f(\mathbf{r}, \mathbf{v}_1; t) f(\mathbf{r}, \mathbf{v}_2; t). \tag{1.27}$$

The dynamics of rapid granular gases has attracted a lot of attention since more than 20 years [14, 17, 18]. It has now become a well studied topic [19, 20]. Flow of granular media is said to be *rapid* when it is collision driven (referred to as *granular gas*), and *quasi-static* when the contact process plays an important role (referred to as *granular liquid*) [21]. The methods of kinetic theory are thus suitable to describe the granular gas regime. The dynamics of granular gases amounts for several spectacular or unexpected manifestations. For a review of some of these effects, see [21, 22, 23]. We shall mention here only a few ones.

Contrarily to the hard sphere gas, it is known that the dynamics of granular gases exhibits density inhomogeneities and clustering [24]. This may ultimately lead to an infinite number of collisions between particles in a finite time, the so-called *inelastic collapse* [25, 26, 27]. This behavior may be understood qualitatively from the fact that more collisions take place per unit time in the dense regions. Therefore the local granular "temperature" defined by the local variance of the velocity distribution decreases and so does the average velocity. Consequently, there is a flux of particles flowing from the more dilute to the denser regions of the system. This leads to the above mentioned inhomogeneities and eventually to the granular collapse. In the case of viscoelastic particles, those density inhomogeneities are transient [12, 13].

Making use of the Chapman-Enskog expansion that we review in Sec. 1.6, one may establish a hydrodynamic description of the granular gas. It is then possible to derive Fourier law's with transport coefficients that are obtained from the microscopic rules. The heat flux is not only proportional to the gradient of the temperature, but also to the *density* gradient. One consequence is that the heat flow may be directed from the region of low temperature to the region of high temperature, which is the so-called *granular temperature inversion* [28], that was also observed experimentally [29, 30].

We then consider a granular mixture made of two different species of particles (defined by different masses, diameters, and normal restitution coefficients). It was then predicted that the equipartition of energy in the equilibrium state is not satisfied. Hence, the kinetic temperature of the two species are different [31, 32, 33]. This was confirmed experimentally [34, 35]. In a rough granular gas with a single species, the equipartition of energy between the average translational and rotational energies was also shown to be broken [36].

Since collisions are dissipative, the stationary state is obtained through an injection of energy that exactly compensates the cooling due to inelastic collisions. Such an injection mechanism is modeled by an external force [through the term $\mathbf{F}$ in Eq. (1.18)], i.e., a "thermostat" which mimics the different possible injection mechanisms [37]. The velocity distribution in the (stationary) homogeneous state shows deviations from the Maxwell distribution both for low and high velocities [37]. Whereas for small velocities the deviations from the Maxwellian are quite small, for large velocities the distribution shows an overpopulated tail proportional to $\exp(-Av^\nu)$, where $\nu = 3/2$ ($\nu = 2$ corresponds to the Maxwell distribution). Again, experiments tend to confirm this prediction [23, 38].

### 1.5.3 The annihilation collision operator

Annihilation dynamics is such that when two particles meet they disappear from the system. Therefore only the loss term of Eq. (1.22) remains, so that

$$J[f,f] = -\sigma^{d-1} \int_{\mathbb{R}^d} \mathrm{d}\mathbf{v}_2 \int \mathrm{d}\widehat{\boldsymbol{\sigma}}\, \theta(\mathbf{g}\cdot\widehat{\boldsymbol{\sigma}})(\mathbf{g}\cdot\widehat{\boldsymbol{\sigma}}) f(\mathbf{r},\mathbf{v}_1;t) f(\mathbf{r},\mathbf{v}_2;t). \tag{1.28}$$

A remarkable feature of ballistic annihilation is that the Boltzmann equation in $d \geqslant 2$ dimensions is likely to become an exact description of the dynamics at late times [39].

Let $\ell$ be the mean free path, then the Grad limit consists in taking simultaneously the limits of vanishing diameter $\sigma \to 0$ and infinite density $n(t) \to \infty$ such that the mean free path $\ell$ is constant $n(t)\sigma^{d-1} = \ell$. Piasecki *et al.* have established the hierarchy equations obeyed by the reduced distribution functions $f_k(\mathbf{r}_1, \mathbf{v}_1, \ldots, \mathbf{r}_k, \mathbf{v}_k; t)$ for annihilation dynamics. In the Grad limit the hierarchy takes the form of a Boltzmann-like hierarchy, where all terms hindering the propagation of the molecular chaos have vanished. Consequently, if the initial state is factorized, then the whole hierarchy reduces to one single nonlinear equation for the one point distribution function $f(\mathbf{r}, \mathbf{v}; t)$: the Boltzmann equation (1.18) with the collision operator (1.19). Annihilation dynamics is such that the particle density decreases in time. Therefore the ratio of particle diameter to mean free path $\sigma/\ell \to 0$ for long times, which is a common point with the Grad limit. The long time limit of annihilation dynamics for $d \geqslant 2$ is thus likely to be adequately described by the Boltzmann equation. This conclusion was confirmed by molecular dynamics simulations (see Chap. 2 or Refs. [39, 40]).

### 1.5.4 The Maxwell and VHP collision operators

We consider particles interacting through a two body potential $V(r) \propto r^{-n}$. For dimensional reasons the energy conservation implies $r^{-n} \sim g^2$. Again, for dimensional reasons and from the definition of $B(g, \Omega)$, the differential cross section satisfies $B(g, \Omega) \propto r^{d-1}$ [see Eq. (1.19)]. Consequently $gB(g, \chi) \propto g^{\mu}$, $\mu = 1 - 2(d-1)/n$. The hard sphere gas is such that $\mu = 1$, or equivalently $gB(g, \chi) \propto g$, therefore $n \to \infty$.

The *Maxwell gas* (or the gas of Maxwell molecules) is defined by a velocity independent $gB(g, \Omega)$, therefore $\mu = 0$ and the particles interact through a pair potential defined by $n = 2(d-1)$. On the other hand, the case $\mu > 1$ cannot be obtained from any positive $n$, i.e., from any simple power-law interaction. In this sense we say that the interaction is "harder" than for hard spheres. We shall consider here the gas of *very hard particles* (VHP) defined by $gB(g, \chi) \propto g^2$.

The collision operator for the Maxwell and VHP models can be obtained from Eq. (1.22). For this purpose, one may average the collision frequency $(\mathbf{g} \cdot \widehat{\boldsymbol{\sigma}})$ over the solid angle and include the effects of a particular cross section into an effective collision frequency $n\sigma^{d-1}\phi v_T^{1-x}$. The dimensionless parameter $\phi(x)$ defines the relevant time scale (or equivalently the amplitude of the effective collision frequency) of the system, where $x$ is an index for the model considered ($x = 0$ corresponds to the Maxwell model, $x = 1$ to the hard spheres, and $x = 2$ to the VHP model). $\phi(x)$ may be freely chosen to optimize the agreement with PBA of hard spheres, see, for example, [41]. One thus obtains

$$J[f, f] = \sigma^{d-1} \frac{\phi(x) v_T^{1-x}}{S_d} \int_{\mathbb{R}^d} \mathrm{d}\mathbf{v}_2 \, v_{12}^x \int \mathrm{d}\widehat{\boldsymbol{\sigma}} \, (b^{-1} - 1) f(\mathbf{r}, \mathbf{v}_1; t) f(\mathbf{r}, \mathbf{v}_2; t), \tag{1.29}$$

where $S_d = 2\pi^{d/2}/\Gamma(d/2)$ is the solid angle surface, $\Gamma$ the Euler gamma function, $v_T = \sqrt{2/\beta m}$ the time-dependent thermal velocity, $\beta = (k_B T)^{-1}$, and $\sigma$ is the diameter of the particles (or the range of the interaction potential).

Note that we shall consider Maxwell and VHP models of granular gases [41, 42], pure annihilation [43, 44], or PBA [45].

## 1.6 The Chapman-Enskog expansion

The Chapman-Enskog expansion is based on the general concept of separation of time scales. The dynamics of a system may be such that different physical processes take place on different time scales. The identification of those time scales allows to develop a perturbation theory in order to reconstruct the solution in terms of a convergent time series: this is the so-called *method of the multiple time scales* [46, 47]. We shall describe here the particular case of the Chapman-Enskog expansion. This expansion is targeted at building a solution to the Boltzmann equation where the spatial average of the hydrodynamic (coarse-grained) fields $n$, $\mathbf{u}$, and $T$ (density, momentum, and temperature, respectively) are conserved by the evolution. Since those fields are conserved, it is expected that their evolution is much slower than any microscopic portion of the system. This allows to state that for long times (as compared to the mean free path) all space and time dependence of the velocity distribution occurs through a functional dependence on the hydrodynamic fields: this is the so-called *normal solution* for the distribution function. It is the starting point for the Chapman-Enskog expansion. Of course, more subtle questions arise if one or some of the hydrodynamic fields are not conserved by the dynamics. We shall therefore discuss this expansion in more details in the following subsections.

### 1.6.1 The hypothesis

The Chapman-Enskog expansion relies on two key hypothesis. The first one is the existence of a normal solution. The second one is based on the existence of two well-separated time scales. However, as it will be shown below, these hypothesis are related to each other. In the following we shall consider for the sake of simplicity the case where there is no external force field, i.e., $\mathbf{F} = 0$.

As explained in Sec. 1.4.1, in order to derive the Boltzmann equation it is required to have a dilute gas. The time scale associated to a collision event $\tau_c$ is therefore much smaller than the mean collision time $\tau$ between two particles. This was shown to be compatible with the condition $\sigma \ll \ell$, where $\sigma$ is the range of the interaction and $\ell$ the mean free path. We now introduce a new length scale, the hydrodynamic length $\ell_h$ such that on this scale the hydrodynamic fields vary "significantly". The corresponding time scale is $\tau_h = \ell_h/v_T$. The hypothesis for the existence of a normal solution is that the variations of the hydrodynamic fields are small on the scale of the mean free path. This means, for example, $\ell|\boldsymbol{\nabla} \ln n| \ll 1$, which is equivalent to $\ell \ll \ell_h$, or $\tau \ll \tau_h$. Assuming this hypothesis, we shall see how the existence of the normal solution becomes justified.

We consider a time $t$ such that $\tau \ll t \ll \tau_h$, and a small volume $\delta V$ of typical size much smaller than $\ell_h$. Due to the collisions we then expect that the gas in $\delta V$ reaches a state *close* to the local equilibrium characterized by the local values of $n$, $\mathbf{u}$, and $T$

(these values may vary depending on where $\delta V$ is located). This first rapid stage is the so-called *kinetic stage* which depends on the initial conditions. Since $t \ll \tau_h$, the hydrodynamic fields do not significantly vary over the period $t$. On the other hand, for $t \simeq \tau_h$ the particles have moved over distances of the order of $\ell_h$ and the system reaches the local equilibrium state. This second slower stage is the *hydrodynamic stage*, which does not depend on the initial conditions. Consequently, for times $t$ of the order of $\tau_h$ the state may be entirely characterized by the hydrodynamic fields $n$, $\mathbf{u}$, and $T$. The choice of these fields is motivated by the fact that in elastic gases (which is the class of system for which the Chapman-Enskog procedure was originally developed) they represent conserved quantities. Therefore, these fields vary only over very long timescales $\tau_h \gg \tau$. All spatial and temporal dependence of the distribution function $f(\mathbf{r}, \mathbf{v}; t)$ may consequently be expressed as a functional dependence on the hydrodynamic fields, the so-called *normal solution*:

$$f(\mathbf{r}, \mathbf{v}; t) = f[\mathbf{v}, n(\mathbf{r}, t), \mathbf{u}(\mathbf{r}, t), T(\mathbf{r}, t)]. \tag{1.30}$$

In order to determine $f$ at one point the knowledge of the fields over the whole system is therefore required. As discussed before, the choice of these hydrodynamic fields is motivated by the fact that they are conserved by the collisions and therefore vary only on time scales that are much bigger than the mean collision time $\tau$. The question that arises is to determine if the conditions for the existence of a normal solution are met when some (or all) of the fields are *not* conserved. This is typically the case of granular gases where particles collide inelastically, or annihilation where particles are removed upon collision. For such *dissipative* systems (in the broader sense), one may associate a non zero decay rate to each non-conserved field. The question is to determine whether the new time scales thereby introduced by those decay rates are shorter than what is allowed for the existence of a normal solution. This point is not yet quantitatively clarified and is still subject to discussion [48, 49, 50]. The justification of the normal solution may be done *a posteriori* by studying the relevance of the results through the appearance of the homogeneous cooling state (HCS) for example [39, 51]. Note that the existence of conserved fields is not a condition required for the Chapman-Enskog expansion to hold. It is only necessary that the time scales introduced are bigger than those associated to the microscopic non hydrodynamic excitations, e.g., $\tau$. In the case of granular gases for example, the temperature decay rate in proportional to $(1 - \alpha^2)$ where $\alpha$ is the restitution coefficient. The time scale is inversely proportional to the decay rate. Therefore $\alpha$ may be chosen as close to unity as required in order to have an arbitrary long time scale.

The second hypothesis states the existence of two distinct time scales. The microscopic time scale $\tau$ is characterized by the average collision time, and the spatial length is defined by the corresponding mean free path $\ell$. On the other hand, the macroscopic time scale is defined by a typical time $\tau_h$ describing the evolution of the hydrodynamic fields and of their inhomogeneities. The hydrodynamic fields thus vary only slightly on a time of the order of $\tau_c$. They are only very weakly inhomogeneous on such length and time scales. This allows for a series expansion in orders of the gradients of the fields:

$$f = f^{(0)} + \lambda f^{(1)} + \lambda^2 f^{(2)} + \dots, \tag{1.31}$$

where each power of the small parameter $\lambda \ll 1$ means a given order in a spatial gradient. Since $\tau/\tau_h \approx \ell/\ell_h \ll 1$ and $|\boldsymbol{\nabla} \ln f| \approx 1/\ell_h$, the formal parameter $\lambda$ may be seen as the ratio of the mean free path to the typical length of the hydrodynamic variations $\lambda \approx \ell/\ell_h \ll 1$. Note that the existence of those two well separated time scales is already required for the formal construction of the normal solution. Therefore the existence of a normal solution and the separation of time scales appear to be related hypothesis.

Since $f^{(0)}$ describes the homogeneous solution of the local equilibrium distribution, it has the same velocity moments $\mathbf{v}^n$, $n = 0, 1, 2$, as the complete distribution $f$. Therefore $\int_{\mathbb{R}^d} \mathrm{d}\mathbf{v}\mathbf{v}^n f^{(k)} = 0,\ n = 0, 1, 2,\ k \geqslant 1$. The evolution of the system exhibits several time scales $\tau_k \sim \lambda^k t,\ k \geqslant 0$. To obtain hierarchical equations for the approximations $f^{(k)}$, we thus have to expand the time derivative operator as [46]

$$\frac{\partial}{\partial t} = \frac{\partial}{\partial \tau_0} + \lambda \frac{\partial}{\partial \tau_1} + \lambda^2 \frac{\partial}{\partial \tau_2} + \ldots \equiv \frac{\partial^{(0)}}{\partial t} + \lambda \frac{\partial^{(1)}}{\partial t} + \lambda^2 \frac{\partial^{(2)}}{\partial t} + \ldots, \tag{1.32}$$

where we have made use of the shorthand notation $\partial^{(k)}/\partial t$. To a given order in $\lambda$ in the temporal hierarchy (1.32) corresponds thus the same order in the spatial hierarchy (1.31).

### 1.6.2 The hierarchy

Inserting the expansions (1.32) and (1.31) in the Boltzmann equation (1.18) yields

$$\left( \sum_{k \geqslant 0} \lambda^k \frac{\partial^{(k)}}{\partial t} + \mathbf{v}_1 \cdot \boldsymbol{\nabla} \right) \sum_{l \geqslant 0} \lambda^l f^{(l)} = J \left[ \sum_{l \geqslant 0} \lambda^l f^{(l)}, \sum_{l \geqslant 0} \lambda^l f^{(l)} \right]. \tag{1.33}$$

Equating the terms of the same order in $\lambda$ and solving the equations order by order allows one to build the Chapman-Enskog solution. Since $f$ depends on time only through the hydrodynamic fields, the action of the time derivative is given by

$$\frac{\partial^{(k)}}{\partial t} = \frac{\partial^{(k)} n}{\partial t} \frac{\partial}{\partial n} + \frac{\partial^{(k)} u_i}{\partial t} \frac{\partial}{\partial u_i} + \frac{\partial^{(k)} T}{\partial t} \frac{\partial}{\partial T}, \tag{1.34}$$

where we have used Einstein's summation convention. The time derivative $\partial^{(k)}/\partial t$ describes the evolution of the field on the corresponding time scale. The time derivative of the hydrodynamic fields are obtained upon integrating the Boltzmann equation over the velocities $\mathbf{v}_1$ with weight 1, $m\mathbf{v}_1$, and $mv_1^2/2$, and making use of the expansions (1.31) and (1.32). Of course, the form of the balance equations thus obtained depends on the system being modeled.

To zeroth order in the gradients, Eq. (1.33) gives

$$0 = J[f^{(0)}, f^{(0)}]. \tag{1.35}$$

The solution is given by the local homogeneous equilibrium distribution. Note that depending on the system, this solution may or not be given by the local Maxwellian.

For granular gases [37], ballistic annihilation [39], or PBA [52], it was shown that the local equilibrium distribution was not Maxwellian in several aspects (although "close" to the Maxwellian for small velocities).

To first order in the gradients, Eq. (1.33) gives the equation governing the first correction to the homogeneous state:

$$\left[\frac{\partial^{(0)}}{\partial t}+\mathcal{L}\right] f^{(1)}=-\left[\frac{\partial^{(1)}}{\partial t}+\mathbf{v}_1\cdot\boldsymbol{\nabla}\right] f^{(0)}. \tag{1.36}$$

Note from Eq. (1.34) that the zeroth order derivative $\partial^{(0)}/\partial t$ applied on $f^{(1)}$ is equal to zero if all hydrodynamic fields are conserved. $\mathcal{L}$ is the *linearized collision operator* defined by

$$\mathcal{L}f^{(1)}=-J[f^{(0)},f^{(1)}]-J[f^{(1)},f^{(0)}]. \tag{1.37}$$

### 1.6.3 The linear collision operator

The linearized collision operator $\mathcal{L}$ depends of the model considered. In general it is not possible to find the first order distribution function without further approximations. The usual approximation, irrespective of the model, is to expand the distribution function to first nonzero order in a set of orthogonal polynomials [7, 20, 53]. These so-called *Sonine polynomials* are eigenfunctions of the linearized collision operator for Maxwell molecules.

In order to discuss some useful properties of the linearized collision operator, we shall consider the particular class of systems where the homogeneous solution is given by the Maxwellian velocity distribution function. For this class of systems, all hydrodynamic fields are conserved. Note that the knowledge of some of the properties of the linearized collision operator will allow then to build in a similar way the appropriate series expansion of the solution in the general case where the homogeneous state is not Maxwellian (the Sonine polynomial expansion).

Since the hydrodynamic fields are conserved, the term $\partial^{(0)}f^{(1)}/\partial t$ in Eq. (1.36) vanishes. Dividing both sides of the latter equation by $f^{(0)}(\mathbf{v}_1)$ one obtains

$$\mathcal{L}\frac{f^{(1)}}{f^{(0)}}=-\left[\frac{\partial^{(1)}}{\partial t}+\mathbf{v}_1\cdot\boldsymbol{\nabla}\right]\ln f^{(0)}. \tag{1.38}$$

$f^{(0)}$ is Maxwellian and thus $f^{(0)}(\mathbf{v}_1)f^{(0)}(\mathbf{v}_2)=f^{(0)}(\mathbf{v}_1')f^{(0)}(\mathbf{v}_2')$. The linear collision operator then reads

$$\mathcal{L}\Phi(\mathbf{v}_1)=\int_{\mathbb{R}^d}\mathrm{d}\mathbf{v}_2\int \mathrm{d}\Omega\, gB(g,\chi)f^{(0)}(\mathbf{v}_2)[\Phi(\mathbf{v}_1)+\Phi(\mathbf{v}_2)-\Phi(\mathbf{v}_1')-\Phi(\mathbf{v}_2')], \tag{1.39}$$

where $\Phi^{(1)}=f^{(1)}/f^{(0)}$.

The properties of the linear collision operator (1.39) were studied for several differential cross sections [7]. We shall recall here only the main properties of interest in the context of the work presented in the next chapters. For the sake of simplicity, we shall consider the three-dimensional case. Let

$$\langle \Phi_1 | \Phi_2 \rangle = \int_{\mathbb{R}^3} \mathrm{d}\mathbf{v}\, f^{(0)}(\mathbf{v}) \Phi_1^\dagger(\mathbf{v}) \Phi_2(\mathbf{v}) \tag{1.40}$$

be the scalar product in $L^2(\mathbb{R}^3, \mathrm{e}^{-v^2}\mathrm{d}\mathbf{v})$. It is then easy to verify that $\mathcal{L}$ is Hermitian, i.e., $\langle \Phi_1 | \mathcal{L}\Phi_2 \rangle = \langle \Phi_2 | \mathcal{L}\Phi_1 \rangle^\dagger$, and $\langle \Phi | \mathcal{L}\Phi \rangle \geqslant 0$. The eigenvalues of $\mathcal{L}$ are therefore real and positive. It can be shown that for two-body interaction potentials of the form $V(r) \propto r^{-n}$, $n \in ]2, \infty[$ the spectrum has a continuous part, and moreover that $\mathcal{L}$ is isotropic, i.e., $\mathcal{L}$ commutes with the rotation operators in the velocity space [54, 55, 56]. Therefore $\mathcal{L}[Y_l^m(\widehat{\mathbf{V}})X_1(V)] = Y_l^m(\widehat{\mathbf{V}})X_2(V)$ where $X_1$ and $X_2$ are functions that depend only on $V = |\mathbf{V}|$. $Y_l^m(\widehat{\mathbf{V}})$ are the spherical harmonics. The eigenfunctions $\Psi_{nlm}$ of $\mathcal{L}$ thus take the form

$$\Psi_{nlm}(\mathbf{V}) = \psi_{nl}(V) Y_l^m(\widehat{\mathbf{V}}). \tag{1.41}$$

There is a 5-time degenerated zero eigenvalue corresponding to the collisional invariants 1, $\mathbf{v}$, and $v^2$. The eigenvalues $\lambda_{nl}$ depend only on the two indices $n$ and $l$. The exact calculation of the eigenvalues and of the eigenvectors is possible only for Maxwell molecules. In this case [7, 54, 55, 56]

$$\Psi_{nlm}(\mathbf{V}) = \sqrt{\frac{2n!}{\Gamma(n+l+1)}}\, c^l S_{l+1/2}^{(n)}(c^2) Y_l^m(\widehat{\mathbf{c}}), \tag{1.42}$$

where $\mathbf{c} = \mathbf{V}/v_T$, $v_T = \sqrt{2k_BT/m}$ is the thermal velocity. $S_l^n(x)$ are the Sonine polynomials defined by

$$S_l^{(n)}(c) = \sum_{k\geqslant 0} (-c)^k \frac{\Gamma(n+l)}{\Gamma(l+k)(n-k)!k!} \tag{1.43}$$

which are related to the generalized Laguerre polynomials $L_n^l$ by

$$L_n^{l+1/2} = \sqrt{\frac{\Gamma(n+l+3/2)}{\Gamma(n+l+1)}}\, S_{l+1/2}^{(n)}. \tag{1.44}$$

The Sonine polynomials are orthogonal in $L^2([0, \infty[, c^l \mathrm{e}^{-c^2}\mathrm{d}c)$, i.e.,

$$\int_0^\infty \mathrm{d}c\, c^l \mathrm{e}^{-c^2} S_l^{(n)}(c) S_l^{(n')}(c) = \frac{\Gamma(n+l+1)}{n!}\delta_{nn'}. \tag{1.45}$$

The eigenvectors (1.42) are thus orthonormal by respect to the scalar product in $L^2(\mathbb{R}^3, \mathrm{e}^{-c^2}\mathrm{d}\mathbf{c})$. The corresponding eigenvalues may be found in [6, 7, 55, 56]. They are defined as functionals of the differential cross section, and their explicit form may only be found for Maxwell molecules where $gB(g, \chi)$ does not depend neither on $g$ nor on the scattering angle $\chi$. For other interaction potentials, the eigenvalues are obtained numerically [7]. Since for Maxwell molecules $f^{(0)}$ is the local Maxwellian, the collision operator (1.39) expresses a scalar product of the form (1.45) (with an additional angular integration).

In the case of the hard spheres gas it is possible to rewrite Eq. (1.38) in the form

$$\mathcal{L}\Phi^{(1)}(\mathbf{V}) = S_i(\mathbf{V})\nabla_i \ln T + C_{ij}(\mathbf{V})\nabla_i u_j, \tag{1.46}$$

where $\mathbf{S}(\mathbf{V})$ is proportional to $S_{3/2}^{(1)}(V^2)\mathbf{V}$, the tensor $\mathbf{C}(\mathbf{V})$ is proportional to $S_{5/2}^{(0)}(V^2)$ $(V_iV_j - \delta_{ij}V^2/3)$, and $\Phi^{(1)}(\mathbf{V}) = f^{(1)}(\mathbf{V})/f^{(0)}(\mathbf{V})$. Since the operator $\mathcal{L}$ is isotropic, the solution for $\Phi^{(1)}(\mathbf{V})$ has the form

$$\Phi^{(1)}(\mathbf{V}) = A(V^2)V_i\nabla_i \ln T + B(V^2)C_{ij}(\mathbf{V})\nabla_i u_j, \tag{1.47}$$

with the additional conditions

$$\mathcal{L}[A(V^2)V_i] = S_i(\mathbf{V}), \tag{1.48a}$$
$$\mathcal{L}[B(V^2)C_{ij}(\mathbf{V})] = C_{ij}(\mathbf{V}). \tag{1.48b}$$

In the case of Maxwell molecules, $\mathbf{S}(\mathbf{V})$ and $\mathbf{C}(\mathbf{V})$ are proportional to the eigenfunctions $\Psi_{11m}(V)$ and $\Psi_{02m}(V)$, respectively. Therefore $\mathcal{L}\mathbf{S}(\mathbf{V}) = \lambda_{11}\mathbf{S}(\mathbf{V})$ and $\mathcal{L}\mathbf{C}(\mathbf{V}) = \lambda_{02}\mathbf{C}(\mathbf{V})$, which combined to Eqs. (1.48) gives $A(V^2)V_i = S_i(\mathbf{V})/\lambda_{11}$ and $B(V^2)B(V^2)C_{ij}(\mathbf{V}) = C_{ij}(\mathbf{V})/\lambda_{02}$ where $\lambda_{nl}$ are the eigenvalues. However, for other models the right-hand side of Eqs. (1.48) is in general not proportional to an eigenvalue of the linearized collision operator. One therefore expands the unknown functions $A(V^2)$ and $B(V^2)$ in the basis of the eigenfunctions of the linearized collision operator of Maxwell molecules. Moreover, it is required that for the particular case of Maxwell molecules the expansion satisfies Eqs. (1.48) *exactly*. This leaves only the choice $l = 1$ for the expansion of $A(V^2)$:

$$A(V^2) = \sum_{n\geqslant 0} a_n S_{3/2}^{(n)}(c^2), \tag{1.49}$$

and $l = 2$ for the expansion of $B(V^2)$:

$$B(V^2) = \sum_{n\geqslant 0} b_n S_{5/2}^{(n)}(c^2). \tag{1.50}$$

Since the moments 1, $\mathbf{V}$, and $V^2$ of $\Phi^{(1)}$ must be equal to zero, one has $\langle A(V^2)|V^2\rangle = 0$, which leads to $a_0 = 0$. Consequently, we verify that for Maxwell molecules only the first terms $a_1$ and $b_0$ are different from zero, and thus the expansions satisfy Eq. (1.48), i.e., $A(V^2) \propto \psi_{11}$ and $B(V^2) \propto \psi_{02}$. For other interaction models, the unknown coefficients $a_i$, $i \geqslant 1$, and $b_i$, $i \geqslant 0$, have to be determined from Eqs. (1.48). However, in order to simplify the problem one usually truncates the series (1.49) and (1.50) to their first nonzero coefficients $a_1$ and $b_0$, truncation referred to as the first Sonine approximation [6, 7, 55, 56, 57].

# Chapter 2

# Some exact results for Boltzmann's annihilation dynamics

## 2.1 Outline of the chapter

The problem of ballistic annihilation for a spatially homogeneous system is revisited within Boltzmann's kinetic theory in two and three dimensions. Analytical results are derived for the time evolution of the particle density for some isotropic discrete bimodal velocity modulus distributions. According to the allowed values of the velocity modulus, different behaviors are obtained: power law decay with non-universal exponents depending continuously upon the ratio of the two velocities, or exponential decay. When one of the two velocities is equal to zero, the model describes the problem of ballistic annihilation in presence of static traps. The analytical predictions are shown to be in agreement with the results of two-dimensional molecular dynamics simulations. The content of this chapter is based on Ref. [40].

## 2.2 Introduction

In ballistically controlled reactions, particles with a given initial velocity distribution move freely (ballistic motion) in a $d$-dimensional space. When two of them meet, they annihilate and disappear from the system. This apparently simple problem has attracted a lot of attention during the past years [39, 43, 58, 59, 60, 61, 62, 63, 64, 65, 66, 67, 68, 69, 70] for the following reasons. First, this is one of the few problems of nonequilibrium statistical physics that can be exactly solved in some cases, and second it models some growth and coarsening processes [71].

This field was entered with the pioneering work by Elskens and Frisch [58], where a one-dimensional system with only two possible velocities $+c$ or $-c$ was studied. Using combinatorial analysis, they showed that the density of particles was decreasing according to a power law ($t^{-1/2}$) in the case of a symmetric initial velocity distribution. The investigation of this one-dimensional problem was generalized by Droz *et al.* [63, 64] to the three-velocity case where the initial velocity distribution is given by $\varphi(v;0) = p_+\delta(v-c) + p_0\delta(v) + p_-\delta(v+c)$ with $p_+ = p_-$ (symmetric case) and $p_+ + p_0 + p_- = 1$. It turns out that the decay of the particle density depends on the details of the initial velocity distribution. The following analytical results were obtained. For $p_0 < 1/4$, the density $n(v;t)$ of particles with velocity $v = \{0, +c, -c\}$, behaves in the long-time limit as $n(0;t) \sim t^{-1}$, $n(\pm c;t) \sim t^{-1/2}$. When $p_0 = 1/4$, $n(0;t) \sim n(\pm c;t) \sim t^{-2/3}$. Finally, for $p_0 > 1/4$, one finds that $n(0;t)$ saturates to a nonzero stationary value, while $n(\pm c;t)$ decays faster than a power law. Moreover, it was shown that in one dimension, annihilation dynamics creates strong correlations between the velocities of colliding particles, which excludes a Boltzmann-like approximation. Pairs of nearest neighbor particles have the tendency to align their velocities and propagate in the same direction [63, 64].

An analytical investigation of the one-dimensional case with a continuous velocity distribution is much more difficult. A dynamical scaling theory, whose validity was supported by extensive numerical simulations for several velocity distributions, led Rey *et al.* [65] to the conjecture that all the continuous velocity distributions $\varphi(v)$ that are symmetric, regular and, such that $\varphi(0) \neq 0$ are attracted in the long-time regime towards the same Gaussian-like distribution and thus belong to the same universality class.

For higher dimensions, most of the studies are based on an uncontrolled Boltzmann-like description [43, 59, 60] or numerical simulations [69]. However, based on phenomenological mean-field-like arguments, Krapivsky *et al.* have studied the annihilation kinematics of a bimodal velocity modulus distribution in $d > 2$ dimensions [61]. In the case of a mixture of moving and motionless particles they showed that the stationary particles always persist, while the density of moving particles decays exponentially. This approach contains unknown phenomenological parameters, and thus a complete comparison with the results obtained by numerical simulation is not possible.

In a recent paper, Piasecki *et al.* [39] gave an analytical derivation of the hierarchy equations obeyed by the reduced distributions for the annihilation dynamics. In dimension $d > 1$ for a spatially homogeneous system, and in the limit (the so-called Grad limit) for which the particle diameter $\sigma \to 0$, and the particle density $n(t) \to \infty$ such that $n(t)\sigma^{d-1} = \ell^{-1}$, where $\ell$ is the mean free path, the hierarchy reduces to the Boltzmann-like hierarchy. This hierarchy propagates the factorization of the reduced $k$-particle distribution in terms of one-particle distribution functions. Thus, if the initial state is factorized, the whole hierarchy reduces to one nonlinear equation for the one-particle distribution. For annihilation kinetics, the ratio of particle diameter to mean free path vanishes in the long-time limit and the situation becomes similar to the Grad limit discussed above for $\ell \to \infty$. Thus the long-time limit of the annihilation dynamics (for $d > 1$) is likely to be adequately described by the nonlinear Boltzmann equation.

A scaling analysis of the nonlinear Boltzmann equation led to analytical expressions for the exponents describing the decay of the particle density and of the root-mean-square velocity in the case of continuous velocity distributions [39].

In view of the different behaviors observed in one dimension for discrete or continuous velocity distributions, it is relevant to study the case of distributions with discrete modulus spectrum in dimensions higher than 1. The goal of this chapter is to investigate simple examples of this kind in two dimensions for which the non linear Boltzmann equation with collision operator given by Eq. (1.28) can be exactly solved. The generalization of this approach to an arbitrary dimension is straightforward [40].

The validity of the Boltzmann description in the long-time limit will be confirmed by comparing our analytical predictions with the results obtained by a molecular dynamics simulation.

The chapter is organized as follows. In Sect. 2.3 we define the model. In Sect. 2.4 the two-dimensional Boltzmann equation is solved analytically for a two velocity modulus ($c_1$ and $c_2$) isotropic distribution. For simplicity we first consider the one velocity model $c_1 = c_2 > 0$ in three dimensions that allows to draw interesting comparisons with the same model in one dimension. Then the implicit solution for the particle densities in the general case $c_1 > c_2 > 0$ is established in two dimensions. It is shown analytically that in the long-time limit the particle densities decay according to power laws, with exponents depending continuously on the value of the velocity modulus ratio. We show that in arbitrary dimension and for any number of velocity modulus such that $c_1 < \ldots < c_N$, the density describing particles with velocity modulus $c_1$ always decays as the inverse of a rescaled time. We also find upper and lower bounds to the particle densities that are compared with the numerical solution of the dynamical equation. The particular case of a mixture of moving ($c_2 > 0$) and motionless ($c_1 = 0$) particles is also investigated. It turns out that the particle densities decay exponentially to zero for the moving particles, and to a nonzero value for the motionless ones. This phenomenology is independent of space dimension, and in Sect. 2.5, it will be shown explicitly to hold in two dimensions by implementing molecular dynamics simulations. This numerical method has the advantage of being free of the approximations underlying Boltzmann's dynamics and, therefore, provides an interesting test for the analytical predictions. Section 2.6 contains our interpretations and conclusions.

## 2.3 An exactly solvable model

We consider a system made of spheres of diameter $\sigma$ moving ballistically in $d$-dimensional space. If two particles touch each other, they annihilate and thus disappear from the system. We consider only two-body collisions. The initial spatial distribution of particles is supposed to be and to remain uniform uniform during the evolution. Existing numerical simulations seem to be compatible with this assumption of homogeneity [39]. We are interested in the time evolution of the number density of particles with a given velocity modulus.

Let $f(\mathbf{v};t)$ be the distribution function of the density of particles in $\mathbb{R}^d$ with velocity $\mathbf{v} \in \mathbb{R}^d$ at time $t$. For spatially homogeneous states, the distribution function has the form

$$f(\mathbf{v};t) = n(t)\varphi(\mathbf{v};t), \tag{2.1}$$

where $\varphi(\mathbf{v};t)$ is the velocity probability density. In the long-time limit, Piasecki *et al.* [39] have shown that the hierarchy satisfied by the reduced distributions approached the Boltzmann hierarchy. If the initial state is factorized, the nonlinear Boltzmann equation provides then the complete description of annihilation dynamics,

$$\frac{\partial}{\partial t} f(\mathbf{v}_1;t) = -\sigma^{d-1} \int \mathrm{d}\widehat{\boldsymbol{\sigma}}\ \theta(\widehat{\boldsymbol{\sigma}} \cdot \widehat{\mathbf{v}}_{12})(\widehat{\boldsymbol{\sigma}} \cdot \widehat{\mathbf{v}}_{12}) \int_{\mathbb{R}^d} \mathrm{d}\mathbf{v}_2\, |\mathbf{v}_{12}| f(\mathbf{v}_1;t) f(\mathbf{v}_2;t). \tag{2.2}$$

Here $\theta$ is the Heaviside function, $\mathbf{v}_{12} = \mathbf{v}_1 - \mathbf{v}_2$ the relative velocity of two particles, $\widehat{\mathbf{v}}_{12} = \mathbf{v}_{12}/v_{12}$ a unit vector, $v_{12} = |\mathbf{v}_{12}|$, and the integration with respect to $\mathrm{d}\widehat{\boldsymbol{\sigma}}$ is the angular integration over the solid angle.

We consider spherically symmetric initial conditions $f(v;0)$, $v = |\mathbf{v}|$. This symmetry property is propagated by the dynamics. The Boltzmann equation (2.2) then takes the form

$$\frac{\partial}{\partial t} f(v_1;t) = -\sigma^{d-1} \beta_1 f(v_1;t) \int_{\mathbb{R}^d} \mathrm{d}\mathbf{v}_2\, |\mathbf{v}_{12}| f(\mathbf{v}_2;t), \tag{2.3}$$

where $\beta_k$ is given by (see App. A.1)

$$\beta_k = \int \mathrm{d}\widehat{\boldsymbol{\sigma}}\ \theta(\widehat{\boldsymbol{\sigma}} \cdot \widehat{\boldsymbol{v}}_{12})(\widehat{\boldsymbol{\sigma}} \cdot \widehat{\mathbf{v}}_{12})^k = \pi^{\frac{d-1}{2}} \frac{\Gamma\left(\frac{k+1}{2}\right)}{\Gamma\left(\frac{k+d}{2}\right)}. \tag{2.4}$$

Equation (2.3) is a nonlinear homogeneous integral equation for the distribution function $f(v;t)$. A simplification arises if the initial velocity distribution has a discrete modulus spectrum. This spectrum is preserved by the annihilation dynamics as no new velocities are created. A simple case is provided by the bimodal distribution

$$\varphi(v,0) = \frac{A}{S_d c_1^{d-1}} \delta(v - c_1) + \frac{1-A}{S_d c_2^{d-1}} \delta(v - c_2), \tag{2.5}$$

where $c_2 > c_1 \geqslant 0$, $A$ denotes the fraction of particles with velocity modulus $c_1$, and

$$S_d = \frac{2\pi^{d/2}}{\Gamma(d/2)} \tag{2.6}$$

is the surface of a $d$-dimensional sphere of unit radius, where $\Gamma$ is the gamma function.

## 2.4 Exact results

Before addressing the general case, we first consider the single-species problem for $d = 3$ where $c_2 = c_1 > 0$. The rest of the section presents the details of the calculations for $d = 2$. We have carried out the $d = 3$ case (which is technically a bit easier) in [40], and we will only quote the results (that are similar to those of $d = 2$).

### 2.4.1 Single-velocity modulus distribution

The Boltzmann equation (2.3) for $d = 3$ takes the form

$$\begin{aligned} \frac{\partial}{\partial t} f(v;t) &= -\sigma\pi f(v;t) \int_0^\infty \mathrm{d}u\, u^2 f(u;t) \int_0^{2\pi} \mathrm{d}\varphi \int_0^\pi \mathrm{d}\theta\, \sqrt{u^2 + v^2 - 2uv\cos\theta} \\ &= -\frac{2}{3}(\pi\sigma)^2 f(v;t) \int_0^\infty \mathrm{d}u\, u^2 f(u;t) \left[\frac{(u+v)^3 - |u-v|^3}{uv}\right]. \end{aligned} \tag{2.7}$$

Setting $c_2 = c_1 = c > 0$ in Eq. (2.5), one obtains from Eq. (2.1)

$$f(v;t) = n(t)\frac{1}{2\pi c}\delta(v-c). \tag{2.8}$$

From the kinetic equation (2.7), we find

$$\frac{1}{4\pi c^2}\delta(v-c)\frac{\partial}{\partial t}n(t) = -\frac{2}{3}(\pi\sigma)^2\frac{n(t)^2}{4\pi c^2}\delta(v-c)\int_0^\infty \mathrm{d}u\,\frac{\delta(u-c)}{4\pi c^2}\left[\frac{(u+v)^3-|u-v|^3}{uv}\right], \tag{2.9}$$

which gives

$$\frac{\mathrm{d}}{\mathrm{d}t}n(t) = -\frac{4}{3}\pi\sigma^2 c\, n(t)^2, \tag{2.10}$$

whose solution is

$$n(t) = \frac{n_0}{1+\frac{4}{3}\pi\sigma^2 n_0 ct}, \tag{2.11}$$

where $n(0) = n_0$. A striking observation is that, in the limit $t \to \infty$, the density (2.11) becomes independent of its initial value $n_0$. Note that the same phenomenon is also present for simple diffusion limited annihilation such as $A + A \to 0$, when the dimension of the system is larger than 2 [72].

Contrary to the one-dimensional case for which it has been rigorously shown that the density decays proportionally to $t^{-1/2}$ [58], one sees from Eq. (2.11) that in three dimensions, Boltzmann's dynamics is faster as the density decays according to $t^{-1}$, which is the mean-field value [61]. We note, however, that the same behavior $n(t) \propto 1/t$ holds in all dimensions within Boltzmann's kinetic theory (and in fact, more generally within the framework of a scaling analysis of the hierarchy governing the dynamics of ballistic annihilation [39]). This discrepancy between Boltmann's prediction and the exact result in one dimension illustrates the crucial importance of dynamical correlations when $d = 1$. On the other hand, as suggested in Ref. [39] and explicitly shown below by molecular dynamics simulations, the nonlinear Boltzmann equation is relevant for describing the long-time dynamics of ballistic annihilation when $d \geqslant 2$. In this case the particles are very diluted and no dynamical correlations can develop during the time evolution, which would violate the molecular chaos hypothesis.

### 2.4.2 Mixture of particles with two nonzero velocity moduli

In the following we will present the details of the calculations for $d = 2$. The $d = 3$ case (which is technically a bit easier) was done in details in [40], and we will only quote the results that are similar to $d = 2$.

Consider the case where particles with velocities $c_1 > 0$ and $c_2 > c_1$ are initially present. Thus $f(v;t)$ is of the form

$$f(v;t) = X(t)\frac{1}{2\pi c_1}\delta(v-c_1) + Y(t)\frac{1}{2\pi c_2}\delta(v-c_2), \tag{2.12}$$

where $X(t)$ and $Y(t)$ are, respectively, the densities of particles with velocities $c_1$ and $c_2$. They add up to the total density $X(t) + Y(t) = n(t)$. Inserting Eq. (2.12) into

Eq. (2.3) gives

$$\frac{\mathrm{d}}{\mathrm{d}t}X(t) = -\frac{\sigma}{\pi}\left[X^2(t)\frac{I_{11}}{c_1} + X(t)Y(t)\frac{I_{21}}{c_2}\right], \tag{2.13a}$$

$$\frac{\mathrm{d}}{\mathrm{d}t}Y(t) = -\frac{\sigma}{\pi}\left[X(t)Y(t)\frac{I_{12}}{c_1} + Y^2(t)\frac{I_{22}}{c_2}\right], \tag{2.13b}$$

where

$$I_{ij} = \int_{\mathbb{R}^2} \mathrm{d}\mathbf{v}_2\,|\mathbf{v}_1 - \mathbf{v}_2|\delta(v_2 - c_i)\Big|_{|\mathbf{v}_1|=c_j} = c_i\int_{\mathbb{R}^2}\mathrm{d}\mathbf{u}\,|\widehat{\mathbf{v}}_1 c_j - \widehat{\mathbf{u}}c_i|\delta(u-1), \tag{2.14}$$

with $\mathbf{u} = \mathbf{v}_2/c_i$ and $\widehat{\mathbf{u}} = \mathbf{u}/|\mathbf{u}|$. The integration is straightforward and leads to

$$I_{ij} = \begin{cases} 8c_i^2, & i = j, \\ 4c_i|c_i - c_j|E[k], & i \neq j, \end{cases} \tag{2.15}$$

where

$$E[k] = \int_0^{\pi/2}\mathrm{d}x\,\sqrt{1 + k^2\sin^2(x)}, \qquad k = 2\frac{\sqrt{c_i c_j}}{|c_i - c_j|}. \tag{2.16}$$

Upon rescaling the time according to $\tau = 2\pi\sigma c_2 t$, it follows from Eq. (2.13) that

$$\dot{X}(\tau) = -4\gamma X(\tau)^2 - \kappa(\gamma)X(\tau)Y(\tau), \tag{2.17a}$$

$$\dot{Y}(\tau) = -4Y(\tau)^2 - \kappa(\gamma)X(\tau)Y(\tau), \tag{2.17b}$$

where $0 \leqslant \gamma = c_1/c_2 < 1$, $\kappa(\gamma) = \int_0^\pi \mathrm{d}\varphi\sqrt{1 + \gamma^2 - 2\gamma\cos\varphi}$, and the overdot denotes time derivative with respect to $\tau$.

The set of equations (2.17) is a nonlinear homogeneous system of coupled differential equations with constant coefficients. An implicit solution can be obtained by introducing the function $V(\tau)$ defined as $V(\tau) = Y(\tau)/X(\tau)$. From Eq. (2.17) we get

$$\frac{\mathrm{d}Y}{\mathrm{d}X} = \frac{4Y^2 + \kappa XY}{4\gamma X^2 + \kappa XY} = \frac{4V^2 + \kappa V}{4\gamma + \kappa V}. \tag{2.18}$$

According to the definition of $V$, the left-hand-side of Eq.(2.18) becomes $\mathrm{d}Y/\mathrm{d}X = V + X\mathrm{d}V/\mathrm{d}X$ which yields

$$X\frac{\mathrm{d}V}{\mathrm{d}X} = \frac{(4-\kappa)V^2 + (\kappa - 4\gamma)V}{4\gamma + \kappa V}, \tag{2.19}$$

so that

$$\frac{\mathrm{d}X}{X} = \frac{4\gamma + \kappa V}{(4-\kappa)V^2 + (\kappa - 4\gamma)V}\,\mathrm{d}V. \tag{2.20}$$

The decomposition of the latter equation in simple elements gives

$$\frac{\mathrm{d}X}{X} = \mathrm{d}V\left(\frac{\alpha}{V} + \frac{\beta}{V + 4 - \kappa}\right), \tag{2.21}$$

with $\alpha = 4\gamma/(\kappa - 4\gamma) \geqslant 0$ and $\beta = \kappa/(4-\kappa) - \alpha > 0$. Integrating Eq. (2.21) yields

$$\frac{X_0}{X} = \left(\frac{V_0}{V}\right)^{\alpha} \left(\frac{V_0 + \frac{\kappa-4\gamma}{4-\kappa}}{V + \frac{\kappa-4\gamma}{4-\kappa}}\right)^{\beta}, \tag{2.22}$$

with $V(0) = V_0 = Y_0/X_0$, $X_0 = X(0)$, $Y_0 = Y(0)$. The special case of $\gamma = 0$ will be discussed in Sec. 2.4.3, hence from now on we assume that $\gamma > 0$, so that $\alpha > 0$. Equations (2.17) can also be written as

$$\frac{\mathrm{d}}{\mathrm{d}\tau}\left(\frac{1}{X}\right) = 4\gamma + \kappa\frac{Y(\tau)}{X(\tau)}, \tag{2.23a}$$

$$\frac{\mathrm{d}}{\mathrm{d}\tau}\left(\frac{1}{Y}\right) = 4 + \kappa\frac{X(\tau)}{Y(\tau)}. \tag{2.23b}$$

Multiplying the right-hand side of Eq. (2.23a) by $X_0$ and making use of $\mathrm{d}/\mathrm{d}\tau = (\mathrm{d}V/\mathrm{d}\tau)\mathrm{d}/\mathrm{d}V$ one obtains

$$\frac{\mathrm{d}V}{\mathrm{d}\tau}\frac{\mathrm{d}}{\mathrm{d}V}\left(\frac{X_0}{X}\right) = (4\gamma + \kappa V)X_0, \tag{2.24}$$

so that making use of the derivative of the right-hand side of Eq. (2.22), one obtains upon integration from 0 to $\tau$ the relation

$$X_0\tau = \int_V^{V_0} \mathrm{d}u\, \frac{1}{4\gamma + \kappa u}\left\{-\frac{\mathrm{d}}{\mathrm{d}u}\left[\left(\frac{V_0}{u}\right)^{\alpha}\left(\frac{V_0 + \frac{\kappa-4\gamma}{4-\kappa}}{u + \frac{\kappa-4\gamma}{4-\kappa}}\right)^{\beta}\right]\right\}. \tag{2.25}$$

Equation (2.25) implicitly defines the time dependence of the function $V(\tau)$. The procedure to obtain the densities $X(\tau)$ and $Y(\tau)$ from Eq. (2.25) is as follows. The integration in Eq. (2.25) leads to Appel functions, that may be inverted (at least numerically) in order to give $V(\tau)$. The insertion of $V(\tau)$ in Eq. (2.22) then gives $X(\tau)$. It is then straightforward to obtain $Y(\tau)$, having determined $V(\tau)$ and $X(\tau)$. The structure of the implicit relation (2.25) permits us to establish interesting analytical results.

First, let us investigate the long time behavior of the particle densities $X(\tau)$ and $Y(\tau)$. When $\tau \to \infty$, the left-hand side of Eq. (2.25) diverges linearly which implies that $\lim_{\tau\to\infty} V(\tau) = 0$. So, in the long-time limit, the implicit relation (2.25) leads to the asymptotic formula

$$\begin{aligned} X_0\tau &\overset{\tau\to\infty}{\simeq} \frac{1}{4\gamma}\left(\frac{V_0 + \frac{\kappa-4\gamma}{4-\kappa}}{\frac{\kappa-4\gamma}{4-\kappa}}\right)^{\beta} \int_V^{V_0} \mathrm{d}s\left[-\frac{\mathrm{d}}{\mathrm{d}u}\left(\frac{V_0}{u}\right)^{\alpha}\right] \\ &= \frac{1}{4\gamma}\left(\frac{V_0 + \frac{\kappa-4\gamma}{4-\kappa}}{\frac{\kappa-4\gamma}{4-\kappa}}\right)^{\beta}\left[-1 + \left(\frac{V_0}{V}\right)^{\alpha}\right]. \end{aligned} \tag{2.26}$$

Since $\lim_{\tau\to\infty} V(\tau) = 0$, then $-1 + (V_0/V)^{\alpha} \simeq (V_0/V)^{\alpha}$, then from Eq. (2.26) one obtains

$$X_0\tau V^{\alpha} \overset{\tau\to\infty}{\simeq} \frac{1}{4\gamma}\left(\frac{V_0 + \frac{\kappa-4\gamma}{4-\kappa}}{\frac{\kappa-4\gamma}{4-\kappa}}\right)^{\beta} V_0^{\alpha}, \tag{2.27}$$

so that

$$V(\tau) \overset{\tau\to\infty}{\simeq} V_0 \left( \frac{V_0 + \frac{\kappa-4\gamma}{4-\kappa}}{\frac{\kappa-4\gamma}{4-\kappa}} \right)^{\beta/\alpha} (4\gamma X_0 \tau)^{-1/\alpha}. \tag{2.28}$$

On the other hand, Eq. (2.23b) may be written as

$$\frac{\mathrm{d}}{\mathrm{d}\tau}\left(\frac{1}{Y}\right) = 4 + \frac{\kappa}{V}, \tag{2.29}$$

in which we insert Eq. (2.28) in order to obtain the long-time relation

$$\frac{\mathrm{d}}{\mathrm{d}\tau}\left(\frac{1}{Y}\right) \overset{\tau\to\infty}{\simeq} 4 + \kappa \frac{1}{V_0} \left( \frac{V_0 + \frac{\kappa-4\gamma}{4-\kappa}}{\frac{\kappa-4\gamma}{4-\kappa}} \right)^{-\beta/\alpha} (4\gamma X_0 \tau)^{1/\alpha}. \tag{2.30}$$

For $\tau \to \infty$ the constant term on the right-hand side of the latter equation is neglectible by comparison to $\tau^{1/\alpha}$, so that upon integration we obtain

$$Y(\tau) \overset{\tau\to\infty}{\simeq} \frac{V_0}{4\gamma}(4\gamma X_0)^{-1/\alpha} \left( \frac{4-\kappa}{\kappa-4\gamma} V_0 + 1 \right)^{\beta/\alpha} \tau^{-\kappa/4\gamma}. \tag{2.31}$$

Note that the exponent for the density $Y(\tau)$ is a function of the ratio $\gamma = c_1/c_2$ and thus is nonuniversal. In the limit $\gamma \to 1$ one recovers the asymptotic behavior of the single-velocity modulus distribution (see Sec. 2.4.4). On the other hand as $\lim_{\tau\to 0} V(\tau) = 0$, Eq. (2.23a) takes the asymptotic form $\mathrm{d}/\mathrm{d}\tau(1/X) = 4\gamma$. Hence we conclude that

$$X(\tau) \overset{\tau\to\infty}{\simeq} \frac{X_0}{1 + 4\gamma X_0 \tau} \overset{\tau\to\infty}{\simeq} \frac{1}{4\gamma}\tau^{-1}. \tag{2.32}$$

Second, we may find analytical upper and lower bounds for $X(\tau)$ and $Y(\tau)$. Granted that $\alpha > 0$ and $\beta > 0$, the integrand of Eq. (2.25) is a strictly monotonic decreasing positive function of $u$, therefore $V(\tau) < V_0$ for all $\tau > 0$. Considering that $(4\gamma)^{-1} \geqslant [4\gamma + \kappa u]^{-1}$ for $u \geqslant 0$, the insertion of Eq. (2.22) in Eq. (2.25) provides the inequality $X_0 \tau \leqslant (X_0/X - 1)/4\gamma$, which leads to an upper bound for $X(\tau)$. On the other hand, the inequality $(4\gamma + \kappa u)^{-1} \leqslant [4\gamma + \kappa V_0]^{-1}$ yields a lower bound, so that we finally get

$$\frac{X_0}{1 + (4\gamma X_0 + \kappa Y_0)\tau} \leqslant X(\tau) \leqslant \frac{X_0}{1 + 4\gamma X_0 \tau}. \tag{2.33}$$

Note that for times such that

$$4\gamma X_0 \tau \gg 1, \tag{2.34}$$

the upper bound (2.33) coincides with the exact asymptotic relation (2.32). The same kind of analysis as that leading to Eq. (2.33) yields the upper bound,

$$0 \leqslant Y(\tau) \leqslant \frac{Y_0}{1 + \kappa X_0 \tau}. \tag{2.35}$$

The width defined by the difference of the bounds in both cases (2.33) and (2.35) is $\mathcal{O}(\tau^{-1})$. Figures 2.1 and 2.2 show the numerical solution for $X(\tau)$, $Y(\tau)$, the bounds (2.33) and (2.35), as well as their asymptotic behaviors (2.32) and (2.31) on a logarithmic scale.

The knowledge of the numerical solution (see Figs. 2.1 and 2.2) allows to determine the crossover time, separating the early and long-time (power law) regimes.

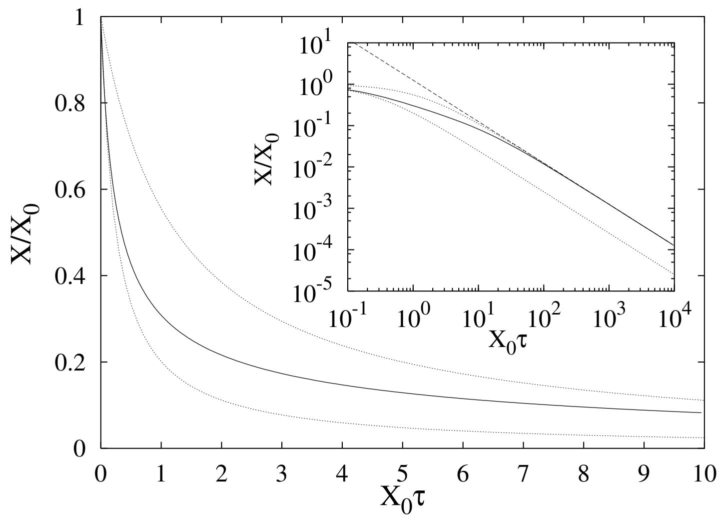


Figure 2.1: Upper and lower bounds (2.33) (dotted lines) as well as the numerical solution of the set of equations (2.17) for $X(\tau)$ with $X_0 = Y_0$, $\gamma = 0.2$ (continuous line). The inner logarithmic plot shows indeed the power law behavior $X(\tau) \sim \tau^{-1}$ for $\tau \to \infty$, where the asymptotic solution (2.32) is represented by the dashed straight line. Moreover, in this regime the solution converges to the upper bound (2.33).

### 2.4.3 Mixture of moving and motionless particles

We now consider a particular case of Sec. 2.4.2 that we solve exactly in the asymptotic limit $\tau \to \infty$. The system is now characterized by a certain number of motionless particles (zero velocity, $c_1 = 0$) whereas the rest of the particles have a given nonzero velocity modulus. Thus, setting $\gamma = 0$ in Eq. (2.22) we obtain

$$\frac{X}{X_0} = \left(\frac{\beta + V}{\beta + V_0}\right)^{\beta}, \tag{2.36}$$

where $\beta = \pi/(4-\pi)$. Since $V(\tau)$ tends to zero, in the asymptotic limit $\tau \to \infty$ the right-hand side of Eq. (2.36) is finite and positive. The density $X(\tau)$ cannot thus tend to zero, and must approach a strictly positive value $X(\infty) = X_\infty > 0$. We thus obtain

$$\lim_{\tau\to\infty} \frac{X}{X_0} = \frac{X_\infty}{X_0} = \left(\frac{\beta}{\beta + V_0}\right)^{\beta} = \frac{1}{(1 + V_0/\beta)^{\beta}}, \tag{2.37}$$

so that

$$X_\infty = \frac{X_0}{(1 + V_0/\beta)^{\beta}}. \tag{2.38}$$

The long-time behavior of $X(\tau)$ is obtained from Eq. (2.23a) by setting $\gamma = 0$ and rescaling the time to absorb the term $\kappa(\gamma = 0) = \pi$ so that

$$\frac{\mathrm{d}}{\mathrm{d}\tau}\left(\frac{1}{X}\right) = V. \tag{2.39}$$

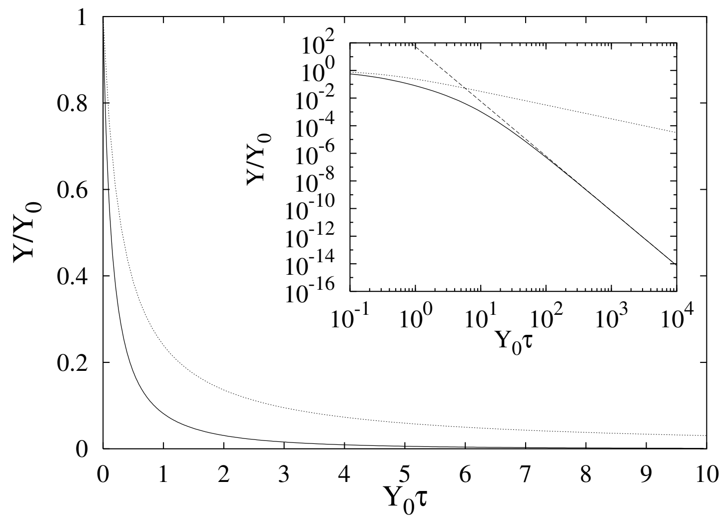


Figure 2.2: Upper bound (2.35) (dashed lines) as well as the numerical solution of the set of equations (2.17) for $Y(\tau)$ with $X_0 = Y_0$, $\gamma = 0.2$ (continuous line). The inner logarithmic plot of the numerical solution shows indeed the power law behavior $Y(\tau) \sim \tau^{-\kappa/4\gamma}$ for $\tau \to \infty$, where the asymptotic solution (2.31) is represented by the dashed straight. Furthermore, the use of both the upper bound (2.35) and the asymptotic form (2.31) allows to find an analytical approximation for $Y(\tau)$, which turns out to be exact in both limits $\tau \to 0$ and $\tau \to \infty$.

Again, multiplying the latter equation by $X_0$, inserting Eq. (2.36) in the left-hand side, and making use of $\mathrm{d}/\mathrm{d}\tau = (\mathrm{d}V/\mathrm{d}\tau)\mathrm{d}/\mathrm{d}V$ we obtain

$$X_0 \mathrm{d}\tau = \frac{1}{V}\mathrm{d}V\frac{\mathrm{d}}{\mathrm{d}V}\left(\frac{\beta+V_0}{\beta+V}\right)^{\beta}, \tag{2.40}$$

which upon integration yields

$$X_0\tau = \int_V^{V_0} \mathrm{d}u\,\frac{1}{u}\frac{\mathrm{d}}{\mathrm{d}u}\left[-\left(\frac{\beta+V_0}{\beta+u}\right)^{\beta}\right]. \tag{2.41}$$

Integrating by parts we obtain

$$X_0\tau = -\int_V^{V_0} \mathrm{d}u\,\ln(u)\frac{\mathrm{d}^2}{\mathrm{d}u^2}\left[-\left(\frac{\beta+V_0}{\beta+u}\right)^{\beta}\right] + \ln(u)\beta\frac{(\beta+V_0)^{\beta}}{(\beta+u)^{\beta+1}}\bigg|_V^{V_0}. \tag{2.42}$$

Since $\tau \to \infty$ we may replace $V$ by 0 in the lower bound of the first integral of the right-hand side of Eq. (2.42) so that

$$X_0\tau \overset{\tau\to\infty}{\simeq} -J - \ln\left[\frac{V^{(1+V_0/\beta)^{\beta}}}{V_0^{1/(1+V_0/\beta)}}\right], \tag{2.43}$$

where

$$J = \int_0^{V_0} \mathrm{d}u \, \ln(u) \frac{\mathrm{d}^2}{\mathrm{d}u^2} \left[ - \left( \frac{\beta + V_0}{\beta + u} \right)^{\beta} \right]. \tag{2.44}$$

Extracting $V(\tau)$ from Eq. (2.43) we obtain

$$V(\tau) \overset{\tau\to\infty}{\simeq} V_0^{1/(1+V_0/\beta)^{\beta+1}} \mathrm{e}^{-JX_\infty/X_0} \mathrm{e}^{-X_\infty \tau} \doteqdot \varepsilon_2(X_0, Y_0; \tau). \tag{2.45}$$

Inserting Eq. (2.45) in Eq. (2.39) yields the expression

$$\frac{\mathrm{d}}{\mathrm{d}\tau} \left( \frac{1}{X} \right) \overset{\tau\to\infty}{\simeq} V_0^{1/(1+V_0/\beta)^{\beta+1}} \mathrm{e}^{-JX_\infty/X_0} \mathrm{e}^{-X_\infty \tau} \tag{2.46}$$

that we integrate in order to find

$$X(\tau) \overset{\tau\to\infty}{\simeq} \frac{X_\infty}{1 - \varepsilon_2(X_0, Y_0; \tau)} \simeq X_\infty [1 + \varepsilon_2(X_0, Y_0; \tau)]. \tag{2.47}$$

Making use of Eq. (2.17a) for $\gamma = 0$ with the appropriate rescaling of the time in order to absorb $\kappa(\gamma = 0) = \pi$ we obtain $\dot{X} = -XY$. Eq. (2.47) then allows to find

$$Y(\tau) \overset{\tau\to\infty}{\simeq} X_\infty \varepsilon_2(X_0, Y_0; \tau). \tag{2.48}$$

Hence we have

$$X(\tau) \overset{\tau\to\infty}{\simeq} X_\infty + Y(\tau). \tag{2.49}$$

There is a qualitative difference from the case $c_1 > 0$. As shown in Fig. 2.3, the density of particles at rest approaches the asymptotic value $X_\infty > 0$ exponentially fast, while the density of moving particles goes to zero exponentially. Table 2.1 summarizes the long-time behavior for the different cases.

| | $c_2 = c_1 > 0$ | $c_2 > c_1 \neq 0$ | $c_2 > c_1 = 0$ |
|---|---|---|---|
| $X(\tau)$ | $\tau^{-1}$ | $\tau^{-1}$ | $X_\infty[1 + A\exp(-X_\infty \tau)]$ |
| $Y(\tau)$ | $\tau^{-1}$ | $\tau^{-\kappa/4\gamma}$ | $X_\infty A \exp(X_\infty \tau)$ |

Table 2.1: Summary of the density long-time behavior in two dimensions, where $A = A(X_0, Y_0) = \varepsilon_2(X_0, Y_0; \tau) \exp(X_\infty \tau)$.

Note that generalizing our results to any dimension $d \geqslant 2$ is straightforward (see [40], the main results for $d = 3$ being recalled in Table 2.2). The algebraic or exponential decay of the particle densities hold irrespective of $d$. In particular, for the general case $c_1 > 0$ the exponent of the density of "slow" particles is independent of $d$ so that $X(\tau) \overset{\tau\to\infty}{\sim} \tau^{-1}$ (see Sec. 2.4.4). Finally the relation (2.49) still holds.

### 2.4.4 Generalization to $d \geqslant 2$ and many-velocity moduli

We shall now show that in arbitrary dimension $d \geqslant 2$ and for any number of velocity modulus satisfying $c_1 < \ldots < c_N$ the density of the slowest particles $n_1$ in the long-time limit always decays as $n_1 \simeq (4\gamma_1 \tau)^{-1}$, where $\gamma_1 = c_1/c_N$.

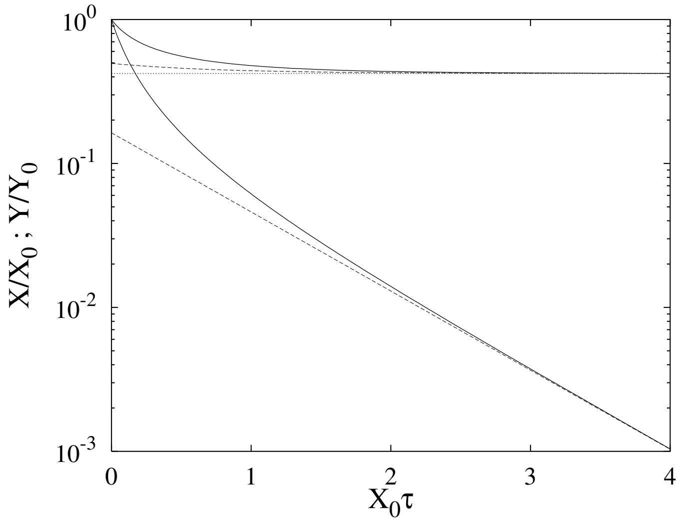


Figure 2.3: Linear-logarithmic plot of the numerical solution of the set of equations (2.17) for $X_0 = Y_0$, $\gamma = 0$ (continuous lines). The asymptotic relations (2.47) and (2.48) are shown by the dashed lines, and the asymptotic limit (2.38) by the dotted line.

| | $c_2 = c_1 > 0$ | $c_2 > c_1 \neq 0$ | $c_2 > c_1 = 0$ |
|---|---|---|---|
| $X(\tau)$ | $\tau^{-1}$ | $\tau^{-1}$ | $X_\infty[1 + 3\exp(-3X_\infty\tau)]$ |
| $Y(\tau)$ | $\tau^{-1}$ | $\tau^{-(3+\gamma^2)/4\gamma}$ | $X_\infty 3\exp(-3X_\infty\tau)$ |

Table 2.2: Summary of the density long-time behavior in three dimensions.

The distribution function is of the form

$$f(\mathbf{v};t) = \sum_{i=1}^{N} \frac{n_i(t)}{S_d c_i^{d-1}} \delta(v - c_i), \tag{2.50}$$

where $S_d$ is the surface of a $d$-dimensional sphere of unit radius given by Eq. (2.6). Inserting Eq. (2.50) into the kinetic equation (2.3) yields

$$\frac{\mathrm{d}}{\mathrm{d}t} n(t) = -\frac{\sigma^{d-1}\beta_1}{S_d} n_i(t) \sum_{j=1}^{N} \frac{n_j(t)}{c_j^{d-1}} I_{ji}, \tag{2.51}$$

where $I_{ij}$ is the $d$-dimensional counterpart of Eq. (2.14):

$$I_{ij} = 2\pi J_d \sqrt{c_i^2 + c_j^2}\, c_i^{d-1} F_d(c_i, c_j), \qquad \forall i, j = 1, \ldots, N, \tag{2.52}$$

and

$$J_d = \begin{cases} \pi^{-1}, & d = 2, \\ 1, & d = 3, \\ \prod_{k=1}^{d-3} \int_0^\pi \mathrm{d}\theta_k \, (\sin\theta_k)^k, & d > 3, \end{cases} \tag{2.53}$$

$$F_d(c_i, c_j) = \int_0^\pi \mathrm{d}\theta \sqrt{1 - 2\frac{c_i c_j}{c_i^2 + c_j^2}\cos\theta} \sin^{d-2}\theta. \tag{2.54}$$

We note that the particular case $F_d(c_i, c_i) \doteqdot F_d$ does not depend on any velocity moduli. Upon rescaling the time according to (such that one recovers the previously used rescaling for $d = 2$ or $d = 3$ [40])

$$\tau = t\sigma^{d-1}\frac{\beta_1 J_d F_d}{S_d}\frac{\pi}{\sqrt{2}}c_N, \tag{2.55}$$

Eq. (2.51) becomes

$$\dot{n}_i(\tau) = -\frac{2\sqrt{2}}{F_d} n_i(\tau) \sum_{j=1}^{N} n_j(\tau) \sqrt{\gamma_i^2 + \gamma_j^2} F_d(c_i, c_j), \tag{2.56}$$

where $\gamma_i = c_i/c_N$. Since $n_i < n_j$ for all $i < j$, in the limit $\tau \to \infty$ the density products $n_1 n_j$ for all $j \neq 1$ may be neglected. Therefore the evolution of the density $n_1(\tau)$ of slowest particles is asymptotically given by $\dot{n}_1(\tau) \overset{\tau\to\infty}{\simeq} -4\gamma_1 n_1^2(\tau)$. It follows upon integration

$$n_1(\tau) \overset{\tau\to\infty}{\simeq} \frac{1}{4\gamma_1}\tau^{-1}. \tag{2.57}$$

Fig. 2.4 shows the numerical solution of Eq. (2.56) for $d = 3$ and the prediction (2.57).

## 2.5 Comparison with molecular dynamics simulations

The analytical predictions obtained in the preceding section rely on the validity of the molecular chaos assumption, leading to the Boltzmann equation. It is therefore instructive to compare these predictions to the results of molecular dynamics (MD) simulations, where the exact equations of motion of the particles are integrated (see Ref. [39] for more details concerning the method).

MD simulations are most efficiently performed in two dimensions, where the best statistical accuracy can be achieved.

MD simulations have been implemented with systems of typically $N = 10^5$ to $4 \times 10^5$ spheres in two dimensions (discs). Periodic boundary conditions were enforced, and low densities considered, in order to minimize the excluded volume effects discarded at the Boltzmann level (note that these effects are necessarily transient since the density decreases with time).

Figure 2.5 compares the MD results obtained with $\gamma = 1/10$ to the predictions of Eqs. (2.32) (for $\gamma = 1/10$, the time decay of the "fast" particles is governed by the

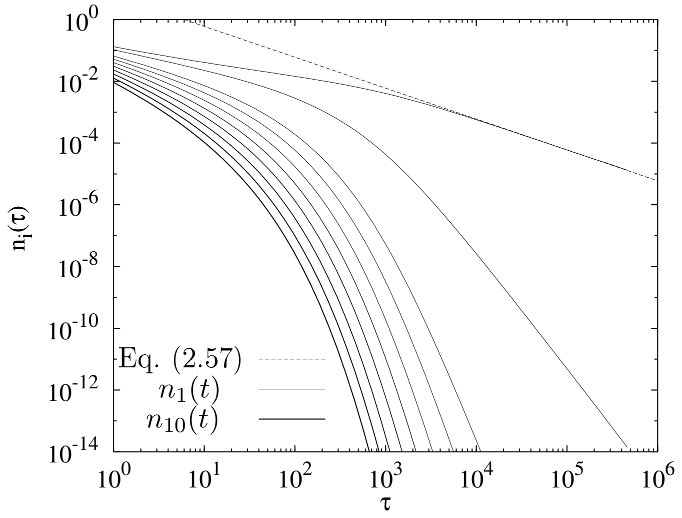


Figure 2.4: Numerical solution of the system (2.56) using a fourth-order Runge-Kutta method for $N = 10$ velocity modulus $c_i$ such that $c_1 < \ldots < c_N$, with $c_1 = 0.1$ and $c_{10} = 2.4$. Each curve corresponds to a density $n_i(\tau)$, and the thicker the curve that larger the value of $c_i$. The dashed line represents the asymptotic behavior of Eq. (2.57), which is seen to match the numerical solution for $n_1(\tau)$ in the long-time regime.

exponent $\kappa/4\gamma \simeq 7.9$). Although the large-time behaviors for $X$ and $Y$ are compatible with those given by Eqs. (2.31) and (2.32), it may be observed that the corresponding asymptotic regime is difficult to probe, even for large systems. The parametric plot [or "trajectory" $Y(X)$] shown in the inset is however in agreement with the relation $Y \propto X^{\kappa/4\gamma}$ deduced from Eqs. (2.31) and (2.32).

We have also performed MD simulations for a mixture of moving and motionless particles ($\gamma = 0$), where it is expected that the density $X$ of particles at rest decreases down to a nonvanishing value $X_\infty$. In the situation of an equimolar mixture ($X_0 = Y_0$), we have $V_0 = 1$ so that according to Eq. (2.37), $X_\infty/X_0 \simeq 0.414$. The MD simulations are in agreement with this scenario, and we find $X_\infty/X_0 \simeq 0.408$ irrespective of the initial conditions for a system with initially $N = 2 \times 10^5$ particles. The results for the time dependence of $X$ and $Y$ are displayed in Fig. 2.6. We conclude that the numerical simulations are again in agreement with the prediction of Boltzmann's kinetic theory.

## 2.6 Conclusions

We have shown that for some simple spatially homogeneous systems, characterized by a velocity distribution with a discrete velocity modulus spectrum, it is possible to find the exact solution for the nonlinear integral equation describing the dynamics of ballistic annihilation. These results, obtained at the level of a Boltzmann equation,

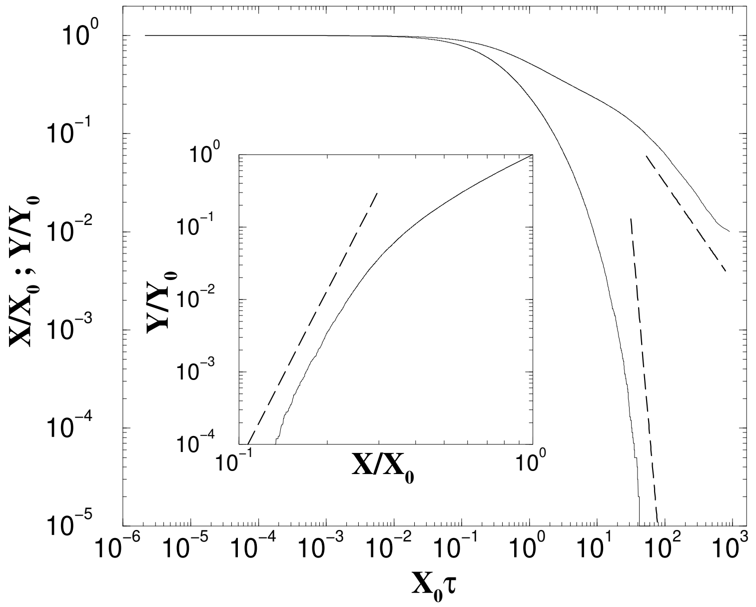


Figure 2.5: Log-log plot of the densities $X$ (upper curve) and $Y$ (lower curve) as a function of rescaled time, as obtained in the MD simulations of a two-dimensional system with $\gamma = 0.1$. The initial condition corresponds to an equimolar mixture ($X_0 = Y_0$) of $N = 2 \times 10^5$ particles, with reduced density $(X_0 + Y_0)\sigma^2 = 0.1$ at $\tau = 0$ (both species have the same diameter). The dashed lines have slopes $-1$ and $-7.9$ [as predicted by Eqs. (2.31) and (2.32)]. Inset: log-log plot of $Y$ as a function of $X$, where the broken line has slope $-7.9$.

have been validated by explicit comparison with molecular dynamics simulations in two dimensions.

For a single-velocity modulus distribution, the particle density of the model decays asymptotically as $n(t) \sim t^{-1}$, irrespective of space dimension. It was however rigorously shown that in one dimension, the decay is slower, $n(t) \sim t^{-1/2}$. This difference is a consequence of the fact that in one dimension strong dynamical correlations are created [63, 64], which invalidate the approximation underlying Boltzmann's dynamics. In higher dimensions, the Boltzmann equation becomes exact in the long-time limit.

In the case of a distribution with two different finite nonzero velocity moduli, we found that both particle densities decay for a large time according to a power law. The interesting feature is that the density of the slow particles decays as $t^{-1}$, while the density of the fast particles decays more rapidly (e.g., as $t^{-\kappa/4\gamma}$ in two dimensions and as $t^{-(3+\gamma^2)/4\gamma}$ in three dimensions [40]), with a nonuniversal exponent depending continuously on the velocity modulus ratio $\gamma = c_1/c_2$. A rough criterion for the crossover time separating the short- and long-time regimes has been given in Eq. (2.34). For $N \geqslant 2$ different finite nonzero velocity moduli the large-time decay of the density according to $t^{-1}$ was shown to hold irrespectively of the dimension.

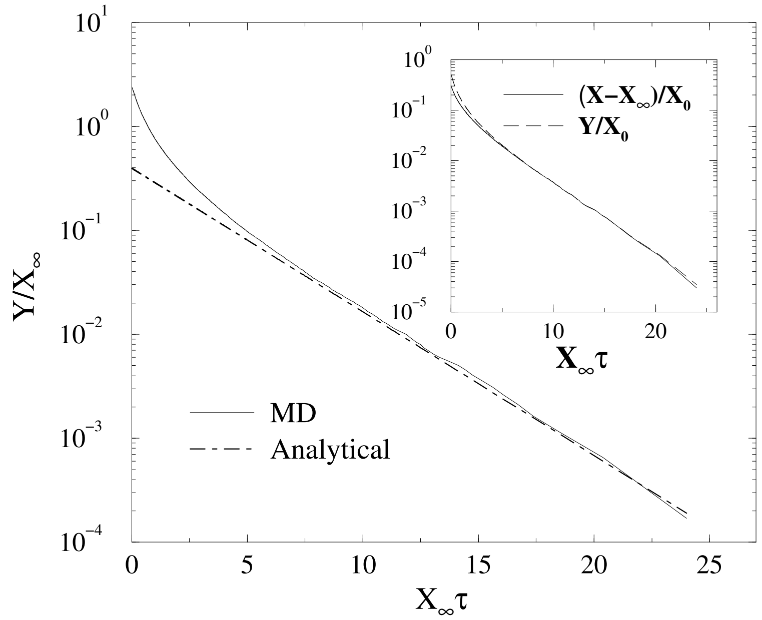


Figure 2.6: Linear-logarithmic plot of the density of moving particles. Here, $\gamma = 0$, $X_0 = Y_0 = 5 \times 10^{-3}/\sigma^2$ [corresponding to a very low total initial packing fraction $\eta_0 \equiv \pi(X_0 + Y_0)\sigma^2/4 = 0.0078$]. The initial number of particles is $N = 4 \times 10^5$. The results of MD simulations (continuous curve) are compared to the predictions of Eqs. (2.47) and (2.48), shown by the broken line. The inset shows that $X - X_\infty$ and $Y$ (obtained in MD) have asymptotically the same time decay [see Eqs. (2.47) and (2.48)].

Finally, the case $c_1 = 0$ leads to a particularly interesting behavior. Independently of the initial conditions, the densities of the moving and the motionless particles both decrease exponentially fast; however down to a nonzero value for particles at rest. This behavior is quite different from that observed in the one-dimensional case where the initial value of the density of motionless particles plays an important role in the long-time regime. This difference between one dimension and higher dimensions reflects once again the important role played by the dynamically created correlations for $d = 1$.

The case with motionless particles can be viewed as a problem of ballistic annihilation of particles with one-velocity moduli moving in a random medium containing immobile traps (the motionless particles) that can capture a moving particle and then disappear. Here again, the situation can be compared to similar problems in diffusion limited annihilation where the presence of traps can modify the long-time dynamics from a power law to an exponential decay [73].

It would be interesting to compare the above theoretical predictions with some experimental data. Besides growth and coarsening problems, ballistic annihilation could model other physical systems such as, for example, the fluorescence of laser excited gas atoms with quenching on contact [74]. However, the correspondence between such experimental situations and our model is not yet close enough to allow comparison. We would be highly interested in the knowledge of other physical systems that could be described by the models studied here.

# Chapter 3

# On the first Sonine correction for granular gases

## 3.1 Outline of the chapter

We consider the velocity distribution for a granular gas of inelastic hard spheres described by the Boltzmann equation. We investigate both the free of forcing case and a system heated by a stochastic force. We propose a new method to compute the first correction to Gaussian behavior in a Sonine polynomial expansion quantified by the fourth cumulant $a_2$. Our expressions are compared to previous results and to those obtained through the numerical solution of the Boltzmann equation. It is numerically shown that our method yields very accurate results for small velocities of the rescaled distribution. We finally discuss the ambiguities inherent to a linear approximation method in $a_2$. This chapter follows the content of Ref. [75].

## 3.2 Introduction

Most theories of rapid granular flows consider a granular gas as an assembly of inelastic hard spheres and assume uncorrelated binary collisions described by the Boltzmann equation, with a possible Enskog correction to account for excluded volume effects [24, 31, 51, 76, 77, 37, 78, 79, 80, 81, 82, 83]. The deviations from the Maxwellian velocity distribution may be accounted for by an expansion in Sonine polynomials, and it is often sufficient to retain only the leading term in this expansion, quantified by $a_2$, the fourth cumulant of the velocity distribution [24, 51, 79, 84, 85]. The purpose of this chapter is twofold: first, we present a novel route to compute $a_2$, directly inspired from a method that has been recently proposed to compute with accuracy the decay exponents and non Maxwellian features of gas subjected to ballistic annihilation dynamics [39, 70] (where particles undergoing free flight motion disappear upon contact [43, 59]). In essence, this method considers the limit of vanishing velocities of the Boltzmann equation, and deduces $a_2$ from moments of the velocity distribution that are *a priori* of lower order than those involved in the standard derivation [37, 79].

We may consequently expect a better precision from this alternative approach, that is analytically simpler to work out. We also know that the velocity distribution is non Gaussian at high energies [37, 79], so that extracting the relevant kinetic information from the behavior at vanishing velocities seems a promising route. The second goal of this chapter is to discuss the ambiguities –common to both approaches– encountered performing computations up to linear order in $a_2$, neglecting not only higher order Sonine contributions but also terms in $a_2^k$, $k = 2, 3$. Such an ambiguity has first been mentioned by Montanero and Santos [79].

## 3.3 The limit method for the first Sonine correction

Within the framework of the Boltzmann equation, as shown in Sec. 1.5.2 the one-particle velocity distribution function $f(\mathbf{v};t)$ for a homogeneous system free of forcing obeys the relation

$$\partial_t f(\mathbf{v}_1;t) = I[f,f], \tag{3.1}$$

where the collision integral reads

$$I[f,f] = \sigma^{d-1} \int_{\mathbb{R}^d} \mathrm{d}\mathbf{v}_2 \int \mathrm{d}\widehat{\boldsymbol{\sigma}}\, \theta(\widehat{\boldsymbol{\sigma}}\cdot\widehat{\mathbf{v}}_{12})(\widehat{\boldsymbol{\sigma}}\cdot\mathbf{v}_{12}) \left(\alpha^{-2}b^{-1} - 1\right) f(\mathbf{v}_1;t) f(\mathbf{v}_2;t). \tag{3.2}$$

In Eq. (3.2), $\sigma$ is the diameter of the particles, $\theta$ the Heaviside distribution, $\mathbf{v}_{12} = \mathbf{v}_1 - \mathbf{v}_2$ the relative velocity of two particles, $\widehat{\mathbf{v}}_{12} = \mathbf{v}_{12}/v_{12}$, $v_{12} = |\mathbf{v}_{12}|$, and $\widehat{\boldsymbol{\sigma}}$ a unit vector joining the centers of the grains. The space dimension is $d$. The precollisional velocities $\mathbf{v}_i'$ and the postcollisional ones $\mathbf{v}_i$ are related through the operator $b^{-1}$ and read

$$\mathbf{v}_1' = b^{-1}\mathbf{v}_1 = \mathbf{v}_1 - \frac{1+\alpha}{2\alpha}(\mathbf{v}_{12}\cdot\widehat{\boldsymbol{\sigma}})\widehat{\boldsymbol{\sigma}}, \tag{3.3a}$$

$$\mathbf{v}_2' = b^{-1}\mathbf{v}_2 = \mathbf{v}_2 + \frac{1+\alpha}{2\alpha}(\mathbf{v}_{12}\cdot\widehat{\boldsymbol{\sigma}})\widehat{\boldsymbol{\sigma}}, \tag{3.3b}$$

with $\alpha \in [0,1]$ the restitution coefficient. Note that $b^{-1}g(\mathbf{v}_1,\mathbf{v}_2;t) = g[b^{-1}\mathbf{v}_1, b^{-1}\mathbf{v}_2;t]$. If energy is supplied to the system, an additional forcing term is present in Eq. (3.1) [79], but the general arguments and method presented below remain valid. To be more specific, we shall also consider the situation where the system is driven into a non equilibrium steady state by a random force acting on the particles [37, 78, 79]. With this energy feeding mechanism, coined "stochastic thermostat", the Fokker-Planck term $\xi_0^2\nabla_{\mathbf{v}}^2 f$ should be added to the right-hand side of Eq. (3.1) [37], where $\xi_0$ is related to the amplitude of the random force acting on the grains.

We are searching for an isotropic scaling solution $\widetilde{f}(c)$ of Eq. (3.2). The requirement of a time independent behavior with respect to the typical velocity $\overline{v}(t) = \sqrt{2\langle v^2\rangle_f/d}$ imposes that [51, 37, 79, 86]

$$f(\mathbf{v};t) = \frac{n}{\overline{v}^d(t)}\widetilde{f}(c), \tag{3.4}$$

where the rescaled velocity is given by $c = v/\overline{v}(t)$ and the angular brackets $\langle\cdot\rangle_f$ denote the average over $f(\mathbf{v};t)$: $\langle \mathbf{v}^2\rangle_f = \int_{\mathbb{R}^d} \mathrm{d}\mathbf{v} v^2 f(\mathbf{v},t)/n$. The scaling form (3.4) is physically "reasonable" within the scaling theory [86], and this form may be justified a posteriori making use of numerical simulations [51, 37, 79]. The presence of the density $n$ on the right-hand side of Eq. (3.4) ensures that $\int \mathrm{d}c\widetilde{f}(c) = 1$ and $\langle c^2 \rangle = \int \mathrm{d}c\, c^2 \widetilde{f}(c) = d/2$. Integrating Eq. (3.1) over $\mathbf{c}_1$ with weight $c_1^p$, this scaling function describing the homogeneous cooling state satisfies the time-independent equation [51, 37, 79]

$$\frac{\mu_2}{d}\left(d + c_1 \frac{\mathrm{d}}{\mathrm{d}c_1}\right)\widetilde{f}(c_1) = \widetilde{I}(\widetilde{f},\widetilde{f}), \tag{3.5}$$

where

$$\mu_p = -\int_{\mathbb{R}^d} \mathrm{d}\mathbf{c}_1\, c_1^p \widetilde{I}(\widetilde{f},\widetilde{f}), \tag{3.6}$$

and

$$\widetilde{I}(\widetilde{f},\widetilde{f}) = \int_{\mathbb{R}^d} \mathrm{d}\mathbf{c}_2 \int \mathrm{d}\widehat{\boldsymbol{\sigma}}\, \theta(\widehat{\boldsymbol{\sigma}} \cdot \widehat{\mathbf{c}}_{12})(\widehat{\boldsymbol{\sigma}} \cdot \mathbf{c}_{12}) \left[\frac{1}{\alpha^2}\widetilde{f}(c_1')\widetilde{f}(c_2') - \widetilde{f}(c_1)\widetilde{f}(c_2)\right]. \tag{3.7}$$

It is useful to consider the hierarchy of moment equations obtained by integrating Eq. (3.5) over $c_1$ with weight $c_1^p$ [37]

$$\mu_p = \frac{\mu_2}{d} p \langle c^p \rangle. \tag{3.8}$$

The solution of Eq. (3.5) is non-Gaussian in several respects. The high energy tail is overpopulated compared to the Maxwellian [37], a generic although not systematic feature for granular gases (a particular heating mechanism leading to an underpopulation at large velocities has been studied in [79]). Deviation from Gaussian behavior may also be observed at thermal scale or near the velocity origin. To study the latter correction, it is convenient to resort to a Sonine expansion for the distribution function $\widetilde{f}(c)$ [87]

$$\widetilde{f}(c) = \widetilde{\mathcal{M}}(c)\left[1 + \sum_{i \geqslant 1} a_i S_i(c^2)\right], \tag{3.9}$$

where $\widetilde{\mathcal{M}}(c) = \pi^{-d/2}\exp(-c^2)$ is the Maxwellian, and $S_i(c^2)$ the Sonine polynomials (that may be found in [87]; the first few are recalled in [37]). Such an expansion is non perturbative in $\alpha$ since the distribution function is close to the Maxwellian for all values of $\alpha$. Due to the constraint $\langle c^2 \rangle = d/2$ the first correction $a_1$ vanishes [37], and for our purposes it is sufficient to know $S_2(x) = x^2/2 - (d+2)x/2 + d(d+2)/8$. If we define the normalization factor $N_i$ by

$$\int_{\mathbb{R}^d} \mathrm{d}\mathbf{c}\, \widetilde{\mathcal{M}}(c) S_i(c^2) S_j(c^2) = \delta_{ij} N_i, \tag{3.10}$$

then for $j > 0$ and making use of $S_0(c^2) = 1$ one obtains the coefficients $a_i$ as polynomial moments of the scaling function:

$$\frac{1}{N_j}\int_{\mathbb{R}^d} \mathrm{d}\mathbf{c}\, \widetilde{f}(c) S_j(c^2) = a_j. \tag{3.11}$$

In particular, the coefficient $a_2$ is related to the kurtosis of the velocity distribution

$$\langle c^4 \rangle = \frac{d(d+2)}{4}(a_2+1), \tag{3.12}$$

so that, upon taking $p = 4$ in Eq. (3.8), we get

$$\mu_4 = (d+2)(1+a_2)\mu_2. \tag{3.13}$$

### 3.3.1 The free cooling gas

#### 3.3.1.1 The first Sonine correction

In the following analysis, we will only retain the first correction in the expansion (3.9): $\widetilde{f} = \widetilde{\mathcal{M}}(1 + a_2 S_2)$. Computing $\mu_2$ and $\mu_4$ to linear order in $a_2$ with this functional ansatz [and further linearizing Eq. (3.13)], one deduces $a_2$ [37, 79]. This approach is nonperturbative in the restitution coefficient. However, since the high energy tail of $\widetilde{\mathcal{M}}(1 + a_2 S_2)$ is very distinct from that of the exact solution of Eq. (3.5), computing $a_2$ from relation (3.8) with $p > 4$ is expected to give a poor estimate, all the worse as $p$ increases. With this in mind, it appears that the limit of vanishing velocity of the rescaled Boltzmann equation (3.5) contains an interesting piece of information:

$$\mu_2 \widetilde{f}(0) = \lim_{c_1 \to 0} \widetilde{I}(\widetilde{f}, \widetilde{f}). \tag{3.14}$$

The main steps to compute this limit are given in appendix A.2. Up to a geometrical prefactor, the loss term of $\lim \widetilde{I}$ on the right-hand side reads $\widetilde{f}(0)\langle c_1 \rangle$ and is thus of lower order than the quantities appearing in (3.13). Working at linear order in $a_2$, one may therefore expect to achieve a better accuracy when computing the various terms (except may be the gain term) appearing in (3.14) than in (3.13). In the context of ballistic annihilation, a related remark lead to analytical predictions for the decay exponents of the dynamics and non-Gaussian features of the velocity statistics, in excellent agreement with the numerical simulations [39, 70]. In the present situation, the gain term of $\widetilde{I}$ in (3.14) cannot be written as a collisional moment, so that the situation is less clear and deserves some investigation. We propose to compare the value of $a_2$ following this route to the standard one of Refs. [37, 79, 84]. Evaluating (3.14) at first order in $a_2$, we obtain:

$$a_2 = \frac{4(\alpha^2+1)^2(\alpha^2-1)\left[\sqrt{2}(\alpha^2+1)-2\right]}{A(\alpha,d)}. \tag{3.15}$$

where

$$\begin{aligned} A(\alpha, d) = {} & 5 + d(2-d) + 8\alpha(\alpha^2+1)(d-1) - \alpha^2(23 - 6d + d^2) + \alpha^4(3 + 6d + d^2) \\ & + \alpha^6(-1 + 2d + d^2) - \sqrt{2}(\alpha^2+1)^3(\alpha^2-1)(3 + 4d + 2d^2)/4. \end{aligned} \tag{3.16}$$

In Fig. 3.1, we compare this result with the analytical expression of van Noije and Ernst [37]. We also display the fourth cumulant $a_2$ obtained by Monte Carlo simulations from the numerical solution of the nonlinear Boltzmann equation (3.1) (so

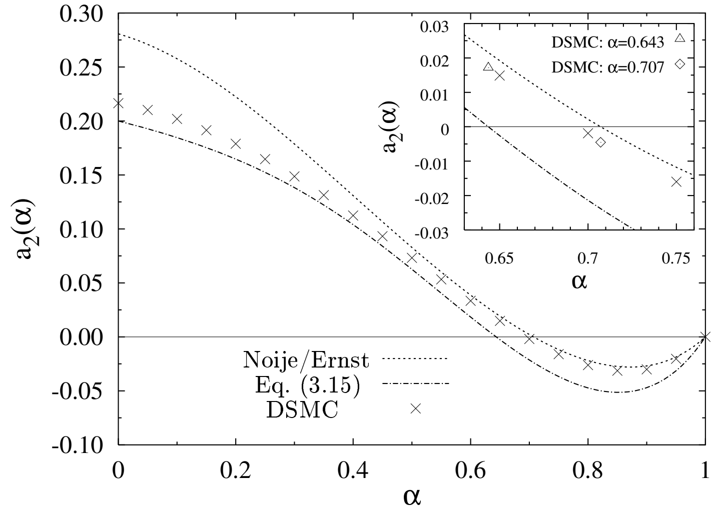


Figure 3.1: Comparison of the correction $a_2(\alpha)$ for the free cooling in two dimensions obtained in [37], with Eq. (3.15). The crosses correspond to the "exact" result, obtained by solving the Boltzmann equation with the DSMC method, for $10^6$ particles and approximately 500 collisions for each particle. The inset is a zoom in the region of the smallest root of the fourth cumulant.

called DSMC technique [88, 89]). Our expression appears more accurate at small inelasticity, but less satisfying close to elastic behavior. The smallest root of $a_2 = 0$ obtained with Eq. (3.15) is $\alpha^* = (\sqrt{2}-1)^{1/2} \simeq 0.643\ldots$. This root differs from the value $\alpha^{**} = 1/\sqrt{2} \simeq 0.707\ldots$ obtained upon solving (3.13) (both $\alpha^*$ and $\alpha^{**}$ do not depend on space dimension $d$). The inset shows that the exact root is located in the interval $]\alpha^*, \alpha^{**}[$, and seems closer to $\alpha^{**}$.

In order to understand the discrepancy close to the elastic limit shown in Fig. 3.1, it is useful to study the first Sonine correction $\widetilde{f}(c_i)/\widetilde{\mathcal{M}}(c_i) = 1 + a_2 S_2(c_i^2)$. The result for $\alpha = 0.8$ where our method seems to be the less accurate is shown in Fig. 3.2, and in Fig. 3.3 for $\alpha = 0.5$.

In spite of the imprecision of our analytical expression for $a_2$ seen in Fig. 3.1, Fig. 3.2 shows that the limit method is very accurate for small velocities, but turns to quickly become more imprecise for bigger velocities. This suggests that computing the fourth cumulant from the limit of vanishing velocities gives more weight to this region which leads to a better behavior of the Sonine expansion for small velocities. On the other hand, the traditional route yields a global interpolation for all velocities. The good precision of our result for small velocities and the lower accuracy for higher velocities is confirmed in Fig. 3.3. Exploiting the above qualitative interpretation of the limit method, we expect to archieve a good accuracy using Eq. (3.15) in order to find the first moment [39]:

$$\langle |c| \rangle = \frac{\sqrt{\pi}}{2}\left(1 - \frac{a_2}{8}\right). \tag{3.17}$$

Indeed, we suppose that the function $a_2$ obtained from the limit method gives a precise

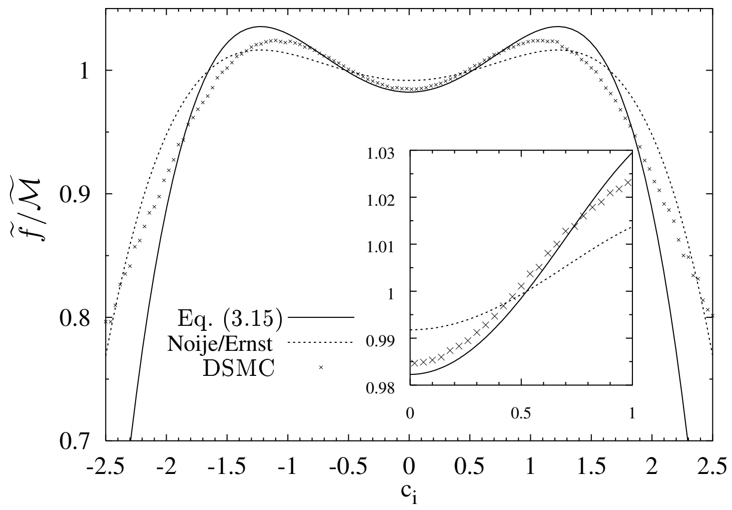


Figure 3.2: Plot of $\widetilde{f}(c_i)/\widetilde{\mathcal{M}}(c_i)$ for $\alpha = 0.8$. The curve labelled "Eq. (3.15)" and "Noije/Ernst" correspond to $1 + a_2 S_2$ where $a_2$ is given respectively by Eq. (3.15) and by the Sonine correction obtained by Noije and Ernst following the traditional route [37]. "DSMC" refers to the full distribution obtained from the solution of the Boltzmann equation (using $10^6$ particles and averaging over 300 independent samples).

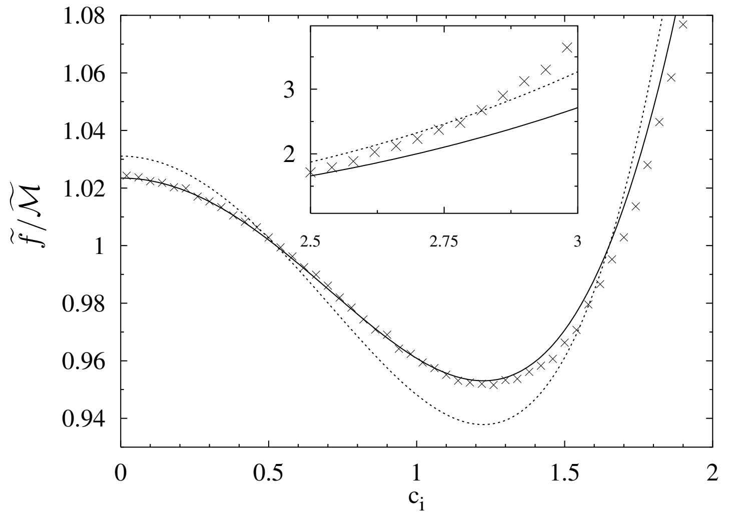


Figure 3.3: Same as Fig. 3.2 for $\alpha = 0.5$.

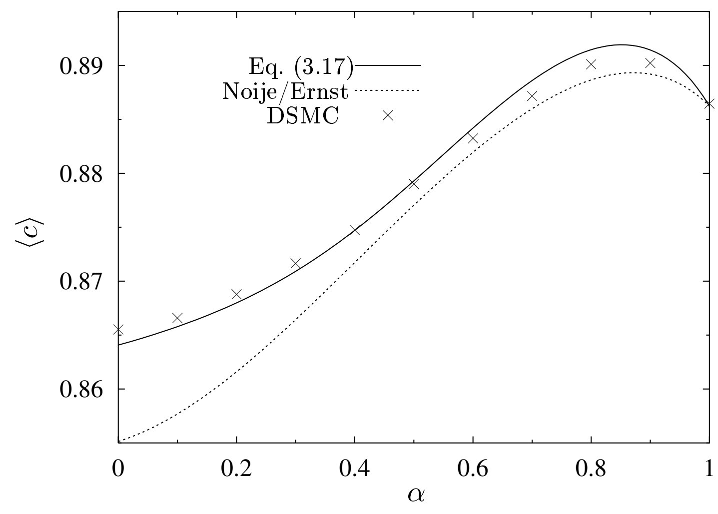


Figure 3.4: First rescaled velocity moment $\langle |c| \rangle$ as a function of the restitution coefficient. DSMC is done for $10^5$ particles and approximately 500 collisions for each particle.

description of the rescaled velocity distribution for small velocities. Thus our $a_2$ is likely to describe more accurately a low order velocity moment than a high order one. This is confirmed by Fig. 3.4.

#### 3.3.1.2 Ambiguities inherent to the linear approximation

As emphasized by Montanero and Santos [79], a certain degree of ambiguity is present when evaluating an identity such as (3.13) or (3.14) to first order in $a_2$. According to the way we rearrange the terms $\mu_4$, $\mu_2$, and $(d+2)(1+a_2)$ in say Eq. (3.13) and subsequently apply a Taylor series expansion in $a_2$, we obtain different predictions for $a_2(\alpha)$. For instance van Noije and Ernst did expand the relation (3.13) [37], whereas Montanero and Santos also considered other possibilities such as $\mu_4/\mu_2 = (d+2)(1+a_2)$ (this leads to a result which turns out to be fairly close to the one in [37]) and also $\mu_4/(1+a_2) = (d+2)\mu_2$. For small $\alpha$ in the latter case, the resulting $a_2$ turns out to be 20% lower than the previous ones, and very close to the exact (within Boltzmann's equation framework) numerical results, for all the values of the restitution coefficient [79]. We push further this remark and show in Fig. 3.5 the eight simplest different possible functions $a_2(\alpha)$ obtained upon rearranging the terms of Eq. (3.13) and expanding the result to first order in $a_2$. A similar ambiguity is present making use of Eq. (3.14). The corresponding eight different possibilities are plotted in Fig. 3.6. It appears that the envelope of the curves following from this method is less spread than within the "traditional" route, by a factor of approximately 2. We thus achieve a better accuracy at small $\alpha$.

The dispersion of the curves in Figs. 3.5 and 3.6 illustrates the nonvalidity of the

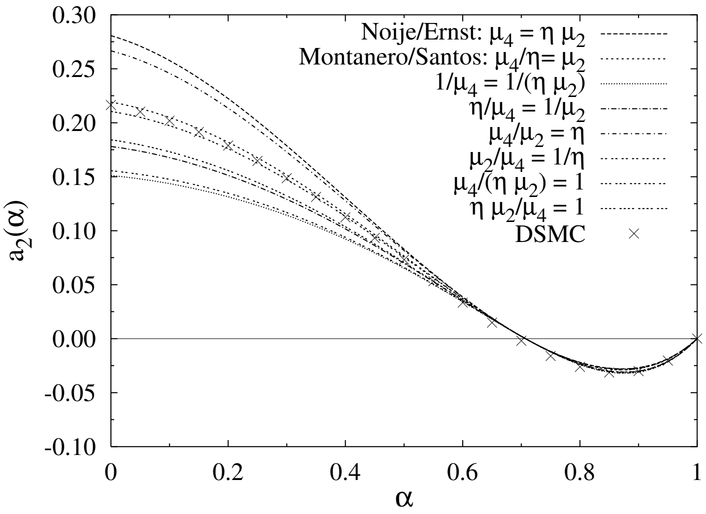


Figure 3.5: The eight possible fourth cumulant $a_2$ obtained from Eq. (3.13), corresponding to the two-dimensional homogeneous free cooling. We define $\eta = (d+2)(1+a_2)$, then rewrite the equation $\mu_4 = \eta\mu_2$ according to the eight possible different combinations mentioned in the legend, before doing the linear Taylor expansion around $a_2 = 0$. The first curve is the plot of the function $a_2$ obtained by van Noije and Ernst [37], whereas the second one – obtained by Montanero and Santos [79]– is very close to the exact results shown by crosses.

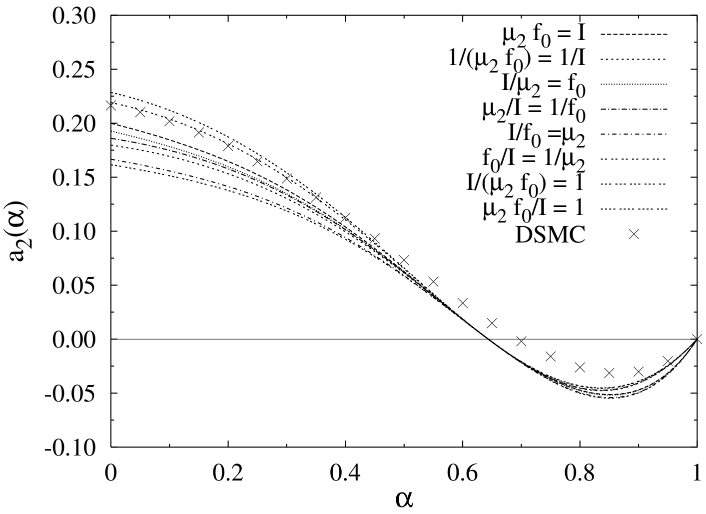


Figure 3.6: Same as Fig. 3.5, making use of Eq. (3.14) instead of (3.13) to compute the first Sonine correction. In the legend, $I$ denotes $\lim \widetilde{I}$ and $f_0 = \widetilde{f}(0)$.

linearization approximation at small $\alpha$. However –and concentrating on Fig. 3.5– it appears that all curves do not have the same status. Brilliantov and Pöschel have indeed solved analytically the full nonlinear problem [i.e., working again with the distribution function $\widetilde{f} = \widetilde{\mathcal{M}}(1 + a_2 S_2)$ but keeping nonlinear terms in $a_2$], and obtained results that are very close to those of Noije/Ernst, except for $\alpha < 0.2$ where they found slightly larger fourth cumulants [80]. Their result is therefore farther away from the exact one obtained by DSMC (see, e.g., Fig. 3.1 where it appears than the Noije/Ernst expression already overestimates the exact curve). The difference between the DSMC results and those of Brilliantov/Pöschel therefore illustrates the relevance of Sonine terms $a_i$ with $i \geqslant 3$ in expansion (3.9). However, some of the curves shown in Fig. 3.5 lie close to the exact one, which means that it is possible to correct the deficiencies of truncating $\widetilde{f}$ at second Sonine order by an ad-hoc linearizing scheme. The agreement obtained is nevertheless incidental, and the corresponding analytical expression should be considered as a semi-empirical interpolation supported by numerical simulations. One should thus emphasize that the right way to compute $a_2$ is to use its definition involving the fourth rescaled velocity cumulant of Eq. (3.12) because this relation is not sensitive to higher order Sonine terms, nor to nonlinearities, even if this route doesn't give the most accurate description in the small velocity domain (as seen from Figs. 3.2 and 3.3)

### 3.3.2 The heated granular gas

For completeness, we now briefly consider the stochastic thermostat situation [37, 78, 79, 85], where the counterpart of Eq. (3.5) reads

$$-\frac{\mu_2}{2d}\,\nabla^2_{\mathbf{c}_1}\widetilde{f}(c_1) \;=\; \widetilde{I}(\widetilde{f},\widetilde{f}). \tag{3.18}$$

The Fokker-Planck diffusion term $\nabla^2_{\mathbf{c}_1}$ represents the change of the distribution function caused by small random kicks (see, e.g., [90]). Considering again the limit $c_1 \to 0$ and retaining only the first correction in the expansion (3.9), we get

$$\frac{\mu_2}{2\pi^{d/2}}\left[2 + a_2\frac{(d+2)(d+4)}{4}\right] \;=\; \lim_{c_1\to 0}\widetilde{I}(\widetilde{f},\widetilde{f}). \tag{3.19}$$

Given that the right-hand side is already known from the free cooling calculation, it is straightforward to extend the previous results to the present case. As before, there are 8 possible ways to extract $a_2$ from Eq. (3.19) working at linear order. The resulting expressions are displayed in Fig. 3.7. On the other hand, the moment method described in Refs. [37, 79] makes use of the identity $\mu_2(d+2) = \mu_4$, that is a direct consequence of Eq. (3.18). There are thus 4 possible rearrangements leading to the different cumulants shown in the inset of Fig. 3.7. For comparison, we have also implemented Monte Carlo simulations in the present heated situation (see the crosses in Fig. 3.7). It is difficult to compare the dispersion of the curves with both methods (8 possibilities versus 4), since our approach makes use of Eq. (3.19) which is of higher order in $a_2$ than $\mu_2(d+2) = \mu_4$, the starting point used in Refs. [37, 79]. Our method appears here less accurate than for the free cooling, with again an underestimation of $a_2$ at large $\alpha$. However, this should be put in the context of the results of Sec. 3.3.1.2.

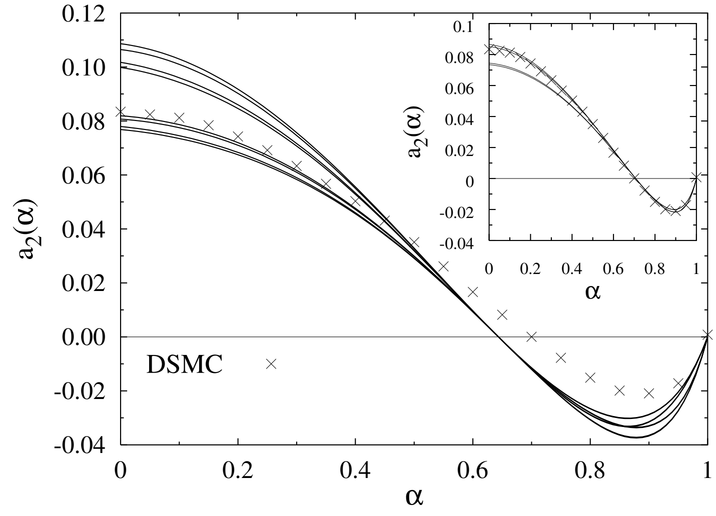


Figure 3.7: The counterpart of Fig. 3.6 for the two dimensional stochastic thermostat. The inset shows the 4 possibilities associated with the method of Refs. [37, 79]. The symbols show the results of DSMC simulations.

## 3.4 The nonlinear problem

In order to get free from the ambiguities inherent to a linear computation in $a_2$, we have also solved the full nonlinear problem. The computation becomes cumbersome, and since Brilliantov and Pöschel [80] have already initiated this route in 3 dimensions for the homogeneous free cooling (thereby providing the calculation of $\mu_2$ and $\mu_4$), we will turn our attention to the three dimensional situation. First and for the sake of comparison, we have repeated the nonlinear derivation of Ref. [80] for the stochastic thermostat. Second, we have computed the right-hand sides of Eqs. (3.14) and (3.19) without any linearization, from the form $\widetilde{f} = \widetilde{\mathcal{M}}(1 + a_2 S_2)$. The left-hand sides only require the knowledge of $\mu_2$. For both free and forced situations, we subsequently obtain a polynomial equation of degree 3 for $a_2$ from which we extract the physical root, the two others corresponding to unstable scaling solutions [80]. The results are displayed in Fig. 3.8. In particular, our approach again suffers from an underestimation of $a_2$ for $\alpha > 0.5$, already observed within the linear computation, and that is thus ascribable to Sonine terms of order 3 or higher. In this respect, it is surprising that these terms do not affect similarly the moment method of Ref. [80] in the same range of inelasticities.

## 3.5 Conclusions

To sum up, using a new approach we obtain the first non-Gaussian correction $a_2$ to the scaled velocity distribution. In view of the above results, we conclude that our approach constitutes an improvement over the previous procedures in the small

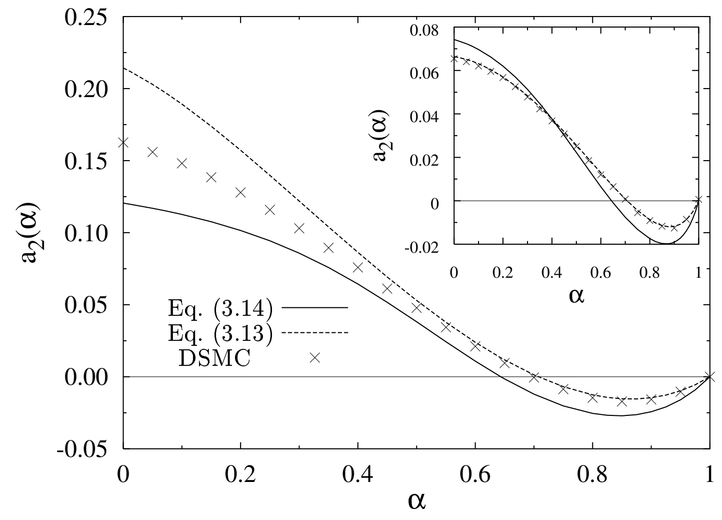


Figure 3.8: Fourth cumulant in 3 dimensions for a force free system in the regime of homogeneous cooling. The curves correspond to the nonlinear solutions of Eqs. (3.13) ("traditional route") and (3.14) (limit method, see text for details). The crosses correspond to the Monte Carlo results. The inset shows the same curves for the stochastic thermostat.

velocity regime, and our analysis turns to be technically simpler to perform. We have also discussed the ambiguities that arise 1) when restricting ourselves to second Sonine order, and 2) when a further linearization of the various relevant relations is performed. It appears that an *ad-hoc* linearization scheme (point 2) may circumvent the limitations inherent to point 1. In any case, the computation of a non-Gaussian correction suffers from uncontrolled approximations that systematically need to be confronted against numerical simulations.

# Chapter 4

# Probabilistic ballistic annihilation

## 4.1 Outline of the chapter

We investigate the problem of ballistically controlled reactions in dimension $d \geqslant 2$ where particles either annihilate upon collision with probability $p$, or undergo an elastic shock with probability $1-p$. Restricting to homogeneous systems, we provide in the scaling regime that emerges in the long time limit, analytical expressions for the exponents describing the time decay of the density and the root-mean-square velocity, as continuous functions of the probability $p$ and of a parameter related to the dissipation of energy. We work at the level of molecular chaos (non-linear Boltzmann equation), and using a systematic Sonine polynomials expansion of the velocity distribution, we obtain in arbitrary dimension the first non-Gaussian correction and the corresponding expressions for the decay exponents. We implement Monte-Carlo simulations in two dimensions, that are in excellent agreement with our analytical predictions. For $p < 1$, numerical simulations lead to conjecture that unlike for pure annihilation ($p = 1$), the velocity distribution becomes universal, i.e., does not depend on the initial conditions. For such a system neither mass, momentum, nor kinetic energy are conserved quantities. We establish the hydrodynamic equations from the Boltzmann equation description. Within the Chapman-Enskog scheme, we determine the transport coefficients up to Navier-Stokes order, and give the closed set of equations for the hydrodynamic fields chosen for the above coarse grained description (density, momentum and kinetic temperature). Linear stability analysis is performed, and the conditions of stability for the local fields are discussed. The content of this chapter is strongly based on Refs. [52, 53]

## 4.2 Introduction

We consider an assembly of particles that move freely in $d$-dimensional space between collisions, where only two body collisions are taken into account. The purpose of this chapter is to present a model that unifies both the dynamics of annihilation [39, 43, 59, 60, 63, 64, 70] and of hard-sphere gases [56] using a continuous parameter $p \in [0, 1]$, the probability that two particles annihilate when they touch each other [44]. The model of probabilistic ballistic annihilation in one dimension for bimodal discrete initial velocity distributions was introduced in [67, 91], whereas for higher dimensions and arbitrary continuous initial velocity distributions it was considered in [52]. In the limiting case $p = 1$, we recover the annihilation model originally defined by Elskens and Frisch [58], that has attracted some attention since [39, 40, 43, 59, 60, 62, 65, 68, 70] and for $p = 0$ the system of hard-spheres. In our system in the limit $p \to 0$, $p > 0$ (denoted $p \to 0^+$), a particle will collide elastically many times before being annihilated. Thus the particles have a diffusing-like motion before annihilating. In one dimension (again for $p = 1$), the problem is well understood for discrete initial velocity distributions [62, 65]. On the contrary, higher dimensions introduce complications that make the problem much more difficult to treat [39, 70]. Only a few specific initial velocity conditions lead to systems that are tractable using the standard tools of kinetic theory [40].

Another extensively studied class of problems is the one of diffusion-limited annihilation in which diffusing particles annihilate on contact with a given rate [72, 92, 93]. The simplest case corresponds to the reaction $A + A \to \varnothing$. The number of particles decays, in the long time regime, as a power law $n(t) \sim t^{-\xi}$. The decay exponent can be exactly computed [94] and is $\xi = \min(1, d/2)$, where $d$ is the dimension of the system. However, the time decay exponents for the density found in our case when $p \to 0^+$ are different from the exponents found in diffusion-limited systems. The reason for this difference is that the underlying microscopic mechanisms responsible for diffusion are different. In our case, particles which have a bigger velocity modulus have a bigger annihilation rate than the slow particles. The velocity dependence of the annihilation rate is not present in the usual diffusion-limited annihilation.

It was recently shown [39] that in the long time limit, the annihilation dynamics for dimensions higher than one is adequately described by the nonlinear Boltzmann equation. This may be understood in a qualitative way by the fact that the density of the gas decays as a function of time, so that the packing fraction (which is the total volume occupied by the particles divided by the total volume of the system) decreases, and the role played by correlations (re-collisions) becomes neglectible. The Boltzmann equation thus becomes relevant at late times. With this phenomenology in mind, we conjecture that in the case of probabilistic ballistic annihilation, the Boltzmann equation adequately describes the dynamics for $p > 0$. For $p = 0$, the resulting elastic hard sphere system would be correctly described by Boltzmann's equation in the low density regime only [56, 95].

The second part of the chapter (Sec. 4.4 and below) reports on the hydrodynamic description of the system. The hydrodynamic description of a low density gas of elastic hard spheres supported by an underlying kinetic theory has attracted a lot of attention already more than 40 years ago [7, 96, 97]. It has now become a well established description [20]. A key ingredient in the hydrodynamic approach is the existence of collisional invariants (quantities conserved by the collisions). The question of the relevance of a coarse-grained hydrodynamic approach is therefore more problematic when the kinetic energy is no longer a collisional invariant [98]. This is the case of rapid granular flows (that may be modeled by inelastic hard spheres in a first approach), where the hydrodynamic picture, despite including a hydrodynamic field associated with the kinetic energy density, is nevertheless reliable (see, e.g., [78, 99, 100, 101] and Dufty for a review [48]). It seems natural to test hydrodynamic-like approaches further and in more extreme conditions, and investigate a system where particles react so that there exist *no collisional invariants*. This chapter, focusing on the derivation of the hydrodynamic description for such a system, is a first step in this direction.

Our starting point will be the Boltzmann equation, which describes correctly the low density limit of granular gases (see [102] and [56, 95] for the elastic case). For annihilation dynamics, the ratio of particle diameter to mean free path vanishes in the long-time limit, such that for $d > 1$ the Boltzmann equation is valid at least at late times [39, 40]. For such a dynamics, none of the standard hydrodynamic fields (i.e., mass, momentum, and energy) is associated with a conserved quantity. There are therefore three nonzero decay rates, one for each field. Numerical evidences show that in the long time limit, a non-Maxwellian scaling solution for the homogeneous system appears (homogeneous cooling state HCS [39, 70], which also exists for inelastic hard spheres [51]). Nothing is known about the stability of the latter solution, the only existing result being that in one dimension, with a bimodal initial velocity distribution, clusters of particles are spontaneously formed by the dynamics [65]. In view of this situation we develop a hydrodynamic description for probabilistic ballistic annihilation. The limiting case of vanishing annihilation probability $p \to 0$ gives the known results for elastic dilute gases [24], whereas the other limit $p \to 1$ yields the case of pure annihilation.

In order to derive the hydrodynamic equations, we make use of the Chapman-Enskog method. We thus consider (at least) two distinct time scales in the system. The microscopic time scale is characterized by the average collision time and the corresponding length scale defined by the mean free path. The macroscopic time scale is characterized by the typical time of evolution of the hydrodynamic fields and their inhomogeneities. The fact that those two time scales are very different implies that on the microscopic time scale the hydrodynamic fields vary only slightly. Therefore they are on such length- and time scales only very weakly inhomogeneous. Combined with the existence of a normal solution for the velocity distribution function (i.e., a solution such that all time dependence may be expressed through the hydrodynamic fields), this allows for a series expansion in orders of the gradients, i.e., to apply the Chapman-Enskog method. The knowledge of the hydrodynamic equations thus obtained to first order allows us to perform a stability analysis. Taking the HCS as a reference state, we study the corresponding small spatial deviations of the hydrodynamic fields.

The chapter is organized as follows: in Sec. 4.3.1, we first introduce the Boltzmann kinetic equation describing the probabilistic annihilation dynamics of a *homogeneous* system in the scaling regime, that corresponds to asymptotically large times. We then provide analytical expressions for the exponents $\xi$ and $\gamma$ governing the algebraic time decay of the particle density and the root mean-square-velocity respectively. Next, we give the first non-Gaussian correction $a_2$ to the rescaled velocity distribution by means of a Sonine polynomial expansion. This allows to give explicit expressions for the exponents $\xi$ and $\gamma$ up to the first correction in $a_2$. Sect. 4.3.2 shows the results of direct Monte-Carlo simulations (DSMC) that are in very good agreement with the analytical results. In the insight of those simulations we clarify the ambiguities following from the analytical computation of $a_2$ [75] and select the simplest and most accurate relation for $a_2$. It is numerically shown that unlike for pure annihilation, the first Sonine correction for $0 < p < 1$ does not depend on the parameter $\mu$ characterizing the initial distribution $f$ for small velocities: $\lim_{|\mathbf{v}|\to 0} f(\mathbf{v}; t=0) \propto |\mathbf{v}|^{\mu}$. We also show analytical and numerical evidence that the conjecture put forward in [70] according to which the exponent $\xi = 4d/(4d+1)$ becomes exact in the limiting case $p \to 0^+$ [70]. Sect. 4.3.3 contains conclusions concerning the first part of the chapter. In Section 4.4.1 we present the *inhomogeneous* Boltzmann equation for probabilistic ballistic annihilation, and establish the subsequent balance equations. Section 4.4.2 is devoted to the Chapman-Enskog solution of the balance equations. For this purpose we consider an expansion of the latter equations in a small formal parameter. The solution to zeroth order provides the hydrodynamic fields of the HCS. Assuming small spatial inhomogeneities, we make use of an explicit normal solution for the velocity distribution function to first order. This allows us to establish the expression for the transport coefficients and for the decay rates to first order, and thus the closed set of equations for the hydrodynamic fields. The technical aspects of the derivations are presented in the appendices while our main results are gathered in Eqs. (4.72). In Section 4.4.3, we study the linear stability of those equations around the HCS. Finally, Section 4.4.4 contains the discussion of the results and our conclusions. Since from the point of view of dissipation probabilistic ballistic annihilation shares some features with granular gases, making several parallels between those two systems will prove to be instructive.

## 4.3 The first Sonine correction

### 4.3.1 Boltzmann kinetic equation

#### 4.3.1.1 Scaling regime

We consider a system made of spheres of diameter $\sigma$ moving ballistically in $d$-dimensional space. If two particles touch each other, they annihilate with probability $p$ and thus disappear from the system. With probability $1-p$, they undergo an elastic collision. We consider only two body collisions. The initial spatial distribution of particles is supposed to be and assumed to remain homogeneous. The Boltzmann equation for the instantaneous one particle distribution function $f(\mathbf{v};t)$ of a homogeneous free of forcing low-density system of hard-spheres annihilating with probability $p$ is given by

$$\partial_t f(\mathbf{v}_1;t) = pJ_a[f,f] + (1-p)J_c[f,f], \tag{4.1}$$

where the annihilation operator $J_a$ is defined by [39]

$$\begin{aligned} J_a[f,g] &= -\sigma^{d-1}\int_{\mathbb{R}^d}\mathrm{d}\mathbf{v}_2\int \mathrm{d}\widehat{\boldsymbol{\sigma}}\,\theta\left(\widehat{\boldsymbol{\sigma}}\cdot\widehat{\mathbf{v}}_{12}\right)\left(\widehat{\boldsymbol{\sigma}}\cdot\mathbf{v}_{12}\right) f(\mathbf{v}_2;t)g(\mathbf{v}_1;t) \\ &= -\sigma^{d-1}\beta_1\int_{\mathbb{R}^d}\mathrm{d}\mathbf{v}_2\, v_{12} f(\mathbf{v}_2;t)g(\mathbf{v}_1;t), \end{aligned} \tag{4.2}$$

and the elastic collision operator $J_c$ is defined by [103, 95, 102]

$$J_c[f,g] = \sigma^{d-1} \int_{\mathbb{R}^d} \mathrm{d}\mathbf{v}_2 \int \mathrm{d}\widehat{\boldsymbol{\sigma}}\, (\widehat{\boldsymbol{\sigma}} \cdot \mathbf{v}_{12}) \theta(\widehat{\boldsymbol{\sigma}} \cdot \mathbf{v}_{12}) (b^{-1} - 1) g(\mathbf{v}_1; t) f(\mathbf{v}_2; t). \tag{4.3}$$

Note that Eq. (4.3) is obtained from Eq. (3.2) in the elastic limit $\alpha \to 1$. In the above expressions, $\sigma$ is the diameter of the particles, $\mathbf{v}_{12} = \mathbf{v}_1 - \mathbf{v}_2$ the relative velocity, $v_{12} = |\mathbf{v}_{12}|$, $\theta$ is the Heaviside distribution, $\widehat{\boldsymbol{\sigma}}$ a unit vector joining the centers of two particles at collision and the corresponding integral is running over the solid angle,

$$\beta_1 = \pi^{(d-1)/2} / \Gamma[(d+1)/2] \tag{4.4}$$

is a particular case of Eq. (2.4), where $\Gamma$ is the gamma function, and $b^{-1}$ an operator acting on the velocities as follows [104]:

$$b^{-1}\mathbf{v}_{12} = \mathbf{v}_{12} - 2(\mathbf{v}_{12} \cdot \widehat{\boldsymbol{\sigma}})\widehat{\boldsymbol{\sigma}}, \tag{4.5a}$$

$$b^{-1}\mathbf{v}_1 = \mathbf{v}_1 - (\mathbf{v}_{12} \cdot \widehat{\boldsymbol{\sigma}})\widehat{\boldsymbol{\sigma}}. \tag{4.5b}$$

Eqs. (4.5) follow from Eqs. (3.3) in the elastic limit. Since $J_c$ describes elastic collisions, this operator conserves the mass, momentum, and energy. On the other hand, $J_a$ describes the annihilation process and thus none of the previous quantities are conserved.

We are searching for an isotropic scaling solution of the homogeneous system, where the time dependence of the distribution function is absorbed into the particles density $n(t)$ and in the typical velocity $\overline{v}(t) = \sqrt{2\langle v^2 \rangle / d}$, where $\langle v^2 \rangle$ is the mean squared velocity. This imposes the scaling form [39, 37]

$$f(\mathbf{v}; t) = \frac{n(t)}{\overline{v}^d(t)} \widetilde{f}(c), \tag{4.6}$$

where the rescaled velocity is given by $c = v/\overline{v}(t)$. By construction, $\int \widetilde{f} = 1$. For both the elastic ($p = 0$) and pure annihilation ($p = 1$) cases the form (4.6) was shown to be an adequate solution [39, 37]. It is therefore expected to remain adequate for arbitrary $p \in [0, 1]$.

#### 4.3.1.2 Decay exponents in the scaling regime

Making use of Eq. (4.6) and integrating Eq. (4.1) over $\mathbf{v}_1$ with weights 1 and $v_1^2$, we obtain the number density and energy time evolution

$$\frac{\mathrm{d}n}{\mathrm{d}t} = -p\omega(t)n, \tag{4.7a}$$

$$\frac{\mathrm{d}(n\overline{v}^2)}{\mathrm{d}t} = -p\alpha_e\omega(t)n\overline{v}^2, \tag{4.7b}$$

where the collision frequency $\omega$ is given by

$$\omega(t) = n(t)\overline{v}(t)\sigma^{d-1} \int \mathrm{d}\mathbf{c}_1 \mathrm{d}\mathbf{c}_2 \mathrm{d}\widehat{\boldsymbol{\sigma}}\; (\widehat{\boldsymbol{\sigma}} \cdot \mathbf{c}_{12})\, \theta\, (\widehat{\boldsymbol{\sigma}} \cdot \mathbf{c}_{12})\, \widetilde{f}(c_1) \widetilde{f}(c_2), \tag{4.8}$$

and the time-independent energy dissipation parameter $\alpha_e$ by

$$\alpha_e = \frac{\int \mathrm{d}\mathbf{c}_1 \mathrm{d}\mathbf{c}_2 \mathrm{d}\widehat{\boldsymbol{\sigma}}\ (\widehat{\boldsymbol{\sigma}} \cdot \mathbf{c}_{12})\, \theta\, (\widehat{\boldsymbol{\sigma}} \cdot \mathbf{c}_{12})\, c_1^2 \widetilde{f}(c_1) \widetilde{f}(c_2)}{\left[\int \mathrm{d}\mathbf{c} c^2 \widetilde{f}(c)\right] \left[\int \mathrm{d}\mathbf{c}_1 \mathrm{d}\mathbf{c}_2 \mathrm{d}\widehat{\boldsymbol{\sigma}}\ (\widehat{\boldsymbol{\sigma}} \cdot \mathbf{c}_{12})\, \theta\, (\widehat{\boldsymbol{\sigma}} \cdot \mathbf{c}_{12})\, \widetilde{f}(c_1) \widetilde{f}(c_2)\right]}. \tag{4.9}$$

The time dependence of $\omega(t)$ occurs only through $n(t)\overline{v}(t)$. We made use of the fact that the elastic dynamics does not contribute to the decay of energy or density, thus the integration over the elastic collision term vanishes. The resolution of Eqs. (4.7) follows the method of Ref. [39]. We define the variable $\mathcal{C}$ counting the number of collisions, such that $\mathrm{d}\mathcal{C} = \omega \mathrm{d}t$. With this variable, the integration of the system (4.7) is straightforward and gives

$$n(t) = n_0 \exp[-p\mathcal{C}(t)], \tag{4.10a}$$

$$\overline{v}^2(t) = \overline{v}_0^2 \exp[-p(\alpha_e - 1)\mathcal{C}(t)]. \tag{4.10b}$$

From the definition of $\mathcal{C}(t)$ and Eq. (4.8)

$$\frac{\mathrm{d}\mathcal{C}}{\mathrm{d}t} = \omega = \omega_0 \frac{n(t)\overline{v}(t)}{n_0 \overline{v}}, \tag{4.11}$$

where $\omega_0 = \omega(t = 0)$. Making use of Eqs. (4.10) one obtains

$$\frac{\mathrm{d}\mathcal{C}}{\mathrm{d}t} = \omega_0 \exp\left[-p\frac{1+\alpha_e}{2}\mathcal{C}(t)\right], \tag{4.12}$$

which upon integration yields

$$\mathcal{C}(t) = \frac{1}{p}\frac{2}{1+\alpha_e} \ln\left(1 + p\frac{1+\alpha_e}{2}\omega_0 t\right). \tag{4.13}$$

The time evolution of $n(t)$ and $\overline{v}(t)$ is therefore

$$\frac{n}{n_0} = \left(1 + p\frac{1+\alpha_e}{2}\omega_0 t\right)^{-2/(1+\alpha_e)}, \tag{4.14a}$$

$$\frac{\overline{v}}{\overline{v}_0} = \left(1 + p\frac{1+\alpha_e}{2}\omega_0 t\right)^{(1-\alpha_e)/(1+\alpha_e)}, \tag{4.14b}$$

where $\omega_0 = \omega(t = 0)$ and $\overline{v}_0 = \overline{v}(t = 0)$. Note that Eqs. (4.14) are still valid for the non factorized two-point distributions [39]. We conclude from this result that the dynamics are up to the time rescaling $t \to t/p$ (and importantly up to the numerical value of $\alpha_e$) the same as the ones obtained for pure annihilation [39]. The decay exponents are given by $n(t) \propto t^{-\xi}$ and $\overline{v}(t) \propto t^{-\gamma}$, with

$$\xi = \frac{2}{1+\alpha_e}, \tag{4.15a}$$

$$\gamma = \frac{\alpha_e - 1}{\alpha_e + 1}. \tag{4.15b}$$

The scaling exponents consequently satisfy the constraint $\xi + \gamma = 1$.

#### 4.3.1.3 Rescaled kinetic equation

Inserting the scaling form (4.6) in Eq. (4.1) and making use of Eqs. (4.14), we obtain (see App. A.3)

$$\langle c_{12}\rangle \left[1+\frac{1-\alpha_e}{2}\left(d+c_1\frac{\mathrm{d}}{\mathrm{d}c_1}\right)\right]\widetilde{f}(c_1) \\ = \widetilde{f}(c_1)\int_{\mathbb{R}^d}\mathrm{d}\mathbf{c}_2\,|c_{12}|\widetilde{f}(c_2)-\frac{1-p}{p}\frac{1}{\beta_1}\widetilde{I}(\widetilde{f},\widetilde{f}), \quad (4.16)$$

where

$$\widetilde{I}[\widetilde{f},\widetilde{f}]=\int_{\mathbb{R}^d}\mathrm{d}\mathbf{c}_2\int \mathrm{d}\widehat{\boldsymbol{\sigma}}\,\theta(\widehat{\boldsymbol{\sigma}}\cdot\widehat{\mathbf{c}}_{12})(\widehat{\boldsymbol{\sigma}}\cdot\mathbf{c}_{12})\left[\widetilde{f}(c_1')\widetilde{f}(c_2')-\widetilde{f}(c_1)\widetilde{f}(c_2)\right] \quad (4.17)$$

and $\beta_1$ is given by Eq. (4.4). In equation (4.16), the angular brackets denote average with weight $\widetilde{f}$: for a given function $q(\mathbf{c}_1,\mathbf{c}_2)$

$$\langle q\rangle = \int \mathrm{d}\mathbf{c}_1\mathrm{d}\mathbf{c}_2\,q(\mathbf{c}_1,\mathbf{c}_2)\,\widetilde{f}(\mathbf{c}_1)\widetilde{f}\mathbf{c}_2) \quad (4.18)$$

Making use of the identity [37]

$$\int_{\mathbb{R}^d}\mathrm{d}\mathbf{c}\,c^k\left(d+c\frac{\mathrm{d}}{\mathrm{d}c}\right)\widetilde{f}(c)=-k\langle c^k\rangle, \quad (4.19)$$

and integrating Eq. (4.16) over $\mathbf{c}_1$ with weight $c_1^k$, one obtains

$$\alpha_e=1+\frac{2}{k}\left(\frac{\langle c_{12}c_1^k\rangle}{\langle c_{12}\rangle\langle c_1^k\rangle}-1\right)+\frac{1-p}{p}\frac{2}{k\beta_1}\frac{\mu_k}{\langle c_{12}\rangle\langle c_1^k\rangle}, \qquad \forall k\geqslant 0, \quad (4.20)$$

where $\mu_k = -\int_{\mathbb{R}^d}\mathrm{d}\mathbf{c}_1 c_1^k\widetilde{I}(\widetilde{f},\widetilde{f})$ and from Eq. (4.9) $\alpha_e = \langle c_{12}c_1^2\rangle/(\langle c_{12}\rangle\langle c_1^2\rangle)$ is the energy dissipation parameter.

#### 4.3.1.4 First non-Gaussian correction

The solution of the Boltzmann equation for pure annihilation dynamics ($p = 1$) is non Gaussian in several aspects. The tail of the distribution is overpopulated [39], and deviations from the Gaussian behavior may also be observed near to the velocity origin [39, 70]. It is thus reasonable to think that the velocity distribution function obtained upon solving Eq. (4.16) will show similar deviations. To study the correction close to the origin, it is convenient to apply a Sonine expansion for the distribution function $\widetilde{f}(c)$ [87]

$$\widetilde{f}(c)=\widetilde{\mathcal{M}}(c)\left[1+\sum_{i\geqslant 1}a_iS_i(c^2)\right], \quad (4.21)$$

where $\widetilde{\mathcal{M}}(c)=\pi^{-d/2}\exp(-c^2)$ is the Maxwellian, and $S_i(c^2)$ the Sonine polynomials. Due to the constraint $\langle c^2\rangle = d/2$, the first correction $a_1$ vanishes [37]. For our purposes, it is sufficient to push the truncation of expression (4.21) to second order, where $S_2(x) = x^2/2 - (d+2)x/2 + d(d+2)/8$. In order to compute $\alpha$ and $a_2$, one may follow the method used for inelastic granular gases in Ref. [37]: we may use the hierarchy (4.20) for $k = 2$ and $k = 4$ to obtain a system of two equations for the two unknowns $\alpha_e$ and $a_2$. The calculations are however tedious and it appears useful to consider the alternative method that consists in invoking the limit of vanishing velocities of Eq. (2.3) [39]. Indeed, since we expect that the tail of the exact solution for the distribution function differs significantly from $\widetilde{\mathcal{M}}(c)[1 + \sum_{i\geqslant 1} a_i S_i(c^2)]$, the computation of low order moments of $\widetilde{f}$ should give a more accurate result. From Eq. (4.16)

$$\langle c_{12}\rangle \left[1 + d\frac{1-\alpha_e}{2}\right] \widetilde{f}(0) = \widetilde{f}(0)\langle c_1\rangle - \frac{1-p}{p}\frac{1}{\beta_1}\lim_{c_1\to 0} \widetilde{I}[\widetilde{f},\widetilde{f}]. \tag{4.22}$$

We see that the limit in Eq. (4.22) involves moments of a lower order than $\mu_4$. Neglecting the corrections $a_i$, $i \geqslant 3$, the computation of the latter limit is obtained from the elastic limit of the result in App. A.2:

$$\lim_{c_1\to 0} \widetilde{I}[\widetilde{f},\widetilde{f}] = \frac{\mathcal{S}_d\widetilde{\mathcal{M}}(0)}{2\sqrt{\pi}} \left[\frac{1-d}{2}a_2 + \frac{d(d+2)}{16}a_2^2 + \mathcal{O}(a_2^3)\right], \tag{4.23}$$

where $\mathcal{S}_d = 2\pi^{d/2}/\Gamma(d/2)$ is the surface of the $d$-dimensional sphere. Inserting Eq. (4.23) in Eq. (4.22), one obtains a relation between $\alpha_e$ and $a_2$ that is supplemented with that corresponding to $k = 2$ in (4.20), in order to finally obtain $\alpha_e$ and $a_2$. To this end, we make use of the various relations between moments of the velocity distribution and the fourth cumulant $a_2$ derived in [39]. To linear order in $a_2$, the corresponding system reads

$$\alpha_e = 1 + \frac{2}{d}\left(1 - \frac{\sqrt{2}}{2}\right) + a_2\frac{\sqrt{2}}{2d}\left[\frac{1}{8} - \frac{1-p}{p}(d-1)\right]. \tag{4.24}$$

$$\alpha_e = \frac{\langle c_{12}c_1^2\rangle}{\langle c_{12}\rangle\langle c_1^2\rangle} = 1 + \frac{1}{2d} + a_2\frac{1}{8}\left(2 + \frac{3}{d}\right) + \mathcal{O}(a_2^2), \tag{4.25}$$

where use have been made of the relation $\mu_2 = 0$ (the elastic shocks conserve the total kinetic energy of the colliding pairs), which consequently eliminates $p$ in the second relation. However, as it was shown in previous works [75, 79], there are some ambiguities arising from the linearization procedure, that may affect $a_2$ if this quantity is not small enough. We have thus solved the full nonlinear problem, and then in order to have a simpler expression of $a_2$, chosen the linearizing scheme that yields the closest result (the difference does not exceed 10%) to the nonlinear solution. It turns out as well that this scheme is the closest one to the numerical simulations of Sect. 4.3.2. This correction is given by:

$$a_2(p) = 8\frac{3 - 2\sqrt{2}}{4d + 6 - \sqrt{2} + \frac{1-p}{p}8\sqrt{2}(d-1)}. \tag{4.26}$$

In the limiting case of pure annihilation $p \to 1$, one recovers the result of Ref. [39].

Inserting this result into the definition Eqs. (4.15), we obtain the decay exponents $\xi$ and $\gamma = 1 - \xi$. In the limit $p \to 0^+$, we note that $a_2$ vanishes, as may have been anticipated: the velocity distribution then becomes close to its elastic Maxwellian counterpart that holds for $p = 0$. In this limit, the decay exponent is $\xi = 4d/(4d+1)$, as conjectured in [70]. We emphasize that the limit $p \to 0$ is singular: $\xi$ is bounded from above by $4d/(4d+1)$ for any $p > 0$, whereas $\xi$ vanishes for $p = 0$. It is therefore important to exclude $p = 0$ from the limit of small annihilation probabilities $p$ in order to get well behaved limiting expressions.

### 4.3.2 Simulation results

We implement a direct Monte-Carlo simulation (DSMC) scheme in order to solve the Boltzmann equation. The algorithm may briefly be described as follows. We choose at random two different particles $\{i, j\}$. If their velocity is such that $\omega = \mathbf{v}_{ij} \cdot \widehat{\boldsymbol{\sigma}} > 0$, they may collide. Time is subsequently increased by $(N^2\omega)^{-1}$, where $N$ is the number of remaining particles. With probability $p$ the two particles are then removed from the system, and with probability $1 - p$ their velocity is modified according to Eqs. (4.5). For more details on the method see [39, 88, 89, 105, 106]. As the number of particles decreases, the statistics at late times suffers from enhanced noise. It is thus necessary to average over many independent realizations.

In dimension one, the dynamics of annihilation creates strong correlations between particles [63, 64]. This precludes a Boltzmann approach that relies on the molecular chaos assumption. We will thus focus on numerical simulations of two-dimensional systems, and we expect the role of correlations to diminish when the dimensionality increases.

#### 4.3.2.1 First Sonine correction

Making use of the relation between $a_2$ and the fourth cumulant of the rescaled velocity distribution [79]

$$a_2 = \frac{4}{d(d+2)}\langle c^4 \rangle - 1, \tag{4.27}$$

we show in Fig. 4.1 the numerical values of the first Sonine correction $a_2$ for different values of $p$. The agreement with Eq. (4.26) is good in most cases.

It turns out that the discrepancy between Eq. (4.26) and DSMC is mainly due to the limit method of computing $a_2$. This method yields a very precise distribution $\widetilde{f}$ in the relevant region of interest in the framework of a Sonine polynomial expansion, namely the small velocity region. On the other hand, it is less accurate in the less interesting high velocity region, hence the discrepancy (see Chap. 3 or [75]).

#### 4.3.2.2 Decay exponents

Plotting the density $n/n_0$ (and the root-mean-squared velocity $\overline{v}/\overline{v}_0$) as a function of time $t$ on a log-log plot gives the decay exponents (see Fig. 4.2).

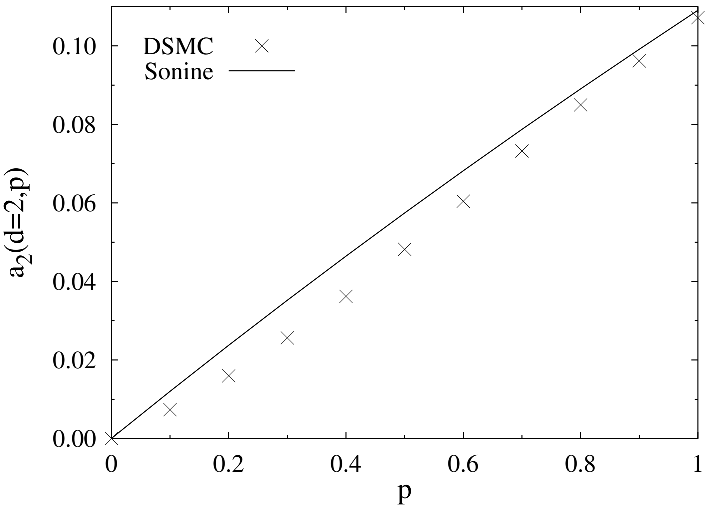


Figure 4.1: First Sonine correction $a_2$ from the analytical estimate (4.26) and from DSMC as a function of the annihilation probability, for $d = 2$. The initial number of particles is $5 \times 10^6$, and each value is obtained from approximately $10^4$ independent runs. The results are not sensitive to the initial velocity distribution. However, the convergence process is much faster starting from a Gaussian distribution.

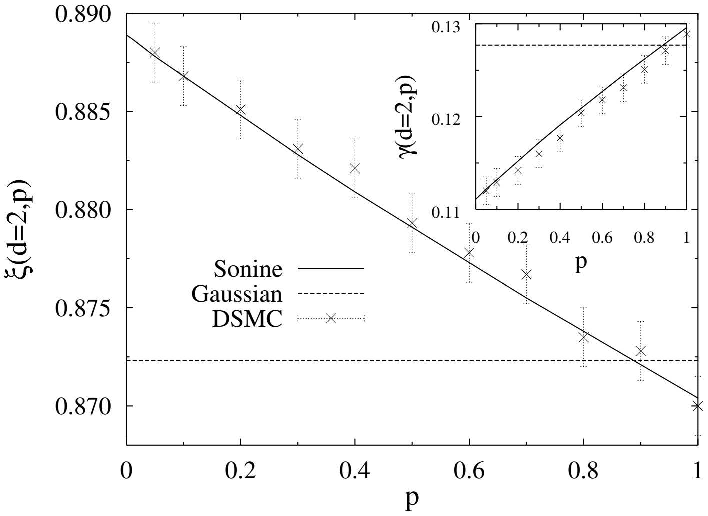


Figure 4.2: The decay exponents $\xi$ and $\gamma$ (inset) in two dimensions, obtained analytically from Eqs. (4.24) and (4.25) that are inserted in Eq. (4.15), and from DSMC (symbols). The initial number of particles is $5 \times 10^6$, and the number of independent runs approximately 100. The values of the exponents are not very sensitive to the probability $p$. The horizontal line shows the Maxwellian analytical prediction to zeroth order in $a_2$, i.e., $\xi$ and $\gamma$ from (4.24) and (4.15) with $a_2 = 0$.

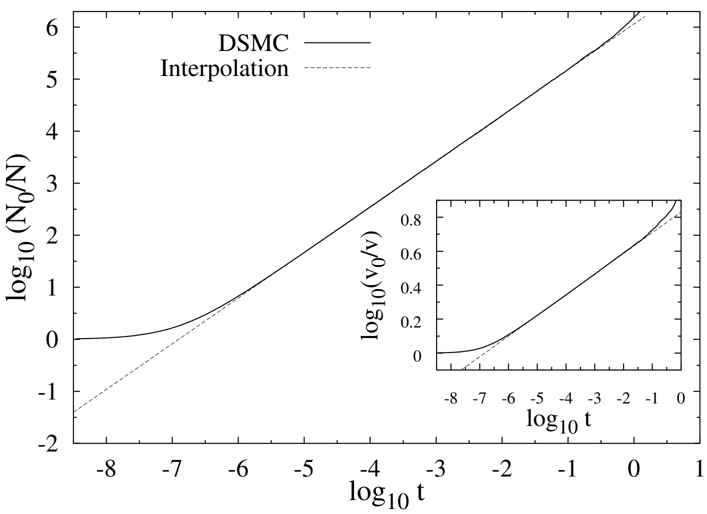


Figure 4.3: The time dependence in two dimensions of $n$ and $\overline{v}$ (inset) on a logarithmic scale for $p = 0.6$ and a Gaussian initial velocity distribution, showing a clear power law behavior. The straight line is the linear interpolation giving the decay exponent. $N_0$ ($N$) is the initial (remaining) number of particles. We have denoted $v_0$ the initial root-mean-square velocity $\overline{v}$. The same quantity is denoted $v$ for $t > 0$. The deviation observed for large times is due to the low number of remaining particles.

The numerical results are in agreement with the analytical predictions obtained from the set of Eqs. (4.24) and (4.25) that is inserted in Eq. (4.15). The predicted power-law behavior is observed over several decades, as shown by Fig. 4.3 for $p = 0.5$.

In Fig. 4.4, we show that the scaling relation $\xi + \gamma = 1$ is well obeyed for all values of $p$. Such a relation holds in fact independently of the molecular chaos assumption underlying the Boltzmann equation.

#### 4.3.2.3 Evolution toward the asymptotic distribution

In order to have a more precise understanding and accuracy check of our results, it is useful to study the velocity distribution in the scaling regime. Indeed, the distribution may be adequately described by the Sonine correction $a_2$ at late times only. Before the scaling regime is reached, the velocity distribution $\widetilde{f}(c_1)$ is time-dependent. A very precise check consists in studying the evolution of the non-Gaussianities. To this end, it is useful to consider numerically the quantity $\widetilde{f}(c_i)/\widetilde{\mathcal{M}}(c_i) = 1 + a_2 S_2(c_i)$. Fig. 4.5 shows the evolution of $\widetilde{f}(c_i)/\widetilde{\mathcal{M}}(c_i)$ for different times corresponding to different densities, starting from an initial Gaussian distribution.

It turns out that both methods of computing $a_2$ [directly using its definition in terms of the fourth cumulant (4.27) or using $\widetilde{f}(c_i)/\widetilde{\mathcal{M}}(c_i)$], are fully compatible numerically. However, the latter method requires much more extensive simulations. It is instructive to investigate the evolution toward the asymptotic solution starting

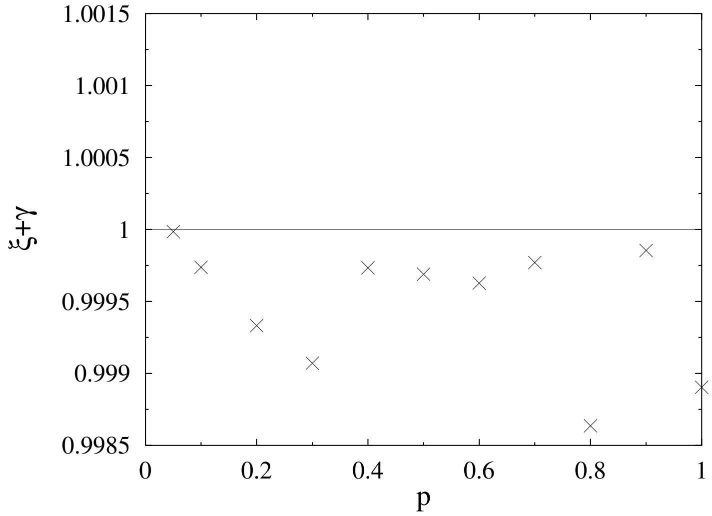


Figure 4.4: Numerical verification of the relation $\xi + \gamma = 1$ in two dimensions for different values of $p$. Note the $y$-scale.

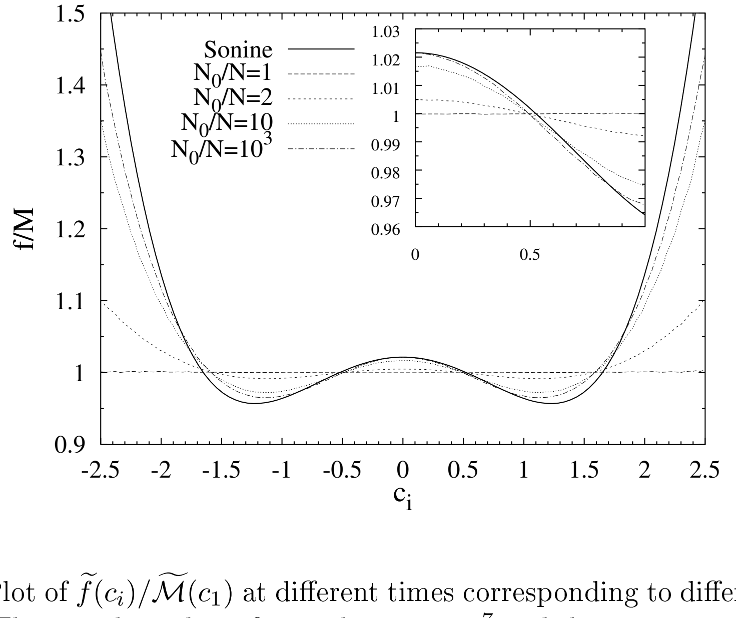


Figure 4.5: Plot of $\widetilde{f}(c_i)/\widetilde{\mathcal{M}}(c_1)$ at different times corresponding to different densities, for $p = 0.5$. The initial number of particles is $2 \times 10^7$ and there are approximately $10^5$ independent runs. The initial distribution is Gaussian and thus corresponds to the flat curve. The continuous curve is the analytical prediction $1 + a_2 S_2$ with $a_2$ given by Eq. (4.26). The inset shows a magnification of the small velocities region.

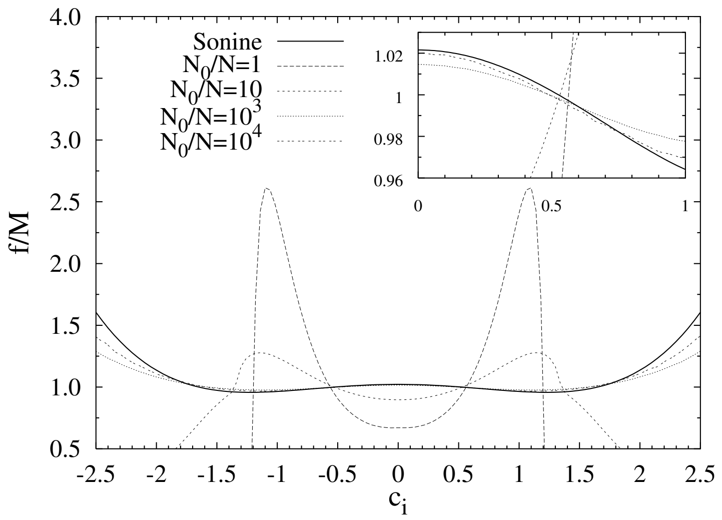


Figure 4.6: Same as Fig. 4.5 but for an initial distribution such that $\mu = 3$.

from different initial distributions, which are characterized by their behavior near the origin. To this extend we define the exponent $\mu$ by the behavior $\widetilde{f}(c) \simeq |c|^\mu$ for $c \to 0$. Fig. 4.6 shows the non-Gaussianities of the evolution towards the scaling function for an initial distribution characterized by $\mu = 3$, and Fig. 4.7 for $\mu = -3/2$. Note that in order that the Boltzmann equation (1.29) is integrable close to the velocity origin, it is required that $\mu + x + d > 0$.

For both initial distributions $\mu = 3$ and $\mu = -3/2$, the solution is attracted toward a scaling function characterized by $\mu = 0$. Hence, there is a qualitative difference between probabilistic annihilation and pure annihilation. Indeed, it was shown in a previous work that for pure annihilation $\mu$ is conserved [70], and more importantly that $\mu$ indexes the "universality classes" of this process (two distributions with the same $\mu$ are characterized by the same long time exponent $\xi$). Obviously, adding the effect of elastic collisions in the dynamics of probabilistic annihilation violates the conservation of $\mu$. Next, the question is to know whether the asymptotic distribution depends on $\mu$ or not. We consequently show in Fig. 4.8 the ratio $\widetilde{f}^{(\mu=0)}(c_1)/\widetilde{f}^{(\mu=3)}(c_1) = [1 + a_2^{(\mu=0)}]/[1 + a_2^{(\mu=3)}]$.

The ratio tends to unity, which implies that $a_2^{(\mu=0)} = a_2^{(\mu=3)}$. Moreover, we checked that for the negative value $\mu = -3/2$, the same conclusion holds. The convergence is however slower due to the divergence of the initial distribution near the velocity origin. We thus conjecture that not only the first Sonine coefficient of probabilistic annihilation but also the full velocity distribution (and hence, all decay exponents) show an universal property in the sense that they do not depend on the initial velocity distribution if $0 < p < 1$. This is a nontrivial result since it was shown that this is not true in the case of pure annihilation $p = 1$ [70].

Finally, in order to clarify the relevance of the scaling function, we studied the fourth cumulant $a_2$ as a function of $N_0/N$, for the same parameters as those in

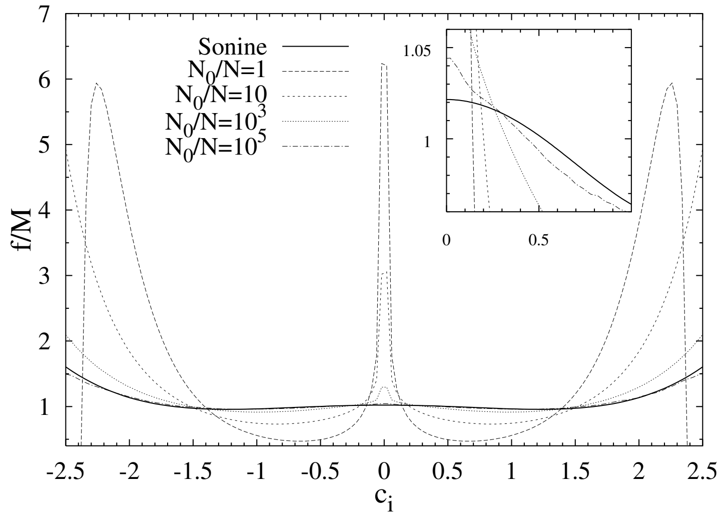


Figure 4.7: Same as Fig. 4.5 but for an initial distribution such that $\mu = -3/2$ and initially $4 \times 10^7$ particles.

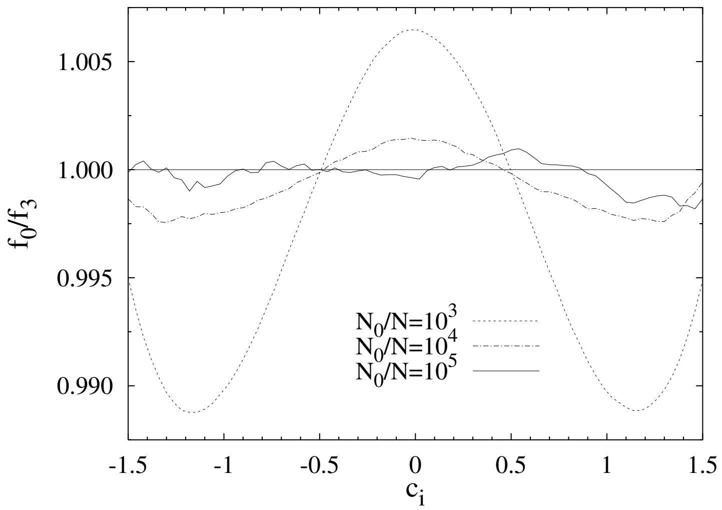


Figure 4.8: Plot of $\widetilde{f}^{(\mu=0)}(c_1)/\widetilde{f}^{(\mu=3)}(c_1)$ for three different times, and $p = 0.5$. We see that for late times the ratio of the two distributions tends to unity, which leads to conjecture that the first Sonine corrections $a_2$ are the same in both cases $\mu = 0$ and $\mu = 3$. The results reported here correspond to particularly extensive simulations (note the vertical scale).

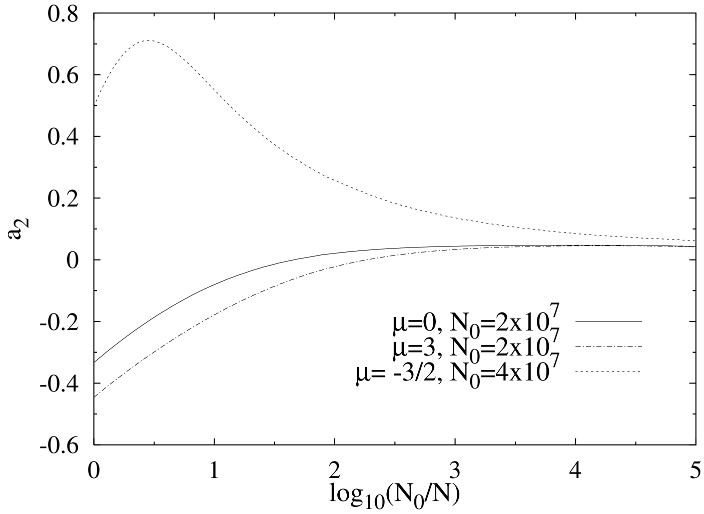


Figure 4.9: Plot of $a_2$ as a function of the densities $N_0/N$ for different values of $\mu$. There are approximately $5 \times 10^4$ independent runs.

Figs. 4.5-4.7. The result is shown in Fig. 4.9. The fact that $a_2$ reaches a plateau indicates that the system enters a scaling regime at late times. For $\mu = -3/2$ (Fig. 4.7), due to the initial central peak, the initial distribution is extremely different from its late time asymptotic counterpart, so that the transient evolution takes longer and the plateau regime is only approached. Finally, it may be observed in Fig. 4.9 that for the 3 initial conditions the fourth cumulants converge to the same value. This is a further illustration of the universal behaviour discussed above.

### 4.3.3 Summary of the section

We gave empirical arguments for the relevance of the Boltzmann description for probabilistic ballistic annihilation in dimensions greater than one. We obtained analytically the decay exponents of the density of particles and of the root-mean-squared velocity in terms of the energy dissipation parameter $\alpha$. It turns out that upon rescaling time according to $t \to t/p$, $p > 0$, the formal structure of the decay equations is the same as in the case of pure annihilation $p = 1$.

In the scaling regime (that emerges in the long time limit), the first Sonine correction $a_2$ to the Maxwellian distribution was obtained as a function of the continuous parameter $p$. This allows to establish an explicit relation for the decay exponents. We have shown that in the limit $p \to 0^+$, the exponent $\xi$ governing the decay of particles, $n(t) \propto t^{-\xi}$, is given by $\xi = 4d/(4d + 1)$, thereby confirming a conjecture put forward in [70].

Numerical simulations (DSMC) in two dimensions are in agreement with the analytical correction $a_2(p)$. Moreover, the analytical values for the decay exponents obtained from the first correction $a_2$ are in good agreement as well with numerics.

The relation $\xi+\gamma=1$ was shown to hold for all values of $p$. The study of the dynamics of non-Gaussianities embodied in $a_2 S_2$ reveals a qualitative difference with pure annihilation dynamics: the parameter $\mu$ describing the small velocity behavior of the rescaled distribution is not conserved for probabilistic annihilation when $0<p<1$. Numerical results for different values of $\mu$ leads to conjecture the universality of the rescaled velocity distribution in this process (this universality being lost for pure annihilation only, i.e., for $p=1$).

## 4.4 The hydrodynamic description

Since the notations in this section are quite involved, Appendix A.4 contains a summary of the notations used.

We now consider a local inhomogeneity of the distribution functions.[1] Thus the Boltzmann equation (4.1) now reads

$$(\partial_t + \mathbf{v}_1 \cdot \boldsymbol{\nabla}) f(\mathbf{r}, \mathbf{v}_1; t) = p J_a[f,f] + (1-p) J_c[f,f], \tag{4.28}$$

where the annihilation operator $J_a$ is defined by [39]

$$J_a[f,g] = -\sigma^{d-1}\beta_1 \int_{\mathbb{R}^d} \mathrm{d}\mathbf{v}_2\, v_{12} f(\mathbf{r},\mathbf{v}_2;t) g(\mathbf{r},\mathbf{v}_1;t), \tag{4.29}$$

where $\beta_1$ is given by Eq. (4.4) and the elastic collision operator $J_c$ is defined by [103, 95, 102]

$$J_c[f,g] = \sigma^{d-1} \int_{\mathbb{R}^d} \mathrm{d}\mathbf{v}_2 \int \mathrm{d}\widehat{\boldsymbol{\sigma}}\, (\widehat{\boldsymbol{\sigma}} \cdot \mathbf{v}_{12}) \theta(\widehat{\boldsymbol{\sigma}} \cdot \mathbf{v}_{12}) (b^{-1} - 1) g(\mathbf{r},\mathbf{v}_1;t) f(\mathbf{r},\mathbf{v}_2;t). \tag{4.30}$$

### 4.4.1 Balance equations

In order to write hydrodynamic equations, we need to define the following local hydrodynamic fields:

$$n(\mathbf{r},t) = \int_{\mathbb{R}^d} \mathrm{d}\mathbf{v}\, f(\mathbf{r},\mathbf{v};t), \tag{4.31a}$$

$$\mathbf{u}(\mathbf{r},t) = \frac{1}{n(\mathbf{r},t)} \int_{\mathbb{R}^d} \mathrm{d}\mathbf{v}\, \mathbf{v} f(\mathbf{r},\mathbf{v};t), \tag{4.31b}$$

$$T(\mathbf{r},t) = \frac{m}{n(\mathbf{r},t) k_B d} \int_{\mathbb{R}^d} \mathrm{d}\mathbf{v}\, \mathbf{V}^2 f(\mathbf{r},\mathbf{v};t), \tag{4.31c}$$

where $n(\mathbf{r},t)$, $\mathbf{u}(\mathbf{r},t)$, and $T(\mathbf{r},t)$ are the local number density, velocity, and temperature, respectively. The definition of the temperature follows from the principle of equipartition of energy. In Eq. (4.31c), $k_B$ is the Boltzmann constant and $\mathbf{V} = \mathbf{v} - \mathbf{u}(\mathbf{r},t)$ is the deviation from the mean flow velocity. The balance equations

[1] The calculations of this section may be found in even more details in [107].

follow from integrating the moments 1, $m\mathbf{v}$, and $mv^2/2$ with weight given by the Boltzmann equation (4.28). We thus obtain (see App. A.5)

$$\partial_t n + \nabla_i(nu_i) = -p\omega[f,f], \tag{4.32a}$$

$$\partial_t u_i + \frac{1}{mn}\nabla_j P_{ij} + u_j\nabla_j u_i = -p\frac{1}{n}\omega[f,V_i f], \qquad i = 1,\ldots,d, \tag{4.32b}$$

$$\partial_t T + u_j\nabla_j T + \frac{2}{nk_B d}(P_{ij}\nabla_i u_j + \nabla_j q_j) = p\frac{T}{n}\omega[f,f] - p\frac{m}{nk_B d}\omega[f,V^2 f], \tag{4.32c}$$

where we have summation over repeated indices, $\mathbf{u} = (u_1,\ldots,u_d)$, and

$$\omega[f,g] = \sigma^{d-1}\beta_1\int_{\mathbb{R}^{2d}} \mathrm{d}\mathbf{v}_1\mathrm{d}\mathbf{v}_2|\mathbf{v}_{12}|g(\mathbf{r}_1,\mathbf{v}_1;t)f(\mathbf{r}_2,\mathbf{v}_2;t). \tag{4.33}$$

In the balance equations (4.32), the pressure tensor $P_{ij}$ and heat-flux $q_i$ are defined by

$$P_{ij}(\mathbf{r},t) = m\int_{\mathbb{R}^d}\mathrm{d}\mathbf{v}\,V_iV_j f(\mathbf{r},\mathbf{v};t) = \int_{\mathbb{R}^d}\mathrm{d}\mathbf{v}\,f(\mathbf{r},\mathbf{v};t)D_{ij}(\mathbf{V}) + \frac{n}{\beta}\delta_{ij}, \tag{4.34}$$

$$q_i(\mathbf{r},t) = \int_{\mathbb{R}^d} d\mathbf{v}S_i(\mathbf{V})f(\mathbf{r},\mathbf{v};t), \tag{4.35}$$

where

$$D_{ij}(\mathbf{V}) = m\left(V_iV_j - \frac{V^2}{d}\delta_{ij}\right), \tag{4.36}$$

$$S_i(\mathbf{V}) = \left(\frac{m}{2}V^2 - \frac{d+2}{2}k_BT\right)V_i. \tag{4.37}$$

One sees from Eqs. (4.32) that when the annihilation probability $p \to 0$, all quantities are conserved. In addition, the long time solution of the system in this limit is given by the Maxwell distribution [52].

### 4.4.2 Chapman-Enskog solution

In order to solve Eqs. (4.32), it is necessary to obtain a closed set of equations for the hydrodynamic fields. This can be done using the Chapman-Enskog method, by expressing the functional dependence of the pressure tensor $P_{ij}$ and of the heat flux $q_i$ in terms of the hydrodynamic fields. Note that other routes have been developed as well [103, 108]. A thorough comparison of the different approaches seems however to be a difficult attempt [108]. In order to apply the Chapman-Enskog method, it is necessary to make two assumptions. The first one is that all temporal and spatial dependence of the distribution function $f(\mathbf{r},\mathbf{v};t)$ may be expressed as a functional dependence on the hydrodynamic fields:

$$f(\mathbf{r},\mathbf{v};t) = f\left[\mathbf{v}, n(\mathbf{r},t), \mathbf{u}(\mathbf{r},t), T(\mathbf{r},t)\right]. \tag{4.38}$$

What is the physical justification for the existence of such a *normal solution*? Suppose that the variations of the hydrodynamic fields are small on the scale of the mean free path $\ell \simeq 1/(n\sigma^{d-1})$, i.e., $\ell|\boldsymbol{\nabla} \ln n| \ll 1$. Therefore, to first order the functional dependence of the distribution function may be made local in the hydrodynamic fields, leading to the normal solution written above. Note that none of the hydrodynamic fields is associated with a conserved quantity. The theoretical question that arises is to know if the new timescales thereby introduced by the cooling rates are shorter than what is allowed for the existence of a normal solution [48]. For sufficiently small $p$ this should be the case. However, in the related context of granular gases, this point is not yet quantitatively clarified and is still subject to discussions [48, 49, 50]. The justification of the normal solution may be done *a posteriori* by studying the relevance of the results through the appearance of the homogeneous cooling state (HCS) for example [39, 51]. The second assumption is based on the existence of (at least) two distinct timescales. The microscopic timescale is characterized by the average collision time and the spatial length defined by the corresponding mean free path. On the other hand, the macroscopic timescale is defined by a typical timescale describing the evolution of the hydrodynamic fields and their inhomogeneities. The difference in those two timescales implies that on the microscopic timescale the hydrodynamic fields vary only very slightly. Thus, those fields are on such time and space scales only very weakly inhomogeneous. This allows for a series expansion in orders of the gradients of the fields:

$$f = f^{(0)} + \lambda f^{(1)} + \lambda^2 f^{(2)} + \dots, \tag{4.39}$$

where each power of the formal small parameter $\lambda$ means a given order in a spatial gradient. The formal parameter $\lambda$ may be seen as the ratio of the mean free path to the wavelength of the variation of the hydrodynamic fields. This shows again the idea of the separation of both microscopic and macroscopic time and length scales. The Chapman-Enskog method assumes the existence of a timescale hierarchy, and thus of a time derivative hierarchy as well:

$$\frac{\partial}{\partial t} = \frac{\partial^{(0)}}{\partial t} + \lambda \frac{\partial^{(1)}}{\partial t} + \lambda^2 \frac{\partial^{(2)}}{\partial t} + \dots, \tag{4.40}$$

where a given order in the temporal hierarchy (4.40) corresponds to the same order in the spatial hierarchy (4.39). One thus concludes that the higher the order of the spatial gradient, the slower the corresponding temporal variation. Inserting expansions (4.39) and (4.40) in the Boltzmann equation (4.28) one obtains

$$\begin{aligned}\left[\sum_{k\geqslant 0} \lambda^k \frac{\partial^{(k)}}{\partial t} + \mathbf{v}_1 \cdot \boldsymbol{\nabla}\right] \sum_{l\geqslant 0} \lambda^l f^{(l)} \\ = pJ_a \left[\sum_{l\geqslant 0} \lambda^l f^{(l)}, \sum_{l\geqslant 0} \lambda^l f^{(l)}\right] + (1-p) J_c \left[\sum_{l\geqslant 0} \lambda^l f^{(l)}, \sum_{l\geqslant 0} \lambda^l f^{(l)}\right].\end{aligned} \tag{4.41}$$

Collecting the terms of a given order in $\lambda$ and solving the equations order by order allows us to build the Chapman-Enskog solution.

#### 4.4.2.1 Zeroth order

To zeroth order in the gradients, Eq. (4.41) gives

$$\partial_t^{(0)} f^{(0)} = pJ_a[f^{(0)}, f^{(0)}] + (1-p)J_c[f^{(0)}, f^{(0)}]. \tag{4.42}$$

This equation has a solution, describing the HCS, and which obeys the scaling relation

$$f^{(0)}(\mathbf{r}, \mathbf{v}; t) = \frac{n(t)}{v_T(t)^d}\widetilde{f}(c). \tag{4.43}$$

The approximate expression for $\widetilde{f}(c)$ was established in Sec. 4.3.1.4 and is recalled by Eq. (4.65). In Eq. (4.43), $v_T = [2/(\beta m)]^{1/2}$ is the time dependent thermal velocity, where $\beta = 1/(k_B T)$, and $c = V/v_T$, $\mathbf{V} = \mathbf{v} - \mathbf{u}$. The existence of a scaling solution of the form (4.43) seems to be a general feature that is confirmed numerically (direct Monte-Carlo simulations or molecular dynamics) not only for ballistic annihilation [39] or granular gases [41], but for the dynamics of ballistic aggregation as well [109, 110].

The function $f^{(0)}$ is isotropic. Thus to this order the pressure tensor (4.34) becomes $P_{ij}^{(0)} = p^{(0)}\delta_{ij}$, where $p^{(0)} = nk_BT$ is the hydrostatic pressure, and the heat-flux (4.35) becomes $\mathbf{q}^{(0)} = 0$.

The balance equations (4.32) to zeroth order read

$$\partial_t n = -pn\xi_n^{(0)}, \tag{4.44a}$$
$$\partial_t u_i = -pv_T\xi_{u_i}^{(0)}, \qquad i = 1, \ldots, d, \tag{4.44b}$$
$$\partial_t T = -pT\xi_T^{(0)}, \tag{4.44c}$$

where the decay rates are

$$\xi_n^{(0)} = \frac{1}{n}\omega[f^{(0)}, f^{(0)}], \tag{4.45a}$$
$$\xi_{u_i}^{(0)} = \frac{1}{nv_T}\omega[f^{(0)}, V_i f^{(0)}], \qquad i = 1, \ldots, d, \tag{4.45b}$$
$$\xi_T^{(0)} = \frac{m}{nk_BTd}\omega[f^{(0)}, V^2 f^{(0)}] - \frac{1}{n}\omega[f^{(0)}, f^{(0)}], \tag{4.45c}$$

For antisymmetry reasons, one sees from Eq. (4.45b) that $\xi_{u_i}^{(0)} = 0$. The two other decay rates are given later on by Eqs. (4.68).

#### 4.4.2.2 First order

To first order in the gradients, the Boltzmann equation (4.41) reads

$$[\partial_t^{(0)} + J]f^{(1)} = -[\partial_t^{(1)} + \mathbf{v}_1 \cdot \boldsymbol{\nabla}]f^{(0)}, \tag{4.46}$$

where

$$Jf^{(1)} = pL_a[f^{(0)}, f^{(1)}] + (1-p)L_c[f^{(0)}, f^{(1)}], \tag{4.47}$$

with

$$L_a[f^{(0)}, f^{(1)}] = -J_a[f^{(0)}, f^{(1)}] - J_a[f^{(1)}, f^{(0)}], \tag{4.48}$$

$$L_c[f^{(0)}, f^{(1)}] = -J_c[f^{(0)}, f^{(1)}] - J_c[f^{(1)}, f^{(0)}]. \tag{4.49}$$

The balance equations (4.32) to first order become

$$\partial_t^{(1)} n + \nabla_i (n u_i) = -pn\xi_n^{(1)}, \tag{4.50a}$$

$$\partial_t^{(1)} u_i + \frac{k_B}{mn}\nabla_i (nT) + u_j \nabla_j u_i = -p v_T \xi_{u_i}^{(1)}, \qquad i = 1, \ldots, d, \tag{4.50b}$$

$$\partial_t^{(1)} T + u_i \nabla_i T + \frac{2}{d} T \nabla_i u_i = -pT\xi_T^{(1)}, \tag{4.50c}$$

where the decay rates are given by

$$\xi_n^{(1)} = \frac{2}{n}\omega[f^{(0)}, f^{(1)}], \tag{4.51a}$$

$$\xi_{u_i}^{(1)} = \frac{1}{nv_T}\omega[f^{(0)}, V_i f^{(1)}] + \frac{1}{nv_T}\omega[f^{(1)}, V_i f^{(0)}], \qquad i = 1, \ldots, d, \tag{4.51b}$$

$$\xi_T^{(1)} = -\frac{2}{n}\omega[f^{(0)}, f^{(1)}] + \frac{m}{nk_B T d}\omega[f^{(0)}, V^2 f^{(1)}] + \frac{m}{nk_B T d}\omega[f^{(1)}, V^2 f^{(0)}]. \tag{4.51c}$$

By definition we know that $f^{(1)}$ must be of first order in the gradients of the hydrodynamic fields, therefore for a low density gas [57]

$$f^{(1)} = \mathcal{A}_i \nabla_i \ln T + \mathcal{B}_i \nabla_i \ln n + \mathcal{C}_{ij} \nabla_j u_i. \tag{4.52}$$

The coefficients $\mathcal{A}_i$, $\mathcal{B}_i$, and $\mathcal{C}_{ij}$ depend on the fields $n$, $\mathbf{V}$, and $T$. Inserting Eq. (4.52) in Eq. (4.46) and making use of Eqs. (4.38), (4.43), and (4.44) one obtains the following set of equations for $\mathcal{A}_i$, $\mathcal{B}_i$, and $\mathcal{C}_{ij}$ (see Appendix A.6):

$$\left\{-p\left[\xi_T^{(0)} T\partial_T + \xi_n^{(0)} n\partial_n + \tfrac{1}{2}\xi_T^{(0)}\right] + (J - p\Omega)\right\}\mathcal{A}_i - p\tfrac{1}{2}\xi_n^{(0)}\mathcal{B}_i = A_i, \tag{4.53a}$$

$$\left\{-p\left[\xi_T^{(0)} T\partial_T + \xi_n^{(0)} n\partial_n + \xi_T^{(0)}\right] + (J - p\Omega)\right\}\mathcal{B}_i - p\xi_T^{(0)}\mathcal{A}_i = B_i, \tag{4.53b}$$

$$\left\{-p\left[\xi_T^{(0)} T\partial_T + \xi_n^{(0)} n\partial_n\right] + (J - p\Omega)\right\}\mathcal{C}_{ij} = C_{ij}, \tag{4.53c}$$

where

$$A_i = \frac{V_i}{2}\frac{\partial}{\partial V_j}[V_j f^{(0)}] - \frac{k_B T}{m}\frac{\partial f^{(0)}}{\partial V_i}, \tag{4.54a}$$

$$B_i = -V_i f^{(0)} - \frac{k_B T}{m}\frac{\partial f^{(0)}}{\partial V_i}, \tag{4.54b}$$

$$C_{ij} = \frac{\partial}{\partial V_i}[V_j f^{(0)}] - \frac{1}{d}\frac{\partial}{\partial V_k}[V_k f^{(0)}]\delta_{ij}, \tag{4.54c}$$

and $\Omega$ is a linear operator defined by

$$\Omega g = f^{(0)}\xi_n^{(1)}[f^{(0)}, g] - \frac{\partial f^{(0)}}{\partial V_i} v_T \xi_{u_i}^{(1)}[f^0, g] + \frac{\partial f^{(0)}}{\partial T} T\xi_T^{(1)}[f^{(0)}, g], \tag{4.55}$$

where $g$ is either $\mathcal{A}_i$, $\mathcal{B}_i$, or $\mathcal{C}_{ij}$, and the functionals $\xi_n^{(1)}$, $\xi_{u_i}^{(1)}$, and $\xi_T^{(1)}$ are obtained from Eqs. (4.51) upon replacing $f^{(1)}$ by $g$. It is possible to show that from Eqs (4.54) the solubility conditions ensuring the existence of the functions $\mathcal{A}_i$, $\mathcal{B}_i$, and $\mathcal{C}_{ij}$ are satisfied (see App. A.7).

#### 4.4.2.3 Navier-Stokes transport coefficients

The hydrodynamic description of the flow requires the knowledge of transport coefficients. The concern of the present section is to determine the form and coefficients of the constitutive equations. This can thus be achieved by linking those macroscopic transport coefficients with their microscopic definition. Using a first order Sonine polynomial expansion, it is then possible to find explicitly the transport coefficients to first order. This will allow us to express the functions $\mathcal{A}_i$, $\mathcal{B}_i$, and $\mathcal{C}_{ij}$ in terms of the transport coefficients, thus determining the distribution function $f^{(1)}$.

The pressure tensor may be put in the form

$$P_{ij}(\mathbf{r},t) = p^{(0)}\delta_{ij} - \eta\left(\nabla_i u_j + \nabla_j u_i - \frac{2}{d}\delta_{ij}\nabla_k u_k\right) - \zeta\delta_{ij}\nabla_k u_k, \tag{4.56}$$

where $p^{(0)} = nk_BT$ is the ideal gas pressure, and $\eta$ is the shear viscosity. For a low density gas, the bulk viscosity $\zeta$ vanishes therefore the last term in the pressure tensor may be neglected [57, 111, 48]. Fourier's linear law for heat conduction is

$$q_i = -\kappa\nabla_i T - \mu\nabla_i n, \tag{4.57}$$

where $\kappa$ is the thermal conductivity and $\mu$ a transport coefficient that has no analogue in the elastic case. A similar quantity appears for granular gases, which again is non-vanishing in the inelastic case only [24, 112].

The identification of Eq. (4.56) with Eq. (4.34) using the result of the first-order calculation yields

$$P_{ij}^{(1)} = \int_{\mathbb{R}^d} \mathrm{d}\mathbf{v}\, D_{ij}(\mathbf{V}) f^{(1)}. \tag{4.58}$$

Similarly, the identification of Eq. (4.57) with Eq. (4.35) using the first-order calculation leads to

$$q_i^{(1)} = \int_{\mathbb{R}^d} \mathrm{d}\mathbf{v}\, S_i(\mathbf{V}) f^{(1)}. \tag{4.59}$$

The main steps of the calculation are shown in Appendix A.8, and the result is

$$\eta^* = \frac{\eta}{\eta_0} = \frac{1}{\nu_\eta^* - \frac{1}{2}p\xi_T^{(0)*}}, \tag{4.60a}$$

$$\kappa^* = \frac{\kappa}{\kappa_0} = \frac{1}{\nu_\kappa^* - 2p\xi_T^{(0)*}}\left[\frac{1}{2}p\xi_n^{(0)*}\mu^* + \frac{d-1}{d}(2a_2+1)\right], \tag{4.60b}$$

$$\mu^* = \frac{n\mu}{T\kappa_0} = \frac{2}{2\nu_\mu^* - 3p\xi_T^{(0)*} - 2p\xi_n^{(0)*}}\left[p\xi_T^{(0)*}\kappa^* + \frac{d-1}{d}a_2\right], \tag{4.60c}$$

where $a_2$ is the kurtosis of the distribution

$$a_2 = \frac{4}{d(d+2)}\frac{1}{v_T^4 n}\int_{\mathbb{R}^d} \mathrm{d}\mathbf{V}\, f^{(0)}(V) - 1, \tag{4.61}$$

and

$$\kappa_0 = \frac{d(d+2)}{2(d-1)}\frac{k_B}{m}\eta_0, \tag{4.62}$$

$$\eta_0 = \frac{d+2}{8}\frac{\Gamma(d/2)}{\pi^{(d-1)/2}}\frac{\sqrt{mk_BT}}{\sigma^{d-1}}, \tag{4.63}$$

are the thermal conductivity and shear viscosity coefficients for hard-spheres, respectively [5]. $\xi_n^{(0)*} = \xi_n^{(0)}/\nu_0$ and $\xi_T^{(0)*} = \xi_T^{(0)}/\nu_0$ are the dimensionless decay rates, where $\nu_0 = p^{(0)}/\eta_0$, with $p^{(0)} = nk_BT$. The dimensionless coefficients $\nu_\eta^*$, $\nu_\kappa^*$, and $\nu_\mu^*$ are given by

$$\nu_\kappa^* = \frac{1}{\nu_0}\frac{\int_{\mathbb{R}^d}\mathrm{d}\mathbf{V}\, S_i(\mathbf{V})J\mathcal{A}_i}{\int_{\mathbb{R}^d}\mathrm{d}\mathbf{V}\, S_i(\mathbf{V})\mathcal{A}_i} - p\frac{1}{\nu_0}\frac{\int_{\mathbb{R}^d}\mathrm{d}\mathbf{V}\, S_i(\mathbf{V})\Omega\mathcal{A}_i}{\int_{\mathbb{R}^d}\mathrm{d}\mathbf{V}\, S_i(\mathbf{V})\mathcal{A}_i}, \tag{4.64a}$$

$$\nu_\mu^* = \frac{1}{\nu_0}\frac{\int_{\mathbb{R}^d}\mathrm{d}\mathbf{V}\, S_i(\mathbf{V})J\mathcal{B}_i}{\int_{\mathbb{R}^d}\mathrm{d}\mathbf{V}\, S_i(\mathbf{V})\mathcal{B}_i} - p\frac{1}{\nu_0}\frac{\int_{\mathbb{R}^d}\mathrm{d}\mathbf{V}\, S_i(\mathbf{V})\Omega\mathcal{B}_i}{\int_{\mathbb{R}^d}\mathrm{d}\mathbf{V}\, S_i(\mathbf{V})\mathcal{B}_i}, \tag{4.64b}$$

$$\nu_\eta^* = \frac{1}{\nu_0}\frac{\int_{\mathbb{R}^d}\mathrm{d}\mathbf{V}\, D_{ij}(\mathbf{V})J\mathcal{C}_{ij}}{\int_{\mathbb{R}^d}\mathrm{d}\mathbf{V}\, D_{ij}(\mathbf{V})\mathcal{C}_{ij}} - p\frac{1}{\nu_0}\frac{\int_{\mathbb{R}^d}\mathrm{d}\mathbf{V}\, D_{ij}(\mathbf{V})\Omega\mathcal{C}_{ij}}{\int_{\mathbb{R}^d}\mathrm{d}\mathbf{V}\, D_{ij}(\mathbf{V})\mathcal{C}_{ij}}. \tag{4.64c}$$

It must be emphasized that the above results are still exact within the Chapman-Enskog expansion framework. However, the relations (4.64) and the decay rates (4.45) cannot be evaluated analytically without approximations. For this purpose, we first consider the Sonine expansion for $f^{(0)}$. We have shown in Sec. 4.3.1.4 that to first non-Gaussian contribution in Sonine polynomials the distribution $f^{(0)}$ reads

$$f^{(0)}(\mathbf{V}) = \frac{n}{v_T^d}\widetilde{\mathcal{M}}\left(\frac{V}{v_T}\right)\left\{1 + a_2\left[\frac{1}{2}\left(\frac{V}{v_T}\right)^4 - \frac{d+2}{2}\left(\frac{V}{v_T}\right)^2 + \frac{d(d+2)}{8}\right]\right\} \tag{4.65}$$

where

$$\widetilde{\mathcal{M}}\left(\frac{V}{v_T}\right) = \frac{1}{\pi^{d/2}}\mathrm{e}^{-V^2/v_T^2} \tag{4.66}$$

is the Maxwellian and

$$a_2 = 8\frac{3-2\sqrt{2}}{4d+6-\sqrt{2}+\frac{1-p}{p}8\sqrt{2}(d-1)}. \tag{4.67}$$

The coefficient $a_2$ was shown to be in very good agreement with direct Monte-Carlo simulations [52]. The relation (4.65) allows us to compute the decay rates (see Appendix A.9):

$$\xi_n^{(0)*} = \frac{d+2}{4}\left(1 - a_2\frac{1}{16}\right), \tag{4.68a}$$

$$\xi_T^{(0)*} = \frac{d+2}{8d}\left(1 + a_2\frac{8d+11}{16}\right). \tag{4.68b}$$

Next, we retain only the first order in a Sonine polynomial expansion applied to $\boldsymbol{\mathcal{A}}$, $\boldsymbol{\mathcal{B}}$, and $\boldsymbol{\mathcal{C}}$ (see App. A.10). We thus have

$$\boldsymbol{\mathcal{A}}(\mathbf{V}) = a_1\mathcal{M}(\mathbf{V})\mathbf{S}(\mathbf{V}), \tag{4.69a}$$
$$\boldsymbol{\mathcal{B}}(\mathbf{V}) = b_1\mathcal{M}(\mathbf{V})\mathbf{S}(\mathbf{V}), \tag{4.69b}$$
$$\boldsymbol{\mathcal{C}}(\mathbf{V}) = c_0\mathcal{M}(\mathbf{V})\mathbf{D}(\mathbf{V}), \tag{4.69c}$$

where $a_1$, $b_1$, and $c_0$ are the coefficients of the development. This allows us to compute the relations (4.64). For this purpose, as already shown the probabilistic collision operator $J$ given by Eq. (4.47) can be split into the sum of an annihilation operator and of a collision operator. Each contribution may thus be treated separately. Therefore we make use of previous calculations for the collision process [99]. The calculations for the annihilation operator are shown in Appendix A.11, and the final results read

$$\begin{aligned}\nu_\kappa^* = \nu_\mu^* &= p\frac{1}{32d}\left[16+27d+8d^2+a_2\frac{2880+1544d-2658d^2-1539d^3-200d^4}{32d(d+2)}\right]\\ &\quad +(1-p)\frac{d-1}{d}\left(1+a_2\frac{1}{32}\right),\end{aligned} \tag{4.70a}$$
$$\begin{aligned}\nu_\eta^* &= p\frac{1}{8d}\left[3+6d+2d^2-a_2\frac{278+375d+96d^2+2d^3}{32(d+2)}\right]\\ &\quad +(1-p)\left(1-a_2\frac{1}{32}\right).\end{aligned} \tag{4.70b}$$

One may check that these expressions approach unity when $p \to 0$. The transport coefficients are thus found from Eqs. (4.60) using Eqs. (4.62), (4.63), (4.67), (4.68), and (4.70).

In order to establish the decay rates to first order, one needs the distribution $f^{(1)}$ (see Appendix A.12):

$$f^{(1)}(\mathbf{V}) = -\frac{\beta^3}{n}\mathcal{M}(\mathbf{V})\left[\frac{2m}{d+2}S_i(\mathbf{V})\left(\kappa\nabla_i T+\mu\nabla_i n\right)+\frac{\eta}{\beta}D_{ij}(\mathbf{V})\nabla_j u_i\right]. \tag{4.71}$$

#### 4.4.2.4 Hydrodynamic equations

The pressure tensor and the heat flux defined by Eqs. (4.56) and (4.57), respectively, are of order one in the gradients. Thus their insertion in the balance equations (4.32) yields contributions of order two in the gradients. Consequently there are second order terms (so called Burnett order) that contribute to the first order (so called Navier-Stokes order) transport coefficients, and the knowledge of the distribution $f^{(2)}$ is thus necessary. Indeed, use was made of the zeroth order relations $P_{ij} = p^{(0)}\delta_{ij}$ and $q_i = 0$ to establish the balance equation for energy (4.50c). However, it was shown in the framework of the weakly inelastic gas – consequently for an elastic gas – that those Burnett contributions were three orders of magnitude smaller than the Navier-Stokes contributions [24]. For the sake of simplicity, we will here neglect those second order contributions. For small annihilation probabilities $p$, this approximation is thus likely to be justified. However, we have *a priori* no control on the error made when the annihilation probability $p$ is close to unity.

The hydrodynamic Navier-Stokes equations are given by

$$\partial_t n + \nabla_i(nu_i) = -pn[\xi_n^{(0)} + \xi_n^{(1)}], \tag{4.72a}$$

$$\partial_t u_i + \frac{1}{mn}\nabla_j P_{ij} + u_j\nabla_j u_i = -pv_T\xi_{u_i}^{(1)}, \qquad i = 1,\ldots,d, \tag{4.72b}$$

$$\partial_t T + u_i\nabla_i T + \frac{2}{nk_Bd}(P_{ij}\nabla_i u_j + \nabla_i q_i) = -pT[\xi_T^{(0)} + \xi_T^{(1)}], \tag{4.72c}$$

where the decay rates $\xi_n^{(0)}$ and $\xi_T^{(0)}$ are given by Eqs. (4.68a) and (4.68b), respectively. $P_{ij}$ and $q_j$ are given by Eqs. (4.56) with $\zeta = 0$, and (4.57) respectively. The rates $\xi_n^{(1)}$, $\xi_{u_i}^{(1)}$, and $\xi_T^{(1)}$ may be calculated using their definition (4.50) and the distribution (4.71). We find (see Appendix A.13):

$$\xi_n^{(1)} = 0, \tag{4.73a}$$

$$\xi_{u_i}^{(1)} = -v_T\left(\kappa^*\frac{1}{T}\nabla_i T + \mu^*\frac{1}{n}\nabla_i n\right)\xi_u^*, \tag{4.73b}$$

$$\xi_T^{(1)} = 0, \tag{4.73c}$$

where

$$\xi_u^* = \frac{(d+2)^2}{32(d-1)}\left[1 + a_2\frac{-86 - 101d + 32d^2 + 88d^3 + 28d^4}{32(d+2)}\right]. \tag{4.74}$$

We thus have a closed set of equations for the hydrodynamic fields to the Navier-Stokes order.

### 4.4.3 Stability analysis

The hydrodynamic Eqs. (4.72) form a set of first order nonlinear partial differential equations that cannot be solved analytically in general. However, their linear stability analysis allows us to answer the question of formation of inhomogeneities. The scope of the present study is to find under which conditions the homogeneous solution to zeroth order, i.e., the HCS, is unstable under spatial perturbations. To this end we consider a small deviation from the HCS and the linearization of Eqs. (4.72) in the latter perturbation. Eqs. (4.44) give the time evolution of the HCS, which is found to be (see App. A.14)

$$n_H(t) = n_0\left(1 + p\frac{t}{t_0}\right)^{-\gamma_n}, \tag{4.75a}$$

$$T_H(t) = T_0\left(1 + p\frac{t}{t_0}\right)^{-\gamma_T}, \tag{4.75b}$$

where the decay exponents are $\gamma_n = \xi_n^{(0)}(0)t_0$, $\gamma_T = \xi_T^{(0)}(0)t_0$, and the relaxation time $t_0^{-1} = \xi_n^{(0)}(0) + \xi_T^{(0)}(0)/2$. The subscript $H$ denotes a quantity evaluated in the homogeneous state. The density and temperature fields of the HCS are thus decreasing monotonously in time, with exponents that depend on the annihilation probability through the kurtosis of the velocity distribution. The explicit expression of the decay exponents may be obtained straightforwardly using Eqs. (4.68).

The linearization procedure used here follows the same route as the method used for granular gases [24]. We define the deviations of the hydrodynamic fields from the HCS by

$$\delta y(\mathbf{r},t) = y(\mathbf{r},t) - y_H(t), \tag{4.76}$$

where $y = \{n, \mathbf{u}, T\}$. Inserting the form (4.76) in Eqs. (4.73) yields differential equations with time-dependent coefficients. In order to obtain coefficients that do not depend on time, it is necessary to introduce the new dimensionless space and time scales defined by

$$\mathbf{l} = \frac{1}{2}\nu_{0H}(t)\sqrt{\frac{m}{k_B T_H(t)}}\mathbf{r}, \tag{4.77a}$$

$$\tau = \frac{1}{2}\int_0^t \mathrm{d}s\, \nu_{0H}(s), \tag{4.77b}$$

as well as the dimensionless Fourier fields

$$\rho_{\mathbf{k}}(\tau) = \frac{\delta n_{\mathbf{k}}(\tau)}{n_H(\tau)}, \tag{4.78a}$$

$$\mathbf{w}_{\mathbf{k}}(\tau) = \sqrt{\frac{m}{k_B T_H(\tau)}}\delta\mathbf{u}_{\mathbf{k}}(\tau), \tag{4.78b}$$

$$\theta_{\mathbf{k}}(\tau) = \frac{\delta T_{\mathbf{k}}(\tau)}{T_H(\tau)}, \tag{4.78c}$$

where

$$\delta y_{\mathbf{k}}(\tau) = \int_{\mathbb{R}^d} \mathrm{d}\mathbf{l}\, \mathrm{e}^{-i\mathbf{k}\cdot\mathbf{l}}\delta y(\mathbf{l},\tau). \tag{4.79}$$

From Eq. (4.77a), it appears that lengths are made dimensionless making use of the time dependent mean free path as a reference scale. Making use of Eqs. (4.78) and (4.77) in Eqs. (4.72), the linearized hydrodynamic equations read (see App. A.15)

$$\left[\frac{\partial}{\partial\tau} + 2p\xi_n^{(0)*}\right]\rho_{\mathbf{k}}(\tau) + p\xi_n^{(0)*}\theta_{\mathbf{k}}(\tau) + ikw_{\mathbf{k}_\parallel}(\tau) = 0, \tag{4.80a}$$

$$\left[\frac{\partial}{\partial\tau} - p\xi_T^{(0)*} + \frac{d-1}{d}\eta^* k^2\right]\mathbf{w}_{\mathbf{k}_\parallel} + i\mathbf{k}\Big[\big(1 - p\xi_u^*\mu^*\big)\rho_{\mathbf{k}}(\tau) + \big(1 - p\xi_u^*\kappa^*\big)\theta_{\mathbf{k}}(\tau)\Big] = 0, \tag{4.80b}$$

$$\left[\frac{\partial}{\partial\tau} - p\xi_T^{(0)*} + \frac{1}{2}\eta^* k^2\right]\mathbf{w}_{\mathbf{k}_\perp}(\tau) = 0, \tag{4.80c}$$

$$\left[\frac{\partial}{\partial\tau} + p\xi_T^{(0)*} + \frac{d+2}{2(d-1)}\kappa^* k^2\right]\theta_{\mathbf{k}}(\tau) + \left[2p\xi_T^{(0)*} + \frac{d+2}{2(d-1)}\mu^* k^2\right]\rho_{\mathbf{k}}(\tau) + \frac{2}{d}ikw_{\mathbf{k}_\parallel}(\tau) = 0, \tag{4.80d}$$

where $\mathbf{w}_{\mathbf{k}_\parallel}$ and $\mathbf{w}_{\mathbf{k}_\perp}$ are the longitudinal and transverse part of the velocity vector defined by $\mathbf{w}_{\mathbf{k}_\parallel} = (\mathbf{w}_\mathbf{k} \cdot \widehat{\mathbf{e}}_\mathbf{k})\widehat{\mathbf{e}}_\mathbf{k}$ and $\mathbf{w}_{\mathbf{k}_\perp} = \mathbf{w}_\mathbf{k} - \mathbf{w}_{\mathbf{k}_\parallel}$, where $\widehat{\mathbf{e}}_\mathbf{k}$ is the unit vector along the direction given by $\mathbf{k}$. Eq. (4.80c) for the shear mode is decoupled from the other equations and can be integrated directly so that

$$\mathbf{w}_{\mathbf{k}_\perp}(\tau) = \mathbf{w}_{\mathbf{k}_\perp}(0)\exp[s_\perp(p,k)\tau], \tag{4.81}$$

where

$$s_\perp(p,k) = p\xi_T^{(0)*} - \frac{1}{2}\eta^* k^2. \tag{4.82}$$

The transversal velocity field $\mathbf{w}_{\mathbf{k}_\perp}$ lies in the $(d-1)$ dimensional vector space that is orthogonal to the vector space generated by $\mathbf{k}$, and therefore the mode $s_\perp$ identifies $(d-1)$ degenerated perpendicular modes. The longitudinal velocity field $\mathbf{w}_{\mathbf{k}_\parallel}$ lies in the vector space of dimension one generated by $\mathbf{k}$. Hence there are three hydrodynamic fields to be determined, namely the density $\rho_\mathbf{k}$, temperature $\theta_\mathbf{k}$, and longitudinal velocity field $\mathbf{w}_{\mathbf{k}_\parallel} = w_{\mathbf{k}_\parallel}\widehat{\mathbf{e}}_\mathbf{k}$. The linear system thus reads

$$\begin{pmatrix} \dot{\rho}_\mathbf{k} \\ \dot{w}_{\mathbf{k}_\parallel} \\ \dot{\theta}_\mathbf{k} \end{pmatrix} = \mathbf{M} \cdot \begin{pmatrix} \rho_\mathbf{k} \\ w_{\mathbf{k}_\parallel} \\ \theta_\mathbf{k} \end{pmatrix}, \tag{4.83}$$

with the hydrodynamic matrix

$$\mathbf{M} = \begin{pmatrix} -2p\xi_n^{(0)*} & -ik & -p\xi_n^{(0)*} \\ -ik(1-p\xi_u^*\mu^*) & p\xi_T^{(0)*} - \frac{d-1}{d}\eta^* k^2 & -ik(1-p\xi_u^*\kappa^*) \\ -2p\xi_T^{(0)*} - \frac{d+2}{2(d-1)}\mu^* k^2 & -\frac{2}{d}ik & -p\xi_T^{(0)*} - \frac{d+2}{2(d-1)}\kappa^* k^2 \end{pmatrix}. \tag{4.84}$$

The corresponding eigenmodes are given by $\varphi_n(k) = \exp[s_n(p,k)\tau]$, $n = 1,\ldots,3$, where $s_n(p,k)$ are the eigenvalues of $\mathbf{M}$. Each of the three fields above is a linear combination of the eigenmodes, thus only the biggest real part of the eigenvalue $s_n(p,k)$ has to be taken into account to discuss the limit of marginal stability of the parallel mode of the velocity field. Fig. 4.10 shows the real part of the eigenvalues for $p = 0.1$ and $d = 3$ (obtained numerically).

One may identify three regions from the dispersion relations. We first define $k_\perp$ (dimensionless) by the condition $\Re[s_\perp(k_\perp,p)] = 0$ ($\Re$ denotes the real part), i.e.,

$$k_\perp = \sqrt{\frac{2p\xi_T^{(0)*}}{\eta^*}}, \tag{4.85}$$

and $k_\parallel$ by $\max_{k_\parallel}\Re[s_\parallel(k_\parallel,p)] = 0$ (the expression for $k_\parallel$ is too cumbersome to be given here); we have $k_\parallel < k_\perp$. Figure 4.11 shows the dependence of $k_\perp$ and $k_\parallel$ as a function of the annihilation probability $p$. Then for all $k > k_\perp$ all eigenvalues are negative and therefore, according to Eq. (4.81), correspond to linearly stable modes. For $k \in [k_\parallel, k_\perp]$ only the shear mode $\mathbf{w}_{\mathbf{k}_\perp}$ of the velocity field is linearly unstable. In the case of granular gases in dimension larger than one this region exhibits velocity vortices [26, 27, 51, 113], with a possible subsequent non-linear coupling to density

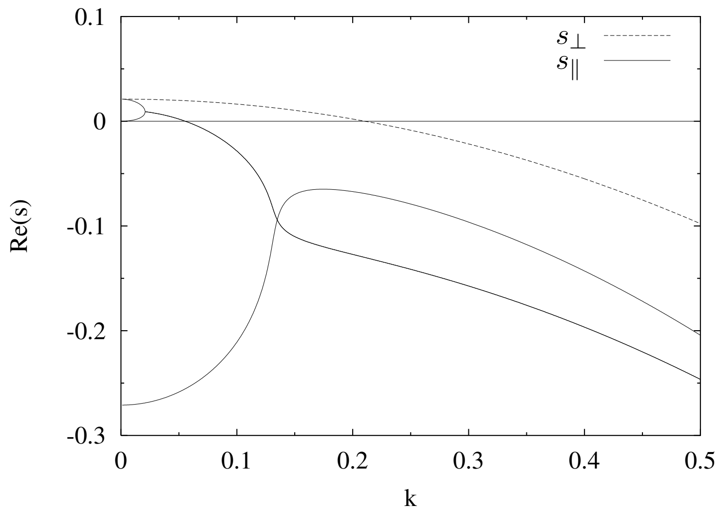


Figure 4.10: Real part of the eigenvalues in dimensionless units for probabilistic ballistic annihilation with $p = 0.1$ and $d = 3$. The dispersion relation obtained from Eq. (4.82) is represented by a dashed line (labeled $s_\perp$) whereas the three remaining relations obtained upon solving Eq. (4.84) are represented by continuous lines (labeled $s_\parallel$).

inhomogeneities. From $\xi_T^{(0)*} = \xi_T^{(0)}/\nu_0$ and Eq. (4.77b) one may integrate Eq. (4.44c) in order to find $T_H(\tau) = T_H(0)\exp[-2p\xi_T^{(0)*}\tau]$. Then equating Eqs. (4.78b) and (4.81), making use of the latter expression for $T_H(\tau)$, of Eq. (4.82), and of Eq. (4.78b) for $\tau = 0$, one finds

$$\delta\mathbf{u}_{\mathbf{k}_\perp}(\tau) = \mathbf{u}_{\mathbf{k}_\perp}(0)\exp\left(-\frac{1}{2}\eta^* k^2\tau\right). \tag{4.86}$$

The exponential decay in the reduced variable $\tau$ translates in a power-law-like decay in the original variable $t$ [since the exponent $k = k(t)$ depends itself on time]. Indeed, the integration of Eq. (4.44c) yields $\tau = -\ln[T_H(t)/T_H(0)]/2\xi_T^{(0)*}$, that we replace in Eq. (4.86) and make use of the homogeneous solution $T_H(t)$ given by Eq. (4.75b) in order to finally obtain

$$\delta\mathbf{u}_{\mathbf{k}_\perp}(t) = \mathbf{u}_{\mathbf{k}_\perp}(0)\left(1 + p\frac{t}{t_0}\right)^{-\frac{\eta^* k^2}{4t_0^*}}, \tag{4.87}$$

where $t_0^* = t_0/\nu_H(0)$ is the dimensionless relaxation time. In the linear approximation the perturbation of the transversal velocity field therefore decays even if $s_\perp(k,p) > 0$. The rescaled modes with $k < k_\parallel$ are linearly unstable.

However, a crucial point is that for any real (finite) system, the wave-numbers are larger than $2\pi/L$ (assuming a cubic box of size $L$), which corresponds to a *time dependent* dimensionless wavenumber $k_{\min} = 2\pi/(Ln\sigma^{d-1})$, which increases with time as $1/n$. This lower cutoff therefore inevitably enters into the stable region $k_{\min} > k_\perp$,

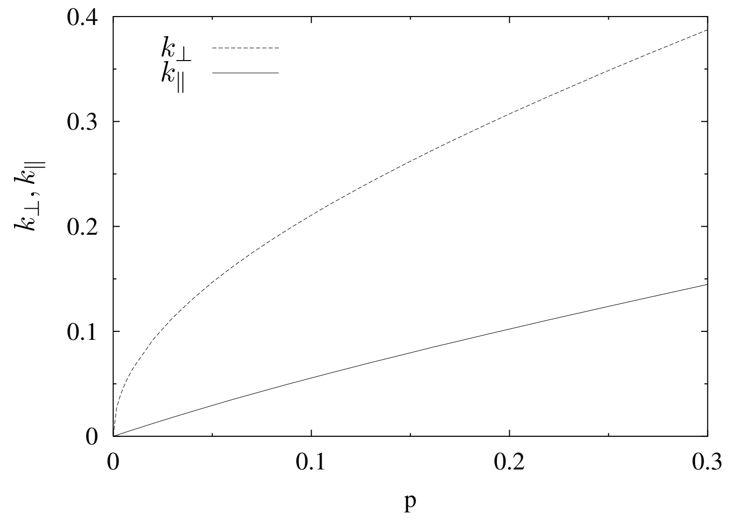


Figure 4.11: Wavenumber $k_\perp$ and $k_\parallel$ in dimensionless units as a function of the annihilation probability $p$ for $d = 3$.

so that an instability may only be a transient effect. In other words, an unstable mode associated to a given value of $k$ corresponds to a perturbation at a wavelength which increases with time in real space, and ultimately becomes larger than system size. However, at late times, the Knudsen number defined as the ratio of mean free path (which is proportional to $k_{\rm min}$) over system size, becomes large, which should invalidate a Navier-Stokes-like description. Similarly, the present coarse-grained approach is *a priori* restricted to low enough values of $k$. Given that $k_\perp$ increases quite rapidly with $p$ (see Figure 4.11), the stable region $k > k_\perp$ might correspond to a "non-hydrodynamic" regime when $p$ is larger than some (difficult to quantify) threshold. Conclusions concerning the stability of the system for such parameters rely on the validity of the hydrodynamic description (that could be tested by Monte Carlo or Molecular Dynamics simulations) which is beyond the scope of the present chapter.

At this point, we conclude that the system may exhibit transient instabilities, but safe statements may only be made for very low values of $p$ for which $k_\perp$ is low enough to guarantee that the hydrodynamic analysis holds. The stable region is then ultimately met irrespective of system size.

With the above possible restrictions in mind, it is instructive to consider the counterpart of Figure 2.1 for "large" values of $p$ (see Fig. 2.3). For $p > 0.893\ldots$, we obtain the unphysical result that some eigenvalues increase and diverge upon increasing $k$. This deficiency, which is *a priori* decoupled from the question of the validity of hydrodynamics or of the Chapman-Enskog procedure, might be ascribable to the approximations made in the present calculations (Sonine expansion limited to leading non Gaussian order, together with a linear approximation with respect to the kurtosis $a_2$).

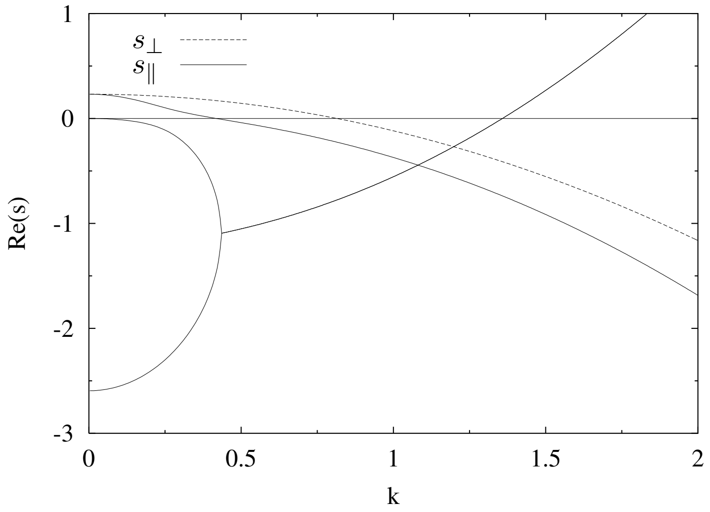


Figure 4.12: Real part of the eigenvalues in dimensionless units for probabilistic ballistic annihilation with $p = 0.95$ and $d = 3$. The figure caption is the same as for Fig. 4.10.

### 4.4.4 Conclusions

In this chapter we construct a hydrodynamic description for probabilistic ballistic annihilation in arbitrary dimension $d \geqslant 2$, where none of the hydrodynamic fields can be associated with a conserved quantity. The motivation is not only to discuss the possibility of large-scale instabilities in such a system, but also to provide the starting point for further (numerical) studies centered on the applicability of hydrodynamics to systems in which there are no collisional invariants. To this aim, we consider the low density and long time regimes in order to make use of the Boltzmann equation with the homogeneous cooling state (HCS) as a reference state. The Chapman-Enskog method then allows us to build a systematic expansion in the gradients of the fields, with an associated timescale hierarchy. We consider only the first (Navier-Stokes) order in the gradients to build the hydrodynamic equations describing the dynamics of probabilistic ballistic annihilation. The transport coefficients and decay rates are established from the microscopic approach neglecting Burnett contributions and restricting ourselves to the first non-Gaussian term in a Sonine expansion. We then linearize the hydrodynamic equations around the HCS. The subsequent dispersion relations inform on the range of the perturbation's wavelength and time-scales for which the system may exhibit density inhomogeneities.

Interestingly, the behavior of the dispersion relations and of the wave-numbers $k_\perp$ and $k_\parallel$ is qualitatively similar to its counterpart obtained for (inelastic) granular gases [24, 114]. This leads us to conclude that some features of those models do not depend on the details of the dynamics, but rather on the parameter controlling the dissipation (referring to the existence of non conserved quantities) in the system, namely $p$ [or $(1-\alpha^2)$ in the case of granular gases, where $\alpha$ is the restitution coefficient]. However, a specific feature of our model is that the mean free path increases rapidly with time. Consequently, even if the stability analysis leads us to the conclusion that this feature drives the system in a region where the homogeneous solution with a vanishing flow field is stable, the associated Knudsen numbers may be too large to validate our coarse-grained approach. At very small values of $p$ however, the stable region ($k > k_\perp$ with the notations of section 4.4.3) should be relevant, but then, the effects of transient instabilities in the case where the system is large enough to allow for $k_{\min} < k_\perp$ or $k_{\min} < k_\parallel$ seem difficult to assess.

Another point to emphasize is the amplitude of the dissipation in the system, which appears through the decay rates of the hydrodynamic fields. Again, there must be a clear separation between the macroscopic timescales described by those decay rates, and between the microscopic timescales. This separation of scales is required in the hydrodynamic approach in order to make use of the hydrodynamic fields $n$, $\mathbf{u}$, and $T$ that are associated with non conserved quantities. The decay rates having the dimension of the inverse of a time, their inverse thus defines a timescale. If those decay rates increase, the associated timescales decay. In our case, we clearly introduce three such timescales that are supposed to be macroscopic; one for each non-conserved field. It is therefore required that the maximum of these decay rates defines a macroscopic timescale that is much bigger than the microscopic one. Nevertheless those decay rates increase as a function of the annihilation probability, hence the decrease of the associated timescale. One question that arises is to determine for which value of $p$ the smallest timescale introduced by the decay rates is of the order of the microscopic timescale – which increases as a function of time because of the decreasing density of particles remaining in the system. When this is the case, the hydrodynamic description becomes irrelevant and one may not make use of the fields $n$, $\mathbf{v}$, and $T$ any more. As the parameter $p$ controls the dissipation in the system, the question at hand here –left for future work– is reminiscent of the controversial issue of the validity of hydrodynamics for granular gases with "low" coefficients of restitution. Probabilistic ballistic annihilation is a particularly well suited system to treat this problem by comparison to granular gases since the phenomenon of granular collapse is absent. The subsequent correlations that may arise are therefore absent for probabilistic ballistic annihilation.

# Chapter 5

# Maxwell and very hard particle models for probabilistic ballistic annihilation: hydrodynamic description

## 5.1 Outline of the chapter

The hydrodynamic description of probabilistic ballistic annihilation, for which no conservation laws hold, is an intricate problem with hard sphere-like dynamics for which no exact solution exists. We consequently focus on simplified approaches, the Maxwell and very hard particles (VHP) models, which allows us to compute analytically upper and lower bounds for several quantities. The purpose is to test the possibility of describing such a far from equilibrium dynamics with simplified kinetic models. The motivation is also in turn to assess the relevance of some singular features appearing within the original model and the approximations invoked to study it. The scaling exponents are first obtained from the (simplified) Boltzmann equation, and are confronted against Monte Carlo simulation (DSMC technique). Then, the Chapman-Enskog method is used to obtain constitutive relations and transport coefficients. The corresponding Navier-Stokes equations for the hydrodynamic fields are derived for both Maxwell and VHP models. We finally perform a linear stability analysis around the homogeneous solution, which illustrates the importance of dissipation in the possible development of spatial inhomogeneities. The content of this chapter is based on Ref. [45].

## 5.2 Introduction

The possibility to describe in terms of hydrodynamic equations the evolution of a system where some physical quantities are not conserved is a challenging problem of non-equilibrium statistical mechanics. Several questions have to be faced as for example the validity of the underlying kinetic theory, the choice of the hydrodynamical fields that are supposed to describe the relevant excitations in the problem, or the consistency of the method itself that is used to deduce the coarse-grained description from the kinetic theory. Much attention has been recently paid to such questions, mainly in the field of granular gas dynamics (see, e.g., [12, 48, 104, 115]). In such systems, the kinetic energy is not conserved, while the linear momentum and number of particles are. However, even for low dissipation, the derivation of the hydrodynamic relations, based on a hard-sphere-like Boltzmann equation is not a simple task and several approximations have to be invoked [48]. These difficulties lead to consider some simpler models by choosing ad-hoc collision term in the Boltzmann equation. The so-called Maxwell and very hard particles (VHP) models [116, 117, 118] are particularly interesting and reproduce some qualitative features of the granular gas of inelastic hard spheres [41, 119, 120, 121, 122, 123].

Another class of problems for which not only energy but also the density and momentum are not conserved is probabilistic ballistic annihilation (PBA). In such a system, the particles move ballistically between collisions. When two particles meet, they undergo an instantaneous collision and are removed from the system with probability $p$ or undergo an elastic scattering with probability $(1-p)$. Since collisions are assumed to be instantaneous, two body events only are taken into account. The PBA model was first introduced in one dimension in [91]. In the limit $p \to 0$, where density, momentum and kinetic energy are conserved, one recovers a system of hard spheres for which the hydrodynamic equations are well known [7, 96, 97]. The other limit $p = 1$ (pure annihilation) has been the object of some work [39, 40, 43, 58, 59, 60, 62, 65, 68, 70]. It was shown that in the long time limit the annihilation dynamics is exactly described by the Boltzmann equation in dimensions higher than one [39]. This may qualitatively be understood by the fact that the density of the gas decays and, at late times, the packing fraction is very low. This fact lead to conjecture that the Boltzmann equation is an adequate description of PBA at late times for $p > 0$ [52].

Given that $p$ may be considered as a perturbation parameter allowing to recover the elastic limit, the PBA model is particularly interesting in view of testing the relevance and validity of the hydrodynamic description in general, which is a controversial issue. The analytical treatment with usual hard sphere dynamics however appears to be quite involved [53], and we study here the simplified Maxwell and VHP versions of PBA. The motivation is here is not only to test the ability of simplified kinetic models to mimic the hard sphere dynamics for a model far from equilibrium (and with no conserved quantity, a more severe situation than that of granular gases) but also to shed some light on some peculiar features obtained in the hydrodynamic study of Ref. [53]. In particular, this work exhibited divergent transport coefficients for a critical value of $p$. We will see that such singularities are absent in the simplified approaches, which may indicate that they are not associated with any physically relevant phenomenon. It will also appear that Maxwell and VHP approaches provide useful bounds for the hard sphere dynamics, so that similar inequalities as those found in [43, 44] concerning the scaling exponents can be obtained.

The chapter is organized as follows. In section 5.3 we introduce the Boltzmann equation for both Maxwell and VHP models of probabilistic ballistic annihilation, as well as the balance equations for the coarse-grained fields. In section 5.4 we briefly describe the Chapman-Enskog scheme while section 5.5 is devoted to the Maxwell model. We first find the homogeneous state, and solve the corresponding homogeneous balance equations. To first order in the Chapman-Enskog expansion we then study the effect of a small spatial inhomogeneity. We follow the traditional route to compute the transport coefficients, which consists in truncating the first-order velocity distribution function to the first nonzero term in a Sonine polynomial expansion [53]. We then show that this truncation does not constitute an approximation for the transport coefficients since they can be obtained by solving the Maxwell model *exactly* to first order. The VHP model is subsequently investigated in section 5.6. We first find the homogeneous cooling state, and then solve the corresponding homogeneous equations. We implement Monte Carlo simulations in order to check the decay exponents found analytically. Next, we establish the transport coefficients to first order in the Chapman-Enskog expansion before presenting a comparison of the transport coefficients of the different models. In Sec. 5.7 we finally perform a linear stability analysis of the Navier-Stokes hydrodynamic equations around the spatially homogeneous state, and compare the results with PBA of hard spheres. Our main findings and conclusions are summarized in section 5.8.

Since the underlying calculations of this chapter are cumbersome, we present only the main steps in order to focus onto the more relevant results. Further technical details or explanations may be found in Chapter 4 [53] and Appendix A.4 contains a summary of the notations used.

## 5.3 The Balance Equations

The Boltzmann equation for the one particle distribution $f(\mathbf{r}, \mathbf{v}; t)$ of particles annihilating upon collision with probability $p$ reads

$$(\partial_t + \mathbf{v}_1 \cdot \boldsymbol{\nabla}) f(\mathbf{r}, \mathbf{v}_1; t) = p J_a[f, f] + (1-p) J_c[f, f], \tag{5.1}$$

where $J_a$ is the annihilation operator defined by

$$J_a[f, g] = -\sigma^{d-1} \phi(x) v_T^{1-x} g(\mathbf{r}, \mathbf{v}_1; t) \int_{\mathbb{R}^d} \mathrm{d}\mathbf{v}_2 \, v_{12}^x f(\mathbf{r}, \mathbf{v}_2; t) \tag{5.2}$$

and $J_c$ is the collision operator:

$$J_c[f, g] = \sigma^{d-1} \frac{\phi(x) v_T^{1-x}}{S_d} \int_{\mathbb{R}^d} \mathrm{d}\mathbf{v}_2 \, v_{12}^x \int \mathrm{d}\widehat{\boldsymbol{\sigma}} \, (b^{-1} - 1) g(\mathbf{r}, \mathbf{v}_1; t) f(\mathbf{r}, \mathbf{v}_2; t). \tag{5.3}$$

In these equations, $d$ denotes the spatial dimension, $v_{12} = |\mathbf{v}_1 - \mathbf{v}_2|$ is the modulus of the relative velocity, $S_d = 2\pi^{d/2}/\Gamma(d/2)$ is the solid angle surface, $\Gamma$ the Euler gamma function, $v_T = \sqrt{2/\beta m}$ the time-dependent thermal velocity, $\beta = (k_B T)^{-1}$, $\sigma$ is the diameter of the particles, $\widehat{\boldsymbol{\sigma}}$ is a unit vector joining the centers of two particles and the corresponding integral is running over the solid angle. Finally, $b^{-1}$ an operator acting on the velocities as given by Eqs. (4.5). The choice $x = 0$ ($x = 2$) corresponds to the Maxwell (VHP) model, respectively. For hard sphere dynamics, that would correspond to $x = 1$, the relative velocity $v_{12}$ gives the rate of collision and its presence makes analytical progress difficult. A convenient simplification [118] to overcome this difficulty is to replace it by $v_{12}^x v_T^{1-x}$ where $v_T$ is introduced for dimensional reasons. The quantity $\phi(x)$ which sets the relevant time scale in the problem can be freely chosen, and will be used in the following analysis to obtain the desired limiting behaviour in the limit $p \to 0$ (see also [41] for related considerations). We also note that particles interacting with an inverse power-law potential are described by a kinetic equation with a cross section of the same form as in Eq. (5.3) [118].

In order to write hydrodynamic equations, we define in Eqs. (4.31) the local hydrodynamic fields number density $n(\mathbf{r}, t)$, velocity $\mathbf{u}(\mathbf{r}, t)$, and temperature $T(\mathbf{r}, t)$ (the latter definition being kinetic with no thermodynamic basis). The definition of the temperature follows from the principle of equipartition of energy. In Eq. (4.31c), $k_B$ is the Boltzmann constant and $\mathbf{V} = \mathbf{v} - \mathbf{u}(\mathbf{r}, t)$ is the deviation from the mean flow velocity. The balance equations follow from integrating the moments 1, $m\mathbf{v}$, and $mv^2/2$ with weight given by the Boltzmann equation (5.1). Following the same route as in Chapter 4 we obtain the balance equations (4.32), where again

$$\omega[f, g] = -\int_{\mathbb{R}^d} \mathrm{d}\mathbf{v}_1 \, J_a[f, g], \tag{5.4}$$

and the pressure tensor $P_{ij}$ and heat-flux $q_i$ are defined by Eqs. (4.34) and (4.35), respectively. As expected, when the annihilation probability $p \to 0$, all three coarse grained fields $n$, $\mathbf{u}$, and $T$ are conserved.

## 5.4 The Chapman-Enskog solution

The Chapman-Enskog method allows from Eqs. (4.32) to build a closed set of equations for the hydrodynamic fields (see, e.g., [12, 48]). For this purpose, it is required to express the functional dependence of the pressure tensor $P_{ij}$ and of the heat flux $q_i$ in terms of the hydrodynamic fields. The Chapman-Enskog approach relies on two important assumptions. The first one is the existence of a normal solution in which all temporal and spatial dependence of the distribution function $f(\mathbf{r}, \mathbf{v}; t)$ may be expressed in terms of the hydrodynamic fields, $f(\mathbf{r}, \mathbf{v}; t) = f\left[\mathbf{v}, n(\mathbf{r}, t), \mathbf{u}(\mathbf{r}, t), T(\mathbf{r}, t)\right]$. The discussion of the relevance of this first assumption can be found elsewhere (e.g., in [48]). The second assumption is based on the separation of the microscopic time scale (the average collision time and the spatial length defined by the corresponding mean free path) and macroscopic time scale (the evolution of the hydrodynamic fields and their inhomogeneities). This separation implies that the hydrodynamic fields are only weakly inhomogeneous, which allows for a series expansion in the gradients of the fields, $f = f^{(0)} + \varepsilon f^{(1)} + \varepsilon^2 f^{(2)} + \ldots$, where each power of the formal small parameter $\varepsilon$ is associated to a given order in spatial gradients. The Chapman-Enskog method assumes the existence of an associated time derivative hierarchy: $\partial/\partial t = \partial^{(0)}/\partial t + \varepsilon\partial^{(1)}/\partial t + \varepsilon^2\partial^{(2)}/\partial t + \ldots$. The insertion of these expansions in the Boltzmann equation yields Eq. (4.41). The Chapman-Enskog solution is obtained upon solving the equations order by order in $\varepsilon$.

## 5.5 The Maxwell Model

### 5.5.1 The homogeneous state

To zeroth order in the gradients, Eq. (4.41) gives

$$\partial_t^{(0)} f^{(0)} = pJ_a[f^{(0)}, f^{(0)}] + (1-p)J_c[f^{(0)}, f^{(0)}]. \tag{5.5}$$

This equation has a solution, describing the homogeneous state, and which obeys the scaling relation

$$f^{(0)}(\mathbf{r}, \mathbf{v}; t) = \frac{n(t)}{v_T^d(t)} \widetilde{f}(c), \tag{5.6}$$

where $v_T = [2/(\beta m)]^{1/2}$ is the time dependent thermal velocity, and $c = V/v_T$, $\mathbf{V} = \mathbf{v} - \mathbf{u}$. The existence of a scaling solution of the form (5.6) seems to be a general feature present in different but related contexts [39, 41, 44]. This solution being isotropic, one has $\mathbf{u} = 0$.

Santos and Brey [124] showed that there exists a relationship between the homogeneous solutions of the Maxwell model with $p = 0$ and $p \neq 0$. We shall here briefly reproduce their arguments. It is possible to rewrite the Boltzmann equation (5.5) for $x = 0$ under the form

$$\partial_{t'}^{(0)} f^{(0)}(\mathbf{v}; t') = -(C_S + C_R) n(t') f^{(0)}(\mathbf{v}; t') + \int_{\mathbb{R}^d} \mathrm{d}\mathbf{v}_1 \int \mathrm{d}\widehat{\boldsymbol{\sigma}}\, \chi(\widehat{\boldsymbol{\sigma}}) f^{(0)}(\mathbf{v}; t') f^{(0)}(\mathbf{v}_1; t'), \tag{5.7}$$

where $t' = (1-p)t$, $C_S = \int \mathrm{d}\widehat{\boldsymbol{\sigma}} \chi(\widehat{\boldsymbol{\sigma}})$, $\chi(\widehat{\boldsymbol{\sigma}}) = \sigma^{d-1}\phi(x = 1) v_T / S_d$, and $C_R = \int d\widehat{\boldsymbol{\sigma}} \chi(\widehat{\boldsymbol{\sigma}}) p/(1-p)$ is the removal collision frequency. Integrating Eq. (5.7) over $\mathbf{v}$, the evolution of the number density is governed by $\partial_{t'} n(t') = -C_R n^2(t')$, the solution being $n(t') = n_0/(1 + n_0 C_R t')$, where $n_0 = n(t' = 0)$. If we define $\tau(t') = \int_0^{t'} \mathrm{d}s\, n(s)/n_0$ and $F(\mathbf{v}; \tau) = f^{(0)}(\mathbf{v}; t') n_0 / n(t')$, then $F(\mathbf{v}; \tau)$ satisfies the Boltzmann equation without annihilation (i.e., $C_R = 0$). $F(\mathbf{v}; \tau)$ therefore evolves towards a Maxwellian, and so does $f^{(0)}$: we have $\widetilde{f}(c) = \mathrm{e}^{-c^2}/\pi^{d/2}$.

### 5.5.2 The zeroth-order Chapman-Enskog solution

Since $f^{(0)}$ is isotropic, to zeroth order the pressure tensor (4.34) becomes $P_{ij}^{(0)} = p^{(0)} \delta_{ij}$, where $p^{(0)} = n k_B T$ is the hydrostatic pressure, and the heat flux (4.35) becomes $\mathbf{q}^{(0)} = 0$. The balance equations to zeroth order read

$$\partial_t^{(0)} n = -pn\xi_n^{(0)}, \tag{5.8a}$$

$$\partial_t^{(0)} u_i = -pv_T \xi_{u_i}^{(0)}, \tag{5.8b}$$

$$\partial_t^{(0)} T = -pT\xi_T^{(0)}, \tag{5.8c}$$

where the decay rates are

$$\xi_n^{(0)} = \frac{1}{n}\omega[f^{(0)}, f^{(0)}], \tag{5.9a}$$

$$\xi_{u_i}^{(0)} = \frac{1}{nv_T}\omega[f^{(0)}, V_i f^{(0)}], \qquad i = 1, \ldots, d \tag{5.9b}$$

$$\xi_T^{(0)} = \frac{m}{k_B T d}\omega[f^{(0)}, V^2 f^{(0)}] - \frac{1}{n}\omega[f^{(0)}, f^{(0)}]. \tag{5.9c}$$

For antisymmetry reasons, one sees from Eq. (5.9b) that $\xi_{u_i}^{(0)} = 0$. The calculation of $\xi_n^{(0)}$ and $\xi_T^{(0)}$ are straightforward and give $\xi_n^{(0)} = n\sigma^{d-1}\phi^{\mathrm{M}} v_T$ and $\xi_T^{(0)} = 0$. We have written $\phi^{\mathrm{M}}$ for $\phi(x = 0)$. The temperature of the Maxwell model is therefore conserved in the homogeneous state (time independent thermal velocity $v_T$). In addition, one has

$$n_H(t) = \frac{n_0}{1 + pt\xi_n^{(0)}(0)}, \tag{5.10}$$

where the subscript $H$ denotes a quantity evaluated in the homogeneous state, and $\xi_n^{(0)}(0)$ is the decay rate for $t = 0$. Note that Eq. (5.10) was already established in Sec. 5.5.1.

### 5.5.3 The first-order Chapman-Enskog solution

To first order in the gradients, the Boltzmann equation (4.41) reads

$$[\partial_t^{(0)} + J]f^{(1)} = -[\partial_t^{(1)} + \mathbf{v}_1 \cdot \boldsymbol{\nabla}]f^{(0)}, \tag{5.11}$$

the operator $J$ being defined by Eqs. (A.31) and (A.32). The balance equations (4.32) to first order become

$$\partial_t^{(1)} n + \nabla_i(nu_i) = -pn\xi_n^{(1)}, \tag{5.12a}$$

$$\partial_t^{(1)} u_i + \frac{k_B}{mn}\nabla_i(nT) + u_j\nabla_j u_i = -pv_T\xi_{u_i}^{(1)}, \qquad i = 1, \ldots, d, \tag{5.12b}$$

$$\partial_t^{(1)} T + u_i\nabla_i T + \frac{2}{d}T\nabla_i u_i = -pT\xi_T^{(1)}, \tag{5.12c}$$

where the decay rates are given by

$$\xi_n^{(1)} = \frac{2}{n}\omega[f^{(0)}, f^{(1)}], \tag{5.13a}$$

$$\xi_{u_i}^{(1)} = \frac{1}{nv_T}\omega[f^{(0)}, V_i f^{(1)}] + \frac{1}{nv_T}\omega[f^{(1)}, V_i f^{(0)}], \qquad i = 1, \ldots, d, \tag{5.13b}$$

$$\xi_T^{(1)} = -\frac{2}{n}\omega[f^{(0)}, f^{(1)}] + \frac{m}{nk_B T d}\omega[f^{(0)}, V^2 f^{(1)}] + \frac{m}{nk_B T d}\omega[f^{(1)}, V^2 f^{(0)}]. \tag{5.13c}$$

By definition $f^{(1)}$ is of first order in the gradients of the hydrodynamic fields; for a low density gas [12]

$$f^{(1)} = \mathcal{A}_i\nabla_i \ln T + \mathcal{B}_i\nabla_i \ln n + \mathcal{C}_{ij}\nabla_j u_i. \tag{5.14}$$

The coefficients $\mathcal{A}_i$, $\mathcal{B}_i$, and $\mathcal{C}_{ij}$ depend on the fields $n$, $\mathbf{V}$, and $T$.

#### 5.5.3.1 The approximate first-order Chapman-Enskog solution

The hydrodynamic description of the flow requires the knowledge of transport coefficients, which may be determined from a Sonine polynomial expansion of the first order distribution function. In addition, the pressure tensor may be put in the form

$$P_{ij}(\mathbf{r},t) = p^{(0)}\delta_{ij} - \eta\left(\nabla_i u_j + \nabla_j u_i - \frac{2}{d}\delta_{ij}\nabla_k u_k\right) - \zeta\delta_{ij}\nabla_k u_k, \tag{5.15}$$

where $p^{(0)} = nk_BT$ is the ideal gas pressure, $\eta$ is the shear viscosity, and $\zeta$ is the bulk viscosity which vanishes for a low density gas [48]. Fourier's linear law for heat conduction is

$$q_i = -\kappa\nabla_i T - \mu\nabla_i n, \tag{5.16}$$

where $\kappa$ is the thermal conductivity and $\mu$ a transport coefficient that has no analogue in the elastic case [24, 28].

The identification of Eq. (5.15) with Eq. (4.34) using the result of the first order calculation yields

$$P_{ij}^{(1)} = \int_{\mathbb{R}^d} \mathrm{d}\mathbf{v}\, D_{ij}(\mathbf{V}) f^{(1)}. \tag{5.17}$$

Similarly, the identification of Eq. (5.16) with Eq. (4.35) using the first order calculation leads to

$$q_i^{(1)} = \int_{\mathbb{R}^d} \mathrm{d}\mathbf{v}\, S_i(\mathbf{V}) f^{(1)}. \tag{5.18}$$

The calculation follows the same route as in Chapter 4, and we obtain

$$\eta^* = \frac{\eta}{\eta_0} = \frac{1}{\nu_\eta^*}, \tag{5.19a}$$

$$\kappa^* = \frac{\kappa}{\kappa_0} = \frac{d-1}{d}\frac{1}{\nu_\kappa^*}, \tag{5.19b}$$

$$\mu^* = \frac{n\mu}{T\kappa_0} = 0, \tag{5.19c}$$

where the thermal conductivity $\kappa_0$ and shear viscosity $\eta_0$ coefficients for hard spheres (used here to obtain dimensionless quantities) are given by Eqs. (A.27) and (A.28), respectively [5]. The dimensionless coefficients $\nu_\eta^*$ and $\nu_\kappa^*$ are given by

$$\nu_\kappa^* = \frac{1}{\nu_0}\frac{\int_{\mathbb{R}^d}\mathrm{d}\mathbf{V}\, S_i(\mathbf{V}) J\mathcal{A}_i}{\int_{\mathbb{R}^d}\mathrm{d}\mathbf{V}\, S_i(\mathbf{V})\mathcal{A}_i} - p\frac{1}{\nu_0}\frac{\int_{\mathbb{R}^d}\mathrm{d}\mathbf{V}\, S_i(\mathbf{V})\Omega\mathcal{A}_i}{\int_{\mathbb{R}^d}\mathrm{d}\mathbf{V}\, S_i(\mathbf{V})\mathcal{A}_i}, \tag{5.20a}$$

$$\nu_\eta^* = \frac{1}{\nu_0}\frac{\int_{\mathbb{R}^d}\mathrm{d}\mathbf{V}\, D_{ij}(\mathbf{V}) J\mathcal{C}_{ij}}{\int_{\mathbb{R}^d}\mathrm{d}\mathbf{V}\, D_{ij}(\mathbf{V})\mathcal{C}_{ij}} - p\frac{1}{\nu_0}\frac{\int_{\mathbb{R}^d}\mathrm{d}\mathbf{V}\, D_{ij}(\mathbf{V})\Omega\mathcal{C}_{ij}}{\int_{\mathbb{R}^d}\mathrm{d}\mathbf{V}\, D_{ij}(\mathbf{V})\mathcal{C}_{ij}}, \tag{5.20b}$$

where $\nu_0 = p^{(0)}/\eta_0$, with $p^{(0)} = nk_BT$. Note that the above relations are still exact within the Chapman-Enskog expansion. The approximation consists in truncating the function $f^{(1)}$ to the first nonzero term in a Sonine polynomial expansion:

$$\boldsymbol{\mathcal{A}}(\mathbf{V}) = a_1\mathcal{M}(\mathbf{V})\mathbf{S}(\mathbf{V}), \tag{5.21a}$$

$$\boldsymbol{\mathcal{B}}(\mathbf{V}) = b_1\mathcal{M}(\mathbf{V})\mathbf{S}(\mathbf{V}), \tag{5.21b}$$

$$\boldsymbol{\mathcal{C}}(\mathbf{V}) = c_0\mathcal{M}(\mathbf{V})\mathbf{D}(\mathbf{V}), \tag{5.21c}$$

where $a_1$, $b_1$, and $c_0$ are the coefficients of the development, and

$$\mathcal{M}(\mathbf{V}) = \frac{n}{v_T^d \pi^{d/2}} \mathrm{e}^{-V^2/v_T^2} \tag{5.22}$$

is the Maxwellian in the scaling regime. This allows one to compute the relations (5.20), and one finds (see Appendix A.16)

$$\nu_\eta^* = \phi^{\mathrm{M}} \frac{\sqrt{2}\Gamma(d/2)}{4\pi^{(d-1)/2}} \left[ p\frac{d+2}{2} + (1-p) \right], \tag{5.23a}$$

$$\nu_\kappa^* = \phi^{\mathrm{M}} \frac{\sqrt{2}\Gamma(d/2)}{4\pi^{(d-1)/2}} \left[ \frac{d+2}{2} + (1-p)\frac{d-1}{d} \right]. \tag{5.23b}$$

The parameter $\phi^{\mathrm{M}}$ governing the collision frequency may be freely chosen to allow for a relevant comparison with hard sphere dynamics (see, e.g., [41]). We choose $\phi$ such that the transport coefficients are normalized to one for $p \to 0$, that is when all collisions are elastic. It is remarkable that for the Maxwell model a single parameter such as $\phi$ is sufficient to ensure normalization of all the transport coefficients (this will not be the case in the VHP approach). This leads to

$$\phi^{\mathrm{M}} = \frac{4\pi^{(d-1)/2}}{\sqrt{2}\Gamma(d/2)}. \tag{5.24}$$

The above value turns out to be the same as the one obtained from the elastic limit of the Maxwell model of granular gases [41]. In the latter case, $\phi$ was chosen matching the temperature decay rate with that characterizing the homogeneous cooling state of inelastic hard spheres. With the choice (5.24) the transport coefficients (5.19) become

$$\eta^* = \frac{1}{p\frac{d+2}{2} + (1-p)}, \tag{5.25a}$$

$$\kappa^* = \frac{1}{p\frac{d(d+2)}{2(d-1)} + (1-p)}, \tag{5.25b}$$

$$\mu^* = 0, \tag{5.25c}$$

Following the same route as in Chapter 4, the first-order distribution function (5.14) reads

$$f^{(1)}(\mathbf{r}, \mathbf{V}; t) = -\frac{\beta^3}{n}\mathcal{M}(\mathbf{V}) \left[ \frac{2m}{d+2} S_i(\mathbf{V})\kappa\nabla_i T + \frac{\eta}{\beta} D_{ij}(\mathbf{V})\nabla_j u_i \right]. \tag{5.26}$$

#### 5.5.3.2 The exact first-order Chapman-Enskog solution

By construction of the Chapman-Enskog method, the velocity moments of $f$ are given by those of the local equilibrium distribution $f^{(0)}$. It is then easy to show that the decay rates to first order (5.13) are equal to zero [therefore $\Omega f^{(1)} = 0$, where the operator $\Omega$ is defined in Appendix A.17]. Proceeding in a similar way as in [41], we obtain in Appendix A.17 the exact transport coefficients for the Maxwell model, i.e., without any approximation on the form of $f^{(1)}$. This may be done by integrating the Boltzmann equation (A.169) over $\mathbf{V}$ with weight $mV_iV_j$ and $mV^2V_i/2$. With the choice for $\phi^{\mathrm{M}}$ given by Eq. (5.24), one finds the same transport coefficients as those given by Eqs. (5.25). This means that the truncation of $f^{(1)}$ to its first nonzero term in a Sonine polynomial expansion is a harmless approximation when looking at the transport coefficients (this is a peculiarity of the Maxwell model). In fact, it turns out that the transport coefficients depend only on the first term in the Sonine polynomial expansion of $f^{(1)}$ [7]. For example, the heat current (4.35) may be rewritten under the form [6, 7]

$$q_i^{(1)} = -\frac{d+2}{2}\frac{n}{m\beta^3}\left(a_1\nabla_i T + b_1\nabla_i n\right), \tag{5.27}$$

where the first nonzero coefficients ($a_1$, $b_1$) (that may depend on $n$ and $T$) in the Sonine expansion are defined by Eqs. (5.21). Therefore the latter coefficients always give an exact result for the transport coefficients, but the problem at hand is to calculate them exactly. This turns out to be possible within the Maxwell model.

### 5.5.4 Hydrodynamic equations

Since the pressure tensor and the heat flux defined by Eqs. (5.15) and (5.16), respectively, are of order 1 in the gradients, their insertion in the balance equations (4.32) yields contributions of order 2. Knowledge of the second order velocity distribution $f^{(2)}$ is therefore required in order to find the correct decay rates that contribute to Navier-Stokes order. It was shown in the framework of the weakly inelastic gas of hard spheres – and consequently for an elastic gas – that those Burnett contributions were three orders of magnitude smaller than the Navier-Stokes contributions [24]. For the sake of simplicity, we shall therefore neglect those terms, with *a priori* no control on the resulting error. Nevertheless, such an approximation is expected to be increasingly more accurate as the annihilation probability is decreased. The corresponding hydrodynamic Navier-Stokes equations are given by

$$\partial_t n + \nabla_i(nu_i) = -pn[\xi_n^{(0)} + \xi_n^{(1)}], \tag{5.28a}$$

$$\partial_t u_i + \frac{1}{mn}\nabla_j P_{ij} + u_j\nabla_j u_i = -pv_T[\xi_{u_i}^{(0)} + \xi_{u_i}^{(1)}], \qquad i = 1,\ldots,d, \tag{5.28b}$$

$$\partial_t T + u_i\nabla_i T + \frac{2}{nk_Bd}(P_{ij}\nabla_i u_j + \nabla_i q_i) = -pT[\xi_T^{(0)} + \xi_T^{(1)}]. \tag{5.28c}$$

$P_{ij}$ and $q_j$ are given by Eqs. (5.15) with $\zeta = 0$, and (5.16) respectively. The rates $\xi_n^{(1)}$, $\xi_{u_i}^{(1)}$, and $\xi_T^{(1)}$ may be calculated using their definition (5.12) and the distribution (5.26) [53]. We find that all decay rates are equal to zero except

$$\xi_n^{(0)} = \frac{d+2}{2}\nu_0. \tag{5.29}$$

We thus have a closed set of equations for the hydrodynamic fields to the Navier-Stokes order.

## 5.6 The VHP model

### 5.6.1 The homogeneous cooling state

Integrating the Boltzmann equation (5.1) over $\mathbf{V}$ for $x = 2$, one obtains

$$\frac{\mathrm{d}n}{\mathrm{d}t} = -p\omega(t)n, \tag{5.30}$$

where

$$\omega(t) = n(t)v_T(t)\sigma^{d-1}\phi^{\mathrm{VHP}}\langle c_{12}^2\rangle, \tag{5.31}$$

and $\langle g(\mathbf{c}_1,\mathbf{c}_2)\rangle = \int_{\mathbb{R}^{2d}} \mathrm{d}\mathbf{c}_1\mathrm{d}\mathbf{c}_2\, g(\mathbf{c}_1,\mathbf{c}_2)\widetilde{f}(c_1)\widetilde{f}(c_2)$ denotes the average of a function $g(\mathbf{c}_1,\mathbf{c}_2)$ in the homogeneous cooling state (HCS). We have written $\phi^{\mathrm{VHP}}$ for $\phi(x=2)$. Following the same route as in [39, 52] or in Appendix A.3, the Boltzmann equation may be rewritten in the form

$$\langle c_{12}^2\rangle\left[1+\frac{1-\alpha_e}{2}\left(d+c_1\frac{\mathrm{d}}{\mathrm{d}c_1}\right)\right]\widetilde{f}(c_1) = \widetilde{f}(c_1)\int_{\mathbb{R}^d}\mathrm{d}\mathbf{c}_2\, c_{12}^2\widetilde{f}(c_2) - \frac{1-p}{p}\frac{1}{S_d}\widetilde{I}[\widetilde{f},\widetilde{f}], \tag{5.32}$$

where

$$\alpha_e = \frac{\int_{\mathbb{R}^{2d}}\mathrm{d}\mathbf{c}_1\mathrm{d}\mathbf{c}_2\int \mathrm{d}\widehat{\boldsymbol{\sigma}}\, c_{12}^2c_1^2\widetilde{f}(c_1)\widetilde{f}(c_2)}{\left[\int_{\mathbb{R}^d}\mathrm{d}\mathbf{c}\, c^2\widetilde{f}(c)\right]\int_{\mathbb{R}^{2d}}\mathrm{d}\mathbf{c}_1\mathrm{d}\mathbf{c}_2\int d\widehat{\boldsymbol{\sigma}}\, c_{12}^2\widetilde{f}(c_1)\widetilde{f}(c_2)} = \frac{\langle c_{12}^2c_1^2\rangle}{\langle c_1^2\rangle\langle c_{12}^2\rangle}, \tag{5.33}$$

and

$$\widetilde{I}[\widetilde{f},\widetilde{f}] = \int_{\mathbb{R}^d}\mathrm{d}\mathbf{c}_1\int \mathrm{d}\widehat{\boldsymbol{\sigma}}\, c_{12}^2(b^{-1}-1)\widetilde{f}(c_1)\widetilde{f}(c_2). \tag{5.34}$$

The limit $c_1 \to 0$ of the Boltzmann equation (5.32) encodes a useful information for ballistically controlled dynamics [39, 52, 70, 75]:

$$\langle c_{12}^2\rangle\left(1+d\frac{1-\alpha_e}{2}\right)\widetilde{f}(0) = \widetilde{f}(0)\langle c^2\rangle - \frac{1-p}{p}\frac{1}{S_d}\lim_{c_1\to 0}\widetilde{I}[\widetilde{f},\widetilde{f}]. \tag{5.35}$$

Next, we consider the first nonzero correction to the Maxwellian in a Sonine polynomial expansion of the HCS:

$$\widetilde{f}(c) = \widetilde{\mathcal{M}}(c)\left[1+a_2S_2(c^2)\right], \tag{5.36}$$

where $\widetilde{\mathcal{M}}(c) = \pi^{-d/2}\mathrm{e}^{-c^2}$ is the Maxwellian and $S_2(c^2) = c^4/2-(d+2)c^2/2+d(d+2)/8$ the second Sonine polynomial [7]. Eqs. (5.35) and (5.33) form a system of two equations for the two unknown $\alpha_e$ and $a_2$. Making use of the relations (A.164), it is a straightforward task to compute the limit in the right-hand side of Eq. (5.35) [75], which gives

$$\lim_{c_1\to 0}\widetilde{I}[\widetilde{f},\widetilde{f}] = -a_2\frac{S_d}{\pi^{d/2}}\frac{d^2(d+2)}{16}. \tag{5.37}$$

Using Eq. (5.36), one easily obtains from Eq. (5.33)

$$\alpha_e = \frac{d+1}{d} + a_2\frac{d+2}{2d}. \tag{5.38}$$

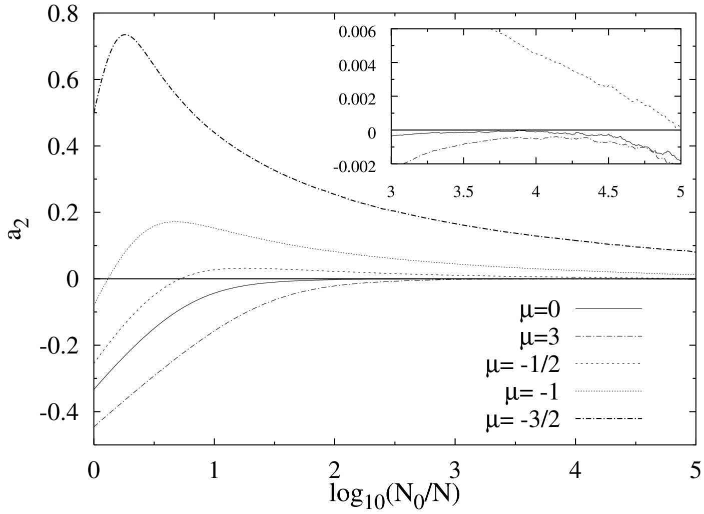


Figure 5.1: Plot of $a_2$ as a function of the densities $N_0/N$ for different values of $\mu$ for the VHP model and $p = 0.5$, $d = 2$, $N_0 = 5 \times 10^7$. There are approximately $5 \times 10^4$ independent runs. The deviation from the asymptotic value of $a_2$ (inset) is due to the low remaining number of particles (large $N_0/N$).

Note that Eqs. (5.37) and (5.38) are exact relations for which all nonlinear contributions in $a_2$ were kept. However, those nonlinear terms cancel out in each case. Making use of $\langle c_{12}^2 \rangle = d$, the insertion of Eqs. (5.37) and (5.36) in (5.35) gives

$$\left(1 - a_2 \frac{d+2}{2}\right) \left[1 + a_2 \frac{d(d+2)}{8}\right] = 1 + a_2 \frac{d(d+2)}{8} \frac{1}{p}. \tag{5.39}$$

Eq. (5.39) admits two solutions, the first one being $a_2 = 0$ and the second one $a_2 = -2[d+p(4-d)]/[d(d+2)p]$. The second solution is not physical since it diverges for $p = 0$. Therefore $a_2 = 0$ and the HCS of the VHP model within the approximation (5.36) is described by the local Maxwellian $\widetilde{\mathcal{M}}(c) = \pi^{-d/2} \mathrm{e}^{-c^2}$. We also note that upon discussing the potential ambiguities resulting from such a linearization scheme in $a_2$ (as done in [75, 79]), the same conclusion is reached.

We study the evolution towards the asymptotic scaling solution starting from different initial distributions characterized by their behavior near the origin. We define the exponent $\mu$ by $\widetilde{f}(c) \simeq |c|^\mu$ for $c \to 0$. Similarly to Sec. 4.3.2.3, we implement DSMC simulations and study the fourth cumulant $a_2$ as a function of $N_0/N$ for several values of $\mu$ (see Fig. 5.1). The fact that $a_2$ reaches a plateau indicates that the distribution enters the scaling regime at late times. Moreover, it seems from the inset that the scaling values for $a_2$ do not (or very weakly, note the $y$ scale of the inset) depend on $\mu$. For negative values of $\mu$, the convergence is however slower due to the divergence of the initial velocity distribution (see, e.g., Fig. 4.7) near the origin (the comparison of Figs. 5.1 and 4.9 shows that the convergence for $\mu = -3/2$ in the VHP case is much slower).

### 5.6.2 The zeroth-order Chapman-Enskog solution

Proceeding in a similar way as already described, we obtain a set of equations formally identical to Eqs. (5.8) and (5.9). The calculation of the decay rates gives $\xi_{u_i}^{(0)} = 0$, $\xi_T^{(0)} = n\sigma^{d-1}\phi^{\text{VHP}} v_T$, and $\xi_n^{(0)} = \xi_T^{(0)} d$. The HCS is therefore given by

$$n_H(t) = n_0(1 + pt/t_0)^{-\gamma_n}, \tag{5.40a}$$

$$T_H(t) = T_0(1 + pt/t_0)^{-\gamma_T}, \tag{5.40b}$$

where the decay exponents are $\gamma_n = \xi_n^{(0)}(0)t_0$, $\gamma_T = \xi_T^{(0)}(0)t_0$, and the relaxation time $t_0^{-1} = \xi_n^{(0)}(0) + \xi_T^{(0)}(0)/2$. In other words, we have

$$\gamma_n = \frac{2d}{2d+1}, \qquad \gamma_T = \frac{2}{2d+1}. \tag{5.41}$$

These quantities do not depend either on $\phi$ nor on the annihilation probability $p$. The former result is an exact property of the dynamics under study (the factor $\phi$ may be absorbed into a rescaling of time $t$, leaving scaling exponents unaffected) while the latter may *a priori* be an artifact of the approximations made (it will however be shown below that the $p$ dependence –if any– is extremely weak). If we define the root-mean-square velocity by $\overline{v} = \sqrt{\langle v^2 \rangle}$, then from the definition (4.31c) of the temperature $\overline{v}(t) \propto T_H^{1/2}(t)$, and from Eq. (5.40b) we have $\overline{v} \sim t^{-\gamma_v}$ for long times, with $\gamma_v = \gamma_T/2$. The decay exponents $\gamma_n$ and $\gamma_v$, as well as the decay exponents for the Maxwell model, agree with the prediction of Krapivsky and Sire [43], and satisfy the scaling constraint $\gamma_n + \gamma_v = 1$, which essentially expresses the unicity of the relevant time scale in the problem. Moreover, making use of the expression for the decay exponents of PBA of hard spheres $\gamma_n^{\text{HS}}$ and $\gamma_v^{\text{HS}}$ obtained to linear order in $a_2$ (see Chapter 4) [52, 53], it is easy to verify explicitly that the Maxwell and VHP models provide bounds [43]

$$\frac{2d}{2d+1} < \gamma_n^{\text{HS}}(p) < 1, \qquad 0 < \gamma_v^{\text{HS}}(p) < \frac{1}{2d+1}, \tag{5.42}$$

for all $p \in [0, 1]$. We emphasized however that the previous inequality have the status of "empirical" observations, and could not be anticipated from rigorous arguments.

We performed Direct Monte Carlo Simulations (DSMC) in order to verify the decay exponents of the VHP model. The algorithm is similar to the one described in [44, 52]. For the sake of completeness, we briefly outline the main steps of the algorithm. We choose at random two different particles $\{i, j\}$. The time is then increased by $v_T/(N^2 v_{ij}^2)$ where $N$ is the number of remaining particles. With probability $p$ the two particles are removed from the system, and with probability $1-p$ their velocities are modified according to Eqs. (4.5). As the fluctuations increase for small $N$, it is necessary to average over several independent realizations in order to diminish the noise. A log-log plot of the density $n/n_0$ and the root-mean-squared velocity $\overline{v}/\overline{v}_0$ as a function of time gives the decay exponents (see Fig. 5.2). The DSMC results are in excellent agreement with the analytical predictions and the expected power-law behaviors are observed over several decades (see. Fig. 5.3).

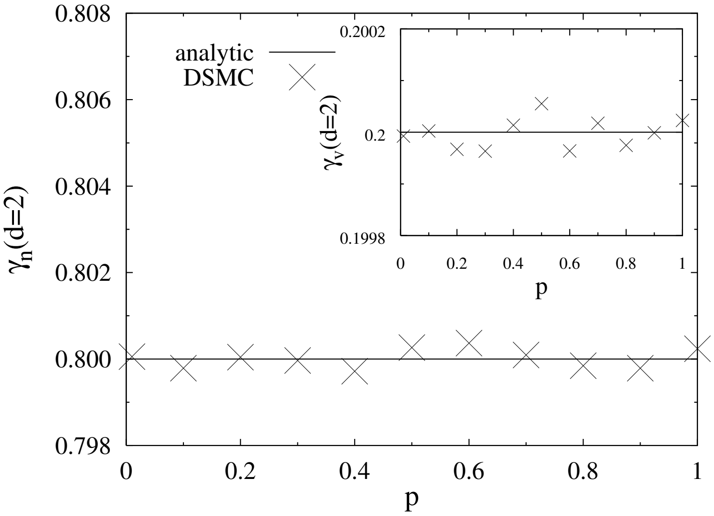


Figure 5.2: The decay exponents $\gamma_n$ and $\gamma_v$ (inset) in two dimensions for the VHP model ($x = 2$). The analytical predictions $\gamma_n = 2d/(2d+1) = 0.8$ and $\gamma_v = 1/(2d+1) = 0.2$ are shown by the continuous lines while the symbols stand for the DSMC results (obtained from approximately 300 independent runs and $10^7$ initial particles). From the above data, it appears that the scaling relation $\gamma_n + \gamma_v = 1$ is well obeyed (the deviation from 1 does not exceed $4 \times 10^{-4}$) and that the scaling exponents do not depend on $p$. Note the $y$ scale.

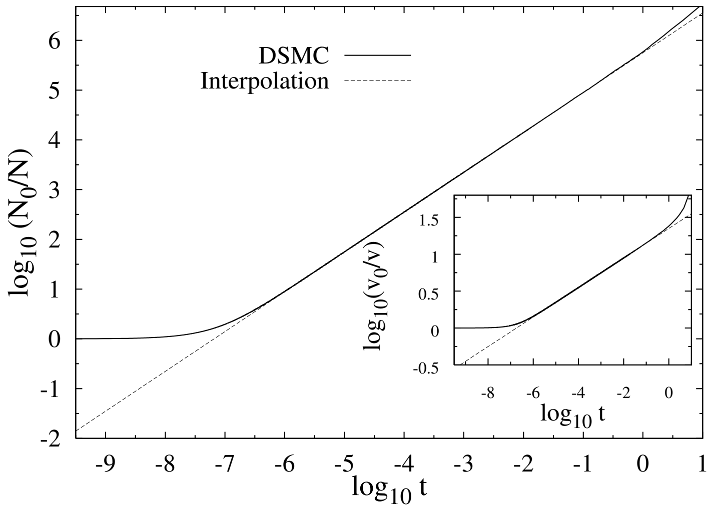


Figure 5.3: Time dependence of $n$ and $\overline{v}$ (inset) for $d = 2$ and $p = 0.5$ on a log-log scale. The initial velocity distribution is Gaussian. $N_0$ (resp. $N$) is the initial (resp. remaining) number of particles. $v_0 = \overline{v}(0)$ is the root-mean-square velocity at $t = 0$, whereas we write $v$ for $\overline{v}(t > 0)$. The dashed straight line is a linear interpolation giving the decay exponent of the power-law, and the deviations to this law for large times is due to the low number of remaining particles.

### 5.6.3 The approximate first-order Chapman-Enskog solution

The procedure is similar to the one followed within the Maxwell model of Sec. 5.5.3 (or [53]), and we find

$$\eta^* = \frac{1}{\nu_\eta^* - \frac{1}{2}p\xi_T^{(0)*}}, \tag{5.43a}$$

$$\kappa^* = \frac{d-1}{d}\frac{2\nu_\mu^* - 2p\xi_n^{(0)*} - 3p\xi_T^{(0)*}}{X}, \tag{5.43b}$$

$$\mu^* = 2p\frac{d-1}{d}\frac{\xi_T^{(0)*}}{X}, \tag{5.43c}$$

where $X = \nu_\kappa^*[2\nu_\mu^* - 2p\xi_n^{(0)*} - 3p\xi_T^{(0)*}] + p\xi_T^{(0)*}\{-4\nu_\mu^* + 3p[\xi_n^{(0)*} + 2\xi_T^{(0)*}]\}$,

$$\nu_\mu^* = \frac{1}{\nu_0}\frac{\int_{\mathbb{R}^d} \mathrm{d}\mathbf{V}\, S_i(\mathbf{V})J\mathcal{B}_i}{\int_{\mathbb{R}^d} \mathrm{d}\mathbf{V}\, S_i(\mathbf{V})\mathcal{B}_i} - p\frac{1}{\nu_0}\frac{\int_{\mathbb{R}^d} \mathrm{d}\mathbf{V}\, S_i(\mathbf{V})\Omega\mathcal{B}_i}{\int_{\mathbb{R}^d} \mathrm{d}\mathbf{V}\, S_i(\mathbf{V})\mathcal{B}_i}, \tag{5.44}$$

and $\xi_n^{(0)*} = \xi_n^{(0)}/\nu_0$, $\xi_T^{(0)*} = \xi_T^{(0)}/\nu_0$. Truncating the function $f^{(1)}$ to the first term in a Sonine polynomial expansion as it was the case for Eqs. (5.21), the coefficients $\nu_\eta^*$,

$\nu_\kappa^*$, and $\nu_\mu^*$ may be calculated with the help of App. A.16. We find

$$\nu_\eta^* = \phi^{\text{VHP}} \frac{\sqrt{2}\Gamma(d/2)}{4\pi^{(d-1)/2}} \left[ p\frac{(d+2)^2}{2} + (1-p)\frac{(d+2)(d+4)}{4} \right], \tag{5.45a}$$

$$\nu_\kappa^* = \nu_\mu^* = \phi^{\text{VHP}} \frac{\sqrt{2}\Gamma(d/2)}{4\pi^{(d-1)/2}} \left[ p\frac{(d+2)(d+3)}{2} + (1-p)\frac{(d-1)(d+4)}{d} \right]. \tag{5.45b}$$

The free parameter $\phi^{\text{VHP}}$ setting the frequency collision has *a priori* no reason for being the same as for the Maxwell model. We choose this quantity such that $\eta^*(p = 0) = 1$, which means that the shear viscosity for the VHP gas is set for vanishing $p$ to coincide with the shear viscosity $\eta_0$ of hard spheres. This allows for a better comparison of the transport coefficients for the Maxwell, hard sphere, and VHP models. Other choices for $\phi^{\text{VHP}}$ are possible. The condition $\eta^*(0) = 1$ leads to

$$\phi^{\text{VHP}} = \phi^{\text{M}} \frac{4}{(d+2)(d+4)}, \tag{5.46}$$

so that

$$\xi_n^{(0)*} = \frac{2d}{d+4}, \tag{5.47a}$$

$$\xi_T^{(0)*} = \frac{2}{d+4}. \tag{5.47b}$$

The first order distribution function reads

$$f^{(1)}(\mathbf{r}, \mathbf{V}; t) = -\frac{\beta^3}{n}\mathcal{M}(\mathbf{V}) \left[ \frac{2m}{d+2} S_i(\mathbf{V}) \left(\kappa \nabla_i T + \mu \nabla_i n\right) + \frac{\eta}{\beta} D_{ij}(\mathbf{V}) \nabla_j u_i \right]. \tag{5.48}$$

where the transport coefficients are given by Eqs (5.43).

### 5.6.4 Hydrodynamic equations

The decay rates to first order may be calculated using the definitions (5.12) and the distribution (5.48) [53], which gives

$$\xi_n^{(1)} = 0, \tag{5.49a}$$

$$\xi_{u_i}^{(1)} = -v_T \left( \kappa^* \frac{1}{T} \nabla_i T + \mu^* \frac{1}{n} \nabla_i n \right) \xi_u^*, \tag{5.49b}$$

$$\xi_T^{(1)} = 0, \tag{5.49c}$$

where

$$\xi_u^* = \frac{d^2(d+2)^2}{8(d-1)} \phi^{\text{VHP}} \frac{\sqrt{2}\Gamma(d/2)}{4\pi^{(d-1)/2}}. \tag{5.50}$$

The Navier-Stokes hydrodynamic equations are thus given by Eqs. (5.28) with the decay rates (5.47) and (5.49).

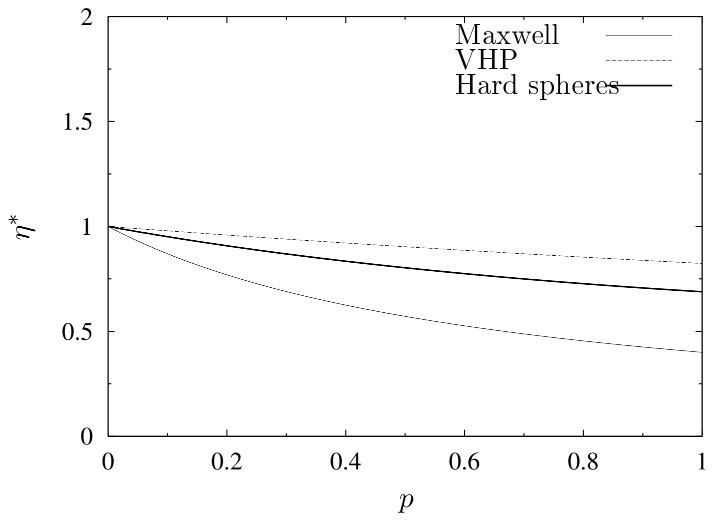


Figure 5.4: Dimensionless shear viscosity $\eta^*$ as a function of the annihilation probability $p$ for the Maxwell (thin continuous line), VHP (dashed line), and hard spheres models (thick continuous line).

### 5.6.5 Comparison of the transport coefficients

We compare the transport coefficients for the Maxwell, VHP, and hard sphere models (the coefficients for the latter model being given in [53]). Figs. 5.4, 5.5, and 5.6 show $\eta^*$, $\kappa^*$, and $\mu^*$, as a function of the annihilation probability.

Note that once we have chosen $\phi(x = 2)$ such that $\eta^* \to 1$ for $p \to 0$ there is no reason to expect $\kappa^* \to 1$ in the same limit. Other choices would have been possible such as enforcing $\kappa^* \to 1$ when $p \to 0$.

From Figures 5.4, 5.5, and 5.6 it first appears that Mawxell and VHP models capture the essential $p$ dependence of the "hard sphere" transport coefficients. In addition, they provide in most cases lower and upper bounds for $\eta^*$, $\kappa^*$ and $\mu^*$. However, as already pointed out in [53], for strong annihilation probability $p \sim p_d$, the hard sphere thermal conductivity and "Fourier" coefficient $\mu$ diverge (see Figs 5.5 and 5.6) which leads to a violation of the VHP upper bound for $\kappa$ and $\mu$ in the vicinity of $p_d$. The fact that VHP and Maxwell models lead to smooth and regular transport coefficients for all values of $p$ is a hint that the hard sphere divergence obtained in previous work [53] is a possible artifact of the underlying approximations and probably does not point towards a change of behavior nor a qualitative difference in the scaling or transport properties. This point will be further discussed in the concluding section. We finally note that an *a priori* similar deficiency was already reported for the Maxwell model of inelastic hard spheres [41].

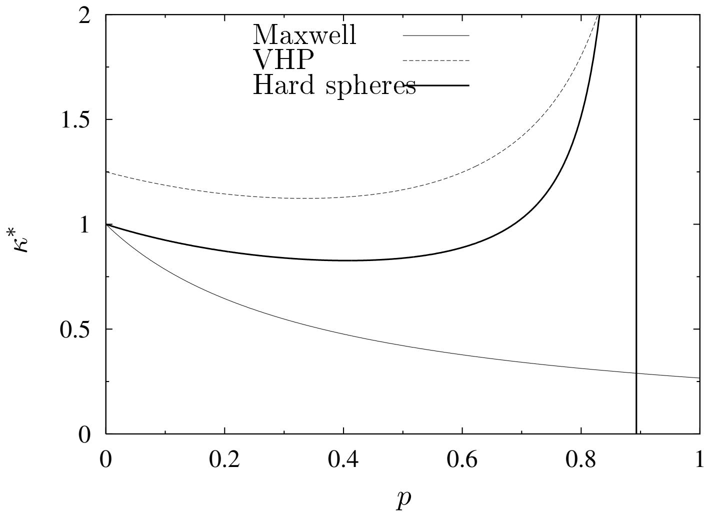


Figure 5.5: Reduced thermal conductivity $\kappa^*$ as a function of the annihilation probability $p$ for the Maxwell (thin continuous line), VHP (dashed line), and hard spheres models (thick continuous line). The vertical lines gives the value $p = 0.893\ldots$ for which a divergence of the hard sphere transport coefficients $\kappa^*$ and $\mu^*$ appears (while the shear viscosity exhibits regular behavior, see Fig. 5.4).

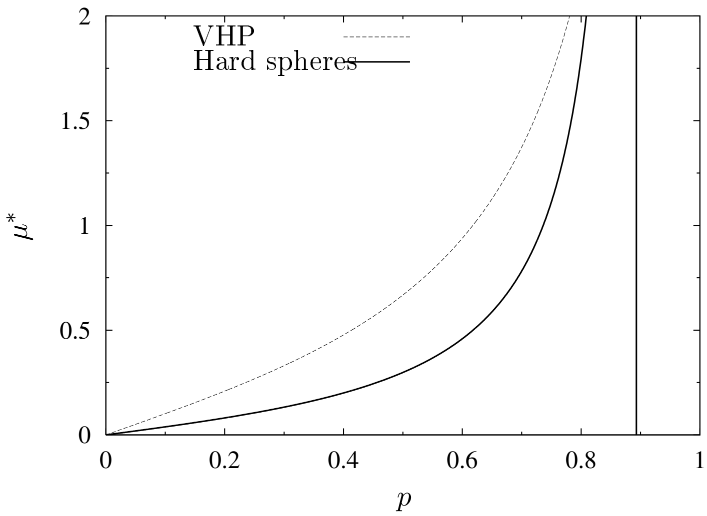


Figure 5.6: Transport coefficient $\mu^*$ as a function of the annihilation probability $p$ (see Fig. 5.5 for more details). The Maxwell model is not represented since in this case $\mu^* = 0$.

## 5.7 Stability analysis of the Navier-Stokes hydrodynamic equations

### 5.7.1 Dispersion relations

The hydrodynamic equations. (5.28) cannot be solved analytically in general. However, their linear stability analysis allows one to answer the question of formation of spatial inhomogeneities. The present study establishes under which conditions the homogeneous state is stable. We consider here a small deviation from spatial homogeneity [see Eqs. (5.10) and (5.40)] and the linearization of Eqs. (5.28) in the latter perturbation. The procedure used here follows the same route as for granular gases [24] or PBA of hard spheres [53]. We define the deviations of the hydrodynamic fields from the homogeneous solution by $\delta y(\mathbf{r},t) = y(\mathbf{r},t) - y_H(t)$, where $y = \{n, \mathbf{u}, T\}$. Inserting this form in the Navier-Stokes-like equations yields differential equations with time-dependent coefficients. In order to obtain coefficients that do not depend on time, it is necessary to introduce the new dimensionless space and time scales defined by $\mathbf{l} = \nu_{0H}(t)\sqrt{m/[k_B T_H(t)]}\mathbf{r}/2$, $\tau = \int_0^t \mathrm{d}s\, \nu_{0H}(s)/2$, as well as the dimensionless Fourier fields $\rho_{\mathbf{k}}(\tau) = \delta n_{\mathbf{k}}(\tau)/n_H(\tau)$, $\mathbf{w}_{\mathbf{k}}(\tau) = \sqrt{m/[k_B T_H(\tau)]}\delta \mathbf{u}_{\mathbf{k}}(\tau)$, and $\theta_{\mathbf{k}}(\tau) = \delta T_{\mathbf{k}}(\tau)/T_H(\tau)$, where $\delta y_{\mathbf{k}}(\tau) = \int_{\mathbb{R}^d} \mathrm{d}\mathbf{l}\, \mathrm{e}^{-i\mathbf{k}\cdot\mathbf{l}}\delta y(\mathbf{l},\tau)$. Note that $\mathbf{l}$ is defined (up to a constant prefactor) in units of the mean free path for a homogeneous gas of density $n_H(t)$. The dimensionless time $\tau(t)$ gives the accumulated number of collisions per particles up to time $t$. Since we will study both the Maxwell and VHP systems, we recall here the general results valid for non-vanishing decay rates $\xi_n^{(0)}$, $\xi_T^{(0)}$, and $\xi_u^{(1)}$. Making use of the dimensionless variables, the linearized hydrodynamic equation for the transverse mode $\mathbf{w}_{\mathbf{k}_\perp} = \mathbf{w}_{\mathbf{k}} - \mathbf{w}_{\mathbf{k}_\parallel}$ appears to be decoupled from the other equations, where the longitudinal velocity field is given by $\mathbf{w}_{\mathbf{k}_\parallel} = (\mathbf{w}_{\mathbf{k}} \cdot \widehat{\mathbf{e}}_{\mathbf{k}})\widehat{\mathbf{e}}_{\mathbf{k}}$ and $\widehat{\mathbf{e}}_{\mathbf{k}}$ is the unit vector along the direction given by $\mathbf{k}$. The transversal velocity field $\mathbf{w}_{\mathbf{k}_\perp}$ consequently defines $(d-1)$ degenerated shear modes. Upon direct integration, we have

$$\mathbf{w}_{\mathbf{k}_\perp}(\tau) = \mathbf{w}_{\mathbf{k}_\perp}(0)\exp[s_\perp(p,k)\tau], \tag{5.51}$$

where

$$s_\perp(p,k) = p\xi_T^{(0)*} - \frac{1}{2}\eta^* k^2. \tag{5.52}$$

On the other hand, the longitudinal velocity field $\mathbf{w}_{\mathbf{k}_\parallel}$ lies in the one dimensional vector space generated by $\mathbf{k}$. Hence there are three hydrodynamic fields to be determined, namely the density $\rho_{\mathbf{k}}$, temperature $\theta_{\mathbf{k}}$, and longitudinal velocity field $\mathbf{w}_{\mathbf{k}_\parallel} = w_{\mathbf{k}_\parallel}\widehat{\mathbf{e}}_{\mathbf{k}}$. The hydrodynamic matrix of the corresponding linear system is given in [53]. The corresponding eigenmodes are given by $\varphi_n(k) = \exp[s_n(p,k)\tau]$, $n = 1,\ldots,3$, where $s_n(p,k)$ are the eigenvalues of $\mathbf{M}$. Each of these three fields is a linear combination of the eigenmodes; thus only the biggest real part of the eigenvalue $s_n(p,k)$ has to be taken into account to discuss the limit of marginal stability of the different modes.

We define $k_\perp$ by the condition $\mathrm{Re}[s_\perp(k_\perp,p)] = 0$, i.e.,

$$k_\perp = \sqrt{\frac{2p\xi_T^{(0)*}}{\eta^*}}, \tag{5.53}$$

and $k_\parallel$ by $\max_{k_\parallel} \mathrm{Re}[s_\parallel(k_\parallel, p)] = 0$, $k_\parallel < k_\perp$. Therefore if $k > k_\perp$ all *rescaled* modes are linearly stable. For $k \in [k_\parallel, k_\perp]$ only the *rescaled* shear mode is linearly unstable (the latter may however be non-linearly coupled to the other modes), and for $k < k_\parallel$ all eigenvalues are positive which leads to instabilities. However, it should be kept in mind that the previous discussion involves rescaled modes only, and should be connected to the original $\mathbf{r}$ variable. Indeed, for any real system (for example a cubic box of volume $L^d$) the smallest wavenumber allowed for a perturbation is given by $2\pi/L$, which from the definition of $\mathbf{l}$ corresponds to the time-dependent dimensionless wavenumber $k_{\min} = 2\pi/(Ln\sigma^{d-1}\mathcal{C})$ where $\mathcal{C} = 4\pi^{(d-1)/2}/[(d+2)\Gamma(d/2)]$. Since the density $n(t)$ is a decreasing function of time, $k_{\min}$ increases monotonously and there exists a time $t_\perp$ such that $k_{\min}(t) > k_\perp$ for $t > t_\perp$. The lower cut-off $k_{\min}$ therefore eventually enters the region where the homogeneous solution is stable. For $t = t_\perp$, the system is however not in a spatially homogeneous state, but it is nevertheless tempting to conclude that the perturbations will be damped for $t > t_\perp$. Although this statement is not rigorously derived, we conclude here that an instability can only be a transient effect (transient instabilities were also predicted for viscoelastic granular gases with velocity-dependent restitution coefficient [13]).

The time $t_\perp$ can be estimated from the condition $k_{\min}(t_\perp) = k_\perp$. Making use of the hypothesis of small spatial inhomogeneities, we may replace the density $n(t)$ appearing in the definition of $k_{\min}(t)$ by the homogeneous density $n_H(t)$ given by Eq. (5.40a). We obtain

$$\frac{t_\perp}{t_0} = \frac{1}{p}\left\{\left[\frac{Ln_0\sigma^{d-1}2\pi^{(d-3)/2}}{(d+2)\Gamma(d/2)}k_\perp(p)\right]^{1/\gamma_n} - 1\right\}. \tag{5.54}$$

Is the transient instability alluded to easily observable in a simulation? A typical number of particles for molecular dynamics simulations is of the order of $10^5$, and $n_0\sigma^2 = 5\times10^{-3}$ (which corresponds to a rather low total initial packing function $\pi n_0\sigma^2/4 \simeq 0.004$). For $p = 0.1$ and $d = 2$ Eq. (5.54) gives $t_\perp \approx 8.6\, t_0 \ldots$. Making use of Eq. (5.40a) to approximate the density, one obtains $n(t_\perp) \approx 0.61 n_0$. The density inhomogeneities therefore start to decrease after that the density decreased to only 0.61 times its initial value, which for $p = 0.1$ corresponds in average to only 4 collisions per particle. For comparison purposes, inhomogeneities in granular gases are observed after a few hundred collisions per particle [12, 113]. In order to observe the previous (and presumably transient) instabilities one would need molecular dynamics simulations with very large systems. Another condition is to have a large enough $p$, which increases $k_\perp$, see Fig. 5.9. Equivalently, increasing $p$ increases the divergence rate $s_\perp$ at fixed $k$, see Eq. (5.52). For sufficiently small $p$ (or small system sizes) Eq. (5.54) does not have a positive solution because $k_{\min} > k_\perp$ already for $t = 0$. To sum up, the typical size of the inhomogeneities may grow as a function of time until $t \simeq t_\perp$ but the subsequent evolution should drive the system back to a time dependent homogeneous regime.

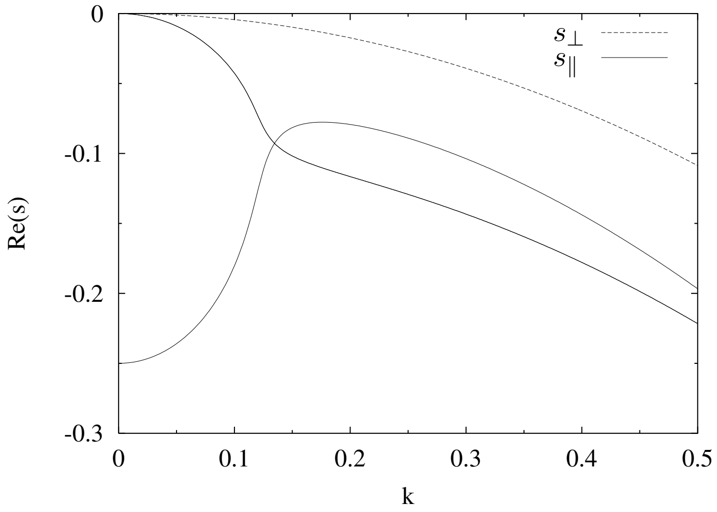


Figure 5.7: Real part of the eigenvalues in dimensionless units for the Maxwell model with $p = 0.1$ and $d = 3$. The dispersion relation obtained from Eq. (5.52) is represented by a dashed line (labeled $s_\perp$) whereas the three remaining relations are represented by continuous lines (labeled $s_\parallel$). The shear mode ($s_\perp$) and sound modes (which are on this figure such that $s = 0$ when $k \to 0$) are degenerated twice.

### 5.7.2 Comparison between Maxwell, very hard particles and hard sphere results

For the Maxwell model, the temperature decay rate $\xi_T^{(0)}$ vanishes. It follows from Eq. (5.52) that $k_\perp = 0$ and the transverse mode is stable, which is confirmed by Fig. 5.7. The Maxwell model appears to be linearly stable for all values of the annihilation probability $p$. On the other hand, within the VHP approach, the decay rate $\xi_T(0) \neq 0$. The transverse mode may consequently be unstable for some wavenumbers $k$ of the perturbation (see Fig. 5.8), which by nonlinear coupling to the other modes may lead to density inhomogeneities. Other modes than the shear may also be linearly unstable, when rescaled wave numbers are such that $k > k_\parallel$. The thresholds $k_\perp$ and $k_\parallel$ are shown in Fig. 5.9 for the 3 models. It appears again that the hard sphere quantity is bounded below by its Maxwell counterpart and above by VHP. Note that the linear stability analysis does not suffer from arbitrariness related to the free parameter $\phi(x)$.

The imaginary part of the eigenvalues embodies the information on the propagation of the perturbations. In Fig. 5.8, we identify 3 different parallel modes for small enough $k$ ($k < 0.05$). Given that the shear mode is always $(d-1)$ times degenerated and that there are $d+2$ modes in total, none of the parallel modes are degenerated for low enough $k$. Increasing $k$ up to the first bifurcation, the sound modes become degenerated and have a nonzero imaginary value. The non-propagating sound modes thus have bifurcated into a pair of propagating modes. Since the eigenvalue for the transverse velocity field is always real, we shall study here only the imaginary part

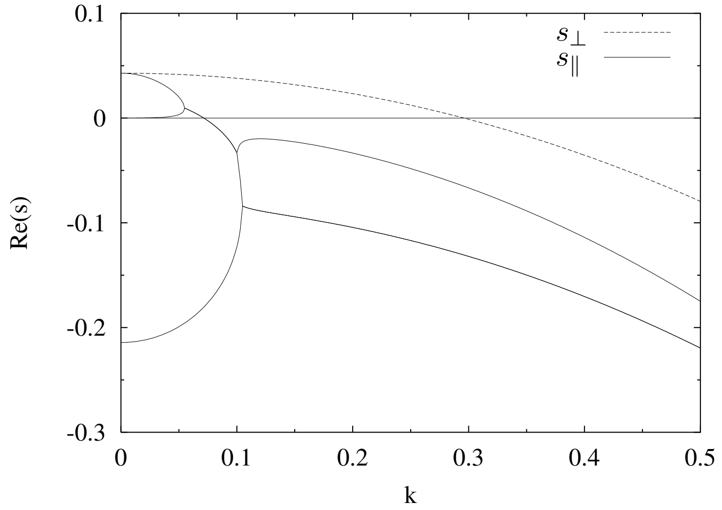


Figure 5.8: Real part of the eigenvalues in dimensionless units for the VHP model with $p = 0.1$ and $d = 3$. The dispersion relation obtained from Eq. (5.52) is represented by a dashed line (labeled $s_\perp$) whereas the three remaining relations are represented by continuous lines (labeled $s_\parallel$). The first two biggest parallel modes are sound modes.

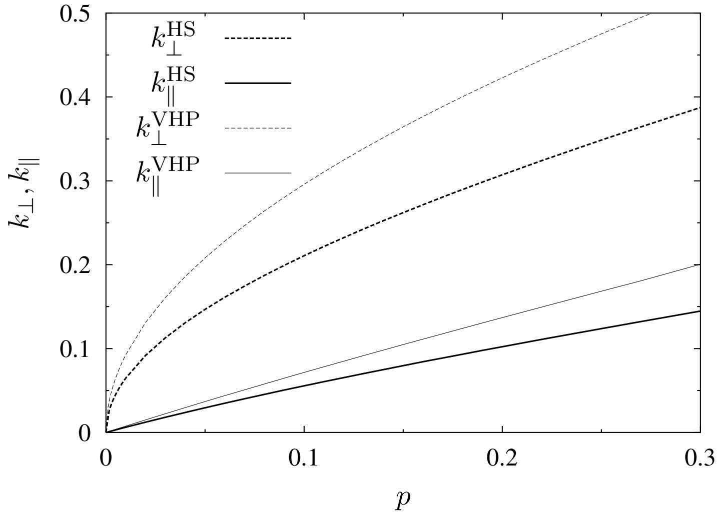


Figure 5.9: Wavenumber $k_\perp$ and $k_\parallel$ in dimensionless units as a function of the annihilation probability $p$ for $d = 3$. HS and VHP superscripts denote the hard spheres and very hard particles models, respectively. Within the Maxwell model, one has $k_\perp = k_\parallel = 0$.

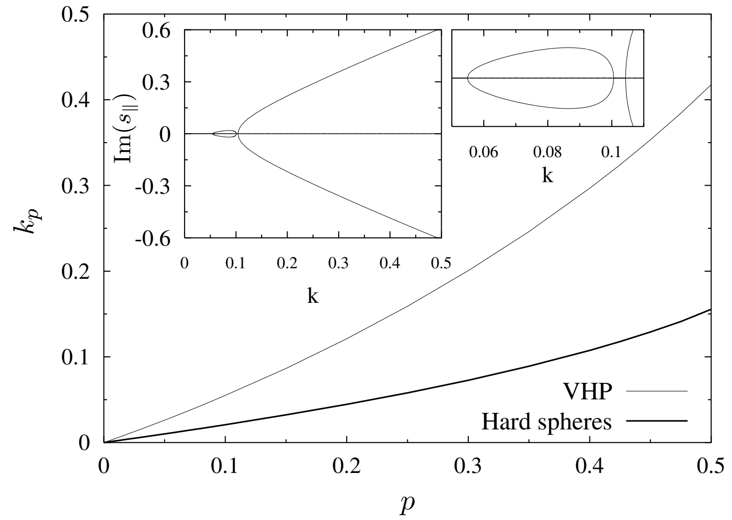


Figure 5.10: Wave number $k_p$ in dimensionless units as a function of the annihilation probability $p$ for $d = 3$. The Maxwell model is not represented since in this case $k_p = 0$ for all $p$. The main inset shows the imaginary part of the eigenvalues in dimensionless units for the VHP model for $d = 3$ and $p = 0.1$. The smaller inset shows the propagation gap $k \in [0.1006\ldots, 0.1046\ldots]$ of the sound modes.

of the other eigenvalues. We define $k_p$ such that for all $k < k_p$ all eigenvalues are real. It means that only perturbations with small enough wave numbers $\lambda$ such that $\lambda^{-1} > k_p/(2\pi n\sigma^{d-1})$ are propagating. Fig. 5.10 shows $k_p$ as a function of the annihilation probability $p$ for the VHP, hard sphere, and Maxwell models. Once more, the VHP and Maxwell models appear as upper and lower bounds, respectively. From Fig. 5.7 the Maxwell sound modes are degenerated for all $k$ and therefore the sound modes of the Maxwell model are always propagating, i.e., $k_p = 0$. In the VHP case, Fig. 5.8 shows a propagation gap for the sound modes, i.e., a $k$- window with $k > k_p$, where the sound modes are not degenerated. This is confirmed by Fig. 5.10 (smaller inset). A propagation gap in the sound mode dispersion relation has been observed in neutron scattering experiments for example [125, 126].

## 5.8 Conclusions

Making use of the Chapman-Enskog scheme, we have derived in this chapter the hydrodynamic equations governing the coarse-grained number density, linear momentum and kinetic energy density fields for an assembly of particles undergoing annihilating collisions with probability $p$ and an elastic scattering otherwise. In between collisions, the motion is ballistic. To this aim, the relevant “hard sphere”-like Boltzmann equation has been simplified first into its Maxwell, and second into its very hard particle (VHP) form. In both cases, the corresponding Navier-Stokes equations take the same form as in the initial hard sphere description and read

$$\partial_t n + \nabla_i (n u_i) = -pn\,\xi_n, \tag{5.55a}$$

$$\partial_t u_i + \frac{1}{mn}\nabla_j P_{ij} + u_j \nabla_j u_i = -p v_T\,\xi_{u_i}, \tag{5.55b}$$

$$\partial_t T + u_i \nabla_i T + \frac{2}{n k_B d}(P_{ij}\nabla_i u_j + \nabla_i q_i) = -pT\,\xi_T, \tag{5.55c}$$

with

$$\xi_n = \frac{d+2}{2}\,\nu_0 = 4\,\frac{\pi^{(d-1)/2}}{\Gamma(d/2)} n \sigma^{d-1}\sqrt{\frac{k_B T}{m}}, \tag{5.56}$$

$$\xi_{u_i} = 0, \tag{5.57}$$

$$\xi_T = 0, \tag{5.58}$$

for the Maxwell model, and

$$\xi_n = \frac{2d}{d+4}\,\nu_0, \tag{5.59}$$

$$\xi_{u_i} = -v_T\left(\kappa^*\frac{1}{T}\nabla_i T + \mu^*\frac{1}{n}\nabla_i n\right)\frac{d^2(d+2)}{2(d-1)(d+4)}, \tag{5.60}$$

$$\xi_T = \frac{2}{d+4}\,\nu_0, \tag{5.61}$$

in the VHP case [the transport coefficients $\kappa^*$ and $\mu^*$ are given by Eqs. (5.43)].

Our analysis showed that the Maxwell and VHP simplifications, that are more amenable to analytic treatment, not only capture the essential features of hard sphere dynamics, but also provide lower and upper bounds for all comparable quantities. Some important differences should however be commented upon. A first difference is that Maxwell and VHP lead to regular transport coefficients for all values of the annihilation probability, whereas a divergence occurs for annihilating hard sphere thermal conductivity $\kappa$ and Fourier coefficient $\mu$. We concluded from this comparison that this divergence is presumably not physical and could result from the more stringent approximations put forward in the hard sphere computation. It turns out that the hard sphere case is such that the velocity distribution is non-Gaussian to zeroth order in spatial gradient, whereas it is Gaussian in Maxwell and VHP cases. This fact could be at the root of the divergence observed in the transport coefficients.

The second important difference between Maxwell, hard sphere and VHP dynamics is that within the Maxwell model, all Fourier modes are found to be linearly stable. This fact is intimately related to the non dissipative nature of the corresponding dynamics, an aspect which may be surprising at first: although particles are permanently removed from the system, the mean kinetic energy is conserved on average ($\xi_T = 0$). This may be considered as a deficiency of the Maxwell (over)simplification. On the other hand, VHP dynamics is such that the collision frequency increases with the velocity of a given population of particles, which in turn implies that the kinetic energy decreases faster than the number of particles, hence $\xi_T > 0$. This dissipation is at the root of possible instabilities in the coarse-grained fields. However, these instabilities manifest themselves for suitably rescaled fields, and we argued in section 5.7

that they should presumably only translate into transient instabilities for the "real" fields. Indeed, due to the decrease of density $n(t)$, an unstable Fourier mode has a wavenumber increasing like $n^{-1}$, and eventually enters into a regime where damping should wash out the perturbation. This feature presumably provides at least a linear saturation mechanism for instabilities, different from usual non-linear saturation effects, that may also play a *transient* role here if the initial conditions are sufficiently unstable [in other words, if $n(t_\perp) \ll n(t=0)$]. Our stability analysis was nevertheless restricted to perturbations around the time dependent homogeneous state, so that strictly speaking, the effects of transient instabilities that may drive the system into a strongly modulated state are unclear at the moment. This calls for a careful numerical (molecular dynamics) study of the coarse-grained fields, which is left for future work. This would also allow to question the validity of the hydrodynamic description, in a regime where the wave number is not much smaller than the inverse mean free path $\ell^{-1} \propto n\sigma^{d-1}$ (in the previous Figures, $k$ is expressed in units of $\ell^{-1}$, up to a prefactor of order one).

# Chapter 6

# Dynamics of the breakdown of granular clusters

## 6.1 Outline of the chapter

Recently van der Meer *et al.* studied the breakdown of a granular cluster [127]. We reexamine this problem using an urn model, which takes into account fluctuations and finite-size effects. General arguments are given for the absence of a continuous transition when the number of urns (compartments) is greater than two. Monte Carlo simulations show that the lifetime of a cluster $\tau$ diverges at the limits of stability as $\tau \sim N^{1/3}$, where $N$ is the number of particles. After the breakdown, depending on the dynamical rules of our urn model, either normal or anomalous diffusion of the cluster takes place. We also study the Yang-Lee theory of phase transitions with a two urn model where the partition function can be expressed as a polynomial of a size-dependent effective fugacity $z$. This chapter is based on Refs. [128, 129].

## 6.2 Introduction

Dissipation of kinetic energy during inelastic collisions in gaseous granular systems has profound consequences [130, 131]. One of the most spectacular is the formation of spatial inhomogeneities [113], which drastically contrast with the uniform distribution of molecules with essentially elastic collisions.

Some time ago Schlichting and Nordmeier presented a simple experiment which demonstrates some consequences of inelasticity of granular systems [132]. They used a container separated into two equal compartments by a wall which has a narrow horizontal slit at a certain height. The container is filled with particles and subjected to vertical shaking. For vigorous shaking the particles distribute equally between the two compartments. However, when the shaking is sufficiently mild, a nonsymmetric distribution occurs. In such a case the compartment with majority of particles, due to numerous inelastic collisions, is effectively "cooler" than the other one. Consequently, less particles are leaving this compartment, which stabilizes such an asymmetric distribution of particles. To explain this experiment, Eggers derived a phenomenological equation for the flux $F(n)$ of particles leaving a given compartment [133]

$$F(n) = Cn^2 \exp(-Bn^2). \tag{6.1}$$

In the above equation $n \in [0,1]$ is the concentration of particles in a given urn and $B$ and $C$ are constants which depend on the properties of particles, typical sizes of the system, and on the parameters of shaking (the constant $C$ may be eliminated by an appropriate redefinition of the time scale). In agreement with the experiment, Eq. (6.1) predicts unequal distribution of particles for sufficiently large $B$. The above type of experiment was repeated in the case when the number of compartments $L$ was greater than two by van der Meer *et al.* [134]. In such a case the appearance of unequal distributions of particles is accompanied by strong hysteresis, which is in agreement with theoretical analysis [135]. Moreover, certain aspects of these phenomena for $L = 2$ were approached using a hydrodynamic description that stems from kinetic theory of granular gases [136].

Another aspect of the $L > 2$ setup was further examined by van der Meer *et al* in [127]. They studied the dynamics of configurations (clusters) starting from all particles localized in a single compartment. Using a theoretical model based on Eq. (6.1), they have shown that when shaking is strong enough such a cluster breaks down and diffuses with the anomalous diffusion exponent 1/3 (in the following we refer to this model as MWL). For less vigorous shaking, the cluster remains relatively stable and only after some time it abruptly breaks down. Some of their predictions were confirmed experimentally.

In the framework of the MWL model it is rather difficult to include the effect of fluctuations. Such fluctuations might originate due, for example, to a finite number of particles and especially close to critical points they might play an important role. In an attempt to take such effects into account a generalization of Ehrenfest's [137, 138] urn model was recently examined in the case $L = 2$ [139]. The relative simplicity of the model allowed for a detailed study of its various characteristics.

The motivation of the present chapter is to re-examine the breakdown of granular clusters using the urn model in the case $L > 2$. In section 6.3 we define the model and present its steady-state phase diagram for $L = 3$. We also argue that, in analogy to the $L$-state Potts model in the mean-field limit, there are no continuous transitions for $L > 2$. In section 6.4 we examine the dynamics of the breakdown of clusters in a similar way as van der Meer *et al.* [127]. Although qualitatively our results are similar to theirs, in our model the diffusion of the cluster is normal with the exponent 1/2. Moreover, we calculate the size dependence of the lifetime of a cluster $\tau$ and show that at the limits of stability it scales as $N^{1/3}$. In section 6.5 we present a modified version of the urn model which in the steady state reproduces the flux (6.1). The diffusion of the broken down cluster is then shown to be anomalous with exponent 1/3, as it was already found [127]. It was suggested that the essential features of the MWL model are independent on the detailed form of the flux (6.1), as long as it has a single hump [127]. On the contrary, our results show that at least the diffusion exponent depends on some details of the flux and not only on its qualitative shape (in our models the flux is also a single hump function). Quantitative criterions on the form of the flux function ensuring the existence of anomalous diffusion were given in [140]. We then turn our attention in section 6.6 to the study the zeros of the partition function of a two-urn model with a size-dependent effective fugacity. We show that several predictions of the Yang-Lee theory of phase transitions apply to our model. In Section 6.7 we mention the connection between the urn model and the class of the so-called zero-range process [141, 142, 143]. Finally, section 6.8 contains our conclusions.

## 6.3 The model and its steady-state properties

Our model is a straightforward generalization of the two-urn model that was introduced to describe spatial separation of vibrated sand [139]. Namely, $N$ particles are distributed between $L \geqslant 2$ urns and the number of particles in $i$-th urn is denoted as $N_i$, with the constraint $\sum_{i=1}^{L} N_i = N$. Urns are connected through slits sequentially: $i$-th urn is connected with $(i-1)$-th and $(i+1)$-th. Moreover, periodic boundary conditions are used, i.e., first and $L$-th urns are connected. Particles in a given urn (say $i$-th) are subject to thermal fluctuations and the temperature $T$ of this urn depends on the number of particles in it as:

$$T(n_i) = T_0 + \Delta(1 - n_i), \tag{6.2}$$

where $n_i$ is a fraction of the total number of particles in a given urn ($n_i = N_i/N$) and $T_0$ and $\Delta$ are positive constants. Equation (6.2) is the simplest function which reproduces the fact that due to inelastic collisions between particles, their kinetic "temperature" decreases as their number in a given urn increases. The relation between the temperature and the number of particles is complicated and depends on several parameters like density of particles or type of driving [144], however indication of a simple dependence of the form (6.2) may also be found in the literature [145, 146]. We suppose that the distribution of particles as a function of height $z$ above the bottom of the urn satisfies the Maxwell-Boltzmann distribution

$$p(z, N_i) = \frac{mgN_i}{k_B T(n_i)} \exp\left[-\frac{mgz}{k_B T(n_i)}\right], \tag{6.3}$$

where $g$ is the Earth acceleration, $m$ the mass of the particles, and $k_B$ the Boltzmann constant. The fraction of particles which are above a certain height $h$ is given by $\int_h^\infty \mathrm{d}z\, p(z, N_i) \propto \exp[-mgh/k_B T(n_i)]$. We measure the temperature in units of $mgh/k_B$, and define the dynamics of the model as:

(i) One of the $N$ particles is selected randomly.

(ii) With probability $\exp[-1/T(n_i)]$ the selected particle is placed in a randomly chosen neighboring urn, where $i$ is the urn of the selected particle.

The above rules implies that the flux of particles leaving $i$-th urn is, up to a proportionality constant [that may be absorbed in the definition of the time in the

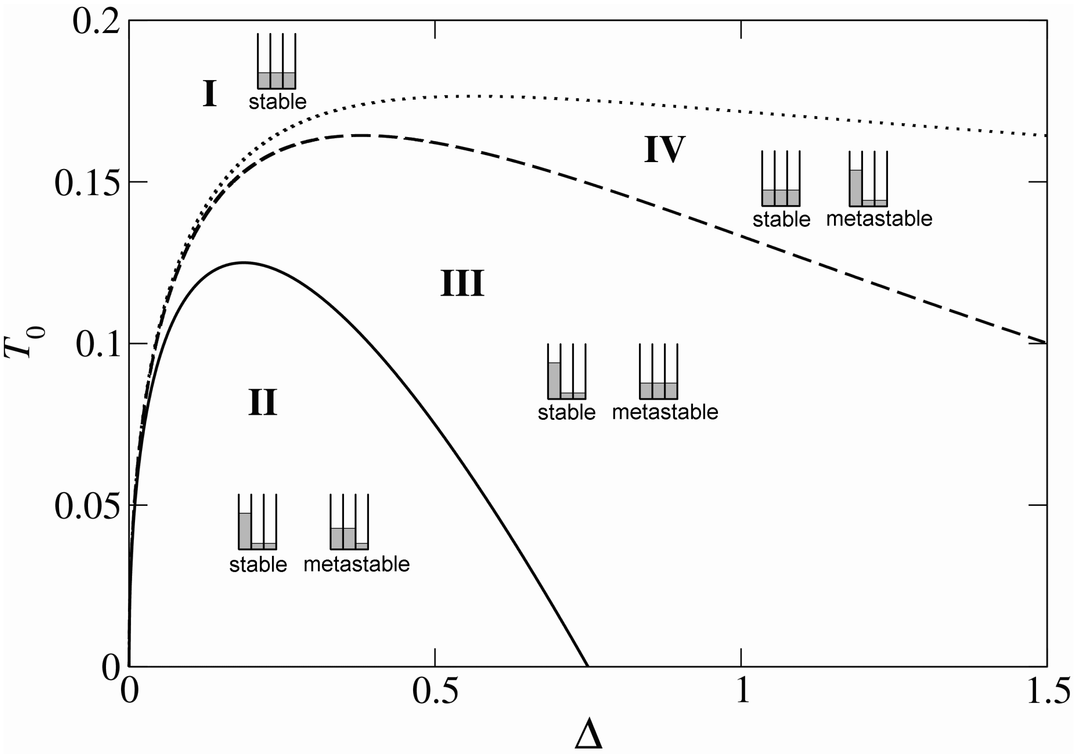


Figure 6.1: The steady-state phase diagram for the three-urn model. The small figures provide a short description of the different regions and their stability. See text for more details of the description of phases.

evolution equations (6.5)], given by

$$F(n_i) = n_i \exp\left[-\frac{1}{T(n_i)}\right], \tag{6.4}$$

where $T(n_i)$ is defined in (6.2). Let us notice that the flux (6.4), similarly to (6.1), is a single hump function. Having an expression for the flux we can write the equations of motion as:

$$\frac{\mathrm{d}n_i}{\mathrm{d}t} = \frac{1}{2}F(n_{i-1}) + \frac{1}{2}F(n_{i+1}) - F(n_i), \tag{6.5}$$

where $i = 1, 2, ..., L$. Steady-state properties of this model can be obtained using similar analysis as in the $L = 2$ case [139] or as for the $L > 2$ case in [135], but with fluxes given this time by Eq. (6.1). The results of this analysis in the $L = 3$ case are presented in Fig. 6.1.

In region I the symmetric $n_1 = n_2 = n_3 = 1/3$ phase is stable. In region II the asymmetric $n_1 > n_2 = n_3$ phase is stable. In the steady state since there is no external driving there are no steady state fluxes. Therefore the flux leaving and entering a given urn must be equal, which means the detailed balance condition

$$\langle n_i \rangle \omega(\langle n_i \rangle) = \langle n_j \rangle \omega(\langle n_j \rangle), \tag{6.6}$$

for all $i, j = 1, \ldots, 3$, where the brackets $\langle\rangle$ denote a time average in the steady state, and $\omega(n) = \exp[-1/T(n)]$ is the transition rate. We define the difference of occupancies of the urns by

$$\varepsilon_1 = \frac{n_1 - n_2}{2N}, \tag{6.7a}$$

$$\varepsilon_2 = \frac{n_1 - n_3}{2N}. \tag{6.7b}$$

In terms of the variables $\langle\varepsilon_1\rangle$ and $\langle\varepsilon_2\rangle$ the detailed balance conditions $\langle n_1\rangle\omega(\langle n_1\rangle) = \langle n_2\rangle\omega(\langle n_2\rangle)$ and $\langle n_1\rangle\omega(\langle n_1\rangle) = \langle n_3\rangle\omega(\langle n_3\rangle)$ give

$$(1 + 2\langle\varepsilon_1\rangle + 2\langle\varepsilon_2\rangle)\,\omega\left[\frac{N}{3}\,(1 + 2\langle\varepsilon_1\rangle + 2\langle\varepsilon_2\rangle)\right] - (1 - 4\langle\varepsilon_1\rangle + 2\langle\varepsilon_2\rangle)\,\omega\left[\frac{N}{3}\,(1 - 4\langle\varepsilon_1\rangle + 2\langle\varepsilon_2\rangle)\right] = 0, \tag{6.8}$$

and

$$(1 + 2\langle\varepsilon_1\rangle + 2\langle\varepsilon_2\rangle)\,\omega\left[\frac{N}{3}\,(1 + 2\langle\varepsilon_1\rangle + 2\langle\varepsilon_2\rangle)\right] - (1 + 2\langle\varepsilon_1\rangle - 4\langle\varepsilon_2\rangle)\,\omega\left[\frac{N}{3}\,(1 + 2\langle\varepsilon_1\rangle - 4\langle\varepsilon_2\rangle)\right] = 0. \tag{6.9}$$

A solution to Eqs. (6.8) and (6.9) is the symmetric state $\langle\varepsilon_1\rangle = \langle\varepsilon_2\rangle = 0$. However, the question is to determine whether this solution is stable against fluctuations. To this purpose, we expand Eq. (6.8) to first order in $\langle\varepsilon_1\rangle$ and $\langle\varepsilon_2\rangle$. Equating the first order terms gives the continuous line in Fig. 6.1 locating the limit of stability of the symmetric phase [note that Eq. (6.9) gives the same result]:

$$T_0 = \sqrt{\frac{\Delta}{3}} - \frac{2\Delta}{3}. \tag{6.10}$$

This equation has a very similar form to the corresponding equation in the $L = 2$ case [139]. In region III (IV) the symmetric (asymmetric) phase is metastable. The line separating regions I and IV (or regions IV and III) can be determined only numerically as a solution of a transcendental equation, similarly to the $L = 2$ case [139]. For example, in order to find the line between regions I and IV, the procedure consists in (i) solving the transcendental equation (e.g., using Newton's method) giving $\varepsilon_1$ and $\varepsilon_2$ in region II in order to obtain the stable asymmetric solution (ii) increasing $\Delta$ by a small amount $\delta\Delta$ and solving the transcendental equation for the steady state, until the solution is such that $\varepsilon_1 = \varepsilon_2 = 0$ (iii) starting again from point (i) but with a slightly different value of $T_0$. There is also a third type of solution where two urns contain majority of particles and the third urn has only a small fraction of them ($n_1 = n_2 > n_3$). Such a solution, which has saddle-like stability, exists only in region II (see Fig. 6.2). Similar solutions can be found for the MWL model [134, 135].

An important, qualitative difference with the case $L = 2$, is that regions I and II are always separated by regions III and IV, hence the tricritical point is located at

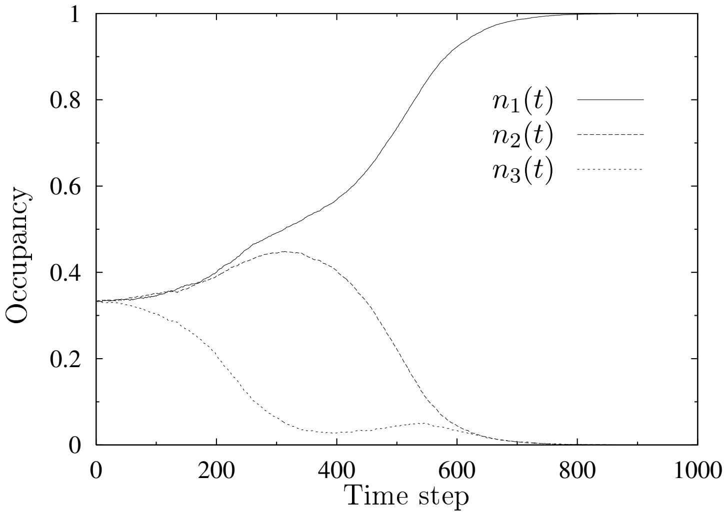


Figure 6.2: Urn occupancies $n_i(t)$, $i = 1, \ldots, 2$, in region II for $T_0 = 0.001$, $\Delta = 0.3$, and $N = 9999$, starting from the symmetric state. One time step corresponds to $N$ iterations. The evolution shows the existence of the metastable phase $n_1 = n_2 > n_3$.

the origin $T_0 = \Delta = 0$. It means that a phase transition between these two phases is always accompanied by hysteresis effects. On the other hand in the $L = 2$ case continuous transitions are possible, which are not accompanied by hysteresis [139]. Such a behaviour is actually in agreement with experimental data and with MWL model [134].

Has this qualitative difference a more general explanation or is it rather a coincidental property? In our opinion, absence of continuous transitions for $L > 2$ is a generic property of such systems and at least to some extent could be understood. First, let us notice that the phase transition for $L = 2$ is a manifestation of the spontaneous symmetry breaking in the system: in certain regime one of the two identical urns is preferentially filled with particles. Such a situation resembles the phase transition in the $S = 1/2$ Ising model, where below certain temperature the up-down symmetry is broken and the system acquires spontaneous magnetization [147]. Actually, this analogy can be confirmed more quantitatively. It was shown that for $L = 2$ and at the critical point the probability distribution has the same moment ratios as in the Ising model in dimension $d$ greater than the so-called upper critical dimension ($d > 4$) for which the critical exponents take mean-field values [148]. Let us notice, that in our model particles are selected randomly which means that this is essentially a mean-field model, and therefore it may be regarded as above the upper critical dimension. Moreover, our model is a *dynamical*, spaceless model, contrary to the Ising model, which is a lattice equilibrium model. The fact that such different models have some similarities shows that as far as the critical behavior is concerned what really matters is symmetry. In both cases this is the $\mathbb{Z}_2$ symmetry which is broken below the critical point.

Pushing this analogy further, we expect that for $L > 2$ the phase transition in our model should be similar to the phase transition of the $L$-state Potts model above the critical dimension (since the Ising model is recovered from the $q = 2$ state Potts model) [149]. In the $L$-state Potts model at sufficiently low temperature one of the $L$ symmetric ground states is preferentially selected. However, it is well-known that above the upper critical dimension and for $L > 2$ there are only discontinuous transitions in the Potts model [149]. Consequently, the transition in the urn model should be discontinuous.

The analogy may be pushed ever further. Let $\xi$ be the correlation length, $\tau$ the relaxation time (that corresponds to the lifetime of the asymmetric state in the urn model, or to a state of broken up-down symmetry for Ising model). At the critical point there is a power-law divergence $\tau \sim \xi^z$. For Ising model above critical dimension with Glauber dynamics (where the order parameter is not conserved by the dynamics, sometimes referred to as "model A") the dynamical critical exponent is $z = 2$ [150]. At the critical point since the correlation length diverges, one may identify the correlation length with the length of the system such that the number of particles $N$ in the system is given by $N = \xi^{d_c}$, the lifetime therefore reads $\tau \sim \xi^2 = N^{2/d_c}$. Going back to the two-urn model, the order parameter corresponding to the Glauber dynamics is the difference of occupancies of the urns $\varepsilon = N_A - N_B$, such that $\varepsilon$ relaxes to zero, which corresponds to the symmetric state. It was shown that the relaxation time diverges as $\tau \sim N^z$, where at the line of continuous transitions $z = 1/2$, at the tricritical point $z = 2/3$, and at the spinodal line $z = 1/3$ [139]. Making use of the latter critical exponents and of $\tau \sim N^{2/d_c}$, one finds for the urn model $d_c = 4$ (line of continuous transitions), $d_c = 3$ (tricritical point), and $d_c = 6$ (spinodal line). The latter critical dimensions are the same ones as those found from a field theory for Ising model [151, 152, 153, 154, 155]. Those results confirm again the analogy at criticality between urn and $L$-state Potts models for Glauber dynamics in high dimensions. However, it should be pointed out that it is not obvious to define the system length $\xi$ for the (spaceless) urn model.

Let us notice that one can easily break the symmetry of the compartments, e.g., changing the boundary conditions, which in our analogy introduces some asymmetry in the Potts model. It is possible that in such a case the system effectively will become similar to the $L = 2$ system and will exhibit a continuous transition. Finally, we expect that for $L > 3$ the phase diagram should be topologically similar to the one for $L = 3$ shown in Fig. 6.1.

## 6.4 Dynamical properties of cluster configurations

In the present section we study certain dynamical properties of cluster configurations. We used Monte Carlo simulation. Since it is rather straightforward, we omit a more detailed description of the numerical implementation of the dynamical rules of our model. Initially, we place all particles in one urn and examine its subsequent evolution. If the parameters $T_0$ and $\Delta$ are such that the system is in region I then such a cluster is unstable and after some time due to fluctuations it breaks down and particles spread

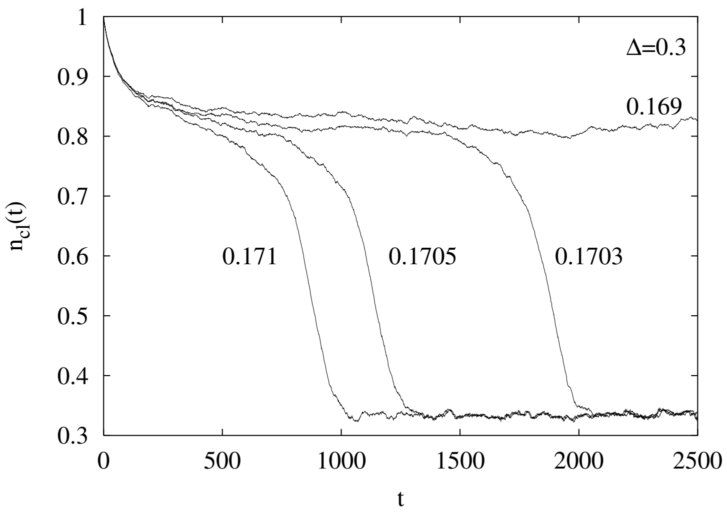


Figure 6.3: The time evolution of the fraction of particles of the cluster $n_{cl}$ close to the limits of stability of the asymmetric phase ($N = 5 \times 10^4,\ L = 3$). The values of $T_0$ are indicated. For $\Delta = 0.3$ the limit of stability of the asymmetric phase is at $T_0 = 0.169829772\ldots$. For a larger number of particles $N$, stochastic fluctuations will diminish.

throughout all urns. This is illustrated in Fig. 6.3 which shows the concentration of particles in the urn in which the particles were initially placed. Let us notice that (i) the breakdown is relatively abrupt and during the evolution up to the breakdown the concentration of particles only slightly decreases; (ii) upon approaching the line separating regions IV and III the lifetime of the cluster $\tau$ increases.

Note the time asymmetry of the clustering process. Indeed, metastable (or unstable) clusters are shown to collapse very abruptly (see Fig. 6.3 or Ref. [127]). On the other hand, formation of clusters starting from a metastble (or unstable) uniform distribution of particles is a much slower process [134, 135].

Since in region III the asymmetric state has an infinite lifetime it means that $\tau$ must diverge upon approaching this region. This behavior is seen in Fig. 6.4. In addition to the three-urn case we also made analogous measurements of $\tau$ for $L = 5$ and 7 and the results are also shown in Fig. 6.4. Let us notice that results presented in Fig. 6.3 and Fig. 6.4 are similar to those obtained by van der Meer [127], although they are parametrized by a different variable.

The limit of stability of the asymmetric phase can be regarded as a critical point. Thus, we expect that exactly at this point, e.g., the lifetime $\tau$ has a power-law divergence $\tau = N^z$, and $z > 0$. Such a behavior is shown in Fig. 6.5. From the slope of the straight line, which is a least-square fit to our data we estimate $z = 0.32(3)$. Let us notice that in the two-urn model at the limits of stability $\tau$ exhibits a very similar divergence [139]. In the case $L = 2$ more precise calculations were possible strongly suggesting that $z = 1/3$ which is also consistent with the present three-urn model

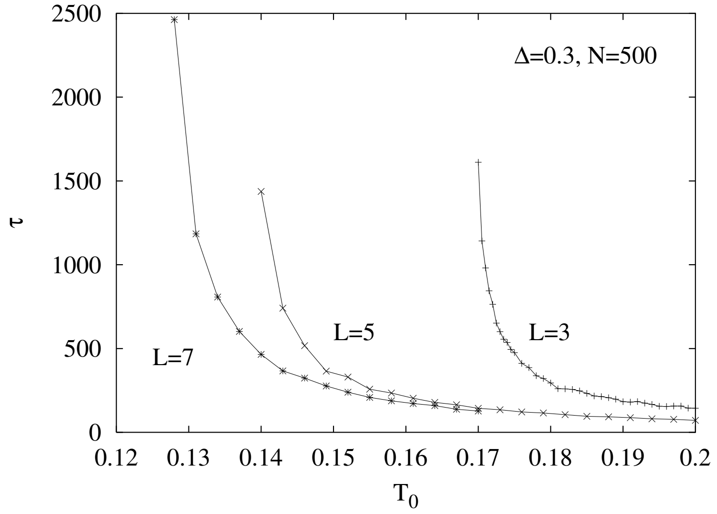


Figure 6.4: The average lifetime of a cluster $\tau$ as a function of $T_0$ for different number of urns $L$. Each point is an average of at least 300 runs.

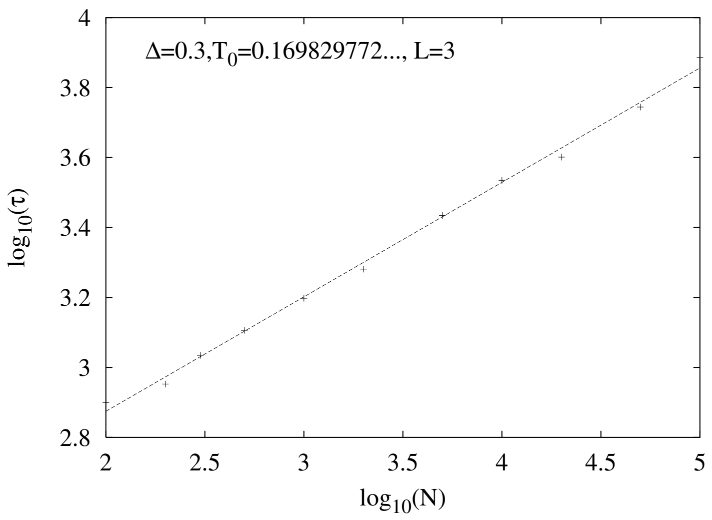


Figure 6.5: The average lifetime of a cluster $\tau$ as a function of the number of particles $N$ at the limits of stability of the asymmetric phase. Each point is an average of at least 300 runs.

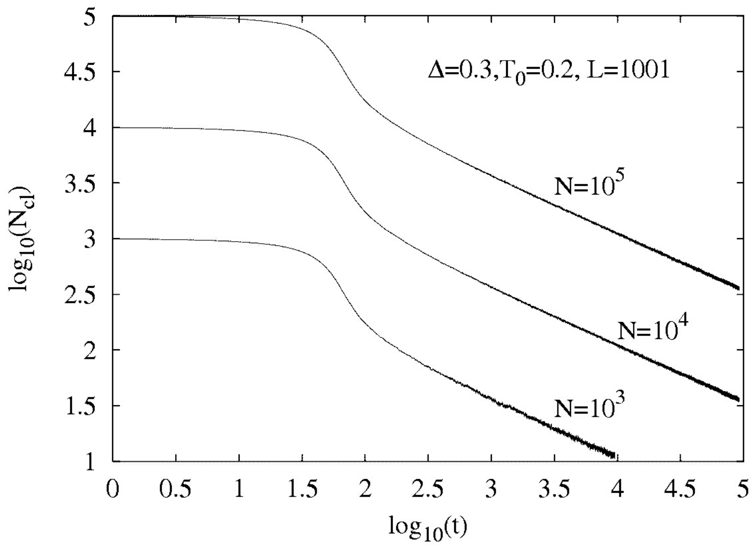


Figure 6.6: The average occupancy of a central urn $N_{cl}$ as a function of time $t$. The slope of decay is very close to 0.5 which confirms the diffusive nature of spreading ($N_{cl} \sim t^{-1/2}$). Each curve is obtained from averaging over 50 independent runs.

result. Let us emphasize that because in our model the number of particles is finite, we can study size dependent quantities as shown in Fig. 6.5.

Finally, let us examine the breakdown of a cluster in the many-urn case $L \gg 1$. In such a case a continuous approach to the MWL model shows that after breaking down, the cluster diffuses with the anomalous exponent 1/3 [127]. Results of our simulations are shown in Fig. 6.6. From these data we conclude that spreading of a cluster occurs with the ordinary exponent 1/2 rather than anomalously. Ordinary diffusion in our model can be also easily explained analytically applying basically the same continuous approach as used in [127]. In this approach the set of equations of motion (6.5) is transformed into a partial differential equation. Then, one immediately realizes that the linear term in front of the exponent in Eq. (6.4) leads to the ordinary diffusion equation. On the other hand, the anomalous diffusion of MWL model can be traced back to the quadratic (in $n$) term in the flux in Eq. (6.1). This quadratic term is related with two-particle collisions [127].

## 6.5 The pair model

One can easily construct urn models for which the expression for the flux will have a different form. In particular, redefining the effective temperature (6.2) and drawing each time a pair of particles we obtain an urn model with the flux of exactly the same form as Eq. (6.1). This dynamics takes into account some of the two particles correlations. It allows us to recover some properties of the MWL model and establish further results.

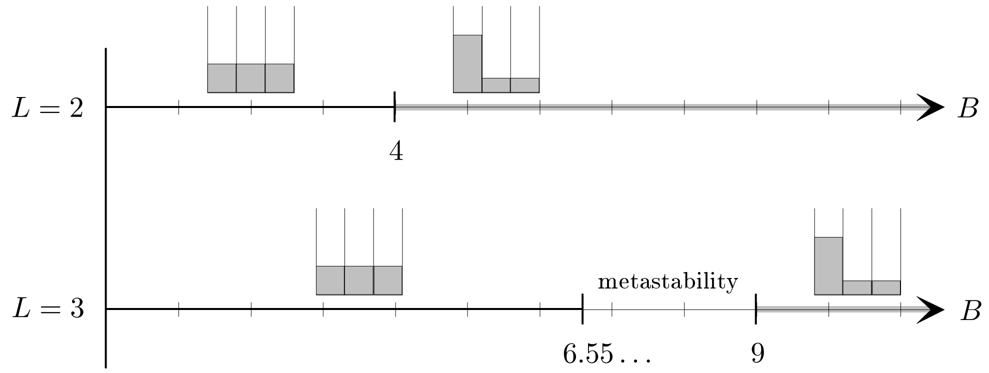


Figure 6.7: The steady-state phase diagram for the two and three-urn pair models. See text for more details of the description of phases.

The model, which we call a pair model, is similar to the previously described one, except that its dynamics is now defined as:

(i) Two different particles are selected randomly.

(ii) If and only if the two particles are in the same urn, with probability $\exp[-Bn_i^2]$ the selected particles are placed in the same randomly chosen neighboring urn, where $i$ is the urn of the selected particles.

One can easily see that the probability that two randomly selected particles belong to the $i$-th urn is given as $N_i(N_i - 1)/[N(N-1)]$, which for $N \to \infty$ becomes $n_i^2$. Multiplying $n_i^2$ with the transition probability $\exp(-Bn_i^2)$ we obtain that the flux in the pair model is proportional to Eq. (6.1). It means that as far as the steady-state properties are concerned, the pair model is equivalent to the MWL [134, 135]. In particular for $L = 2$ one easily obtains the critical value $B = 4$ for the continuous transition between the symmetric ($B < 4$) and asymmetric phase ($B > 4$). For $L = 3$ one obtains two critical points $B_1 = 6.552703411\ldots$ and $B_2 = 9$. The first one can only be determined numerically. Similarly to Fig. 6.1, for $B < B_1$ the symmetric solution is stable whereas for $B > B_2$ the asymmetric solution is stable. In the interval $B \in [B_1, B_2]$ both symmetric and asymmetric solutions are stable, which is the interval showing hysteresis with respect to the driving parameter $B$ (see Fig. 6.7).

Qualitatively the dynamical properties of cluster configurations in the pair model are similar to those described in previous section. In particular for $L = 3$ and $B = B_1$, the average lifetime of a cluster $\tau$ as a function of the number of particles $N$ once more shows a power-law divergence $\tau = N^z$, with $z = 0.31(3)$ suggesting that $z = 1/3$. It shows a certain universality of this exponent with respect to different dynamical rules.

Finally, Fig. 6.8 shows the diffusion of the broken down cluster. Since the asymptotic slope of our data is very close to 1/3 we conclude that in this case the diffusion is anomalous, as already predicted by van der Meer *et al.* who used the

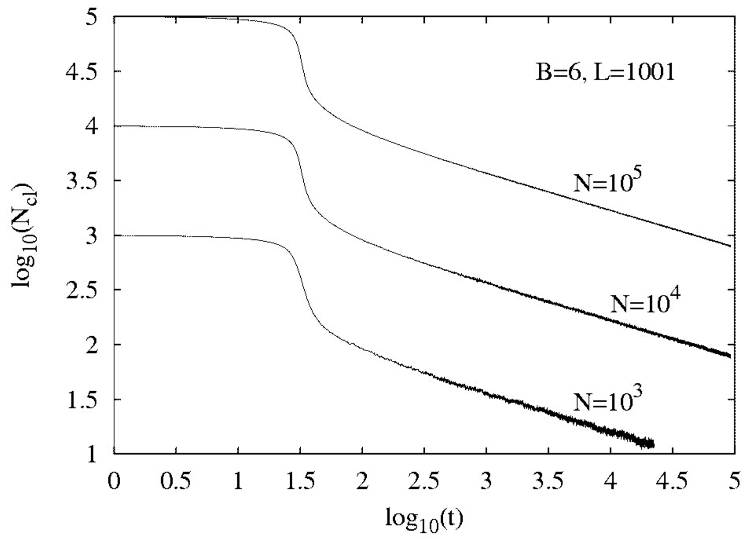


Figure 6.8: The average occupancy of a central urn $N_{cl}$ as a function of time $t$ for the pair model. The slope of decay is very close to 1/3 which confirms the anomalous diffusive nature of spreading ($N_{cl} \sim t^{-1/3}$). Each curve is obtained from averaging over 50 independent runs.

continuous approach [127]. This prediction was recently confirmed from an analytical derivation [141].

The pair model and the model examined in the previous section exhibit qualitatively similar behavior for most of the physical quantities. The main difference is the diffusion: it is anomalous in the pair model and ordinary in model examined in the previous section. It would be desirable to experimentally examine the nature of diffusion in such systems.

## 6.6 The Yang-Lee zeros

The microscopic dynamics of the urn model is out of equilibrium. Indeed, in the stationary state there is a balance between an energy injection mechanism (vertical shaking of the urns) and dissipation (through inelastic collisions between particles). However, level of coarse graining of our description is such that the corresponding stationary probability distribution obeys the detailed balance [140]. Therefore the model we are studying is formally an equilibrium one. Moreover, as it will be shown, it can be mapped onto an equilibrium mean-field Ising model [159, 160]. A basic ingredient of the Yang-Lee theory of equilibrium phase transitions is that the grand-canonical partition function can be expressed as a polynomial of a size-independent control parameter – the fugacity. The purpose of this section is to show, on our simple model, that this might not be a necessary condition. Indeed, this model has a partition function with a polynomial structure in terms of a *size-dependent* effective fugacity, and thus the validity of the Yang-Lee approach might be highly questionable. We show, however, that the Yang-Lee strategy for this model still works.

We first define the model and the partition function is introduced as a polynomial of an effective size-dependent fugacity. Then the zeros of the partition function are studied numerically. They are shown to form a very complicated structure in the plane of the complex fugacity. Nevertheless, they offer information about the nature of the phase transition in our model.

### 6.6.1 The $L = 2$ model

Let us now consider the two-urn model [139], a generalisation of Ehrenfest's urn model [137, 138]. The $N$ particles are distributed between two urns, the first urn containing $M$ particles and the second one $N - M$. The dynamics is defined as follows. At each time step, one particle is chosen at random in one of the urns. Then, with a probability that depends on the number of particles present in the chosen urn, i.e., with a *state-dependent* transition rate, this particle moves to the other urn. Correspondingly, the flux $F(n)$ of particles leaving a given urn at a certain time depends on the fraction $n$ of the total number of particles in the given urn at that moment. This model is thus by construction mean-field like. The master equation for the probability distribution $p(M, t)$ that there are $M$ particles in a given urn at time $t$ writes [139]:

$$p(M, t+1) = F\left(\frac{N-M+1}{N}\right) p(M-1, t) + F\left(\frac{M+1}{N}\right) p(M+1, t) \\ + \left[1 - F\left(\frac{M}{N}\right) - F\left(\frac{N-M}{N}\right)\right] p(M, t). \quad (6.11)$$

Its stationary solution is found to be [141]:

$$p_s(M) = \frac{1}{Z_N} \prod_{i=1}^{M} \frac{F\left(\frac{N-i+1}{N}\right)}{F\left(\frac{i}{N}\right)}, \quad (6.12)$$

where the normalization factor (the partition function) is:

$$Z_N = 1 + \sum_{M=1}^{N} \prod_{i=1}^{M} \frac{F\left(\frac{N-i+1}{N}\right)}{F\left(\frac{i}{N}\right)}. \quad (6.13)$$

This model can describe the transition between a symmetric distribution of the particles in the two urns, associated with a single peak of the probability distribution at $M = N/2$ (for $N$ even), to a symmetry breaking state described by a bimodal distribution with peaks at $M = N(1/2 \pm \varepsilon)$. The order parameter $\varepsilon$ measures the difference in the occupancy of the two urns. To produce this symmetry breaking it is sufficient that the flux function $F(n)$ has a single hump [133, 134, 139]. Indeed, since in the steady-state the flux leaving an urn is equal to the flux entering this urn, it is sufficient that there exists two different values of the density $n_1 \neq n_2$ such that $F(n_1) = F(n_2)$. The simplest possible choice for $F(n)$ having this property is

$$F(n) = n \exp\left(-A\, n\right), \tag{6.14}$$

which corresponds to a state-dependent transition rate $\exp(-An)$. Thus the problem is characterized by a single control parameter $A$. In the thermodynamic limit $N \to \infty$, this symmetry breaking corresponds to a second-order phase transition. In this limit, the probability distribution becomes $\delta$-peaked around the macroscopic stable state, that is determined by the condition that the flux of particles directed from the first urn to the second one equals the flux of particles from the second urn towards the first one, $F\left(1/2 - \varepsilon\right) = F\left(1/2 + \varepsilon\right)$, namely

$$(1/2 - \varepsilon) \exp\left[-A\left(1/2 - \varepsilon\right)\right] = (1/2 + \varepsilon) \exp\left[-A\left(1/2 + \varepsilon\right)\right]. \tag{6.15}$$

A first order Taylor expansion in $\varepsilon$ allows one to find the critical value $A_c = 2$. It follows that in the thermodynamic limit for $A < A_c = 2$ the stationary state is the symmetric one, while for $A > A_c = 2$ the equipartition of particles is broken, i.e., a second order phase transition takes place at $A = A_c = 2$.

### 6.6.2 Analysis of the zeros of the partition function

With such a choice of the flux $F(n)$, one may rewrite the normalization factor (6.13) as:

$$\begin{aligned}
Z_N &= 1 + \sum_{M=1}^{N} \prod_{i=1}^{M} \frac{N-i+1}{i} \exp\left(-A\frac{N+1}{N}\right) \exp\left(\frac{2A}{N} i\right) \\
&= 1 + \sum_{M=1}^{N} \exp\left(-A\frac{N+1}{N} M\right) \exp\left(\frac{2A}{N}\frac{M(M+1)}{2}\right) \frac{1}{M!} \prod_{j=N}^{N-M+1} j \\
&= 1 + \sum_{M=1}^{N} \exp\left(-\frac{A}{N} M(N-M)\right) \frac{N!}{M!(N-M)!} \\
&= \sum_{M=0}^{N} \binom{N}{M} z^{M(N-M)}.
\end{aligned} \tag{6.16}$$

Here $\binom{N}{M} = N!/[M!(N-M)!]$ is the binomial coefficient and $z = \exp\left(-A/N\right)$ is the effective fugacity. One can see that $Z_N$ is a polynomial in $z$, that is related to the control parameter $A$ of the model, but *$z$ is not a size-independent quantity*, and depends on the number of particles $N$. The partition function (6.16) can be mapped onto the partition function of the mean-field Weiss-Ising model. This can be done by setting in Eq. (5) of Ref. [160]: $H = 0$, $n \to M$, $\beta \to A/2$, $z = \exp(-2\beta J)$, and thus the Ising-Weiss canonical partition function becomes $Z_N = z^{-N/4} \sum_{M=0}^{N} \binom{N}{M} z^{M(N-M)}$, up to the prefactor $z^{-N/4}$ that is irrelevant [159].

We embark on studying the zeros of the partition function $Z_N$. As a first step we find zeros of Eq. (6.16), considering $z$ as a complex $N$-independent variable. The results of our numerical calculations, using MATHEMATICA, for three values of $N$ are represented in Fig. 6.9. Note that the order of the polynomial of Eq. (6.16) increases rapidly like $N^2/4$, and therefore we were not able to perform precise calculations of the roots beyond $N = 71$.

With increasing $N$ these roots approach the unit circle. One can argue that this should indeed be the case. First, let us associate with the partition function (6.16) the complex free energy density

$$f_N(z) = (1/N)\ln(Z_N). \tag{6.17}$$

For large $N$ and $|z| > 1$ the partition function is dominated by the central term $M = N/2$ and hence $f_N(|z| > 1) \sim (N/4)\ln z$. Thus we define $f^{(1)}(z) = (N/4)\ln z$ as the free energy of the symmetric ($M = N/2$) phase. On the other hand, for $|z| < 1$ the dominant contribution are coming only from the $M = 0$ and $M = N$ terms, and thus $f_N(|z| < 1) \sim 1/N \to 0$ in the thermodynamic limit. This allows to define $f^{(2)}(z) = 0$ as the free energy of the asymmetric phase. To obtain the location of the zeros of $Z_N$ in this limit we have to equate real parts of the complex free energies on both sides of the transition [161, 162]. Namely, we require that

$$\mathrm{Re}\, f^{(1)}(z) = \mathrm{Re}\, f^{(2)}(z). \tag{6.18}$$

Using a polar representation $z = re^{i\phi}$ we obtain from Eq. (6.18) $\mathrm{Re}(\ln r + i\phi) = 0$ and the only way to satisfy this equation is to have $r = 1$. Hence, asymptotically, the zeros should be located on the unit circle, as confirmed by our numerical calculations.

However, the model with $z$ as a control parameter (which has a transition with a jump of the effective free energy density) is quite different from the original urn model with $A$ as a control parameter (which has a continuous phase transition). Therefore, in order to infer some information about the phase transition in the urn model we have to analyze the behavior of zeros of Eq. (6.16) in the complex $A$-plane, that can be obtained from the zeros in the $z$-plane using the relation $A = -N\ln(z)$. Those zeros are in our model the equivalent of the Fisher zeros (zeros of the canonical partition function in the complex temperature plane for equilibrium systems) [163]. Transformation of zeros into the complex $A$-plane is shown in Fig. 6.10.

With increasing $N$ the zeros approach the critical point $A_c = 2$ with a slope of $\pi/4$, and with a vanishing density of zeros. These numerical observations seem to confirm the second-order nature of the phase transition [156].

In the following we establish analytically the form of the line of zeros close to the critical point, and the final result is presented as a continuous line in Fig. 6.10. As already mentioned, in the thermodynamic limit the partition function is dominated by the stationary state (6.15). Below the critical point the leading term of $Z_N$ for $N \to \infty$ is given by the central peak $M = N/2$:

$$Z_N \sim \binom{N}{N/2} \exp\left(-A\frac{N}{4}\right), \qquad A < A_c = 2. \tag{6.19}$$

On the other hand, for $A > A_c$ there are two leading contributions to $Z_N$ coming, respectively, from $M = N(1/2 - \varepsilon)$ and $M = N(1/2 + \varepsilon)$, where $\varepsilon$ is the solution of

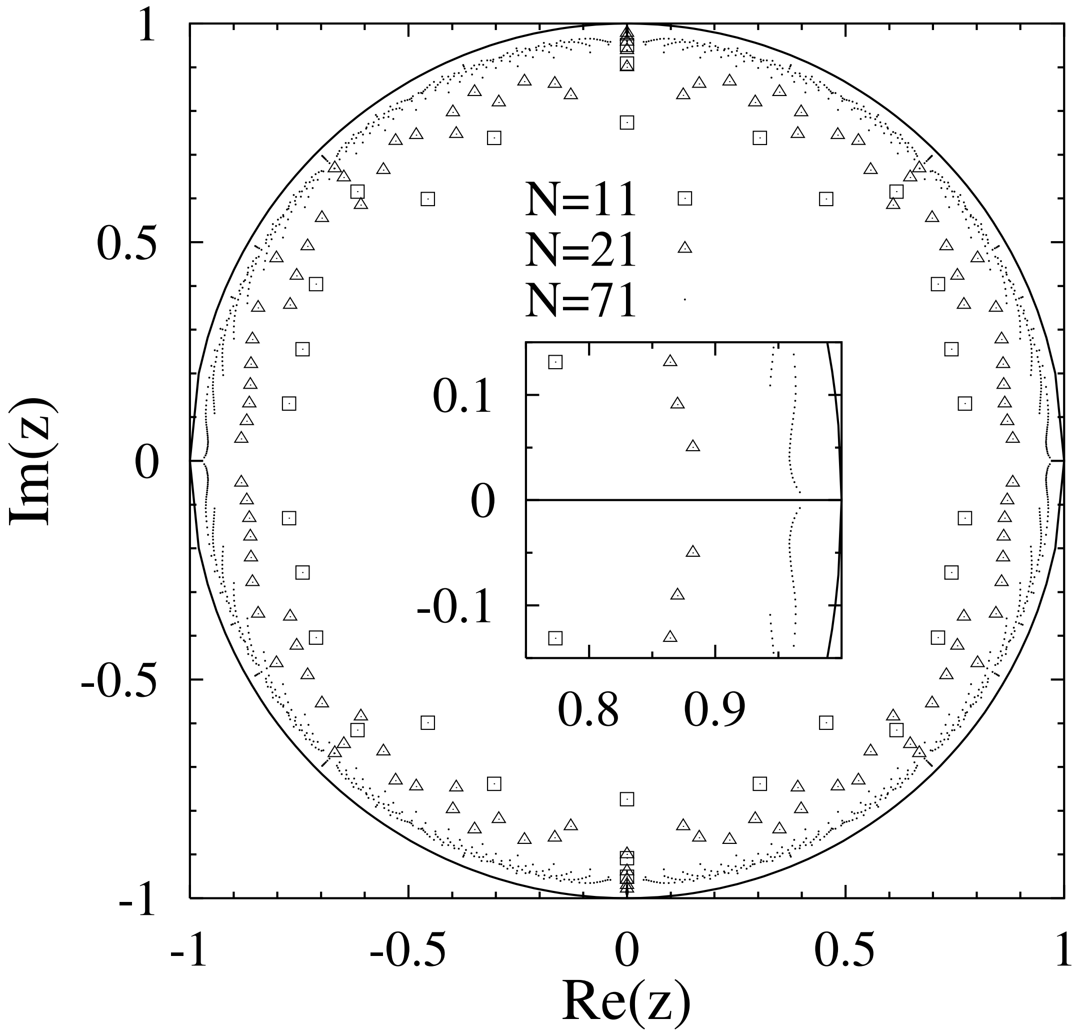


Figure 6.9: Zeroes of the partition function (6.16) in the complex $z$-plane for three values of $N$. The continuous line is the unit circle. The inset illustrates the behavior in the vicinity of $z = 1$.

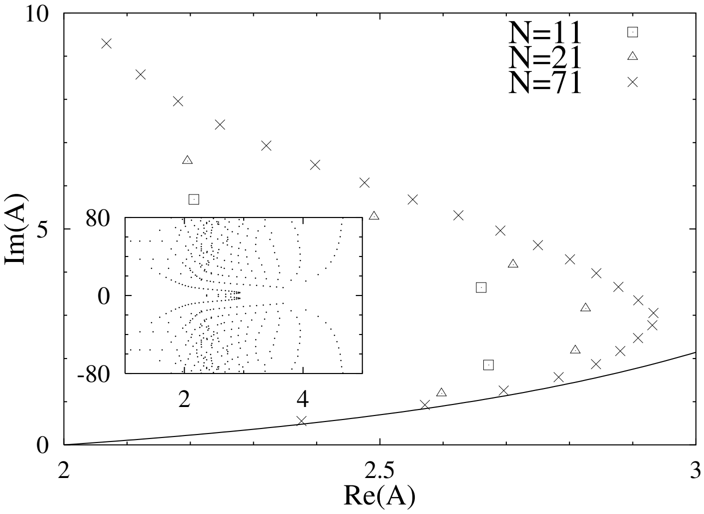


Figure 6.10: Zeroes of Eq. (6.16) in the complex $A$-plane, nearby the critical value $A_c = 2$, for three values of $N$. The inset shows more roots for $N = 71$. The continuous line is the analytical perturbative estimation (6.26) of the line of zeros in the thermodynamic limit, see main text.

the macroscopic stationarity condition (6.15). Therefore:

$$Z_N \sim 2\binom{N}{N(1/2-\varepsilon)} \exp\left[-AN\left(\frac{1}{4}-\varepsilon^2\right)\right], \qquad A > A_c = 2. \tag{6.20}$$

Correspondingly, the effective free energy density $f = \lim_{N\to\infty}(1/N)\ln(Z_N)$ [161, 162] associated with this partition function is

$$f^{(1)} = -A/4 + \ln 2, \qquad A < A_c = 2, \tag{6.21a}$$

$$\begin{aligned} f^{(2)} &= -A(1/4-\varepsilon^2) - (1/2-\varepsilon)\ln(1/2-\varepsilon) \\ &\qquad -(1/2+\varepsilon)\ln(1/2+\varepsilon), \qquad A > A_c = 2. \end{aligned} \tag{6.21b}$$

Let us now consider the behavior of the partition function and of the effective free energy density as a function of the *complex* parameter $A$. Then the condition (6.18), $\operatorname{Re} f^{(1)} = \operatorname{Re} f^{(2)}$, together with Eq. (6.15) determine the line of zeros in the complex $A$-plane. Note that now $\varepsilon$ is a complex variable obtained from the steady-state Eq. (6.15).

However, Eq. (6.18) is now too complicated to allow for a complete analysis of the zeros line in the entire $A$-plane. But we are mainly interested in the behavior of this line in the vicinity of the critical point $A_c = 2$. Therefore, we shall look for a perturbative solution of Eqs. (6.15) and (6.18) in the small real parameter $\alpha = \operatorname{Re} A - 2$ around $A_c$. Making use of the form $A = (2+\alpha) + ia$ and $\varepsilon = x + iy$, Eq. (6.15) gives for the real part

$$4(2+\alpha)x - 4ya + \ln\left[(1/2-x)^2 + y^2\right] - \ln\left[(1/2+x)^2 + y^2\right] = 0, \tag{6.22}$$

and for the imaginary part

$$2(2+\alpha)y + 2ax - \arctan\left(\frac{y}{1/2-x}\right) - \arctan\left(\frac{y}{1/2+x}\right) = 0. \tag{6.23}$$

Equation (6.18) gives

$$(2+\alpha)(x^2-y^2) - 2axy + y\arctan\left(\frac{y}{1/2-x}\right) + y\arctan\left(\frac{y}{1/2+x}\right) - \ln 2$$
$$-\frac{1}{2}(1/2+x)\ln\left[(1/2+x)^2+y^2\right] - \frac{1}{2}(1/2-x)\ln\left[(1/2-x)^2+y^2\right] = 0. \tag{6.24}$$

From Eqs. (6.22) and (6.23) one concludes that $a$ scales like $\alpha$ and that $x$ scales like $y$. Since the model exhibits a second order phase transition, the transition is mean-field-like, which guides us to a scaling for $x$ and $y$ like $\alpha^{1/2}$. We are thus led to consider the following developments:

$$A = (2+\alpha) + i\alpha(a_0 + \alpha a_1 + \alpha^2 a_2 + \ldots), \tag{6.25a}$$
$$\varepsilon = \alpha^{1/2}(x_0 + \alpha x_1 + \alpha^2 x_2 + \ldots) + i\alpha^{1/2}(y_0 + \alpha y_1 + \alpha^2 y_2 + \ldots). \tag{6.25b}$$

We substitute these expressions in Eqs. (6.22) to (6.24), then solve them order by order in $\alpha$. This leads to the following parametric expression for the line of zeros in the $A$-plane, in the vicinity of $A_c = 2$:

$$A = (2+\alpha) + i\alpha\left[1 + 0.6\alpha + 0.2443\ldots\alpha^2 + 0.1749\ldots\alpha^3 + 0.1235\ldots\alpha^4 + \mathcal{O}(\alpha^5)\right]. \tag{6.26}$$

The result of this perturbative calculation up to $\mathcal{O}(\alpha^5)$ is represented by the continuous line in Fig. 6.10. Note that, indeed, the slope of this curve at the critical point is $\pi/4$, sign of a second-order phase transition. For completeness we shall give as well the solution for $\varepsilon$ up to order $\mathcal{O}(\alpha^5)$:

$$x = \alpha^{1/2}[0.6728\ldots - 0.1182\ldots\alpha + 0.0169\ldots\alpha^2$$
$$-0.0137\ldots\alpha^3 + 0.0014\ldots\alpha^4 + \mathcal{O}(\alpha^5)], \tag{6.27a}$$
$$y = \alpha^{1/2}[0.2787\ldots - 0.2854\ldots\alpha + 0.0754\ldots\alpha^2$$
$$-0.0477\ldots\alpha^3 + 0.0115\ldots\alpha^4 + \mathcal{O}(\alpha^5)]. \tag{6.27b}$$

Moreover, one can compute the density of zeros on the curve defined by Eq. (6.26) in the vicinity of the critical point using the relationship [161, 162]:

$$2\pi\mu(s) = \left|\frac{\partial}{\partial s}\,\mathrm{Im}\left(f^{(1)} - f^{(2)}\right)\right|, \tag{6.28}$$

where $\mu(s)$ is the density of zeros at a distance $s$ from the transition point, distance measured along the line of zeros. Making use of Eqs. (6.21) one finds

$$\mathrm{Im}(f^{(1)} - f^{(2)}) = 2(2+\alpha)xy + a(x^2-y^2)$$
$$+ (1/2-x)\arctan\left(\frac{y}{1/2-x}\right) - (1/2+x)\arctan\left(\frac{y}{1/2+x}\right)$$
$$+ y/2\ln\left[(1/2-x)^2+y^2\right] - y/2\ln\left[(1/2+x)^2+y^2\right]. \tag{6.29}$$

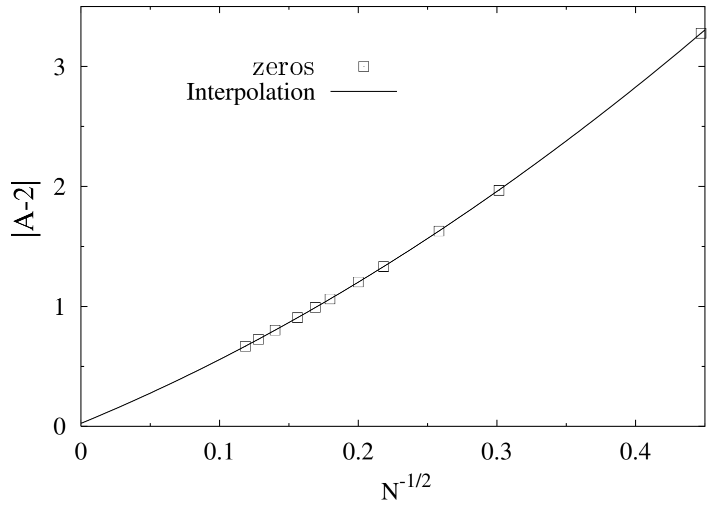


Figure 6.11: The minimum distance between the zeros of $Z_N$ and $A_c = 2$ in the complex $A$-plane as a function of $N^{-1/2}$. The continuous line is a least-square fit of the form $a + bN^{-1/2}(1 + cN^{-1})$, where $a$, $b$, and $c$ are fitting parameters. Note that the correction term $N^{-3/2}$ is used in view of the small values of $N$ that are accessible to calculations. Extrapolating to the $N \to \infty$ limit we obtain $a/A_c \simeq 1\%$, i.e., very close to zero, that confirms the theoretical value $A_c = 2$.

Making use of

$$s = \alpha\sqrt{1 + (1 + 0.6\alpha + \ldots)^2}, \tag{6.30}$$

of $\partial/\partial s = (\partial s/\partial\alpha)^{-1}\partial/\partial\alpha$, and of the solution (6.27), this gives in the vicinity of the transition point $\mu(s) = as + \mathcal{O}(s^2)$, with $s = \sqrt{2}\alpha$ and $a = 0.0045\ldots$. The density of zeros vanishes as a power law towards the transition point on the real axis – i.e., we recovered yet another characteristic of the equilibrium theory for second-order phase transitions.

Up to now, we have shown that the zeros of the partition function indeed provide information about the location and the type of the phase transition. But, as pointed out [157, 158] certain critical exponents are also encoded in the behavior of these zeros. A similar conclusion can be drawn in our model. As shown in Fig. 6.11, the distance $|A - A_c|$ between the closest root $A$ to $A_c = 2$ in the complex $A$-plane decreases like $N^{-1/2}$. A simple scaling argument shows [157, 158] that $|A-A_c|$ should scale with the system size as $N^{-1/\nu}$, where $\nu$ is the correlation length critical exponent. However, our urn model is structureless and the correlation length does not seem to be a well-defined quantity. Nevertheless, we can implement a definition of the critical exponent $\nu$ that is based on the finite-size scaling of moments of the order parameter [164]. Since the probability distribution at the critical point for urn models is known [141], using the standard prescription [164] we obtain $\nu = 2$. Such a value agrees with the finite-size scaling observed in Fig. 6.11.

In conclusion, we considered a simple stochastic model with *state-dependent tran-*

*sition rates* for which the partition function can be computed analytically, and that exhibits a second order phase transition. Our aim was to show that, although it is not a straightforward task to apply the concepts of the Yang-Lee theory, it is a remarkable and non-trivial fact that they still apply when the microscopic transition rates (obtained from a master equations description) of the model are state-dependent. Once more, this system is an equilibrium one in a mathematical sense since it satisfies detailed balance at a certain coarse-grained level of description. On the other hand, from the physical point of view it is a nonequilibrium system, since there is a continuous flow of energy through the system. The energy input is due to the shaking of the container, and energy is continuously dissipated through inelastic collisions between the particles.

## 6.7 The link with zero-range processes

It was possible to write the evolution equations (master equations) for the probability distribution $p(M,t)$ that in a given urn at time $t$ there are $M$ particles [139]. The corresponding master equations were thus solved analytically for $L = 2$ [141] and $L = 3$ [140]. However, in order to obtain results for arbitrary $L$ it is useful to consider the model as a zero-range process (ZRP) [140, 142], as first defined by Spitzer [165]. A ZRP is a process defined on a lattice of arbitrary dimension where the hopping probabilities $u_\mu(n_\mu)$ from one site to another one depend only on the number of particles $n_\mu$ in the initial site. Therefore if $n_\mu$ is the occupation number of site $\mu$, the configuration of the system is defined by the set (which may be infinite) of occupation numbers $\{n_\mu\}_{\mu=1}^{L}$. The total number of particles is conserved by the dynamics: $\sum_\mu n_\mu = N$. The ZRP formalism provides a steady state probability distribution $P(\{n_\nu\})$ which is a product measure of the form

$$P(\{n_\nu\}) = \frac{1}{Z(N,L)} \prod_{\mu=1}^{N} f_\mu(n_\mu), \tag{6.31}$$

where $L$ is the number of states (sites), $Z(N,L)$ the normalization factor, and $f_\mu(n_\mu)$ the *marginals* which are given by [142]

$$f(n) = \begin{cases} \displaystyle\prod_{m=1}^{n} \frac{1}{u(m)}, & n \geqslant 1, \\ 1, & n = 0. \end{cases} \tag{6.32}$$

The urn model corresponds to the particular case of a *homogeneous* ZRP for which the hopping probabilities $u(n_\mu)$ do not depend on the site. The hopping rates $u(n)$ of the urn model are given by Eq. (6.4), so that the probability distribution of finding the system of $L$ urns in the state $\{n_1, \dots, n_L\}$ reads off straightforwardly from Eqs. (6.31) and (6.32).

## 6.8 Conclusions

We examined two versions of the $L$-urn model for vibrated sand ($L \geqslant 2$). Our models recover qualitatively experimental findings and previous steady-state calculations. In addition, they take into account fluctuations caused by the finite number of particles. Using symmetry properties, we relate them with high-dimensional Potts model and argue that for $L \geqslant 3$ the phase transitions in such systems should be discontinuous. Although several quantities exhibit qualitatively similar behaviors for the two different versions of the model, there are important differences too. In particular, these models predict a different diffusion of a broken-down cluster, which can be either ordinary or anomalous, i.e., the type of diffusion is very sensitive to the dynamical rules of the model, and thus to the form of the flux. Next, for $L = 2$ we have shown that the concepts of the Yang-Lee theory still apply for the second order symmetry-breaking phase transition of the system, although the microscopic transition rates of the model are state-dependent. Finally, we have noted that the urn models belong to the class of zero-range processes.

# Chapter 7

# Conclusions and outlook

The class of systems we studied is defined by nonequilibrium dilute dissipative systems made of many interacting particles. The methods we developed may be applied to several systems such as granular gases, granular mixtures, pure annihilation, or probabilistic ballistic annihilation to cite a few ones. We also developed another (although related) model of a nonequilibrium dissipative system, namely the urn model for the separation of sand, which captures an essential feature of granular gases: the formation of clusters and symmetry breaking. We shall first recall the main results presented in this thesis.

## 7.1 Summary of the main results

One of the main objectives of this thesis was to provide a well established hydrodynamic description of probabilistic ballistic annihilation (PBA). In order to reach this goal, we made use of kinetic theory to study several properties of PBA.

We focused first on a model of pure annihilation that was solved exactly. This system is made of hard spheres with isotropic discrete bimodal initial velocity distributions. For such a system colliding particles disappear, therefore the discrete spectrum of the velocity distribution is preserved by the dynamics. This is the key ingredient leading to the analytical solution for the velocity distribution. We implemented molecular dynamics simulations which were confronted with the analytical solution based on Boltzmann's equation. This allowed to draw the important conclusion that Boltzmann's equation provides an accurate description of the dynamics already in two dimensions (it is expected that in higher dimensions the role of correlations diminish, while in dimension one the Boltzmann description fails) [40]. In the following, we turn our attention to continuous initial velocity distributions.

The next step was to develop a new method for building the first nonzero correction to the Maxwell distribution for a homogeneous dissipative ballistic gas. This method mainly consists in taking the limit of vanishing velocities of the rescaled Boltzmann equation. The scope of this method is very wide since it applies to granular gases, mixtures of particles, pure annihilation, probabilistic annihilation, etc. For comparison, we first used our method on granular gases, for which several results based on the "traditional" method are already available in the literature. We implemented Monte Carlo simulations in order to check the predictions of the velocity distribution for granular gases in the scaling regime $\widetilde{f}$ obtained analytically from our limit method. Our conclusion was that $\widetilde{f}$ provides a very accurate description (not attained by the "traditional" method) in the velocity domain of interest (small velocities). Moreover, this new method turns out to be technically simpler to implement than the "traditional" method [75].

Having developed this new general method and tested the accuracy of the Boltzmann equation for annihilation dynamics, we turned our attention to PBA. In this case colliding particles annihilate with probability $p$ and scatter elastically with probability $(1-p)$. The first result was to obtain the velocity distribution function for the homogeneous state and the decay exponents for the coarse grained density and thermal velocity fields. Monte Carlo simulations have shown that the predictions obtained from our limit method turned out to be very accurate (however the limit of vanishing annihilation $p \to 0$ is singular). Let $\mu$ characterize the behavior of the velocity distribution close to the origin: $\widetilde{f}(c) \propto c^{\mu}$, $c \to 0$. It is known that for pure annihilation the dynamics preserves the exponent $\mu$. On the other hand, our simulations led us to conjecture that in the long time limit the velocity distribution does not depend on the continuous initial velocity distribution. All distributions are attracted towards the same distribution characterized by $\mu = 0$, and thus become universal [52].

The next step was to study inhomogeneities in the gas. This allows for the existence of fluxes inside the system, associated with nonzero transport coefficients. Inhomogeneities were described by means of a first order Chapman-Enskog expansion. We thus established a hydrodynamic description of a system where none of the usual hydrodynamic fields is associated with a conserved quantity. The main result was to obtain the Navier-Stokes equations (first correction to the hydrodynamic equations describing a homogeneous flow) with transport coefficients and decay rates that stem from the microdynamics. The linear stability analysis of the latter equations allowed to conclude that presumably any inhomogeneity may only be a very short transient effect. This is to be contrasted to granular gases with constant restitution coefficient, where dense clusters form as a result of an initial inhomogeneity [45]. We have also studied two models that are simpler to treat analytically: the Maxwell and very hard particles models. We have shown that they not only capture the essential features of the hard sphere gas, but also provide upper and lower bounds to all comparable physical quantities [53].

Finally, we developed an urn model for the separation of granular matter. This phenomenological model is based on a master equations description. The model was shown to illustrate interesting and sometimes counterintuitive features like spontaneous symmetry breaking (clusterization), existence of metastable states, or anomalous diffusion of clusters for example. The model recovers qualitatively experimental findings. Moreover, using symmetry properties we argued that for $L \geqslant 2$ urns the model seems to be related with high-dimensional $L$-state Potts model [128]. In the $L = 2$ case, we were also able to show that the Yang-Lee theory adequately describes the phase transition in the case where the partition function is expressed in terms of a size-dependent effective fugacity [129].

## 7.2 Extensions and open problems

We would like to mention some problems opened by and which have not been treated in this thesis.

One peculiarity of probabilistic ballistic annihilation is that for long times the Boltzmann equation is likely to give an adequate description of the dynamics. On the other hand, molecular dynamics simulations allow to reproduce the exact dynamics without any underlying assumption (like molecular chaos). Consequently, an important point would be to implement molecular dynamics simulations of PBA of hard spheres in order to obtain numerically the transport coefficients for different annihilation probabilities $p$. Indeed, comparing those transport coefficients with the ones obtained analytically in this thesis would allow to probe directly the validity of the hydrodynamic description. This comparison would be independent from the problem of molecular chaos. The implementation of such a molecular dynamics program represents, however, a considerable amount of work and is beyond the range of this thesis.

The dynamics of PBA revealed different physical phenomena as compared to granular gases, e.g., inhomogeneities in PBA appear to be transient.[1] One may therefore presumably encounter unexpected behaviors from the study of slightly modified versions of PBA. It would therefore be worth to investigate several other variants of PBA as discussed below.

The undriven system of PBA of hard spheres is such that none of the hydrodynamic fields is associated with a conserved quantity. However, one could consider the action of a generalized "thermostat" $\mathbf{F}$ that plays the role of a source term in the Boltzmann equation (1.18). One usually considers a deterministic force proportional to the velocity $\mathbf{V}$ (Gaussian thermostat) [166, 167]

$$\boldsymbol{\nabla}_{\mathbf{v}} \cdot \mathbf{F} f(\mathbf{r}, \mathbf{v}; t) = \gamma(\mathbf{r}, v) \boldsymbol{\nabla}_{\mathbf{v}} \cdot [\mathbf{V} f(\mathbf{r}, \mathbf{v}; t)] \tag{7.1}$$

or a stochastic force (white noise thermostat) [37, 78, 168, 169, 170]

$$\boldsymbol{\nabla}_{\mathbf{v}} \cdot \mathbf{F} f(\mathbf{r}, \mathbf{v}; t) = -\frac{\gamma(\mathbf{r}, t) T(\mathbf{r}, t)}{m} \nabla_{\mathbf{v}}^2 f(\mathbf{r}, \mathbf{v}; t), \tag{7.2}$$

where $\gamma(\mathbf{r}, t)$ describes the amplitude of the force. However, the latter two thermostats are such that the number of particles and the impulsion are conserved: $\int \mathrm{d}\mathbf{v} \mathbf{v}^k \boldsymbol{\nabla}_{\mathbf{v}} \cdot \mathbf{F} f(\mathbf{r}, \mathbf{v}; t) = 0$, $k = 0, 1$. One has therefore to invent an additional particle and momentum injection mechanism. It would then be possible to have source terms that compensate exactly the loss of particles, momentum, and kinetic energy. The system could therefore be driven into a nonequilibrium steady state (different from the

[1] We shall make a comparison with granular gases since it is a well studied system which unveils a rich variety of models.

homogeneous cooling state). Since the density would be conserved, the conclusions regarding the linear stability of the hydrodynamic equations are likely to change. This study would provide some valuable theoretical insight. Indeed, it is probable that inhomogeneities would not show up only as transient phenomena and that they could be observed from molecular dynamics simulations. Again, this analysis could be carried out for PBA of hard spheres, as well as for the simpler Maxwell and VHP models which allow for a higher order analysis in the Chapman-Enskog expansion.

Besides probing the validity of hydrodynamics there is a very large amount of possible studies starting from the PBA formalism developed in this thesis. Indeed, many of the models implemented in the context of granular gases may be translated in the context of PBA (thermostats [37, 166, 171], mixtures of particles [6, 172], particles with internal degrees of freedom [14, 15], more complex collision rules with non-unity tangent restitution coefficient [173, 174], ...) for several interactions (Maxwell [41], hard spheres [53], and VHP models [45]), or numerical approaches (lattice gas automata [175, 176], molecular dynamics [83, 88, 102, 105], or Monte Carlo methods [102, 121, 177]), or even taking into account excluded volume effects with the Enskog equation [57]. Obtaining interesting conclusions for some of those extensions would be a rather straightforward work based on the results of this thesis. We shall mention as well that finding an experimental realization of (probabilistic) ballistic annihilation is a difficult task. However, it seems that the dynamics of point defects in nematic liquid crystals in specific geometries shares some features with ballistic annihilation [178].

Finally, using the results presented in this thesis it is straightforward to generalize the formalism of PBA to inelastic collisions. This would lead to a unified kinetic theory for probabilistic ballistic annihilation of granular gases. Again, a further possible extension would be then to take into account the velocity dependence of the restitution coefficient (PBA of viscoelastic particles), or a random restitution coefficient [84]. In the case of granular gases, it is known that if the restitution coefficient depends on the velocity, then instabilities are transient [12, 13]. It would therefore be interesting to study how this velocity dependence modifies the conclusions regarding the linear stability of PBA, and if inhomogeneities could therefore be observed from molecular dynamics simulations.

# Appendix A

# Appendix

## A.1 Calculation of $\beta_k$

We note $\Omega_d = \int \mathrm{d}\widehat{\boldsymbol{\sigma}} = 2\pi^{d/2}/\Gamma(d/2)$ the surface of a $d$-dimensional sphere, then

$$\begin{aligned}
\beta_k &= \frac{1}{2}\Omega_d \frac{\int \mathrm{d}\widehat{\boldsymbol{\sigma}}\,(\widehat{\boldsymbol{\sigma}}\cdot\widehat{\mathbf{v}}_{12})^k\theta(\widehat{\boldsymbol{\sigma}}\cdot\widehat{\mathbf{v}}_{12})}{\frac{1}{2}\Omega_d} \\
&= \frac{1}{2}\Omega_d \frac{\left(\prod_{l=1}^{d-2}\int_0^{\pi}\mathrm{d}\varphi_l\right)\int_0^{2\pi}\mathrm{d}\psi\prod_{m=1}^{d-2}(\sin\varphi_m)^m\cos(\varphi_{d-2})^k\theta(\cos\varphi_{d-2})}{\left(\prod_{l=1}^{d-2}\int_0^{\pi}\mathrm{d}\varphi_l\right)\int_0^{2\pi}\mathrm{d}\psi\prod_{m=1}^{d-2}(\sin\varphi_m)^m} \\
&= \frac{1}{2}\Omega_d \frac{\int_0^{\pi/2}\mathrm{d}\,\theta(\sin\theta)^{d-2}(\cos\theta)^k}{\int_0^{\pi/2}\mathrm{d}\theta\,(\sin\theta)^{d-2}} \\
&= \frac{1}{2}\Omega_d \frac{\frac{\Gamma[(d-1)/2]\Gamma[(k+1)/2]}{2\Gamma[(d+k)/2]}}{\frac{\Gamma[(d-1)/2]\Gamma(1/2)}{2\Gamma(d/2)}} \\
&= \pi^{\frac{d-1}{2}}\frac{\Gamma\left[(k+1)/2\right]}{\Gamma\left[(k+d)/2\right]},
\end{aligned} \tag{A.1}$$

which is Eq. (2.4).

## A.2 Calculation of the limit $c_1 \to 0$ of the collision term

We define the loss term $\widetilde{I}_l$ and gain term $\widetilde{I}_g$ by

$$\widetilde{I}_l = -\lim_{c_1\to 0}\int_{\mathbb{R}^d}\mathrm{d}\mathbf{c}_2\int d\widehat{\boldsymbol{\sigma}}\,\theta(\widehat{\boldsymbol{\sigma}}\cdot\widehat{\mathbf{c}}_{12})(\widehat{\boldsymbol{\sigma}}\cdot\mathbf{c}_{12})\widetilde{f}(c_1)\widetilde{f}(c_2) \tag{A.2a}$$

$$\widetilde{I}_g = \lim_{c_1\to 0}\frac{1}{\alpha^2}\int_{\mathbb{R}^d}\mathrm{d}\mathbf{c}_2\int d\widehat{\boldsymbol{\sigma}}\,\theta(\widehat{\boldsymbol{\sigma}}\cdot\widehat{\mathbf{c}}_{12})(\widehat{\boldsymbol{\sigma}}\cdot\mathbf{c}_{12})\widetilde{f}(c_1')\widetilde{f}(c_2'), \tag{A.2b}$$

so that $\lim_{c_1\to 0}\widetilde{I}(\widetilde{f},\widetilde{f}) = \widetilde{I}_l + \widetilde{I}_g$.

Taking the limit $c_1 \to 0$ of the loss term yields the exact result

$$\widetilde{I}_l = -\beta_1 \widetilde{f}(0)\langle c_2\rangle, \tag{A.3}$$

where $\beta_1 = \pi^{(d-1)/2}/\Gamma\left[(d+1)/2\right]$ is the particular case $k=1$ of Eq. (2.4). Making use of the relation

$$\int_{\mathbb{R}^d} \mathrm{d}\mathbf{x}\,|\mathbf{x}|^n \mathrm{e}^{-\alpha\mathbf{x}^2} = \frac{\pi^{d/2}}{\alpha^{(d+n)/2}}\frac{\Gamma\left[(d+n)/2\right]}{\Gamma(d/2)} \tag{A.4}$$

for $\alpha \in \mathbb{R}^+$, with $\Gamma$ the Euler gamma function, it is easy to show that within the framework of the Sonine expansion (4.21), neglecting the coefficients $a_i$, $i \geqslant 3$,

$$\langle c_2^n\rangle = \left[1 + \frac{a_2}{8}n(n-2)\right]\frac{\Gamma\left[(d+n)/2\right]}{\Gamma(d/2)}. \tag{A.5}$$

Making use of the particular case $n=1$, Eq. (A.3) becomes

$$\widetilde{I}_l = -\frac{S_d\widetilde{\mathcal{M}}(0)}{2\sqrt{\pi}}\left[1 + a_2\frac{d(d+2)}{8}\right]\left(1 - \frac{a_2}{8}\right), \tag{A.6}$$

where $S_d = \int \mathrm{d}\widehat{\boldsymbol{\sigma}} = 2\pi^{d/2}/\Gamma(d/2)$ is the surface of the $d$-dimensional sphere.

Defining $\beta = (1+\alpha)/(2\alpha) \geqslant 1$, the precollisional rescaled velocities $\mathbf{c}_i'$ and post-collisional ones $\mathbf{c}_i$ are related by

$$\mathbf{c}_1' = \mathbf{c}_1 - \beta(\mathbf{c}_{12}\cdot\widehat{\boldsymbol{\sigma}})\widehat{\boldsymbol{\sigma}}, \tag{A.7a}$$

$$\mathbf{c}_2' = \mathbf{c}_2 + \beta(\mathbf{c}_{12}\cdot\widehat{\boldsymbol{\sigma}})\widehat{\boldsymbol{\sigma}}. \tag{A.7b}$$

The gain term (A.2b) thus reads

$$\widetilde{I}_g = \frac{1}{\alpha^2}\int_{\mathbb{R}^d}\mathrm{d}\mathbf{c}_2\int \mathrm{d}\widehat{\boldsymbol{\sigma}}\,\theta(\widehat{\boldsymbol{\sigma}}\cdot\widehat{\mathbf{c}}_2)(\widehat{\boldsymbol{\sigma}}\cdot\mathbf{c}_2)\,\widetilde{f}\left[\beta(\mathbf{c}_2\cdot\widehat{\boldsymbol{\sigma}})\widehat{\boldsymbol{\sigma}}\right]\widetilde{f}\left[\mathbf{c}_2 - \beta(\mathbf{c}_2\cdot\widehat{\boldsymbol{\sigma}})\widehat{\boldsymbol{\sigma}}\right], \tag{A.8}$$

where the function $\widetilde{f}$ is isotropic. Performing the integration over $\mathbf{c}_2$ before that over $\widehat{\boldsymbol{\sigma}}$, we choose the $x$ Cartesian coordinate as corresponding to the $\widehat{\boldsymbol{\sigma}}$ direction. The velocity $\mathbf{c}_2$ is thus written $\mathbf{c}_2 = c_x\widehat{\mathbf{x}} + \mathbf{c}_\perp$, with $c_x = (\mathbf{c}_2\cdot\widehat{\boldsymbol{\sigma}}) \in \mathbb{R}$ and $\mathbf{c}_\perp = \mathbf{c}_2 - c_x\widehat{\mathbf{x}} \in \mathbb{R}^{d-1}$. Eq. (A.8) becomes

$$\widetilde{I}_g = \frac{1}{\alpha^2}\int \mathrm{d}\widehat{\boldsymbol{\sigma}}\int_{\mathbb{R}^d}\mathrm{d}\mathbf{c}_2\,\theta(c_x)\,c_x\widetilde{f}(\beta c_x\widehat{\boldsymbol{\sigma}})\widetilde{f}(\mathbf{c}_2 - \beta c_x\widehat{\boldsymbol{\sigma}}) \tag{A.9}$$

$$= \frac{S_d}{\alpha^2}\int_0^\infty \mathrm{d}c_x\,c_x\int_{\mathbb{R}^{d-1}}\mathrm{d}\mathbf{c}_\perp\,\widetilde{f}(\beta c_x)\widetilde{f}\left(\sqrt{c_\perp^2 + c_x^2(1-\beta)^2}\right). \tag{A.10}$$

Eq. (A.10) is an exact relation within Boltzmann's framework. Making use of the the Sonine expansion (4.21) where we retain only the first correction $a_2$, Eq. (A.10) becomes

$$\widetilde{I}_g = \frac{S_d}{\alpha^2\pi^d}\int_0^\infty \mathrm{d}c_x\,c_x\mathrm{e}^{-\left[\beta^2+(1-\beta^2)\right]c_x^2}\int_{\mathbb{R}^{d-1}}\mathrm{d}\mathbf{c}_\perp\,\mathrm{e}^{-c_\perp^2}\left[1 + a_2S_2(\beta^2c_x^2)\right]$$
$$\times\left\{1 + a_2S_2\left[c_\perp^2 + c_x^2(1-\beta)^2\right]\right\}. \tag{A.11}$$

With the definition of the second Sonine polynomial $S_2(x) = x^2/2 - (d+2)x/2 + d(d+2)/8$, one sees that Eq. (A.11) may be expressed as a sum of products of the integrals

$$J_\perp(n) = \int_{\mathbb{R}^{d-1}} \mathrm{d}\mathbf{c}_\perp\, \mathrm{e}^{-c_\perp^2} c_\perp^n, \tag{A.12a}$$

$$J_x(n) = \int_0^\infty \mathrm{d}c_x\, \mathrm{e}^{-[\beta^2+(1-\beta^2)]c_x^2} c_x^n, \tag{A.12b}$$

that are straightforwardly computed using the relation (A.4). Tedious but technically simple calculations thus lead to

$$\widetilde{I}_g = \frac{S_d \widetilde{\mathcal{M}}(0)}{2\sqrt{\pi}} \left[\frac{2}{1+\alpha^2} + a_2 D_1(\alpha,d) + a_2^2 D_2(\alpha,d)\right], \tag{A.13}$$

where

$$D_1(\alpha,d) = \frac{1}{8(1+\alpha^2)^3}\Big[2(1+\alpha^2)^2(d^2-2d-5) + 4(d-1)(\alpha-1)^2(1+\alpha^2) \\ + 8(\alpha^4+6\alpha^2+1)\Big] \tag{A.14}$$

and

$$D_2(\alpha,d) = \frac{1}{32(1+\alpha^2)^5}\Big[12\alpha^3(1+\alpha^2)(d-1)(d-2) - 4\alpha^2(1+\alpha^4)(24+4d-d^2) \\ + 4\alpha(1+\alpha^6)(d+6)(d-1) - (1+\alpha^8)(26+28d+9d^2)\Big]. \tag{A.15}$$

Finally, the limit $c_1 \to 0$ of Eq. (3.7) is given by the sums of Eqs. (A.6) and (A.13).

## A.3 Boltzmann equation involving moments

Inserting the scaling form (4.6) in the Boltzmann equation (4.1), the contributions of the right-hand side become

$$pJ_a[f,f] = -p\sigma^{d-1}\frac{n^2}{\overline{v}^{d-1}}\beta_1 \int_{\mathbb{R}^d} \mathrm{d}\mathbf{c}_2\, |c_{12}| \widetilde{f}(c_1)\widetilde{f}(c_2), \tag{A.16}$$

and

$$(1-p)J_c[f,f] = (1-p)\sigma^{d-1}\frac{n^2}{\overline{v}^{d-1}}\widetilde{I}[\widetilde{f},\widetilde{f}], \tag{A.17}$$

where

$$\widetilde{I}[\widetilde{f},\widetilde{f}] = \int_{\mathbb{R}^d} \mathrm{d}\mathbf{c}_2 \int \mathrm{d}\widehat{\boldsymbol{\sigma}}\, \theta(\widehat{\boldsymbol{\sigma}}\cdot\widehat{\mathbf{c}}_{12})(\widehat{\boldsymbol{\sigma}}\cdot\widehat{\mathbf{c}}_{12})|c_{12}| \left[\widetilde{f}(c_1')\widetilde{f}(c_2') - \widetilde{f}(c_1)\widetilde{f}(c_2)\right]. \tag{A.18}$$

The left-hand side of Eq. (4.1) becomes

$$\begin{aligned}
\partial_t f(\mathbf{v}_1;t) &= \frac{1}{\overline{v}^d}\widetilde{f}(c_1)\partial_t n - \frac{d}{\overline{v}^{d+1}} n\widetilde{f}(c_1)\partial_t\overline{v} + \frac{n}{\overline{v}^d}\frac{\partial c_1}{\partial t}\frac{\mathrm{d}}{\mathrm{d}c_1}\widetilde{f}(c_1) \\
&= \frac{n}{\overline{v}^d}\left[\widetilde{f}(c_1)\frac{1}{n}\partial_t n - d\widetilde{f}(c_1)\frac{1}{\overline{v}}\partial_t\overline{v} - c_1\frac{\mathrm{d}}{\mathrm{d}c_1}\widetilde{f}(c_1)\frac{1}{\overline{v}}\partial_t\overline{v}\right] \\
&= \frac{n}{\overline{v}^d}\left[\partial_t \ln n - \partial_t \ln\overline{v}\left(d + c_1\frac{\mathrm{d}}{\mathrm{d}c_1}\right)\right]\widetilde{f}(c_1).
\end{aligned} \tag{A.19}$$

On the other hand, Eqs. (4.14) and (4.15) provide:

$$\ln n = -\xi p \ln\left(1 + p\frac{1+\alpha_e}{2}\omega_0 t\right), \tag{A.20a}$$

$$\ln \overline{v} = -\gamma p \ln\left(1 + p\frac{1+\alpha_e}{2}\omega_0 t\right), \tag{A.20b}$$

therefore

$$\partial_t \ln n = -\xi p \frac{p\frac{1+\alpha_e}{2}\omega_0}{1 + p\frac{1+\alpha_e}{2}\omega_0 t}, \tag{A.21a}$$

$$\partial_t \ln \overline{v} = -\gamma p \frac{p\frac{1+\alpha_e}{2}\omega_0}{1 + p\frac{1+\alpha_e}{2}\omega_0 t}, \tag{A.21b}$$

Making use of Eqs. (A.21) in Eq. (A.19), and of Eqs. (A.16) and (A.17) the Boltzmann equation reads

$$\begin{aligned} p\frac{\frac{1+\alpha_e}{2}\omega_0}{1 + p\frac{1+\alpha_e}{2}\omega_0 t}\left[-\xi + \gamma\left(d + c_1\frac{\mathrm{d}}{\mathrm{d}c_1}\right)\right]\widetilde{f}(c_1) \\ = -p\sigma^{d-1} n\overline{v}\beta_1 \int_{\mathbb{R}^d} \mathrm{d}\mathbf{c}_2\, |c_{12}|\widetilde{f}(c_1)\widetilde{f}(c_2) + (1-p)\sigma^{d-1} n\overline{v}\widetilde{I}[\widetilde{f},\widetilde{f}]. \end{aligned} \tag{A.22}$$

Eqs. (4.14) yield

$$n\overline{v} = n_0\overline{v}_0 \frac{1}{1 + p\frac{1+\alpha_e}{2}\omega_0 t}, \tag{A.23}$$

that we insert in Eq. (A.22) in order to obtain

$$\begin{aligned} p\frac{1+\alpha_e}{2}\omega_0\left[-\xi + \gamma\left(d + c_1\frac{\mathrm{d}}{\mathrm{d}c_1}\right)\right]\widetilde{f}(c_1) \\ = -p\sigma^{d-1}\beta_1 \int_{\mathbb{R}^d} \mathrm{d}\mathbf{c}_2\, |c_{12}|\widetilde{f}(c_1)\widetilde{f}(c_2) + (1-p)\sigma^{d-1}\widetilde{I}[\widetilde{f},\widetilde{f}]. \end{aligned} \tag{A.24}$$

Eq. (4.8) gives $\omega_0$:

$$\omega_0 = n_0\overline{v}_0\sigma^{d-1}\beta_1\langle c_{12}\rangle, \tag{A.25}$$

which in Eq. (A.24) yields the form (4.16) of the Boltzmann equation.

## A.4 Summary of the notations

We shall recall here some of the notations used through chapters 4 and 5. $\kappa$ and $\mu$ are the transport coefficients appearing in Fourier's linear heat conduction law (4.57), and $\eta$ is the shear viscosity appearing in the pressure tensor (4.56). A quantity $A$ that is made dimensionless is noted $A^*$. The corresponding dimensionless transport coefficients are written

$$\eta^* = \frac{\eta}{\eta_0}, \tag{A.26a}$$

$$\kappa^* = \frac{\kappa}{\kappa_0}, \tag{A.26b}$$

$$\mu^* = \frac{n\mu}{T\kappa_0}, \tag{A.26c}$$

where

$$\kappa_0 = \frac{d(d+2)}{2(d-1)}\frac{k_B}{m}\eta_0, \tag{A.27}$$

$$\eta_0 = \frac{d+2}{8}\frac{\Gamma(d/2)}{\pi^{(d-1)/2}}\frac{\sqrt{mk_BT}}{\sigma^{d-1}}, \tag{A.28}$$

are the thermal conductivity and shear viscosity coefficients for hard spheres, respectively. The dimensionless coefficients $\nu_\eta^*$, $\nu_\kappa^*$, and $\nu_\mu^*$ are given by

$$\nu_\kappa^* = \frac{1}{\nu_0}\frac{\int_{\mathbb{R}^d}\mathrm{d}\mathbf{V}\, S_i(\mathbf{V})J\mathcal{A}_i}{\int_{\mathbb{R}^d}\mathrm{d}\mathbf{V}\, S_i(\mathbf{V})\mathcal{A}_i} - p\frac{1}{\nu_0}\frac{\int_{\mathbb{R}^d}\mathrm{d}\mathbf{V}\, S_i(\mathbf{V})\Omega\mathcal{A}_i}{\int_{\mathbb{R}^d}\mathrm{d}\mathbf{V}\, S_i(\mathbf{V})\mathcal{A}_i}, \tag{A.29a}$$

$$\nu_\mu^* = \frac{1}{\nu_0}\frac{\int_{\mathbb{R}^d}\mathrm{d}\mathbf{V}\, S_i(\mathbf{V})J\mathcal{B}_i}{\int_{\mathbb{R}^d}\mathrm{d}\mathbf{V}\, S_i(\mathbf{V})\mathcal{B}_i} - p\frac{1}{\nu_0}\frac{\int_{\mathbb{R}^d}\mathrm{d}\mathbf{V}\, S_i(\mathbf{V})\Omega\mathcal{B}_i}{\int_{\mathbb{R}^d}\mathrm{d}\mathbf{V}\, S_i(\mathbf{V})\mathcal{B}_i}, \tag{A.29b}$$

$$\nu_\eta^* = \frac{1}{\nu_0}\frac{\int_{\mathbb{R}^d}\mathrm{d}\mathbf{V}\, D_{ij}(\mathbf{V})J\mathcal{C}_{ij}}{\int_{\mathbb{R}^d}\mathrm{d}\mathbf{V}\, D_{ij}(\mathbf{V})\mathcal{C}_{ij}} - p\frac{1}{\nu_0}\frac{\int_{\mathbb{R}^d}\mathrm{d}\mathbf{V}\, D_{ij}(\mathbf{V})\Omega\mathcal{C}_{ij}}{\int_{\mathbb{R}^d}\mathrm{d}\mathbf{V}\, D_{ij}(\mathbf{V})\mathcal{C}_{ij}}, \tag{A.29c}$$

where $\mathbf{V} = \mathbf{v} - \mathbf{u}$,

$$\nu_0 = \frac{p^{(0)}}{\eta_0} = \frac{8}{d+2}\frac{\pi^{(d-1)/2}}{\Gamma(d/2)}n\sigma^{d-1}\sqrt{\frac{k_BT}{m}}, \tag{A.30}$$

and $p^{(0)} = nk_BT$ is the zeroth order pressure. In Eqs. (A.29), the operator $J$ is given by

$$Jg = pL_a[f^{(0)}, g] + (1-p)L_c[f^{(0)}, g], \tag{A.31}$$

where

$$L_a[f^{(0)}, g] = -J_a[f^{(0)}, g] - J_a[g, f^{(0)}], \tag{A.32a}$$

$$L_c[f^{(0)}, g] = -J_c[f^{(0)}, g] - J_c[g, f^{(0)}], \tag{A.32b}$$

$$\tag{A.32c}$$

$g$ being an arbitrary function. The collision operator $J_c$ (annihilation operator $J_a$) is defined by Eq. (5.3) [Eq. (5.2)]. The linear operator $\Omega$ is defined by Eq. (4.55).

The velocity distribution function is denoted $f(\mathbf{r}, \mathbf{v}; t)$. In the scaling regime

$$f(\mathbf{r}, \mathbf{v}; t) = \frac{n(t)}{v_T^d(t)}\widetilde{f}(c), \tag{A.33}$$

where $c = V/v_T$. The time dependent [through $T(t)$] thermal velocity is

$$v_T = \sqrt{\frac{2k_BT}{m}}. \tag{A.34}$$

We note the Maxwellian in the homogeneous cooling state by

$$\mathcal{M}(V) = \frac{n(t)}{v_T^d(t)\pi^{d/2}}\exp\left(-\frac{V^2}{v_T^2}\right), \tag{A.35}$$

and the Maxwellian by

$$\widetilde{\mathcal{M}}(c) = \pi^{-d/2} \exp(-c^2). \tag{A.36}$$

Therefore, we obtain a similar relation to Eq.(A.33): $\mathcal{M}(V) = (n/v_T^d)\widetilde{\mathcal{M}}(c)$.

The decay rate for the field $A = \{n, u_i, T\}$ reads $\xi_A^{(m)}$, where $m$ denotes the order in the Chapman-Enskog expansion. The corresponding dimensionless decay rate is

$$\xi_A^{(m)*} = \frac{\xi_A^{(m)}}{\nu_0}. \tag{A.37}$$

## A.5 Balance equations

In the following we adopt Einstein's summation convention.

### A.5.1 Mass

Integrating Eq. (4.28) over $\mathbf{v}_1$ we obtain

$$\partial_t \int_{\mathbb{R}^d} \mathrm{d}\mathbf{v}\, f(\mathbf{r},\mathbf{v};t) + \nabla_i \int_{\mathbb{R}^d} \mathrm{d}\mathbf{v}\, v_i f(\mathbf{r},\mathbf{v};t) = p \int_{\mathbb{R}^d} \mathrm{d}\mathbf{v}\, J_a[f,f] + (1-p)\int_{\mathbb{R}^d} \mathrm{d}\mathbf{v}\, J_c[f,f]. \tag{A.38}$$

Using the definition (4.31), the first term of the left-hand side gives $\partial_t n$, and the second $nu_i$. The last term of the right-hand side is equal to zero since the collision operator preserves the number of particles. Finally, using Eqs. (4.29) and (4.33) we see that the first term of the right-hand side is equal to $-p\omega[f,f]$. We thus obtain Eq. (4.32a).

### A.5.2 Momentum

Integrating Eq. (4.28) over $\mathbf{v}_1$ with weight $m\mathbf{v}_1$ we obtain

$$\partial_t \int_{\mathbb{R}^d} \mathrm{d}\mathbf{v}\, m v_i f(\mathbf{r},\mathbf{v};t) + \nabla_j \int_{\mathbb{R}^d} \mathrm{d}\mathbf{v}\, m v_i v_j f(\mathbf{r},\mathbf{v};t) = p \int_{\mathbb{R}^d} \mathrm{d}\mathbf{v}\, m v_i J_a[f,f] + (1-p)\int_{\mathbb{R}^d} \mathrm{d}\mathbf{v}\, m v_i J_c[f,f]. \tag{A.39}$$

Again, for similar reasons Eq. (A.39) becomes

$$\partial_t (n u_i) + \nabla_j \int_{\mathbb{R}^d} \mathrm{d}\mathbf{v}\, v_i v_j f(\mathbf{r},\mathbf{v};t) = -p\omega[f, v_i f]. \tag{A.40}$$

Making use of the definition (4.34) for the pressure tensor, we establish

$$\nabla_j \int_{\mathbb{R}^d} \mathrm{d}\mathbf{v}\, v_i v_j f(\mathbf{r},\mathbf{v};t) = \frac{1}{m}\nabla_j P_{ij} + \nabla_j n u_i u_j, \tag{A.41}$$

that we insert in Eq. (A.40). Making then use of the balance equation for mass (4.32a) we obtain Eq. (4.32b).

### A.5.3 Energy

Integrating Eq. (4.28) over $\mathbf{v}_1$ with weight $m\mathbf{v}_1^2/2$ we obtain

$$\begin{aligned}\partial_t \int_{\mathbb{R}^d} \mathrm{d}\mathbf{v}\, v^2 f(\mathbf{r},\mathbf{v};t) + \nabla_j \int_{\mathbb{R}^d} \mathrm{d}\mathbf{v}\, v^2 v_j f(\mathbf{r},\mathbf{v};t)& \\ = p\int_{\mathbb{R}^d} \mathrm{d}\mathbf{v}\, v^2 J_a[f,f] + (1-p)\int_{\mathbb{R}^d} \mathrm{d}\mathbf{v}\, v^2 J_c[f,f].&\end{aligned} \tag{A.42}$$

The definition (4.35) for the heat-flux allows to find the intermediate result

$$\begin{aligned}\nabla_j q_j = \frac{m}{2}\nabla_j \int_{\mathbb{R}^d} \mathrm{d}\mathbf{v}\, v_j v^2 f(\mathbf{r},\mathbf{v};t) - \frac{m}{2}\nabla_j u_j \int_{\mathbb{R}^d} \mathrm{d}\mathbf{v}\, v^2 f(\mathbf{r},\mathbf{v};t)& \\ - m\nabla_j u_k \int_{\mathbb{R}^d} \mathrm{d}\mathbf{v}\, v_j v_k f(\mathbf{r},\mathbf{v};t) + m\nabla_j n u_j u^2.&\end{aligned} \tag{A.43}$$

Making use of the definition (4.34) for the pressure tensor, Eq. (A.43) yields

$$\begin{aligned}\nabla_j \int_{\mathbb{R}^d} \mathrm{d}\mathbf{v}\, v^2 v_j f(\mathbf{r},\mathbf{v};t) = \frac{2}{m}\left(P_{ij}\nabla_i u_j + \nabla_j q_i\right) + \nabla_j u_j \int_{\mathbb{R}^d} \mathrm{d}\mathbf{v}\, v^2 f(\mathbf{r},\mathbf{v};t)& \\ - 2\nabla_j n u_j u^2 + n u_j \nabla_j u^2 + \frac{2}{m} u_k \nabla_j P_{kj} + 2u_k \nabla_j n u_j u_k.&\end{aligned} \tag{A.44}$$

On the other hand, the definition (4.31c) for the temperature yields

$$\begin{aligned}\partial_t T = \frac{m}{k_B T}\frac{1}{n^2}\left(\partial_t n\right) \int_{\mathbb{R}^d} \mathrm{d}\mathbf{v}\, v^2 f(\mathbf{r},\mathbf{v};t)& \\ + \frac{m}{k_B T} 2u_j\left(\partial_t u_j\right) - \frac{m}{k_B d}\frac{1}{n}\partial_t \int_{\mathbb{R}^d} \mathrm{d}\mathbf{v}\, v^2 f(\mathbf{r},\mathbf{v};t),&\end{aligned} \tag{A.45}$$

in which we use the balance equations (4.32a) and (4.32b) in order to obtain

$$\begin{aligned}\partial_t \int_{\mathbb{R}^d} \mathrm{d}\mathbf{v}\, v^2 f(\mathbf{r},\mathbf{v};t) = -\frac{1}{n}\left(p\omega[f,f] + u_j \nabla_j n + n\nabla_j u_j\right) \int_{\mathbb{R}^d} \mathrm{d}\mathbf{v}\, v^2 f(\mathbf{r},\mathbf{v};t)& \\ + \frac{n k_B d}{m}\partial_t T - 2\left(\frac{1}{m} u_j \nabla_k P_{jk} + n u_j u_k \nabla_k u_j + p\omega[f, u_j V_j f]\right).&\end{aligned} \tag{A.46}$$

Finally, the insertion of Eqs. (A.44) and (A.46) into Eqs. (A.42) leads us to Eq. (4.32c).

## A.6 Equations for $\mathcal{A}_i$, $\mathcal{B}_i$, and $\mathcal{C}_{ij}$ to first order

We would like to rewrite the right-hand side of Eq. (4.46) in a form involving gradients of the hydrodynamic fields. The normal solution (4.38) gives

$$\partial_t f^{(0)}(\mathbf{r},\mathbf{v};t) = \frac{\partial f^{(0)}}{\partial n}\frac{\partial n}{\partial t} + \frac{\partial f^{(0)}}{\partial u_i}\frac{\partial u_i}{\partial t} + \frac{\partial f^{(0)}}{\partial T}\frac{\partial T}{\partial t}, \tag{A.47}$$

and using the lightened notation $\mathbf{v}_1 = (v_1, \ldots, v_d)$, $\mathbf{r}_1 = (r_1, \ldots, r_d)$:

$$\mathbf{v}_1 \cdot \boldsymbol{\nabla} f^{(0)} = v_i \frac{\partial f^{(0)}}{\partial n} \nabla_i n + v_j \frac{\partial f^{(0)}}{\partial u_i} \nabla_j u_i + v_i \frac{\partial f^{(0)}}{\partial T} \nabla_i T. \tag{A.48}$$

Since $f^{(0)}$ is known [Eq. (4.43)], then $\partial f^{(0)}/\partial n = f^{(0)}/n$, and $\partial f^{(0)}/\partial u_i = -\partial f^{(0)}/\partial V_i$, the right-hand side of Eq. (4.42) becomes

$$\begin{aligned} -\left[\partial_t + v_i \nabla_i\right] f^{(0)} = &-f^{(0)} \left( \frac{1}{n}\partial_t n + \frac{1}{n} v_i \nabla_i n \right) \\ &+ \frac{\partial f^{(0)}}{\partial V_i} \left(\partial_t u_i + v_j \nabla_j u_i\right) - \frac{\partial f^{(0)}}{\partial T} \left(\partial_t T + v_i \nabla_i T\right). \end{aligned} \tag{A.49}$$

The terms in parenthesis may be rewritten using the first order balance equations (4.44). Then Eq. (4.46) finally takes the form

$$[\partial_t^{(0)} + J] f^{(1)} = A_i \nabla_i \ln T + B_i \nabla_i \ln n + C_{ij} \nabla_i u_j + p\Omega f^{(1)}, \tag{A.50}$$

where $V_i = v_i - u_i$,

$$\Omega f^{(1)} = f^{(0)} \xi_n^{(1)} - \frac{\partial f^{(0)}}{\partial V_i} v_T \xi_{u_i}^{(1)} + \frac{\partial f^{(0)}}{\partial T} T \xi_T^{(1)}, \tag{A.51}$$

and

$$A_i = -V_i T \frac{\partial f^{(0)}}{\partial T} - \frac{k_B T}{m} \frac{\partial f^{(0)}}{\partial V_i}, \tag{A.52a}$$

$$B_i = -V_i f^{(0)} - \frac{k_B T}{m} \frac{\partial f^{(0)}}{\partial V_i}, \tag{A.52b}$$

$$C_{ij} = \frac{\partial}{\partial V_i}[v_j f^{(0)}] + \frac{2}{d} T \frac{\partial f^{(0)}}{\partial T} \delta_{ij}. \tag{A.52c}$$

The velocity dependence of $f^{(0)}$ occurs only through $V/v_T$. Because of the normalization the temperature dependence of the function $f^{(0)}$ is of the form $T^{-d/2}\overline{f}^{(0)}(V/T^{1/2})$. Therefore

$$\begin{aligned} -T\frac{\partial f^{(0)}}{\partial T} &= -T\frac{\partial}{\partial T}\left[T^{-d/2}\overline{f}^{(0)}(V/T^{1/2})\right] \\ &= \frac{d}{2} f^{(0)} - T T^{-d/2} \frac{\partial}{\partial T} \overline{f}^{(0)}(V/T^{1/2}). \end{aligned} \tag{A.53}$$

If we define $\mathbf{x} = \mathbf{V}/T^{1/2}$, then $\partial/\partial x_i = T^{1/2}\partial/\partial V_i$, and

$$\frac{\partial}{\partial T}\overline{f}^{(0)}(V/T^{1/2}) = -\frac{1}{2} V_i \frac{1}{T} \frac{\partial \overline{f}^{(0)}}{\partial V_i}. \tag{A.54}$$

Inserting Eq. (A.54) in Eq. (A.53) we obtain

$$-T\frac{\partial f^{(0)}}{\partial T} = \frac{d}{2} f^{(0)} + \frac{1}{2} V_i T^{d/2} \frac{\partial}{\partial V_i} \overline{f}^{(0)}(V/T^{1/2}). \tag{A.55}$$

On the other hand

$$\frac{1}{2}\frac{\partial}{\partial V_i}\left[V_i f^{(0)}\right] = \frac{d}{2}f^{(0)} + \frac{1}{2}V_i T^{d/2}\frac{\partial}{\partial V_i}\overline{f}^{(0)}(V/T^{1/2}). \tag{A.56}$$

Comparing Eqs. (A.55) and (A.56) one obtains

$$-T\frac{\partial f^{(0)}}{\partial T} = \frac{1}{2}\frac{\partial}{\partial V_i}[V_i f^{(0)}]. \tag{A.57}$$

The insertion of Eq. (A.57) in the Eqs. (A.52) yields the relations (4.54).

We now turn to the left-hand side of Eq. (4.46). Making use of the form (4.52) for $f^{(1)}$ then

$$\begin{aligned}
\frac{\partial^{(0)} f^{(1)}}{\partial t} &= \nabla_i \ln T\left[\frac{\partial \mathcal{A}_i}{\partial T}\frac{\partial^{(0)}T}{\partial t} + \frac{\partial \mathcal{A}_i}{\partial n}\frac{\partial^{(0)}n}{\partial t} + \frac{\partial \mathcal{A}_i}{\partial u_j}\frac{\partial^{(0)}u_j}{\partial t}\right] \\
&\quad +\nabla_i \ln n\left[\frac{\partial \mathcal{B}_i}{\partial T}\frac{\partial^{(0)}T}{\partial t} + \frac{\partial \mathcal{B}_i}{\partial n}\frac{\partial^{(0)}n}{\partial t} + \frac{\partial \mathcal{B}_i}{\partial u_j}\frac{\partial^{(0)}u_j}{\partial t}\right] \\
&\quad +\nabla_j u_i\left[\frac{\partial \mathcal{C}_{ij}}{\partial T}\frac{\partial^{(0)}T}{\partial t} + \frac{\partial \mathcal{C}_{ij}}{\partial n}\frac{\partial^{(0)}n}{\partial t} + \frac{\partial \mathcal{C}_{ij}}{\partial u_k}\frac{\partial^{(0)}u_k}{\partial t}\right] \\
&\quad +\mathcal{A}_i\nabla_i\frac{1}{T}\frac{\partial^{(0)}T}{\partial t} + \mathcal{B}_i\nabla_i\frac{1}{n}\frac{\partial^{(0)}n}{\partial t} + \mathcal{C}_{ij}\nabla_j\frac{\partial^{(0)}u_i}{\partial t}.
\end{aligned} \tag{A.58}$$

The derivatives of the hydrodynamic fields are expressed using the zeroth-order balance equations (4.44):

$$\begin{aligned}
\nabla_i\frac{1}{T}\frac{\partial^{(0)}T}{\partial t} &= -p\nabla_i\xi_T^{(0)} \\
&= -p\left(n\frac{\partial \xi_T^{(0)}}{\partial n}\nabla_i \ln n + T\frac{\partial \xi_T^{(0)}}{\partial T}\nabla_i \ln T + \frac{\partial \xi_T^{(0)}}{\partial u_j}\nabla_i u_j\right),
\end{aligned} \tag{A.59a}$$

$$\begin{aligned}
\nabla_i\frac{1}{n}\frac{\partial^{(0)}n}{\partial t} &= -p\nabla_i\xi_n^{(0)} \\
&= -p\left(n\frac{\partial \xi_n^{(0)}}{\partial n}\nabla_i \ln n + T\frac{\partial \xi_n^{(0)}}{\partial T}\nabla_i \ln T + \frac{\partial \xi_n^{(0)}}{\partial u_j}\nabla_i u_j\right),
\end{aligned} \tag{A.59b}$$

$$\begin{aligned}
\nabla_j\frac{\partial^{(0)}u_i}{\partial t} &= -p\nabla_j\xi_{u_i}^{(0)} \\
&= -p\left(n\frac{\partial \xi_{u_i}^{(0)}}{\partial n}\nabla_j \ln n + T\frac{\partial \xi_{u_i}^{(0)}}{\partial T}\nabla_j \ln T + \frac{\partial \xi_{u_i}^{(0)}}{\partial u_k}\nabla_j u_k\right).
\end{aligned} \tag{A.59c}$$

Eqs. (A.59) have to be inserted into Eq. (A.58). On the other hand, since $J$ is a linear operator we have

$$Jf^{(1)} = (J\mathcal{A}_i)\nabla_i \ln T + (J\mathcal{B}_i)\nabla_i \ln n + (J\mathcal{C}_{ij})\nabla_j u_i. \tag{A.60}$$

Eqs. (A.60) and (A.58) [combined with Eqs. (A.59)] allow to express the left-hand side of Eq. (4.46): $[\partial_t^{(0)} + J]f^{(1)}$. Since again $\Omega$ is a linear operator, $\Omega f^{(1)}$ has the same form as in Eq. (A.60) where we replace $J$ by $\Omega$. Making use of Eq. (A.50) we thus obtain

$$-p\alpha_i + (J - p\Omega)\mathcal{A}_i = A_i, \tag{A.61a}$$
$$-p\beta_i + (J - p\Omega)\mathcal{B}_i = B_i, \tag{A.61b}$$
$$-p\gamma_{ij} + (J - p\Omega)\mathcal{C}_{ij} = C_{ij}, \tag{A.61c}$$

where

$$\alpha_i = T\xi_T^{(0)}\frac{\partial \mathcal{A}_i}{\partial T} + n\xi_n^{(0)}\frac{\partial \mathcal{A}_i}{\partial n} + \xi_{u_j}^{(0)}\frac{\partial \mathcal{A}_i}{\partial u_j} + \mathcal{A}_i T\frac{\partial \xi_T^{(0)}}{\partial T} + \mathcal{B}_i T\frac{\partial \xi_n^{(0)}}{\partial T} + \mathcal{C}_{ji} T\frac{\partial \xi_{u_j}^{(0)}}{\partial T}, \tag{A.62a}$$

$$\beta_i = T\xi_T^{(0)}\frac{\partial \mathcal{B}_i}{\partial T} + n\xi_n^{(0)}\frac{\partial \mathcal{B}_i}{\partial n} + \xi_{u_j}^{(0)}\frac{\partial \mathcal{B}_i}{\partial u_j} + \mathcal{A}_i n\frac{\partial \xi_T^{(0)}}{\partial n} + \mathcal{B}_i n\frac{\partial \xi_n^{(0)}}{\partial n} + \mathcal{C}_{ji} n\frac{\partial \xi_{u_j}^{(0)}}{\partial n}, \tag{A.62b}$$

$$\gamma_{ij} = T\xi_T^{(0)}\frac{\partial \mathcal{C}_{ij}}{\partial T} + n\xi_n^{(0)}\frac{\partial \mathcal{C}_{ij}}{\partial n} + \xi_{u_k}^{(0)}\frac{\partial \mathcal{C}_{ij}}{\partial u_k} + \mathcal{A}_i\frac{\partial \xi_T^{(0)}}{\partial u_j} + \mathcal{B}_i\frac{\partial \xi_n^{(0)}}{\partial u_j} + \mathcal{C}_{kj}\frac{\partial \xi_{u_k}^{(0)}}{\partial u_i}. \tag{A.62c}$$

Eqs. (A.61) represents a system of $d(d+2)$ partial differential equations for the $d(d+2)$ unknown $\mathcal{A}_i$, $\mathcal{B}_i$, and $\mathcal{C}_{ij}$. Some simplifications are however possible.

Using the scaling form (4.43) and by definition of the decay rates (4.45) one has

$$\xi_n^{(0)} \sim \xi_T^{(0)} \sim nT^{1/2}. \tag{A.63}$$

Besides the trivial relation $\partial_{u_i}\xi_{n,T}^{(0)} = 0$, this yields

$$T\frac{\partial \xi_{n,T}^{(0)}}{\partial T} = \frac{1}{2}\xi_{n,T}^{(0)}, \tag{A.64}$$

and

$$n\frac{\partial \xi_{n,T}^{(0)}}{\partial n} = \xi_{n,T}^{(0)}, \tag{A.65}$$

where $\xi_{n,T}^{(0)} = \{\xi_n^{(0)}, \xi_T^{(0)}\}$. Making use of the relations (A.64) and (A.65) with $\xi_{u_i}^{(0)} = 0$, as explained in Sec. 4.4.2.1, from the system (A.61) one obtains the relations (4.53).

## A.7 Solubility conditions

The moments of $v^0$, $\mathbf{v}^1$, $v^2$ with weight $f$ are given by those of $f^{(0)}$. Therefore

$$\langle \chi | f^{(k)} \rangle = \int_{\mathbb{R}^d} \mathrm{d}\mathbf{v}\, \chi(\mathbf{v}) f^{(k)} = 0, \qquad \forall k \geqslant 1, \quad \chi(\mathbf{v}) = \{v^0, \mathbf{v}^1, v^2\}. \tag{A.66}$$

Let $\mathcal{P}$ be the projector in the subspace generated by $\{v^0, \mathbf{v}^1, v^2\}$ [57]:

$$\mathcal{P}g(\mathbf{v}) = \frac{1}{n}\sum_{i=1}^{d+2} \psi_i(\mathbf{v}) f^{(0)}(\mathbf{v}) \int_{\mathbb{R}^d} \mathrm{d}\mathbf{v}'\, \psi_i(\mathbf{v}') g(\mathbf{v}'), \tag{A.67}$$

where

$$\{\psi_i(\mathbf{v})\} = \{1, c_1\mathbf{v} + c_2, c_3 v^2\}, \tag{A.68}$$

with $c_i$, $i = 1, \ldots, 3$ are constants defined in [57]. The condition (A.66) means that

$$\mathcal{P}f = \mathcal{P}f^{(0)}. \tag{A.69}$$

In particular

$$f^{(1)} \in \mathcal{P}^{\perp}, \tag{A.70}$$

i.e., $f^{(1)}$ is in the orthogonal subspace to $\mathcal{P}$. This condition reads

$$\mathcal{P}f^{(1)} = \mathcal{P}\left(\mathcal{A}_i \nabla_i \ln T + \mathcal{B}_i \nabla_i \ln n + \mathcal{C}_{ij} \nabla_i U_j\right), \tag{A.71}$$

therefore

$$\mathcal{P}\begin{pmatrix} \boldsymbol{\mathcal{A}} \\ \boldsymbol{\mathcal{B}} \\ \boldsymbol{\mathcal{C}} \end{pmatrix} = 0. \tag{A.72}$$

The condition (A.72) is therefore a direct consequence of the Chapman-Enskog method. Since $\mathcal{P}$ commutes with $\partial_T$, $\partial_n$, and $J$, applying $\mathcal{P}$ on both sides of Eqs. (4.53) with the constraints (A.72) yields the condition for nonzero $\mathcal{A}_i$, $\mathcal{B}_i$, and $\mathcal{C}_{ij}$ to exist (solubility conditions [57]):

$$\mathcal{P}\begin{pmatrix} \mathbf{A} \\ \mathbf{B} \\ \mathbf{C} \end{pmatrix} = 0. \tag{A.73}$$

It is possible to verify explicitly that the relations (A.73) are satisfied [57].

## A.8 Equations for the transport coefficients

As we will apply a Sonine expansion, the symmetry properties of $\boldsymbol{\mathcal{A}}(\mathbf{V})$ and $\boldsymbol{\mathcal{B}}(\mathbf{V})$ are the same as those of $\mathbf{S}(\mathbf{V})$, whereas the properties of $\boldsymbol{\mathcal{C}}(\mathbf{V})$ are the same as those of $\mathbf{D}(\mathbf{V})$. Thus the insertion of Eq. (4.52) in Eq. (4.58) yields

$$P_{ij}^{(1)} = \int_{\mathbb{R}^d} \mathrm{d}\mathbf{v}\, D_{ij}(\mathbf{V})\mathcal{C}_{kl}(\mathbf{V})\nabla_k u_l. \tag{A.74}$$

The identification of Eqs. (A.74) and (4.56) yields (see, e.g., [111])

$$\eta = -\frac{1}{(d-1)(d+2)} \int_{\mathbb{R}^d} \mathrm{d}\mathbf{V}\, D_{ij}(\mathbf{V})\mathcal{C}_{ij}(\mathbf{V}). \tag{A.75}$$

Integrating Eq. (4.53c) over $\mathbf{V}$ in $\mathbb{R}^d$ with weight $-1/[(d-1)(d+2)]D_{ij}(\mathbf{V})$ and making use of Eq. (A.75) one obtains

$$\left[-p\xi_T^{(0)} T\partial_T - p\xi_n^{(0)} n\partial_n + \nu_\eta\right]\eta = -\frac{1}{(d-1)(d+2)} \int_{\mathbb{R}^d} \mathrm{d}\mathbf{V}\, D_{ij}(\mathbf{V})C_{ij}, \tag{A.76}$$

where $\nu_\eta$ is given by Eq. (4.64c). Functional dependence analysis shows that $n\partial_n\eta = 0$ and $T\partial_T\eta = \eta/2$. Using the definitions (4.36) for $D_{ij}(\mathbf{V})$ and (A.170c) for $C_{ij}(\mathbf{V})$, it is possible to compute the right-hand side of (A.76) which gives

$$\eta = \frac{1}{\nu_\eta - \frac{1}{2}p\xi_T^{(0)}}\frac{1}{d}\int_{\mathbb{R}^d} \mathrm{d}\mathbf{V}\, mV^2 f^{(0)}. \tag{A.77}$$

Using the hydrostatic pressure $p^{(0)} = nk_BT$ with the definition (4.31c) for the temperature, and dividing Eq. (A.77) by $\eta_0$ [see Eq. (4.63)] we finally obtain Eq. (4.60a).

The insertion of Eq. (4.52) in Eq. (4.59) gives

$$q_i = \int_{\mathbb{R}^d} \mathrm{d}\mathbf{V}\, S_i(\mathbf{V})\mathcal{A}_k(\mathbf{V})\nabla_k \ln T + \int_{\mathbb{R}^d} \mathrm{d}\mathbf{V}\, S_i(\mathbf{V})\mathcal{B}_k(\mathbf{V})\nabla_k \ln n. \tag{A.78}$$

It is easy to show that

$$\int_{\mathbb{R}^d} \mathrm{d}\mathbf{V} S_i(\mathbf{V})\mathcal{A}_k(\mathbf{V})\nabla_k \ln T = \frac{1}{d}\int_{\mathbb{R}^d} \mathrm{d}\mathbf{V} S_k(\mathbf{V})\mathcal{A}_k(\mathbf{V})\nabla_i \ln T, \tag{A.79}$$

therefore the identification of Eqs. (A.78) and (5.16) yields

$$\kappa = -\frac{1}{dT}\int_{\mathbb{R}^d} \mathrm{d}\mathbf{V}\, S_i(\mathbf{V})\mathcal{A}_i(\mathbf{V}), \tag{A.80a}$$

$$\mu = -\frac{1}{dn}\int_{\mathbb{R}^d} \mathrm{d}\mathbf{V}\, S_i(\mathbf{V})\mathcal{B}_i(\mathbf{V}). \tag{A.80b}$$

The fact that $\mu \neq 0$ is due to the annihilation process (or in general to a dissipative mechanism of the dynamics). Integrating Eqs. (4.54a) and (4.54b) over $\mathbf{V}$ in $\mathbb{R}^d$ with weight $-S_i(\mathbf{V})/d$ and making further use of Eq. (A.80), then making use of $T\partial_T(T\kappa) = 3T\kappa/2$, $T\partial_T(n\mu) = 3n\mu/2$, and $n\partial_n(T\kappa) = n\partial_n(n\mu) = 0$ obtained from functional dependence analysis, it follows

$$\kappa = \frac{1}{\nu_\kappa - 2p\xi_T^{(0)}}\frac{1}{T}\left[\frac{1}{2}p\xi_n^{(0)}n\mu - \frac{1}{d}\int_{\mathbb{R}^d} d\mathbf{V}\, S_i(\mathbf{V})A_i(\mathbf{V})\right], \tag{A.81a}$$

$$\mu = \frac{1}{\nu_\mu - \frac{3}{2}p\xi_T^{(0)} - p\xi_n^{(0)}}\frac{1}{n}\left[p\xi_T^{(0)}T\kappa - \frac{1}{d}\int_{\mathbb{R}^d} d\mathbf{V}\, S_i(\mathbf{V})B_i(\mathbf{V})\right]. \tag{A.81b}$$

Using Eqs. (4.54a), (4.54b), (4.37), and (4.67) one may calculate the integrals appearing in the right-hand side of Eqs. (A.81):

$$\frac{1}{dT}\int_{\mathbb{R}^d} \mathrm{d}\mathbf{V}\, S_i(\mathbf{V})A_i(\mathbf{V}) = -\frac{d+2}{2}\frac{nk_B}{m\beta}(2a_2+1), \tag{A.82a}$$

$$\frac{1}{dn}\int_{\mathbb{R}^d} \mathrm{d}\mathbf{V}\, S_i(\mathbf{V})B_i(\mathbf{V}) = -\frac{d+2}{4}\frac{1}{\beta^2 m}2a_2, \tag{A.82b}$$

where $\nu_\kappa$ and $\nu_\mu$ are given by Eqs. (4.64a) and (4.64b). The insertion of Eqs. (A.82) in (A.81) yields Eqs. (4.60b) and (4.60c).

## A.9 Evaluation of $\xi_n^{(0)*}$ and $\xi_T^{(0)*}$

The decay rates (4.45a) and (4.45c) may be computed using the definition (4.33) and Eqs. (4.65) and (4.66). We first change variables to $\mathbf{c}_i = \mathbf{V}_i/v_T$, $i = 1, 2$, then to $\mathbf{c}_{12} = \mathbf{c}_1 - \mathbf{c}_2$ and $\mathbf{C} = (\mathbf{c}_1 + \mathbf{c}_2)/2$ in order to decouple the integrals. Next, the integrals being isotropic with a symmetric weight, only even powers of the components of $\mathbf{C}$ and $\mathbf{c}_{12}$ will give nonzero contributions. Thus the terms $(\mathbf{C}\cdot\mathbf{c}_{12})^2$ in the integrals become $C^2c_{12}^2/d$. Finally, the resulting integrals may be computed using the following relation [70]: if we define

$$M_{np}^0 = \frac{1}{\pi^d}\int_{\mathbb{R}^{2d}} \mathrm{d}\mathbf{c}_{12} d\mathbf{C}\, \mathrm{e}^{-c_{12}^2/2}\mathrm{e}^{-2C^2} c_{12}^n C^p, \tag{A.83}$$

$$\begin{aligned} M_{np} = \langle c_{12}^n C^p\rangle = \frac{1}{\pi^d}\int_{\mathbb{R}^{2d}} &\mathrm{d}\mathbf{c}_{12}\mathrm{d}\mathbf{C}\, \mathrm{e}^{-c_{12}^2/2}\mathrm{e}^{-2C^2} c_{12}^n C^p \\ \times \left[1 + a_2\left\{C^4 + \frac{1}{16}c_{12}^4 + \frac{d+2}{2d}C^2c_{12}^2 - (d+2)C^2 - \frac{d+2}{4}c_{12}^2 + \frac{d(d+2)}{4}\right\}\right]&, \end{aligned} \tag{A.84}$$

then

$$M_{np}^0 = 2^{(n-p)/2}\frac{\Gamma[(d+n)/2]\Gamma[(d+p)/2]}{\Gamma(d/2)^2}, \tag{A.85}$$

$$\frac{M_{np}}{M_{np}^0} = 1 + \frac{a_2}{16d}\left[d(n^2+p^2) - 2d(n+p) + 2np(d+2)\right]. \tag{A.86}$$

Equations (A.85) and (A.86) may be easily verified using the relation (A.4). We thus obtain the decay rates to zeroth order (4.68).

## A.10 First order Sonine polynomial expansion for $f^{(1)}$

The decay rates to zeroth order being known, it is next required to compute the coefficients $\nu_\eta^*$, $\nu_\kappa^*$, and $\nu_\mu^*$. It is however beyond the scope of the present study if the general functions $\mathcal{A}_i$, $\mathcal{B}_i$, and $\mathcal{C}_{ij}$ are used. In order to turn the problem to a tractable one, it is required to expand the latter functions in Sonine polynomials, keeping only the first nonzero contribution.

The generalized Sonine polynomials are defined by Eq. (1.43). Then $\mathbf{S}(\mathbf{V}) = -S_{3/2}^{(1)}(V^2/v_T^2)\mathbf{V}^1/\beta$, and $\mathbf{D}(\mathbf{V}) = mS_{5/2}^{(0)}(\mathbf{VV} - V^2/d)$. For the sake of simplicity and as mentioned in Sec. 1.6.3, only the first nonzero contribution in the expansion of $\mathcal{A}_i$, $\mathcal{B}_i$, and $\mathcal{C}_{ij}$ is kept. This approximation however yields accurate results [24, 57].

As an example, we shall expand $\boldsymbol{\mathcal{A}}$ in the base of eigenvectors of the linear collision operator $L_c$:

$$\boldsymbol{\mathcal{A}}(\mathbf{V}) = \mathcal{M}(\mathbf{V})\sum_{i\geqslant 0} a_i S_{3/2}^{(i)}(V^2)\mathbf{V}, \tag{A.87}$$

where $a_i$ is the projection of $\boldsymbol{\mathcal{A}}$ on the $i$-th eigenvector. The eigenvectors are given by (see Sec. 1.6.3 or [6, 7])

$$\Psi_{nlm}(\mathbf{V}) \sim V^l S^{(n)}_{l+1/2}(V^2) Y_l^m(\widehat{\mathbf{V}}), \tag{A.88}$$

where $Y_l^m(\widehat{\mathbf{V}})$ are the spherical harmonics, $\widehat{\mathbf{V}} = \mathbf{V}/V$. The latter eigenvectors are orthogonal in $L^2(\mathbb{R}^d, \mathcal{M}(\mathbf{V})\mathrm{d}\mathbf{V})$. The condition that the moments of $f$ are given by those of $f^{(0)}$ implies $f^{(1)} \in \mathcal{P}^{\perp}$, i.e., $\mathcal{P}\boldsymbol{\mathcal{A}} = 0$ (see App. A.7). Therefore since Eq, (A.87) is odd in $\mathbf{V}$, one concludes from the projection operator (A.67) that the condition $\mathcal{P}\boldsymbol{\mathcal{A}} = 0$ writes

$$\int_{\mathbb{R}^d} \mathrm{d}\mathbf{V}\, \mathbf{V} f^{(1)}(\mathbf{V}) = \int_{\mathbb{R}^d} \mathrm{d}\mathbf{V}\, \mathbf{V}\mathcal{M}(\mathbf{V})\boldsymbol{\mathcal{A}}(\mathbf{V}) \cdot \boldsymbol{\nabla} \ln T = 0, \tag{A.89}$$

which implies

$$\int_{\mathbb{R}^d} \mathrm{d}\mathbf{V}\, \mathbf{V}\mathcal{M}(\mathbf{V})\boldsymbol{\mathcal{A}}(\mathbf{V}) = 0. \tag{A.90}$$

Inserting the expansion (A.87) gives

$$\sum_{i\geqslant 0} a_i \int_{\mathbb{R}^d} \mathrm{d}\mathbf{V}\, \mathcal{M}(\mathbf{V}) S^{(i)}_{3/2}(V^2)\mathbf{V} S^{(0)}_{3/2}(V^2)\mathbf{V} = 0, \tag{A.91}$$

where we have made use of $S^{(0)}_{3/2} = 1$. The latter equation may be written as a scalar product in $L^2(\mathbb{R}^d, \mathcal{M}(\mathbf{V})\mathrm{d}\mathbf{V})$:

$$\int_{\mathbb{R}^d} \mathrm{d}\mathbf{V}\, \mathbf{V} f^{(1)}(\mathbf{V}) \propto \sum_{i\geqslant 0} a_i \left\langle S^{(i)}_{3/2}\mathbf{V} | S^{(0)}_{3/2}\mathbf{V} \right\rangle_{L^2(\mathbb{R}^d, \mathcal{M}(V)\mathrm{d}\mathbf{V})} \propto \sum_{i\geqslant 0} a_i \delta_{i,0} = 0. \tag{A.92}$$

Therefore $a_0 = 0$ and the first nonzero term is $a_1$. The truncation of the series to first order yields $\boldsymbol{\mathcal{A}}(\mathbf{V}) = a_1\mathcal{M}(\mathbf{V})\mathbf{S}(\mathbf{V})$. Note that this result does not depend on the form of the collision operator, thus is valid for annihilation as well. The first nonzero order expansion in Sonine polynomials thus yields Eqs. (4.69) [24, 7, 57].

## A.11 Evaluation of $\nu_\kappa^*$, $\nu_\mu^*$, and $\nu_\eta^*$

Using the first order Sonine expansion (4.69), Eqs. (4.64) reduce to

$$\begin{aligned} \nu_\eta^* = {} & \frac{1}{\nu_0} \frac{\int_{\mathbb{R}^d} \mathrm{d}\mathbf{V}\, D_{ij}(\mathbf{V}) J[\mathcal{M}D_{ij}]}{\int_{\mathbb{R}^2} \mathrm{d}\mathbf{V}\, D_{ij}(\mathbf{V})\mathcal{M}(\mathbf{V})D_{ij}(\mathbf{V})} \\ & - p\frac{1}{\nu_0} \frac{\int_{\mathbb{R}^d} \mathrm{d}\mathbf{V}\, D_{ij}(\mathbf{V}) \Omega[\mathcal{M}D_{ij}]}{\int_{\mathbb{R}^2} \mathrm{d}\mathbf{V}\, D_{ij}(\mathbf{V})\mathcal{M}(\mathbf{V})D_{ij}(\mathbf{V})}, \end{aligned} \tag{A.93a}$$

$$\begin{aligned} \nu_\kappa^* = \nu_\mu^* = {} & \frac{1}{\nu_0} \frac{\int_{\mathbb{R}^d} d\mathbf{V}\, S_i(\mathbf{V}) J[\mathcal{M}S_i]}{\int_{\mathbb{R}^2} d\mathbf{V}\, S_i(\mathbf{V})\mathcal{M}(\mathbf{V})S_i(\mathbf{V})} \\ & - p\frac{1}{\nu_0} \frac{\int_{\mathbb{R}^d} \mathrm{d}\mathbf{V}\, S_i(\mathbf{V}) \Omega[\mathcal{M}S_i]}{\int_{\mathbb{R}^2} \mathrm{d}\mathbf{V}\, S_i(\mathbf{V})\mathcal{M}(\mathbf{V})S_i(\mathbf{V})}. \end{aligned} \tag{A.93b}$$

The denominators of Eqs. (A.93) are straightforward to compute using the formula (A.4). We thus find

$$\nu_\eta^* = \frac{\beta^2}{(d+2)(d-1)n\nu_0}\left[\int_{\mathbb{R}^d} \mathrm{d}\mathbf{V}\, D_{ij}(\mathbf{V}) J[\mathcal{M}D_{ij}] \right.$$
$$\left. -p\int_{\mathbb{R}^d} \mathrm{d}\mathbf{V}\, D_{ij}(\mathbf{V})\Omega[\mathcal{M}D_{ij}]\right], \quad \text{(A.94a)}$$

$$\nu_\kappa^* = \nu_\mu^* = \frac{2m\beta^3}{d(d+2)n\nu_0}\left[\int_{\mathbb{R}^d} \mathrm{d}\mathbf{V}\, S_i(\mathbf{V}) J[\mathcal{M}S_i] \right.$$
$$\left. -p\int_{\mathbb{R}^d} \mathrm{d}\mathbf{V}\, S_i(\mathbf{V})\Omega[\mathcal{M}S_i]\right]. \quad \text{(A.94b)}$$

The collision operator $J$ defined by Eq. (4.47) is made of the sum of the annihilation operator $L_a$ with weight $p$ and of the elastic collisional operator $L_c$ with weight $(1-p)$. Using previous calculations for $L_c$ [99] [or making use of Eqs. (A.166) to (A.168)], we obtain the elastic gas contributions proportional to $(1-p)$ in the right-hand side of Eqs. (4.70), namely

$$\nu_\eta^{*c} = (1-p)\left(1 - a_2\frac{1}{32}\right), \quad \text{(A.95)}$$

$$\nu_\kappa^{*c} = (1-p)\frac{d-1}{d}\left(1 + a_2\frac{1}{32}\right). \quad \text{(A.96)}$$

The following computations are technically simple, but lengthy. We shall thus only give the main steps. The annihilation contributions, written $\nu_\eta^{*a}$, $\nu_\kappa^{*a}$, and $\nu_\mu^{*a}$, are given by

$$\nu_\eta^{*a} = \frac{\beta^2}{(d+2)(d-1)n\nu_0}\int_{\mathbb{R}^d} \mathrm{d}\mathbf{V}\, D_{ij}(\mathbf{V}) L_a[\mathcal{M}D_{ij}] + \nu_\eta^{*a'}, \quad \text{(A.97a)}$$

$$\nu_\kappa^{*a} = \nu_\mu^{*a} = \frac{2m\beta^3}{d(d+2)n\nu_0}\int_{\mathbb{R}^d} \mathrm{d}\mathbf{V}\, S_i(\mathbf{V}) L_a[\mathcal{M}S_i] + \nu_\kappa^{*a'}, \quad \text{(A.97b)}$$

where $L_a$ is given by Eqs. (4.48) and (4.29), and

$$\nu_\eta^{*a'} = -\frac{\beta^2}{(d+2)(d-1)n\nu_0}\int_{\mathbb{R}^d} \mathrm{d}\mathbf{V}\, D_{ij}(\mathbf{V})\Omega[\mathcal{M}D_{ij}], \quad \text{(A.98a)}$$

$$\nu_\kappa^{*a'} = \nu_\mu^{*a'} = -\frac{2m\beta^3}{d(d+2)n\nu_0}\int_{\mathbb{R}^d} \mathrm{d}\mathbf{V}\, S_i(\mathbf{V})\Omega[\mathcal{M}S_i]. \quad \text{(A.98b)}$$

Using the relation (which may easily be checked from a change of variables $\mathbf{v}_i \to \mathbf{v}_j$, $i \neq j$.)

$$\int_{\mathbb{R}^d} \mathrm{d}\mathbf{v}_1\, Y(\mathbf{v}_1) L_a[\mathcal{M}X]$$
$$= \sigma^{d-1}\beta_1 \int_{\mathbb{R}^{2d}} \mathrm{d}\mathbf{v}_1 \mathrm{d}\mathbf{v}_2\, |\mathbf{v}_{12}| f^{(0)}(\mathbf{v}_1)\mathcal{M}(\mathbf{v}_2)X(\mathbf{v}_2)\left[Y(\mathbf{v}_1) + Y(\mathbf{v}_2)\right], \quad \text{(A.99)}$$

where $X$ and $Y$ are arbitrary functions, changing variables to $\mathbf{c}_i = \mathbf{v}_i/v_T$ for $i = 1, 2$, then changing variables to $\mathbf{c}_{12} = \mathbf{c}_1 - \mathbf{c}_2$ [in the following we adopt the notation $\mathbf{c}_{12} = (c_{12_1}, \dots, c_{12_d})$] and $\mathbf{C} = (\mathbf{c}_1+\mathbf{c}_2)/2$ in order to decouple the integrals, replacing under the integral sign for symmetry reasons the relations $(\mathbf{C}\cdot\mathbf{c}_{12})^2$ by $C^2c_{12}^2/d$, and using

$$\int_{\mathbb{R}^{2d}} \mathrm{d}\mathbf{C}\mathrm{d}\mathbf{c}_{12}\, F(C)G(c_{12})(\mathbf{C}\cdot\mathbf{c}_{12})^4 = \int_{\mathbb{R}^{2d}} \mathrm{d}\mathbf{C}\mathrm{d}\mathbf{c}_{12}\, F(C)G(c_{12})\left(\frac{3}{d^2}C^4c_{12}^4 - 2dC_i^4c_{12_j}^4\right) \quad \text{(A.100)}$$

where $i$ and $j$ can be chosen arbitrarily in the set $\{1, \dots, d\}$ and $F$, $G$ are arbitrary isotropic integrable functions, one obtains

$$\nu_\eta^{*a} = \frac{1}{d(d-1)\pi^d\sqrt{2}}\frac{\Gamma(d/2)}{\Gamma\left[(d+1)/2\right]}H_1(a_2, d) + \nu_\eta^{*a'}, \quad \text{(A.101a)}$$

$$\nu_\kappa^{*a} = \nu_\mu^{*a} = \frac{1}{d\pi^d\sqrt{2}}\frac{\Gamma(d/2)}{\Gamma\left[(d+1)/2\right]}H_2(a_2, d) + \nu_\kappa^{*a'}, \quad \text{(A.101b)}$$

where

$$H_k(a_2, d) = \sum_{(i,j)\in\Omega_\alpha^k} \alpha_{ij}\int_{\mathbb{R}^d}\mathrm{d}\mathbf{C}\,\mathrm{e}^{-2C^2}C^i\int_{\mathbb{R}^d}\mathrm{d}\mathbf{c}_{12}\mathrm{e}^{-c_{12}^2/2}c_{12}^{j+1} + \sum_{(i,j)\in\Omega_\gamma^k}\gamma_{ij}\int_{\mathbb{R}^d}\mathrm{d}\mathbf{C}\,\mathrm{e}^{-2C^2}C^iC_1^4\int_{\mathbb{R}^d}\mathrm{d}\mathbf{c}_{12}\mathrm{e}^{-c_{12}^2/2}c_{12}^{j+1}c_{12_1}^4, \quad \text{(A.102)}$$

with $\alpha_{ij}$ and $\gamma_{ij}$ that are functions of $d$ and $a_2$, $\Omega_\alpha^k$ and $\Omega_\gamma^k$ being the sets of allowed values for the pairs $(i, j)$ defining the moments in the integrals (A.102). Since the calculations are technically simple but cumbersome, expressions for $\alpha_{ij}$, $\gamma_{ij}$, $\Omega_\alpha^k$, and $\Omega_\gamma^k$ will not be given here. The integrals in the first sum of the right-hand side of Eq. (A.102) may be computed using the formula (A.4). Eq. (A.100) may easily be verified. If $\mathbf{x}$, $\mathbf{y} \in \mathbb{R}^d$, then

$$(\mathbf{x}\cdot\mathbf{y})^4 = \sum_{ijkl=1}^{d} x_ix_jx_kx_ly_iy_jy_ky_l\left[(1-\delta_{ijkl}) + (1-\delta_{ij}\delta_{kl}) + (1-\delta_{ik}\delta_{jl}) + (1-\delta_{il}\delta_{jk})\right] + \sum_{ijkl=1}^{d} x_ix_jx_kx_ly_iy_jy_ky_l\left[\delta_{ijkl} + (1-\delta_{ijkl})\left(\delta_{ij}\delta_{kl} + \delta_{ik}\delta_{jl} + \delta_{il}\delta_{jk}\right)\right]. \quad \text{(A.103)}$$

The second sum contains all even moments, whereas the first sum the odd moments. The latter one will not contribute if integrated over a symmetric domain with an even weight. Therefore

$$
\begin{aligned}
\int_{\mathbb{R}^{2d}} \mathrm{d}\mathbf{x}\mathrm{d}\mathbf{y} F(x)G(y)(\mathbf{x}\cdot\mathbf{y})^4 = & \int_{\mathbb{R}^{2d}} \mathrm{d}\mathbf{x}\mathrm{d}\mathbf{y} F(x)G(y)\Bigg[\sum_{ijkl=1}^{d} x_i x_j x_k x_l y_i y_j y_k y_l \delta_{ijkl} \\
& + \sum_{ijkl=1}^{d} x_i x_j x_k x_l y_i y_j y_k y_l \delta_{ij}\delta_{kl}(1-\delta_{ij}\delta_{kl}\delta_{ik}) \\
& + \sum_{ijkl=1}^{d} x_i x_j x_k x_l y_i y_j y_k y_l \delta_{ik}\delta_{jl}(1-\delta_{ij}\delta_{kl}\delta_{ik}) \\
& + \sum_{ijkl=1}^{d} x_i x_j x_k x_l y_i y_j y_k y_l \delta_{il}\delta_{jk}(1-\delta_{ij}\delta_{kl}\delta_{ik})\Bigg] \\
= & \int_{\mathbb{R}^{2d}} \mathrm{d}\mathbf{x}\mathrm{d}\mathbf{y} F(x)G(y) 3 \sum_{ij=1}^{d} x_i^2 x_j^2 y_i^2 y_j^2 (1-\delta_{ij}) \\
& + \int_{\mathbb{R}^{2d}} \mathrm{d}\mathbf{x}\mathrm{d}\mathbf{y} F(x)G(y) \sum_{i=1}^{d} x_i^4 y_i^4 . \qquad \text{(A.104)}
\end{aligned}
$$

The latter expression may be simplified making use of isotropy, thus yielding Eq. (A.100).

The integrals in the second sum of Eq. (A.102) may be computed using the particular case $i = j = k = l$ of the following lemma.

**Lemma A.1** *Let* $\mathbf{x} = (x_1, \ldots, x_d) \in \mathbb{R}^d$, $a > 0$, $d \geqslant 2$, $n \in \mathbb{N}$, *then:*

$$
\begin{aligned}
M_{ijkl}[n] \doteqdot & \int_{\mathbb{R}^d} \mathrm{d}\mathbf{x}\, |\mathbf{x}|^n \mathrm{e}^{-ax^2} x_i x_j x_k x_l \\
& = \pi^{d/2} \frac{3}{4} \frac{(d+n)(d+n+2)}{d(d+2)} \frac{\Gamma\left[(d+n)/2\right]}{\Gamma\left(d/2\right)} \frac{1}{a^{(d+n+4)/2}} \\
& \times \left\{ \delta_{ijkl} + \frac{1}{3}\Big[\delta_{ij}\delta_{kl}(1-\delta_{ik}) + \delta_{ik}\delta_{jl}(1-\delta_{ij}) + \delta_{il}\delta_{jk}(1-\delta_{ij})\Big]\right\}. \qquad \text{(A.105)}
\end{aligned}
$$

**Proof:** by isotropy the integral does not depend on the orientation of the coordinate system therefore $M_{iiii}[n] = M_{jjjj}[n] \doteqdot b$, $\forall i, j$. The coordinate system being invariant under rotations, in order that $M_{ijkl}$ is nonzero it is necessary that $(i, j) = (k, l)$, or $(i, k) = (j, l)$, or $(i, l) = (j, k)$, which implies

$$
\begin{aligned}
M_{ijkl}[n] &= b\delta_{ijkl} + c(1-\delta_{ijkl})\left(\delta_{ij}\delta_{kl} + \delta_{ik}\delta_{jl} + \delta_{il}\delta_{jk}\right) \\
&= b\delta_{ijkl} + c\Big[\delta_{ij}\delta_{kl}(1-\delta_{ik}) + \delta_{ik}\delta_{jl}(1-\delta_{ij}) + \delta_{il}\delta_{jk}(1-\delta_{ij})\Big], \text{(A.106)}
\end{aligned}
$$

with

$$
\begin{aligned}
b &= \int_{\mathbb{R}^d} \mathrm{d}\mathbf{x}\, |\mathbf{x}|^n \mathrm{e}^{-ax^2} x_1^4 \\
&= \int_0^\infty \mathrm{d}r\, r^n \mathrm{e}^{-ar^2} \int_0^{2\pi} \mathrm{d}\varphi \int_0^\pi \mathrm{d}\theta_1 \ldots \int_0^\pi \mathrm{d}\theta_{d-2}\, r^4 \cos^4\varphi \\
&\quad \times \left[\prod_{k=1}^{d-2} (\sin\theta_k)^4\right] r^{d-1} \left[\prod_{k=1}^{d-2} (\sin\theta)^k\right] \\
&= \int_0^\infty \mathrm{d}r\, r^{d+n+3} \mathrm{e}^{-ar^2} \int_0^{2\pi} \mathrm{d}\varphi\, \cos^4\varphi \prod_{k=1}^{d-2} \int_0^\pi \mathrm{d}\theta (\sin\theta)^{k+4}. \qquad \text{(A.107)}
\end{aligned}
$$

The first integral may be calculated using Eq. (A.4), the second one gives

$$
\int_0^{2\pi} \mathrm{d}\varphi\, \cos^4\varphi = \frac{3\pi}{4}, \qquad \text{(A.108)}
$$

and the last one

$$
\int_0^\pi \mathrm{d}\theta (\sin\theta)^{k+4} = \sqrt{\pi} \frac{\Gamma\left(\frac{k+5}{2}\right)}{\Gamma\left(\frac{k+6}{2}\right)}. \qquad \text{(A.109)}
$$

Eq. (A.107) thus becomes

$$
\begin{aligned}
b = \frac{3}{32} 2^{d-2} \pi^{d/2} (d+n)(d+n+2) \Gamma\left(\frac{d+n}{2}\right) \frac{1}{a^{(d+n+4)/2}} \\
\times \left[\prod_{k=1}^{d-2} \frac{(k+1)(k+3)}{k(k+2)(k+4)}\right] \left[\prod_{k=1}^{d-2} \frac{\Gamma\left(\frac{k+1}{2}\right)}{\Gamma\left(k/2\right)}\right]. \qquad \text{(A.110)}
\end{aligned}
$$

Making use of

$$
\begin{aligned}
\prod_{k=1}^{d-2} \frac{(k+1)(k+3)}{k(k+2)(k+4)} &= \frac{8(d+1)(d-1)}{\Gamma(d+3)}, \qquad \text{(A.111)} \\
\prod_{k=1}^{d-2} \frac{\Gamma\left(\frac{k+1}{2}\right)}{\Gamma\left(k/2\right)} &= \frac{\Gamma\left[\frac{(d-2)+1}{2}\right]}{\Gamma(1/2)}, \qquad \text{(A.112)}
\end{aligned}
$$

and

$$
\frac{\Gamma\left(\frac{d-1}{2}\right)}{\Gamma(d-1)} = \frac{2^{2-d}\sqrt{\pi}}{\Gamma(d/2)}, \qquad \text{(A.113)}
$$

we finally obtain

$$
b = \pi^{d/2} \frac{3}{4} \frac{(d+n)(d+n+2)}{d(d+2)} \frac{\Gamma\left[(d+n)/2\right]}{\Gamma(d/2)} \frac{1}{a^{(d+n+4)/2}}. \qquad \text{(A.114)}
$$

On the other hand

$$
\begin{aligned}
c &= \int_{\mathbb{R}^d} \mathrm{d}\mathbf{x}|\mathbf{x}|^n \mathrm{e}^{-ax^2} x_1^2 x_2^2 \\
&= \int_0^\infty \mathrm{d}r\, r^n \mathrm{e}^{-ar^2} \int_0^{2\pi} \mathrm{d}\varphi \int_0^\pi \mathrm{d}\theta_1 \ldots \int_0^\pi \mathrm{d}\theta_{d-1}\, r^4 \cos^2\varphi \sin^2\varphi \\
&\quad \times \left[\prod_{k=1}^{d-2} (\sin\theta_k)^4\right] r^{d-1} \left[\prod_{k=1}^{d-2} (\sin\theta_k)^k\right] \\
&= \frac{b}{\int_0^{2\pi} \mathrm{d}\varphi\, \cos^4\varphi} \int_0^{2\pi} \mathrm{d}\varphi\, \cos^2\varphi \sin^2\varphi \\
&= b \frac{4}{3\pi} \frac{\pi}{4} \\
&= \frac{b}{3}.
\end{aligned} \tag{A.115}
$$

Inserting Eqs. (A.114) and (A.115) in Eq. (A.106) leads to the result (A.105). ■

Finally, in order to evaluate $\nu_\eta^{*a'}$, $\nu_\kappa^{*a'}$, and $\nu_\mu^{*a'}$ we need the following lemma.

**Lemma A.2** *Let* $\mathbf{x} = (x_1, \ldots, x_d) \in \mathbb{R}^d$, $a > 0$, $d \geqslant 2$, $n \in \mathbb{N}$, *then:*

$$
M_{ij}[n] \doteqdot \int_{\mathbb{R}^d} \mathrm{d}\mathbf{x}\, |\mathbf{x}|^n \mathrm{e}^{-ax^2} x_i x_j = \pi^{d/2} \frac{d+n}{2d} \frac{\Gamma[(d+n)/2]}{\Gamma(d/2)} \frac{1}{a^{(d+n+2)/2}} \delta_{ij}. \tag{A.116}
$$

**Proof:** again, by isotropy the integral does not depend on the orientation of the coordinate system therefore $M_{ii}[n] = M_{jj}[n] \doteqdot b, \forall i, j$. By definition $M_{ij}[n] = M_{ji}[n]$ and the coordinate system being invariant under rotations $M_{ij}[n] = M_{i+1,j+1}[n]\ \forall i, j$, which implies

$$
M_{ij}[n] = M\delta_{ij} + C(1 - \delta_{ij}). \tag{A.117}
$$

In order to see that $C = 0$ it is sufficient to calculate $M_{ij}[n]$ for given values of $i$ and $j$:

$$
M_{12}[n] = \int_0^\infty \mathrm{d}r\, r^{n+d-1} \mathrm{e}^{-ar^2} \left[\prod_{k=1}^{d-2} \int_0^\pi \mathrm{d}\theta_k\, (\sin\theta_k)^k\right] \int_0^{2\pi} \mathrm{d}\varphi\, \cos\varphi \sin\varphi, \tag{A.118}
$$

which is equal to zero since $\int_0^{2\pi} \mathrm{d}\varphi\, \cos\varphi \sin\varphi = 0$. Therefore $M_{ij} = M\delta_{ij}$ with

$$
\begin{aligned}
M &= \int_{\mathbb{R}^d} \mathrm{d}\mathbf{x}\, |\mathbf{x}^n| \mathrm{e}^{-ax^2} x_1^2 \\
&= \int_0^\infty \mathrm{d}r\, r^{n+d+1} \mathrm{e}^{-ar^2} \int_0^{2\pi} \mathrm{d}\varphi\, \cos^2\varphi \prod_{k=1}^{d-2} \int_0^\pi \mathrm{d}\theta_k\, (\sin\theta_k)^{k+2}.
\end{aligned} \tag{A.119}
$$

The first integral may be calculated using Eq. (A.4), and the last one is obtained from Eq. (A.108). We thus have

$$
M = \frac{\pi}{4}(n+d) \frac{\Gamma\left(\frac{n+d}{2}\right)}{a^{(n+d+2)/2}} \pi^{(d-2)/2} 2^{d-2} \left[\prod_{k=1}^{d-2} \frac{k+1}{k(k+2)}\right] \left[\prod_{k=1}^{d-2} \frac{\Gamma\left(\frac{k+1}{2}\right)}{\Gamma(k/2)}\right].
$$

Making use of

$$\prod_{k=1}^{d-2}\frac{k+1}{k(k+2)}=\frac{2(d-1)}{\Gamma(d+1)} \tag{A.120}$$

and of Eqs. (A.112) and (A.113) we finally obtain Eq. (A.116). ■

The calculation can thus be performed and since $\nu_\kappa^{*a'}=\nu_\mu^{*a'}=0$, as it will be shown in the rest of this appendix, we obtain the first terms in the right-hand side of Eqs. (4.70).

### A.11.1 Evaluation of $\nu_\kappa^{*a'}$ and $\nu_\mu^{*a'}$

Since $S_i(\mathbf{V})$ is odd in $\mathbf{V}$ (and $\mathcal{M}$ even) only the odd terms of $\Omega[\mathcal{M}S_i]$ will give a nonzero contribution to the integral (A.98b), i.e., the term proportional to $\xi_{u_i}^{(1)}$ in Eq. (4.55). Making use of Eq. (4.51b) we therefore obtain

$$\nu_\kappa^{*a'}=\nu_\mu^{*a'}=\frac{2m\beta^3}{d(d+2)n\nu_0}K_{ij}\int_{\mathbb{R}^d}\mathrm{d}\mathbf{V}\,S_i(\mathbf{V})\frac{\partial f^{(0)}}{\partial V_j}, \tag{A.121}$$

where

$$K_{ij}=\frac{1}{n}\left(\omega\big[f^{(0)},V_j\mathcal{M}S_i\big]+\omega\big[V_jf^{(0)},\mathcal{M}S_i\big]\right) \tag{A.122}$$

are coefficients that do not depend on $\mathbf{V}$. Making use of Eq. (A.4) and of the lemma A.2 we obtain $\nu_\kappa^{*a'}=\nu_\mu^{*a'}=0$.

### A.11.2 Evaluation of $\nu_\eta^{*a'}$

We are going to show that $\nu_\eta^{*a'}=0$ from the result $\Omega\mathcal{C}_{ij}=0$. Indeed, we recall that to first nonzero order $\mathcal{C}_{ij}=c_0\mathcal{M}D_{ij}$, therefore the conditions $\Omega\mathcal{C}_{ij}=0$ and Eq. (A.98a) imply $\nu_\eta^{*a'}=0$.

Since $\Omega$ is a linear operator, then

$$\Omega f^{(1)}=(\Omega\mathcal{A}_i)\nabla_I\ln T+(\Omega\mathcal{B}_i)\nabla_i\ln T+(\Omega\mathcal{C}_{ij})\nabla_j u_i. \tag{A.123}$$

From Eqs. (4.69), the symmetry properties of $\boldsymbol{\mathcal{A}}$ and $\boldsymbol{\mathcal{B}}$ are the same as those of $\mathbf{S}(\mathbf{V})$ (i.e., odd in $\mathbf{V}$) and the symmetry properties of $\boldsymbol{\mathcal{C}}$ are the same as those of $D_{ij}(\mathbf{V})$ (i.e., even in $\mathbf{V}$). Therefore using Eqs. (4.55) and (4.51) for symmetry reasons

$$\Omega\mathcal{A}_j=-\frac{\partial f^{(0)}}{\partial V_i}\frac{1}{n}\left(\omega\big[f^{(0)},V_i\mathcal{A}_j\big]+\omega\big[V_if^{(0)},\mathcal{A}_j\big]\right), \tag{A.124a}$$

$$\Omega\mathcal{B}_j=-\frac{\partial f^{(0)}}{\partial V_i}\frac{1}{n}\left(\omega\big[f^{(0)},V_i\mathcal{B}_j\big]+\omega\big[V_if^{(0)},\mathcal{B}_j\big]\right), \tag{A.124b}$$

$$\begin{aligned}\Omega\mathcal{C}_{ij}=\;&f^{(0)}\frac{2}{n}\omega\big[f^{(0)},\mathcal{C}_{ij}\big]+\frac{\partial f^{(0)}}{\partial T}T\Bigg(-\frac{2}{n}\omega\big[f^{(0)},\mathcal{C}_{ij}\big]\\&+\frac{m}{nk_BTd}\omega\big[f^{(0)},V^2\mathcal{C}_{ij}\big]+\frac{m}{nk_BTd}\omega\big[V^2f^{(0)},\mathcal{C}_{ij}\big]\Bigg).\end{aligned} \tag{A.124c}$$

Inserting Eqs. (A.124) in Eq. (A.123) and making use of Eqs. (4.51) we obtain

$$\Omega f^{(1)} = -\frac{\partial f^{(0)}}{\partial V_i} v_T \xi_{u_i}^{(1)} + f^{(0)} \frac{2}{n} \omega\left[f^{(0)}, \mathcal{C}_{ij}\right] \nabla_j u_i \\ + \frac{\partial f^{(0)}}{\partial T} T \left( -\frac{2}{n} \omega\left[f^{(0)}, \mathcal{C}_{ij}\right] + \frac{m}{nk_B T d} \omega\left[f^{(0)}, V^2 \mathcal{C}_{ij}\right] + \frac{m}{nk_B T d} \omega\left[V^2 f^{(0)}, \mathcal{C}_{ij}\right] \right). \tag{A.125}$$

On the other hand, we may use the definition (4.55) for $\Omega$ which gives

$$\Omega f^{(1)} = f^{(0)} \xi_n^{(1)} - \frac{\partial f^{(0)}}{\partial V_i} v_T \xi_{u_i}^{(1)} + \frac{\partial f^{(0)}}{\partial T} T \xi_T^{(1)}. \tag{A.126}$$

We show in App. A.13 that $\xi_n^{(1)} = \xi_T^{(1)} = 0$. Note that the latter result is not affected by the possiblility on a nonzero value for $\Omega \mathcal{C}_{ij}$. Indeed, the term $\Omega \mathcal{C}_{ij}$ contributes to the transport coefficients only, and as it is seen in App. A.13 those coefficients are not responsible for the eventual nullity of the first order decay rates. We may therefore make use of $\xi_n^{(1)} = \xi_T^{(1)} = 0$ without interferring with the conclusions drawn here. Eq. (A.126) thus gives

$$\Omega f^{(1)} = -\frac{\partial f^{(0)}}{\partial V_i} v_T \xi_{u_i}^{(1)}. \tag{A.127}$$

Comparing Eqs. (A.127) and (A.125) we conclude that the last two terms in Eq. (A.125) must cancel each other. But recall that those last two terms originate from $\Omega \mathcal{C}_{ij} \nabla_i u_j$ (and the first one from $\Omega \mathcal{A}_i$ and $\Omega \mathcal{B}_i$). This implies $\Omega \mathcal{C}_{ij} \nabla_i u_j = 0$. By isotropy

$$\Omega \mathcal{C}_{ij} = a\delta_{ij} + b(1 - \delta_{ij}), \qquad a, b \in \mathbb{R}. \tag{A.128}$$

Therefore

$$(\Omega \mathcal{C}_{ij}) \nabla_i u_j = a \nabla_j u_j + \frac{d(d-1)}{2} b \nabla_k u_l, \qquad k, l \in \{1, \ldots, d\}. \tag{A.129}$$

The symmetry properties of $\mathcal{C}_{ij}$ being the same as those of $D_{ij}$, we have $\mathrm{Tr}\, \boldsymbol{\mathcal{C}} = \mathrm{Tr}\, \mathbf{D} = 0$. Since $\Omega$ is a linear operator

$$\mathrm{Tr}(\Omega \boldsymbol{\mathcal{C}}) = \Omega(\mathrm{Tr}\, \boldsymbol{\mathcal{C}}) = 0, \tag{A.130}$$

and from Eq. (A.128)

$$\mathrm{Tr}(\Omega \boldsymbol{\mathcal{C}}) = da. \tag{A.131}$$

Comparing Eqs. (A.130) and (A.131) it follows $a = 0$, that we insert in Eq. (A.129) to obtain $b = 0$. Therefore $\Omega \mathcal{C}_{ij} = 0$, which implies $\nu_\eta^{*a'} = 0$. Note that this result can also be obtained from a direct calculation.

## A.12 The distribution $f^{(1)}$

Using the form (4.52) for $f^{(1)}$ and the first order Sonine expansion (4.69) one has

$$f^{(1)}(\mathbf{V}) = \mathcal{M}(\mathbf{V}) \left[ a_1 S_i(\mathbf{V}) \nabla_i T + b_1 S_i(\mathbf{V}) \nabla_i n + c_0 D_{ij}(\mathbf{V}) \nabla_j u_i \right]. \tag{A.132}$$

The coefficients $a_1$, $b_1$, and $c_0$ may be expressed as functions of the transport coefficients, thus determining $f^{(1)}$. Eq. (A.75) in which we insert the Sonine expansion (4.69) yields

$$\eta = -c_0 \frac{1}{(d-1)(d+2)} \int_{\mathbb{R}^d} \mathrm{d}\mathbf{V}\, D_{ij}(\mathbf{V}) \mathcal{M}(\mathbf{V}) D_{ij}(\mathbf{V}) \tag{A.133}$$

$$= -c_0 \frac{n}{\beta^2}, \tag{A.134}$$

where we have made use of the definitions (4.36) and (4.66).

Proceeding in a similar way with Eq. (A.80) and (4.69) it follows

$$\kappa = -a_1 \frac{1}{dT} \int_{\mathbb{R}^d} \mathrm{d}\mathbf{V}\, S_i(\mathbf{V}) \mathcal{M}(\mathbf{V}) S_i(\mathbf{V}) \tag{A.135}$$

$$= -a_1 \frac{d+2}{2} \frac{n k_B}{m\beta^2}, \tag{A.136}$$

$$\mu = -b_1 \frac{1}{dn} \int_{\mathbb{R}^d} \mathrm{d}\mathbf{V}\, S_i(\mathbf{V}) \mathcal{M}(\mathbf{V}) S_i(\mathbf{V}) \tag{A.137}$$

$$= -b_1 \frac{d+2}{2} \frac{1}{m\beta^3}. \tag{A.138}$$

Replacing in Eq. (A.132) the coefficients $c_0$, $a_1$, and $b_1$ obtained from Eqs. (A.134), (A.136), and (A.138), one obtains the distribution (4.71).

## A.13 Evaluation of $\xi_n^{(1)}$, $\xi_{u_i}^{(1)}$, and $\xi_T^{(1)}$

The zeroth order and first order distributions $f^{(0)}$ and $f^{(1)}$ being known, it is possible to compute the first order decay rates (4.51). The procedure is similar to the calculation of the zero order decay rates of Appendix A.9. We first change variables to $\mathbf{c}_i = \mathbf{V}_i/v_T$, $i = 1, 2$, then to $\mathbf{c}_{12} = \mathbf{c}_1 - \mathbf{c}_2$ and $\mathbf{C} = (\mathbf{c}_1 + \mathbf{c}_2)/2$ so that

$$\begin{aligned} &\omega[Af^{(0)}, Bf^{(1)}] \\ &= -n \frac{\Gamma(d/2)}{\Gamma\left(\frac{d+1}{2}\right)} \frac{\sqrt{2}}{\pi^d} \frac{d+2}{4} \left[ \frac{v_T}{2} \frac{d}{d-1} \left( \kappa^* \frac{1}{T} \nabla_i T + \mu^* \frac{1}{n} \nabla_i n \right) I_1 + \eta^* \nabla_j u_i I_2 \right], \end{aligned} \tag{A.139}$$

where $\omega[f, g]$ is defined by Eq. (4.33), $(A, B) = \{(1, 1), (V_2^2, 1), (1, V_1^2), (V_{2_i}, 1), (1, V_{1_i})\}$, $\mathbf{V}_i = (V_{i_1}, \ldots, V_{i_d})$, and

$$\begin{aligned} I_1 = \int_{\mathbb{R}^d} \mathrm{d}\mathbf{c}_{12}\, |\mathbf{c}_{12}| \mathrm{e}^{-c_{12}^2/2} \int_{\mathbb{R}^d} \mathrm{d}\mathbf{C}\, \mathrm{e}^{-2C^2} A(v_T \mathbf{c}_2) B(v_T \mathbf{c}_1) \left( c_1^2 - \frac{d+2}{2} \right) c_{1_i} \\ \times \left[ 1 + a_2 S_2(c_2^2) \right], \end{aligned} \tag{A.140}$$

$$\begin{aligned} I_2 = \int_{\mathbb{R}^d} \mathrm{d}\mathbf{c}_{12}\, |\mathbf{c}_{12}| \mathrm{e}^{-c_{12}^2/2} \int_{\mathbb{R}^d} \mathrm{d}\mathbf{C}\, \mathrm{e}^{-2C^2} A(v_T \mathbf{c}_2) B(v_T \mathbf{c}_1) \left( c_{1_i} c_{1_j} - \frac{1}{d} \delta_{ij} c_1^2 \right) \\ \times \left[ 1 + a_2 S_2(c_2^2) \right], \end{aligned} \tag{A.141}$$

In the above integrals, $\mathbf{c}_1$ and $\mathbf{c}_2$ are expressed as functions of $\mathbf{C}$ and $\mathbf{c}_{12}$. Then, in order to compute those integrals one needs lemmas A.1 and A.2. Assuming summation over repeated indices, it is easy to show that

$$M_{jk}^{(a)} M_{ik}^{(a')} = M^{(a)} M^{(a')} \delta_{ij}, \tag{A.142}$$

$$M_{kl}^{(a)} M_{kl}^{(a')} = d M^{(a)} M^{(a')}. \tag{A.143}$$

Using the definition (A.105) one can show that

$$M_{ijkl}^{(a)} M_{kl}^{(a')} = \frac{d+2}{3} b^{(a)} M^{(a')} \delta_{ij}, \tag{A.144}$$

$$M_{iklm}^{(a)} M_{jklm}^{(a')} = \frac{d+2}{3} b^{(a)} b^{(a')} \delta_{ij}, \tag{A.145}$$

$$M_{klmn}^{(a)} M_{klmn}^{(a')} = \frac{d(d+2)}{3} b^{(a)} b^{(a')}. \tag{A.146}$$

For symmetry reasons, many of the terms in the integrals (A.140) and (A.141) vanish upon integration. Nevertheless, the expressions are very cumbersome and the use of symbolic computation programs is appreciable [179]. Eqs. (A.4), (A.105), (A.116), and (A.142) to (A.145) thus allow us after a lengthy but technically simple calculation to find the decay rates to first order (4.51).

## A.14 Solution of the homogeneous cooling state

If we define $a$ by $\nu_0 = anT^{1/2}$, where $\nu_0 = p^{(0)}/\eta_0$ with $p^{(0)} = nk_BT$ and $\eta_0$ given by Eq. (4.63), then the zeroth order equations (4.44) take the form

$$\partial_t n = -n^2 T^{1/2} a_n, \tag{A.147a}$$
$$\partial_t T = -n T^{3/2} a_T, \tag{A.147b}$$

where $a_n = \xi_n^{(0)*} pa$ and $a_T = \xi_T^{(0)*} pa$. Guided by Haff's law $T(t) = T_0(1+t/t_0)^{-2}$, $t_0 = \xi_T^{(0)}(0)/2$, for the granular gas [59], we may solve Eqs. (A.147) using

$$n(t) = c_1(1+c_2 t)^{\gamma_1}, \tag{A.148a}$$
$$T(t) = c_3(1+c_4 t)^{\gamma_2}. \tag{A.148b}$$

The substitution of Eqs. (A.148) in Eqs. (A.147) imposes

$$c_2 = c_4 \doteqdot c = c_1\sqrt{c_3}(a_n + a_T/2), \tag{A.149}$$

$$\gamma_2 = -a_T \frac{c_1}{c}\sqrt{c_3} = -\frac{2a_T}{2a_n + a_T}, \tag{A.150}$$

$$\gamma_1 = -1 - \gamma_2/2 = -\frac{2a_n}{2a_n + a_T}. \tag{A.151}$$

Initial conditions $n(0) = n_0$ and $T(0) = T_0$ impose $c_1 = n_0$ and $c_3 = T_0$. Therefore

$$c = p\big[\xi_n^{(0)}(0) + \xi_T^{(0)}/2\big] \doteqdot p t_0^{-1}, \tag{A.152}$$

which leads to the solution given by Eqs. (4.75).

## A.15 Linearized hydrodynamic equations

### A.15.1 Density

From Eqs. (4.72a) and (4.76)

$$\partial_t \delta n + \partial_t n + n_H \nabla_j \delta u_j = -p\delta_n \nu_{0H} \xi_n^{(0)*} - p n_H \nu_0 \xi_n^{(0)*} + \mathcal{O}(\delta^2). \tag{A.153}$$

Making use of Eq. (4.44a), i.e., $\partial_t n = -p n_H \nu_{0H} \xi_n^{(0)*}$, and integrating Eq. (A.153) over $\mathbf{l}$ with weight $\exp(-i\mathbf{k}\cdot\mathbf{l})$ it follows

$$\begin{aligned}\frac{1}{n_H}\partial_\tau n_{\mathbf{k}}(\tau) - 2p\xi_n^{(0)*}\int_{\mathbb{R}^d} \mathrm{d}\mathbf{l}\, \mathrm{e}^{-i\mathbf{k}\cdot\mathbf{l}} + ik\mathbf{w}_{\mathbf{k}_\parallel}(\tau) \\ = -2p\xi_n^{(0)*}\rho_{\mathbf{k}}(\tau) - \frac{2p\xi_n^{(0)*}}{\nu_{0H}}\int_{\mathbb{R}^d} \mathrm{d}\mathbf{l}\, \mathrm{e}^{-i\mathbf{k}\cdot\mathbf{l}}\nu_0,\end{aligned} \tag{A.154}$$

where $\mathbf{w}_{\mathbf{k}_\parallel} = \mathbf{k}\cdot\mathbf{w}_{\mathbf{k}}(\tau)$. Making use of

$$\partial_\tau \rho_{\mathbf{k}}(\tau) = \frac{1}{n_H}\partial_\tau n_{\mathbf{k}}(\tau) + \rho_{\mathbf{k}}(\tau) 2p\xi_n^{(0)*} \tag{A.155}$$

and

$$\begin{aligned}-\frac{2p\xi_n^{(0)*}}{\nu_{0H}}\int_{\mathbb{R}^d} \mathrm{d}\mathbf{l}\, \mathrm{e}^{i\mathbf{k}\cdot\mathbf{l}}\nu_0 \\ = -2p\xi_n^{(0)*}\int_{\mathbb{R}^d} \mathrm{d}\mathbf{l}\, \mathrm{e}^{i\mathbf{k}\cdot\mathbf{l}} - 2p\xi_n^{(0)*}\rho_{\mathbf{k}}(\tau) - p\xi_n^{(0)*}\theta_{\mathbf{k}}(\tau) + \mathcal{O}(\delta^2)\end{aligned} \tag{A.156}$$

in Eq. (A.154) we obtain Eq. (4.80a).

### A.15.2 Momentum

Proceeding in a similar way, we obtain

$$\begin{aligned}\partial_\tau w_{\mathbf{k}j}(\tau) - p\xi_T^{(0)*} w_{\mathbf{k}j}(\tau) + ik_j\theta_{\mathbf{k}}(\tau) + ik_j\rho_{\mathbf{k}}(\tau) + \frac{\eta^*}{2}\left[k_j k_l w_{\mathbf{k}j}(\tau) + \frac{d-2}{d} k_j k_l w_{\mathbf{k}l}(\tau)\right] \\ = -p\sqrt{\frac{m}{k_B T_H}}\frac{2}{\nu_{0H}}\int_{\mathbb{R}^d} \mathrm{d}\mathbf{l}\, \mathrm{e}^{-\mathbf{k}\cdot\mathbf{l}} v_T \xi_{u_i}^{(1)} + \mathcal{O}(\delta^2).\end{aligned} \tag{A.157}$$

**Lemma A.3** *let $\mathbf{w}_{\mathbf{k}_\perp}$ be the perpendicular component of the velocity field to $\mathbf{k}$, and $\mathbf{w}_{\mathbf{k}_\parallel}$ the parallel component, then*

$$\widehat{\mathbf{e}}_i\left[k_i k_j w_{\mathbf{k}i}(\tau) + \frac{d-2}{d} k_i k_j w_{\mathbf{k}j}(\tau)\right] = k^2 \mathbf{w}_{\mathbf{k}_\perp} + \frac{2(d-1)}{d} k^2 \mathbf{w}_{\mathbf{k}_\parallel}. \tag{A.158}$$

**Proof:** we note $\mathbf{k} = k\widehat{\mathbf{e}}_\mathbf{k}$, $\mathbf{w}_\mathbf{k} = \mathbf{w}_{\mathbf{k}_\perp} + \mathbf{w}_{\mathbf{k}_\parallel}$, $\mathbf{w}_{\mathbf{k}_\parallel} = \mathbf{w}_\mathbf{k} \cdot \widehat{\mathbf{e}}_\mathbf{k}$, $\mathbf{w}_{\mathbf{k}_\perp} = \mathbf{w}_\mathbf{k} - \mathbf{w}_{\mathbf{k}_\parallel}$, $|\mathbf{w}_{\mathbf{k}_\parallel}| = w_{\mathbf{k}_\parallel}$, $|\mathbf{w}_{\mathbf{k}_\perp}| = w_{\mathbf{k}_\perp}$. Then:

$$\begin{aligned}
\sum_{i=1}^{d} \widehat{\mathbf{e}}_i \left[ k_i k_j w_{\mathbf{k}i}(\tau) + \frac{d-2}{d} k_i k_j w_{\mathbf{k}j}(\tau) \right] &= \left( \sum_{j=1}^{d} k_j k_j \right) \left( \sum_{i=1}^{d} \widehat{\mathbf{e}}_i w_{\mathbf{k}i}(\tau) \right) \\
&\quad + \frac{d-2}{d} \left( \sum_{i=1}^{d} \widehat{\mathbf{e}}_i k_i \right) \left( \sum_{j=1}^{d} k_j w_{\mathbf{k}j}(\tau) \right) \\
&= k^2 \begin{pmatrix} \mathbf{w}_{\mathbf{k}_\parallel} \\ \mathbf{w}_{\mathbf{k}_\perp} \end{pmatrix} + \frac{d-2}{d} \begin{pmatrix} \mathbf{k} \\ 0 \end{pmatrix} \left[ \begin{pmatrix} \mathbf{k} \\ 0 \end{pmatrix} \cdot \begin{pmatrix} \mathbf{w}_{\mathbf{k}_\parallel} \\ \mathbf{w}_{\mathbf{k}_\perp} \end{pmatrix} \right] \\
&= k^2 \begin{pmatrix} \mathbf{w}_{\mathbf{k}_\parallel} \\ \mathbf{w}_{\mathbf{k}_\perp} \end{pmatrix} + \frac{d-2}{d} k \widehat{\mathbf{e}}_\mathbf{k} \left( k \widehat{\mathbf{e}}_\mathbf{k} \cdot w_{\mathbf{k}_\parallel} \widehat{\mathbf{e}}_\mathbf{k} \right) \\
&= k^2 \mathbf{w}_{\mathbf{k}_\perp} + \frac{2(d-1)}{d} k^2 \mathbf{w}_{\mathbf{k}_\parallel}. \qquad \text{(A.159)}
\end{aligned}$$

■

This lemma allows to rewrite Eq. (A.157) as

$$\begin{aligned}
\left( \partial_\tau - p\xi_T^{(0)*} \right) \begin{pmatrix} \mathbf{w}_{\mathbf{k}_\parallel} \\ \mathbf{w}_{\mathbf{k}_\perp} \end{pmatrix} + ik \left[ \rho_\mathbf{k}(\tau) + \theta_\mathbf{k}(\tau) \right] \begin{pmatrix} \widehat{\mathbf{e}}_\mathbf{k} \\ 0 \end{pmatrix} + \frac{\eta^*}{2} k^2 \begin{pmatrix} \frac{2(d-1)}{d} \mathbf{w}_{\mathbf{k}_\parallel} \\ \mathbf{w}_{\mathbf{k}_\perp} \end{pmatrix} \\
= -p \sqrt{\frac{m}{k_B T_H}} \frac{2}{\nu_{0H}} \widehat{\mathbf{e}}_i \int \mathrm{d}\mathbf{l}\, \mathrm{e}^{-i\mathbf{k}\cdot\mathbf{l}} v_T \xi_{u_i}^{(1)}. \qquad \text{(A.160)}
\end{aligned}$$

Making use of

$$-p \sqrt{\frac{m}{k_B T_H}} \frac{2}{\nu_{0H}} \widehat{\mathbf{e}}_i \int \mathrm{d}\mathbf{l}\, \mathrm{e}^{-i\mathbf{k}\cdot\mathbf{l}} v_T \xi_{u_i}^{(1)} = p\xi_\mathbf{u}^* \kappa^* ik\theta_\mathbf{k}(\tau) \widehat{\mathbf{e}}_\mathbf{k} + p\xi_\mathbf{u}^* \mu^* ik\rho_\mathbf{k}(\tau) \widehat{\mathbf{e}}_\mathbf{k}, \qquad \text{(A.161)}$$

Eq. (A.160) leads to the linearized equations (4.80b) and (4.80c).

### A.15.3 Temperature

From Eq. (4.72c) and proceeding in a similar way as for the previous cases we obtain the linearized equations (4.80d) for the temperature field $\theta_\mathbf{k}(\tau)$.

## A.16 Summary of useful relations for the coefficients $\nu_\kappa^*$ and $\nu_\eta^*$

The expressions (4.64) and (5.44) may be calculated with the help of the following relations. Let $X$ and $Y$ be arbitrary functions, $\mathcal{M}(\mathbf{V}) = n/(v_T^d \pi^{d/2}) \exp(-V^2/v_T^2)$

the Maxwellian in the scaling regime, then

$$\begin{aligned}&\int_{\mathbb{R}^d} \mathrm{d}\mathbf{v}_1\, Y(\mathbf{v}_1) L_a[\mathcal{M}X] \\ &= \sigma^{d-1}\phi(x) v_T^{1-x} \int_{\mathbb{R}^{2d}} \mathrm{d}\mathbf{v}_1 \mathrm{d}\mathbf{v}_2\, v_{12}^x f^{(0)}(\mathbf{v}_1)\mathcal{M}(\mathbf{v}_2)X(\mathbf{v}_2)\left[Y(\mathbf{v}_1)+Y(\mathbf{v}_2)\right], \quad (A.162)\end{aligned}$$

and

$$\begin{aligned}&\int_{\mathbb{R}^d} \mathrm{d}\mathbf{v}_1\, Y(\mathbf{v}_1) L_c[\mathcal{M}X] - \sigma^{d-1}\frac{\phi(x) v_T^{1-x}}{S_d} \\ &\times \int_{\mathbb{R}^{2d}} \mathrm{d}\mathbf{v}_1 \mathrm{d}\mathbf{v}_2\, v_{12}^x f^{(0)}(\mathbf{v}_1)\mathcal{M}(\mathbf{v}_2)X(\mathbf{v}_2) \int \mathrm{d}\widehat{\boldsymbol{\sigma}}(b-1)\left[Y(\mathbf{v}_1)+Y(\mathbf{v}_2)\right], \quad (A.163)\end{aligned}$$

where $L_a g = -J_a[f^{(0)}, g] - L_a[g, f^{(0)}]$ and $L_c g = -J_c[f^{(0)}, g] - J_c[g, f^{(0)}]$ for an arbitrary function $g$. Let $\alpha \in \mathbb{R}^+$, then

$$\int_{\mathbb{R}^d} \mathrm{d}\mathbf{x}|\mathbf{x}|^n \mathrm{e}^{-\alpha x^2} = \frac{\pi^{d/2}}{\alpha^{(d+n)/2}}\frac{\Gamma[(d+n)/2]}{\Gamma(d/2)}, \quad (A.164)$$

$$\int_{\mathbb{R}^d} \mathrm{d}\mathbf{x}\, |\mathbf{x}|^n\, \mathrm{e}^{-\alpha \mathbf{x}^2} x_i x_j = \frac{\pi^{d/2}}{\alpha^{(d+n+2)/2}}\frac{d+n}{2d}\frac{\Gamma\left[(d+n)/2\right]}{\Gamma\left(d/2\right)}\delta_{ij}. \quad (A.165)$$

In the integrals below, the results when $\theta(\widehat{\boldsymbol{\sigma}}\cdot\mathbf{g})$ is absent are obtained upon multiplying the value of $\beta_n$ by two. For $\widehat{\boldsymbol{\sigma}} = (\sigma_1, \ldots, \sigma_d)$, $\mathbf{g} \in \mathbb{R}^d$, $|\widehat{\boldsymbol{\sigma}}| = 1$, we have [79]

$$\int \mathrm{d}\widehat{\boldsymbol{\sigma}}\, \theta(\widehat{\boldsymbol{\sigma}}\cdot\mathbf{g})(\widehat{\boldsymbol{\sigma}}\cdot\mathbf{g})^n \sigma_i\sigma_j = \frac{\beta_n}{n+d} g^{n-2}(n g_i g_j + g^2\delta_{ij}), \quad (A.166)$$

$$\int \mathrm{d}\widehat{\boldsymbol{\sigma}}\, \theta(\widehat{\boldsymbol{\sigma}}\cdot\mathbf{g})(\widehat{\boldsymbol{\sigma}}\cdot\mathbf{g})^n \sigma_i = \beta_{n+1} g^{n-1} g_i, \quad (A.167)$$

$$\beta_n = \int \mathrm{d}\widehat{\boldsymbol{\sigma}}\, \theta(\widehat{\boldsymbol{\sigma}}\cdot\widehat{\mathbf{g}})(\widehat{\boldsymbol{\sigma}}\cdot\widehat{\mathbf{g}})^n = \pi^{(d-1)/2}\frac{\Gamma\left[(n+1)/2\right]}{\Gamma\left[(n+d)/2\right]}. \quad (A.168)$$

## A.17 Exact transport coefficients of the Maxwell model

Following the same route as in [53] (or Chapter 4) we may rewrite the right-hand side of Eq. (4.46) such that

$$[\partial_t^{(0)} + J] f^{(1)} = A_i \nabla_i \ln T + B_i \nabla_i \ln n + C_{ij}\nabla_i u_j + p\Omega f^{(1)}, \quad (A.169)$$

where

$$A_i = \frac{V_i}{2}\frac{\partial}{\partial V_j}[V_j f^{(0)}] - \frac{k_B T}{m}\frac{\partial f^{(0)}}{\partial V_i}, \quad (A.170a)$$

$$B_i = -V_i f^{(0)} - \frac{k_B T}{m}\frac{\partial f^{(0)}}{\partial V_i}, \quad (A.170b)$$

$$C_{ij} = \frac{\partial}{\partial V_i}[V_j f^{(0)}] - \frac{1}{d}\frac{\partial}{\partial V_k}[V_k f^{(0)}]\delta_{ij}, \quad (A.170c)$$

and $\Omega$ is a linear operator defined by

$$\Omega g = f^{(0)}\xi_n^{(1)}[f^{(0)}, g] - \frac{\partial f^{(0)}}{\partial V_i} v_T \xi_{u_i}^{(1)}[f^0, g] + \frac{\partial f^{(0)}}{\partial T} T \xi_T^{(1)}[f^{(0)}, g]. \tag{A.171}$$

The function $g$ is either $\mathcal{A}_i$, $\mathcal{B}_i$, or $\mathcal{C}_{ij}$, and the functionals $\xi_n^{(1)}$, $\xi_{u_i}^{(1)}$, and $\xi_T^{(1)}$ are obtained from Eqs. (5.13) upon replacing $f^{(1)}$ by $g$.

### A.17.1 Pressure tensor

Integrating the Boltzmann equation (A.169) over $\mathbf{V}$ with weight $mV_iV_j$ and taking into account the symmetry properties of the coefficients (A.170) one obtains

$$\begin{aligned}\partial_t^{(0)} P_{ij}^{(1)}(\mathbf{r}, t) + p \int_{\mathbb{R}^d} \mathrm{d}\mathbf{V}\, mV_iV_j L_a[f^{(0)}, f^{(1)}] + (1-p) \int_{\mathbb{R}^d} \mathrm{d}\mathbf{V}\, mV_iV_j L_c[f^{(0)}, f^{(1)}] \\ = \int_{\mathbb{R}^d} \mathrm{d}\mathbf{V}\, mV_iV_j C_{kl}(\mathbf{V}) \nabla_k u_l,\end{aligned} \tag{A.172}$$

where we have made use of the definition (5.17) for the pressure tensor. The same definition further allows us to write

$$\int_{\mathbb{R}^d} \mathrm{d}\mathbf{V}\, mV_iV_j L_a[f^{(0)}, f^{(1)}] = \xi_n^{(0)} P_{ij}^{(1)}(\mathbf{r}, t), \tag{A.173}$$

and using additionally Eq. (A.163), and (A.166) to (A.168):

$$\int_{\mathbb{R}^d} \mathrm{d}\mathbf{V}\, mV_iV_j L_c[f^{(0)}, f^{(1)}] = \xi_n^{(0)} \frac{2}{d+2} P_{ij}^{(1)}(\mathbf{r}, t). \tag{A.174}$$

Finally

$$\int_{\mathbb{R}^d} \mathrm{d}\mathbf{V}\, mV_iV_j C_{kl}(\mathbf{V}) \nabla_k u_l = -p^{(0)} \Delta_{ijkl} \nabla_k u_l, \tag{A.175}$$

where

$$\Delta_{ijkl} = \delta_{ik}\delta_{jl} + \delta_{jk}\delta_{il} - \frac{2}{d}\delta_{ij}\delta_{kl}. \tag{A.176}$$

Insertion of Eqs. (A.173) to (A.175) in (A.172) yields

$$\left[\partial_t^{(0)} + p\xi_n^{(0)} + (1-p)\xi_n^{(0)} \frac{d+2}{2}\right] P_{ij}^{(1)}(\mathbf{r}, t) = -p^{(0)} \Delta_{ijkl} \nabla_k u_l. \tag{A.177}$$

The solution of Eq. (A.177) is $P_{ij}^{(1)} = -\eta \Delta_{ijkl} \nabla_k u_l$. Functional dependence analysis shows that $\eta \propto T^{1/2}$, and since to zeroth order the temperature is conserved $\partial_t P_{ij}^{(1)} = 0$. Eq. (A.177) thus gives

$$\eta^* = \frac{1}{p\frac{d+2}{2} + (1-p)}. \tag{A.178}$$

### A.17.2 Heat flux

Integrating the Boltzmann equation (A.169) over $\mathbf{V}$ with weight $mV^2V_i/2$ and taking into account the symmetry properties of the coefficients (A.170) one obtains

$$\partial_t^{(0)} q_i^{(1)}(\mathbf{r},t) + p\int_{\mathbb{R}^d} \mathrm{d}\mathbf{V}\,\frac{1}{2}mV^2V_iL_a[f^{(0)},f^{(1)}] + (1-p)\int_{\mathbb{R}^d} \mathrm{d}\mathbf{V}\,\frac{1}{2}mV^2V_iL_c[f^{(0)},f^{(1)}]$$
$$= \int_{\mathbb{R}^d} \mathrm{d}\mathbf{V}\,\frac{1}{2}mV^2V_iA_k(\mathbf{V})\nabla_k \ln T + \int_{\mathbb{R}^d} \mathrm{d}\mathbf{V}\,\frac{1}{2}mV^2V_iB_k(\mathbf{V})\nabla_k \ln T, \quad \text{(A.179)}$$

where we have made use of the definition (4.35) for the heat flux to first order. Moreover, one finds

$$\int_{\mathbb{R}^d} \mathrm{d}\mathbf{V}\,\frac{1}{2}mV^2V_iL_a[f^{(0)},f^{(1)}] = \xi_n^{(0)} q_i^{(1)}(\mathbf{r},t), \quad \text{(A.180)}$$

and using additionally Eq. (A.163), and (A.166) to (A.168):

$$\int_{\mathbb{R}^d} \mathrm{d}\mathbf{V}\,\frac{1}{2}mV^2V_iL_c[f^{(0)},f^{(1)}] = \frac{2(d-1)}{d(d+2)}\xi_n^{(0)} q_i^{(1)}(\mathbf{r},t). \quad \text{(A.181)}$$

Finally

$$\int_{\mathbb{R}^d} \mathrm{d}\mathbf{V}\,\frac{1}{2}mV^2V_iA_k(\mathbf{V})\nabla_k \ln T = -\frac{d+2}{2}\frac{p^{(0)}k_B}{m}\nabla_i T, \quad \text{(A.182)}$$

$$\int_{\mathbb{R}^d} \mathrm{d}\mathbf{V}\,\frac{1}{2}mV^2V_iB_k(\mathbf{V})\nabla_k \ln n = 0. \quad \text{(A.183)}$$

Insertion of Eqs. (A.180) to (A.183) in (A.179) gives

$$\left[\partial_t^{(0)} + p\xi_n^{(0)} + (1-p)\xi_n^{(0)}\frac{2(d-1)}{d(d+2)}\right] q_i^{(1)}(\mathbf{r},t) = -\frac{d+2}{2}\frac{p^{(0)}k_B}{m}\nabla_i T. \quad \text{(A.184)}$$

The solution of Eq. (A.184) is $q_i^{(1)} = -\lambda\nabla_i T - \mu\nabla_i n$. Functional dependence analysis shows that $\lambda \propto T^{1/2}$ and $\mu \propto T^{3/2}n^{-1}$, therefore $\partial_t q_i^{(1)} = p\xi_n^{(0)}\mu\nabla_i n$. In order to satisfy Eq. (A.184) it is therefore required that $\mu = 0$ and

$$\lambda^* = \frac{1}{p\frac{d(d+2)}{2(d-1)} + (1-p)}. \quad \text{(A.185)}$$

# Bibliography


[1] E. Bertin, O. Dauchot, and M. Droz, Phys. Rev. Lett. **93**, 230601 (2004).

[2] W. Zippold, R. Kühn, and H. Horner, Eur. Phys. J. B. **13**, 531-537 (1999).

[3] M.R. Evans and R.A. Blythe, Physica A **313**, 110 (2002).

[4] Z. Rácz, e-print: cond-mat/0210435 (2002).

[5] J. Ferziger and H. Kaper, *Mathematical Theory of Transport Process in Gases*, North-Holland, Amsterdam (1972).

[6] V. Garzó and A. Santos, *Kinetic Theory of Gases in Shear Flows* (Kluwer Academic Publishers, The Netherlands, 2003).

[7] S. Chapman and T.G. Cowling, *The mathematical theory of non-uniform gases* (Cambridge University Press, Cambridge, 1970).

[8] J. Lebowitz, J. Percus, and J. Skyes, Phys. Rev. **188**, 487 (1969).

[9] H. van Beijern and M.H. Ernst, Physica A **68**, 437 (1973).

[10] P. Résibois, Phys. Rev. Lett. **40**, 1409 (1978).

[11] J.M. Montanero, V. Garzó, M. Alam, and S. Luding, e-print: cond-mat/0411548.

[12] N.V. Brilliantov and T. Pöschel, *Kinetic Theory of Granular Gases* (Oxford University Press, Oxford, 2004).

[13] N. Brilliantov, C. Salueña, T. Schwager, and T. Pöschel, Phys. Rev. Lett. **93**, 134301 (2004).

[14] J.T. Jenkins and M.W. Phys. Fluids. **28**, 3485 (1985).

[15] T. Aspelmeier, M. Huthmann, and A. Zippelius, in *Granular Gases*, edited by T. Pöschel and S. Luding, *Lecture Notes in Physics* **564** (Springer Verlag, Berlin, 2001), p.31.

[16] S. Luding, H. Herrmann, and A. Blumen, Phys. Rev. E **50**, 3100 (1990).

[17] C.K.K. Lun, S.B. Savage, D.J. Jeffrey, and N. Chepurnity, J. Fluid. Mech. **140**, 223 (1984).

[18] J.T. Jenkins and M.W. Richman, Arch. Ration. Mech. Anal. **87**, 355 (1985).

[19] T.P.C. van Noije, M.H. Ernst, and R. Brito, Physica A **251**, 266 (1998).

[20] A. Santos, J.M. Montanero, J.W. Dufty, and J.J. Brey, Phys. Rev. E **57**, 1644 (1998).

[21] H.M. Jaeger, S.R. Nagel, and R.P. Behringer, Rev. Mod. Phys. **68**, 1259 (1996).

[22] L.P. Kadanoff, Rev. Mod. Phys. **71**, 435 (1999).

[23] A. Barrat, E. Trizac, and M.H. Ernst, , e-print: cond-mat/0411435 (2004).

[24] J.J. Brey, J.W. Dufty, C.S. Kim, and A. Santos, Phys. Rev. E **58**, 4638 (1998).

[25] B. Bernu and R. Mazighi, J. Phys. A **23**, 5745 (1990).

[26] S. McNamara and W.R. Young, Phys. Rev. E **50**, R28 (1994).

[27] S. McNamara and W.R. Young, Phys. Rev. E **53**, 5089 (1996).

[28] R. Soto, M. Mareschal, and D. Risso, Phys. Rev. Lett. **83**, 5003 (1999).

[29] R.D. Wildman, A. Kudrolli, and D.J. Parker, Phys. Rev. E **67**, 061311 (2001).

[30] D.L. Blair and A. Kudrolli, Phys. Rev. E **67**, 041301 (2003).

[31] V. Garzó and J. Dufty, Phys. Rev. E **60**, 5706 (1999).

[32] Ph.A. Martin and J. Piasecki, Europhys. Lett. **46**, 613 (1999).

[33] A. Barrat and E. Trizac, Gran. Matter **4**, 57 (2002) (e-print: cond-mat/0202297).

[34] K. Feitosa and N. Menon, Phys. Rev. Lett. **88**, 198301 (2002).

[35] R.D. Wildman and D.J. Parker, Phys. Rev. Lett. **88**, 064301 (2002).

[36] S. McNamara and S. Luding, Phys. Rev. E **58**, 2247 (1998).

[37] T.P.C. van Noije and M.H. Ernst, Granular Matter **1**, 57 (1998) (e-print: cond-mat/9803042).

[38] I.S. Aranson and J.S. Olafsen, Phys. Rev. E **66**, 061302 (2002).

[39] J. Piasecki, E. Trizac, and M. Droz, Phys. Rev. E **66**, 066111 (2002).

[40] F. Coppex, M. Droz, J. Piasecki, E. Trizac, and P. Wittwer, Phys. Rev. E **67**, 021103 (2002).

[41] A. Santos, Physica A **321**, 442 (2003).

[42] M.H. Ernst and R. Brito, J. Stat. Phys. **109**, 407 (2002) (e-print: cond-mat/0112417).

[43] P.L. Krapivsky and C. Sire, Phys. Rev. Lett. **86**, 2494 (2001).

[44] E. Trizac and P.L. Krapivsky, Phys. Rev. Lett. **91**, 218302 (2003).

[45] F. Coppex, M. Droz, and E. Trizac, e-print: cond-mat/0503102 (submitted to Phys. Rev. E) (2005).

[46] J. Piasecki, *Echelles de temps en théorie cinétique* (PPUR, Lausanne, 1997).

[47] A.H. Nayfeh, *Perturbation Methods* (John Wiley, New York, 1973).

[48] J.W. Dufty, Res. Devel. Stat. Phys. **2**, 21-52 (2002) (e-print: cond-mat/0108444); J.W. Dufty, Adv. Compl. Syst. **4**, 397-406 (2001) (e-print: cond-mat/0109215).

[49] M.-L. Tan and I. Goldhirsch, Phys. Rev. Lett. **81**, 3022 (1998).

[50] J.J. Brey, M.J. Ruiz-Montero, and D. Cubero, Europhys. Lett. **48** (4), 359 (1999).

[51] J.J. Brey, M.J. Ruiz-Montero, and D. Cubero, Phys. Rev. E **54**, 3664 (1996).

[52] F. Coppex, M. Droz, and E. Trizac, Phys. Rev. E. **69**, 011303 (2004).

[53] F. Coppex, M. Droz, and E. Trizac, Phys. Rev. E. **70**, 061102 (2004).

[54] C. Cercignani, *Mathematical Methods in Kinetic Theory* (Plenum Press, New-York, 1990).

[55] C. Cercignani, *The Boltzmann Equation and its Applications* (Springer-Verlag, New-York, 1988).

[56] P. Résibois and M. de Leener, *Classical Kinetic Theory of Fluids*, John Wiley and Sons (1977).

[57] V. Garzó and J.W. Dufty, Phys. Rev. E **59**, 5895 (1999).

[58] Y. Elskens and H.L. Frisch, Phys. Rev. A **31**, 3812 (1985).

[59] E. Ben-Naim, S. Redner, and F. Leyvraz, Phys. Rev. Lett. **70**, 1890 (1993).

[60] E. Ben-Naim, P.L. Krapivsky, F. Leyvraz, and S. Redner, J. Chem. Phys. **98**, 7284 (1994).

[61] P.L. Krapivsky, S. Redner, and F. Leyvraz, Phys. Rev. E **51**, 3977 (1995).

[62] J. Piasecki, Phys. Rev. E **51**, 5535 (1995).

[63] M. Droz, P.-A. Rey, L. Frachebourg, and J. Piasecki, Phys. Rev. Lett. **75**, 160 (1995).

[64] M. Droz, P.-A. Rey, L. Frachebourg, and J. Piasecki, Phys. Rev. E **51**, 5541 (1995).

[65] P.-A. Rey, M. Droz, and J. Piasecki, Phys. Rev. E **57**, 138 (1997).

[66] P.-A. Rey, M. Droz, and J. Piasecki, Phys. Rev. E **59**, 126 (1998).

[67] Y. Kafri, J. Phys. A **33**, 2365 (1999).

[68] R.A. Blythe, M.R. Evans, and Y. Kafri, Phys. Rev. Lett. **85**, 3750 (2000).

[69] B. Chopard, A. Masselot, and M. Droz, Phys. Rev. Lett. **81**, 1845 (1998).

[70] E. Trizac, Phys. Rev. Lett. **88**, 160601 (2002).

[71] J. Krug and H. Spohn, Phys. Rev. A **38**, 4271 (1988).

[72] D. Toussain and F. Wilczek, J. Chem. Phys **78**, 2642 (1983).

[73] M. D. Donsker and S.R.S. Varadhan, Commun. Pure Appl. Math. **28**, 525 (1975).

[74] J. Piasecki, P.-A. Rey, and M. Droz, Physica A **229**, 515 (1996).

[75] F. Coppex, M. Droz, J. Piasecki, and E. Trizac, Physica A **329**, 114 (2003).

[76] S. McNamara and W.R. Young, Phys. Fluids A **5**, 34 (1993).

[77] N. Sela and I. Goldhirsch, J. Fluid Mech. **361**, 41 (1998).

[78] T.P.C. van Noije, M.H. Ernst, E. Trizac, and I. Pagonabarraga, Phys. Rev. E **59**, 4326 (1999).

[79] J.M. Montanero and A. Santos, Granular Matter **2**, 53 (2000) (e-print: cond-mat/0002323).

[80] N.V. Brilliantov and T. Pöschel, Phys. Rev. E **61**, 2809 (2000).

[81] R. Cafiero, S. Luding, and H.J. Herrmann, Phys. Rev. Lett. **84**, 6014 (2000).

[82] R. Soto and M. Maréschal, Phys. Rev. E **63**, 041303 (2001).

[83] A. Barrat and E. Trizac, Phys. Rev. E **66**, 051303 (2002).

[84] A. Barrat, E. Trizac, and J.N. Fuchs, Eur. Phys. J. E **5**, 161 (2001).

[85] A. Barrat, T. Biben, Z. Rácz, E. Trizac, and F. van Wijland, J. Phys. A **35**, 463 (2002) (e-print: cond-mat/0110345).

[86] E. Trizac, Europhys. Lett. **43**, 671 (1998).

[87] L. Landau and E. Lifshitz, *Physical Kinetics*, Pergamon Press (1981).

[88] G. Bird, *Molecular Gas Dynamics and the Direct Simulation of Gas Flows* (Clarendon Press, Oxford, 1994).

[89] J.M. Montanero, V. Garzó, A. Santos, and J.J. Brey, J. Fluid Mech. **389**, 391 (1999).

[90] N.G. van Kampen, *Stochastic Process in Physics and Chemistry* (North-Holland, Amsterdam, 1992).

[91] M.J.E. Richardson, J. Stat. Phys. **89**, 777 (1997).

[92] K. Kang and S. Redner, Phys. Rev. Lett. **52**, 955 (1984).

[93] K. Kang and S. Redner, Phys. Rev. A **30**, 2833 (1984).

[94] M. Droz and L. Sasvári, Phys. Rev. E **48**, R2343 (1993).

[95] O.E. Lanford III, Physica A **106**, 70 (1981).

[96] N.N. Bogolubov, in *Studies in Statistical Mechanics*, edited by J. De Boer and G.E. Uhlenbeck, Vol. I (North-Holland Publ. Co., Amsterdam, 1962), p.5.

[97] E.G.D. Cohen, in *Statistical Mechanics of Equilibrium and Non-Equilibrium*, edited by J. Meixner (North-Holland Publ. Co., Amsterdam, 1962), p.140.

[98] I. Goldhirsch, in *Granular Gases*, edited by T. Pöschel and S. Luding, *Lecture Notes in Physics* **564** (Springer Verlag, Berlin, 2001), p.79.

[99] J.J. Brey and D. Cubero, in *Granular Gases*, edited by T. Pöschel and S. Luding, *Lecture Notes in Physics* **564** (Springer Verlag, Berlin, 2001), p.59.

[100] V. Garzó and J.M. Montanero, Phys. Rev. E **68**, 041302 (2003).

[101] B. Meerson, T. Pöschel, Y. Bromberg, Phys. Rev. Lett. **91** 024301, (2003).

[102] J.J. Brey and M.J. Ruiz-Montero, Phys. Rev. E **69**, 011305 (2004).

[103] H. Grad, "Principles of the kinetic theory of gases", in *Encyclopedia of Physics*, edited by S. Flugge (Springer, NY, 1958).

[104] T.P.C. van Noije and M.H. Ernst, in *Granular Gases*, edited by T. Pöschel and S. Luding, *Lecture Notes in Physics* (Springer Verlag, Berlin, 2001), p. 3.

[105] G. Bird, *Molecular Gas Dynamics* (Oxford University Press, New York, 1976).

[106] A. Frezzotti, Physica A **278**, 161 (2000).

[107] See `http://mpej.unige.ch/~coppex/download/notes.ps`

[108] R. Ramírez, D. Risso, R. Soto, and P. Cordero, Phys. Rev. E **62**, 2521 (2000).

[109] G.F. Carnevale, Y. Pomeau, and W.R. Young, Phys. Rev. Lett. **64**, 2913 (1990).

[110] E. Trizac and J.-P. Hansen, Phys. Rev. Lett. **74**, 4114 (1995).

[111] V. Garzó and J.M. Montanero, Physica A **313**, 336-356 (2002).

[112] R. Soto, M. Mareschal and D. Risso, Phys. Rev. Lett. **83**, 5003 (1999).

[113] I. Goldhirsch and G. Zanetti, Phys. Rev. Lett. **70**, 1619 (1993).

[114] J.J. Brey, M.J. Ruiz-Montero, and D. Cubero, Phys. Rev. E **60**, 3150 (1999).

[115] J.W. Dufty and J.J. Brey, e-print: cond-mat/0410133.

[116] M.H. Ernst and E.M. Hendriks, Phys. Lett. A **70**, 183 (1979).

[117] E.M. Hendriks and M.H. Ernst, Physica A **120**, 545 (1983).

[118] M.H. Ernst, Phys. Rep. **78**, 1 (1981).

[119] U. Marini Bettolo Marconi and A. Puglisi, Phys. Rev. E **66**, 011301 (2002).

[120] J.W. Dufty, A. Baskaran, and L. Zogaib, Phys. Rev. E **69**, 051301 (2004).

[121] V. Garzó and A. Astillero, e-print: cond-mat/0404386 (2004).

[122] A. Baskaran and J.W. Dufty, e-print: cond-mat/0410084.

[123] V. Garzó and J.M. Montanero, e-print: cond-mat/0411221.

[124] A. Santos and J.J. Brey, Phys. Fluids **29**, 1750 (1986).

[125] E.G.D. Cohen, I.M. de Schepper, and M.J. Zuilhof, Physica B **127**, 282 (1984).

[126] E.G.D. Cohen, Physica A **194**, 229 (1993).

[127] D. van der Meer, K. van der Weele, and D. Lohse, Phys. Rev. Lett. **88** 174302 (2002).

[128] F. Coppex, M. Droz, and A. Lipowski, Phys. Rev. E **66**, 011305 (2002).

[129] I. Bena, F. Coppex, M. Droz, and A. Lipowski, Phys. Rev. Lett. **91**, 160602 (2003).

[130] P. B. Umbanhowar, F. Melo, and H. L. Swinney, Nature **382**, 793 (1996).

[131] T. Shinbrot and F. J. Muzzio, Nature **410**, 251 (2001).

[132] H. J. Schlichting and V. Nordmeier, Math. Naturwissenschaften Unterr. **49**, 323 (1996) (in German).

[133] J. Eggers, Phys. Rev. Lett. **83**, 5322 (1999).

[134] K. van der Weele, D. van der Meer, M. Versluis, and D. Lohse, Europhys. Lett. **53**, 328 (2001).

[135] D. van der Meer, K. van der Weele, and D. Lohse, Phys. Rev. E **63** 061304 (2001).

[136] J. J. Brey, F. Moreno, R. García-Rojo, and M. J. Ruiz-Montero, Phys. Rev. E **65**, 011305 (2001).

[137] P. Ehrenfest and T. Ehrenfest, *The Conceptual Foundations of the Statistical Approach in Mechanics* (Dover, New York, 1990).

[138] M. Kac and J. Logan, in *Fluctuation Phenomena* Ed. E. W. Montroll and J. L. Lebowitz (North-Holland, Amsterdam, 1987).

[139] A. Lipowski and M. Droz, Phys. Rev. E **65**, 031307 (2002).

[140] G.M. Shim, B.Y. Park, J.D. Noh, and H. Lee, Phys. Rev. E **70**, 031305 (2004).

[141] G.M. Shim, B.Y. Park, and H. Lee, Phys. Rev. E **67**, 011301 (2003).

[142] M.R. Evans, Braz. J. Phys. **30**, 42, (2000) (e-print: cond-mat/0007293).

[143] M.R. Evans and T. Hanney, e-print: cond-mat/0501338 (2005).

[144] V. Kumaran, Phys. Rev. E **57**, 5660 (1998).

[145] E. Falcon, S. Fauve, and C. Laroche, Eur. Phys. J. B. **9**, 183 (1999).

[146] E. Falcon, S. Fauve, and C. Laroche, J. Chim. Phys. **96**, 1111 (1999).

[147] K. Huang, *Statistical Mechanics* (John Wiley & Sons, New York, 1987).

[148] A. Lipowski and M. Droz, Phys. Rev. E **66**, 016118 (2002).

[149] F. Y. Wu, Rev. Mod. Phys. **54**, 235 (1982).

[150] P.C. Hohenberg and B.I. Halperin, Rev. Mod. Phys. **49**, 435 (1977).

[151] H.K. Janssen and K Oerding, J. Phys. A **27**, 715 (1994).

[152] E.D. Siggia, Phys. Rev. B **11**, 4736 (1974).

[153] B.I. Harlepin, P.C. Hohenberg, and S. Ma, Phys. Rev. B **10**, 139 (1974).

[154] J.D. Gunton and M.C. Yalabik, Phys. Rev. B **18**, 6199 (1978).

[155] W. Klein and C. Unger, Phys. Rev. B **28**, 445 (1983).

[156] R.A. Blythe and M.R. Evans, Braz. J. Phys. **33**, 464 (2003) (e-print: cond-mat/0304120).

[157] P.F. Arndt, S.R. Dahmen, and H. Hinrichsen, Physica A **295**, 128 (2001).

[158] S.M. Dammer, S.R. Dahmen, and H. Hinrichsen, J. Phys. A **35**, 4527 (2002).

[159] R.L. Greenblatt and J. Lebowitz, Phys. Rev. Lett. **93**, 238901 (2004).

[160] R.B. Griffiths, C.Y. Weng, and J.S. Langer, Phys. Rev. **149**, 301 (1966).

[161] S. Grossmann and W. Rosenhauer, Z. Phys. **218**, 437 (1969).

[162] S. Grossmann and V. Lehmann, Z. Phys. **218**, 449 (1969).

[163] M.E. Fisher, in *Lectures in Theoretical Physics, Vol. VIIC - Statistical Physics, Weak Interactions, Field Theory*, Ed. W.E. Brittin (Colorado University Press, Boulder, 1965).

[164] K. Binder and D. W. Heermann, *Monte Carlo Simulations in Statistical Physics* (Springer-Verlag, Berlin, 1997).

[165] F. Spitzer, Adv. Math. **5**, 246 (1970).

[166] M.H. Ernst and R. Brito, Phys. Rev. E **65**, 040301(R) (2002).

[167] W.G. Hoover, *Computational Statistical Mechanics* (Elsevier, Amsterdam, 1991).

[168] E. Ben-Naim and P.L. Krapivsky, Phys. Rev. E **61**, R5 (2000).

[169] J.A. Carrillo, C. Cercignani, and I.M. Gamba, Phys. Rev. E **62**, 7700 (2000).

[170] I. Pagonabarraga, E. Trizac, T.P.C. van Noije, and M.H. Ernst, Phys. Rev. E **65**, 011303 (2002).

[171] J.S. van Zon and F.C. MacKintosh, Phys. Rev. Lett. **93**, 38001 (2004); e-print: cond-mat/0205512.

[172] V. Garzó and J.W. Dufty, *Hydrodynamic Equations for Granular Mixtures - A Review* in *Horizons in Physics Research* (Nova Pubs., Hauppauge, NY, 2003) (e-print: cond-mat/0307426).

[173] C. Thornton, Z. Ning, C. Wu, and M. NasrullahLi, in *Granular Gases*, edited by T. Pöschel and S. Luding, *Lecture Notes in Physics* **564** (Springer Verlag, Berlin, 2001), p.184.

[174] N.V. Brilliantov, F. Spahn, J.M. Hertzsch, and T. Poeschel, Phys. Rev. E **53**, 5382-5392 (1996).

[175] M. Müller and H.J. Herrmann, in *Granular Gases*, edited by T. Pöschel and S. Luding, *Lecture Notes in Physics* **564** (Springer Verlag, Berlin, 2001), p.445.

[176] B. Chopard and M. Droz, *Cellular Automata Modeling of Physical Systems* (Cambridge University Press, 1998).

[177] K. Binder, Rep. Prog. Phys. **60**, 487 (1997).

[178] P.E. Cladis and H.R. Brand, Physica A **326**, 322 (2003).

[179] T. Pöschel and N. V. Brilliantov, in *Granular Gas Dynamics, Vol. 624 - Lecture Notes in Physics*, p. 131-162 (Springer Verlag, New York, 2003).

# List of publications

- Francois Coppex, Michel Droz, and Adam Lipowski, *Dynamics of the breakdown of granular clusters*, Phys. Rev. E **66**, 011305 (2002).
- Francois Coppex, Michel Droz, Jarosław Piasecki, Emmanuel Trizac, and Peter Wittwer, *Some exact results for Boltzmann's annihilation dynamics*, Phys. Rev. E **67**, 021103 (2002).
- Francois Coppex, Michel Droz, Jarosław Piasecki, and Emmanuel Trizac, *On the first Sonine correction for granular gases*, Physica A **329**, 114 (2003).
- Ioana Bena, Francois Coppex, Michel Droz, and Adam Lipowski, *Yang-Lee zeroes for an urn model for the separation of sand*, Phys. Rev. Lett. **91**, 160602 (2003).
- Francois Coppex, Michel Droz, and Emmanuel Trizac, *Probabilistic ballistic annihilation with continuous velocity distributions*, Phys. Rev. E **69**, 011303 (2004).
- Francois Coppex, Michel Droz, and Adam Lipowski, *Extinction dynamics of Lotka-Volterra ecosystems on evolving networks*, Phys. Rev. E **69**, 061901 (2004).
- Francois Coppex, Michel Droz, and Adam Lipowski, *Lotka-Volterra Model of Macro-Evolution on Dynamical Networks*, Proceedings of "Computational Science-ICCS 2004", Eds. Marian Dubak, Geert Dick van Albada, Peter M.A. Sloot and Jack J. Dongarra, Springer Verlag, Lecture Notes in Computer Sciences **3039**, p. 742-749 (2004).
- Francois Coppex, Michel Droz, and Emmanuel Trizac, *Hydrodynamics of probabilistic ballistic annihilation*, Phys. Rev. E **70**, 061102 (2004).
- Ioana Bena, Francois Coppex, Michel Droz, and Zoltán Rácz, *Front motion in an $A+B \to C$ type reaction-diffusion process: Effects of an electric field*, J. Chem. Phys. **122**, 024512 (2005) .
- Francois Coppex, Michel Droz, and Emmanuel Trizac, *Maxwell and very hard particle models for probabilistic ballistic annihilation: hydrodynamic description*, e-print: cond-mat/0503102 (submitted to Phys. Rev. E) (2005).